School of Biomedical Sciences

Characterisation of liver progenitor cells and their microenvironment during chronic liver disease and hepatocarcinogenesis

Julia Köhn

This thesis is presented for the Degree of

Doctor of Philosophy

of

Curtin University

October 2016

DECLARATION

To the best of my knowledge and belief this thesis contains no material previously published by any other person except where due acknowledgment has been made.

This thesis contains no material, which has been accepted for the award of any other degree or diploma in any university.

Human Ethics The research presented and reported in this thesis was conducted in accordance with the National Health and Medical Research Council National Statement on Ethical Conduct in Human Research (2007) – updated March 2014. The proposed research study received human research ethics approval from the Fremantle Hospital Human Research Ethics Committee (96/37) and the Alfred Hospital Ethics Committee (280/13).

Animal Ethics The research presented and reported in this thesis was conducted in compliance with the National Health and Medical Research Council Australian code for the care and use of animals for scientific purposes 8th edition (2013). The proposed research study received animal ethics approval from the Curtin University Animal Ethics Committee, Approval Number AEC_2012_23, AEC_2012_24, AEC_2014_28 and AEC_2014_29.

Signature:

Date:

ACKNOWLEDGEMENTS

The journey through this PhD has been a very exciting but also challenging experience on a personal and professional level. I would like to express my special appreciation and gratitude to all of you who made this possible and accompanied me over the last four years locally or from far away.

First and foremost I would like to thank my supervisor Dr. Nina Tirnitz-Parker for giving me the opportunity to come to Australia and to undertake this PhD project in her research group. I am grateful for all the support, the contributions of ideas, time and funding, the enthusiastic and motivational atmosphere, but also for teaching me to become an independent and conscientious researcher. I am also grateful to my second supervisor Prof. John Olynyk for his support and expertise, in particular with the human study within my project. To Dr. Caryn Elsegood for her valuable advice on immunohistology and for always having an open ear even without being one of my supervisors.

A big thank you goes to my lab colleagues Jully and Frankie. We worked well together as a team, especially during our animal experiments. Jully, thanks for your encouragement, your warm words and chocolate supply in the final stage of my PhD. I also want to acknowledge my "office buddies" from room 145 who created a friendly, enjoyable working environment and for several stimulating discussions. I am particularly grateful to Ganga and Gae for all the conversations, the many laughs we shared, your advice and for entertaining my children when I needed to finish experiments in the lab or during the last period of my thesis write up.

A huge thank you to all my friends from near and far, you guys are the best. I am grateful to Georgia and Kobi who always offered their help when needed, especially during the final countdown. Matt, you took us in warmly when we arrived in Australia helping us to get started down under. *Merc*i to Honorine, my special "French girl", we were so lucky to have you here for three months as friend and an extra pair of hands for the children. *Dankeschön* to my German friends, who supported me from far away or came for a visit. A special thanks goes to Verena for being an encouraging and caring friend throughout many years. I rejoiced in the many parcels sent from Germany which brought "home" a little closer to Australia.

Last but not least, *Dankeschön* to my family for their love and encouragement: For my parents who supported me throughout all my journeys and adventures. My Mum for the three months she spent with us in Australia which meant so much to me and the kids. Thanks to my partner Fillippo for encouraging and supporting me along the way and to my children Mia and Matteo for their patience when I had to work on weekends. I couldn't have made it without you.

ABSTRACT

Chronic liver disease (CLD) is a major health and economic burden and its respective end-stage complications, cirrhosis and hepatocellular carcinoma (HCC), cause high rates of mortality worldwide. The number of patients with a high risk to develop end-stage CLD are increasing in western countries due to changing life styles, obesity, *diabetes mellitus* and insulin resistance, and also more frequently include children. Despite the diversity of causal factors, most CLDs share the common characteristics of hepatocellular necrosis, inflammation, fibrosis and the activation of liver progenitor cells (LPCs) as part of ductular reactions (DRs). The latter has been associated with HCC development, and thus LPCs are of particular interest in the study of hepatocarcinogenesis.

There can be vast differences between experimental models that aim to mimic CLD-related processes and their identification is fundamental for translational research. Chapter 3 of this thesis characterises and compares two common murine CLD models based on (i) choline deficiency and ethionine supplementation (CDE), and (ii) thioacetamide (TAA) supplementation. Overall, great discrepancies were revealed between both regimens. Liver injury markers, including serum alanine transaminase levels, apoptosis, hepatic fat loading and oxidative stress, as well as inflammatory, fibrogenic and LPC responses were analysed at early stages of CLD, defined as injury induction (day 3 and 7), establishment (day 14 and 21) and maintenance phase (day 42). The data defined CDE-driven periportal injury and fibrosis with an early peak and slow normalisation of all parameters. In contrast, TAA induced pericentral patterns of progressive injury and fibrosis, resulting in a more severe hepatic injury phenotype. Importantly, this study is the first to resolve two different patterns of injury and fibrosis in the CDE and TAA model, and to indisputably identify the fibrosis pattern in the TAA model as driven initially from the pericentral vein region. In Chapter 4, a detailed characterisation of the LPC response using common markers in the field, including panCK, CK19, CD133, EpCAM, E cadherin, MIC1-1C3, and Sox9 identified a broad homogenous population of LPCs provoked in both regimens. In addition, small subpopulations with distinct phenotypes were detected within the LPC responses, which were more

prominent in the TAA model. Chapter 5 describes CDE- and TAA-induced disease progression and carcinogenesis that were assessed in a long-term study. Injury dynamics, including hepatocellular tissue damage, and the inflammatory, fibrogenic and LPC response, as well as tumour development were assessed in mice treated for 3, 5, and 7 months. Both regimens provoked progressively increasing levels of all investigated disease parameters throughout the time course study and eventually neoplasms were formed, starting after three months (CDE model) and five months of treatment (TAA), respectively. Importantly, in this thesis, both CDE- and TAA-induced carcinogenesis resulted in the formation of HCC, which is controversial to several studies that reported TAA-associated cholangiocarcinoma development. Interestingly, increased LPC numbers were associated with carcinogenesis in both regimens, and CD44 was proposed to represent a marker that may potentially identify cancer-related LPC populations. To investigate the relevance of the results obtained in experimental models in the human setting, the relationship between the DR, LPC responses and HCC development was investigated in a retrospective study, described in Chapter 6. The data propose a positive correlation between the magnitude and distribution of DRs/LPCs and the development of HCC in CLD patients.

This thesis provides a valuable foundation for future work utilising the CDE and TAA regimens to model a variety of human CLDs that feature DRs, LPC responses, and that predispose to hepatocarcinogenesis. It also highlights the importance of standardised protocols when using experimental models. Furthermore, the data from the human study may be of potential clinical relevance and may help to develop alternative strategies for prevention of HCC development in CLD patients.

PUBLICATIONS

Köhn-Gaone J., Gogoi-Tiwari J., Ramm G.A., Olynyk J.K., Tirnitz-Parker J.E.E. (2016). The role of liver progenitor cells during liver regeneration, fibrogenesis, and carcinogenesis. *American Journal of Physiology Gastrointestinal and Liver Physiology*, **310**: G143-154.

Köhn-Gaone J., Dwyer B.J., Grzelak C.A., Miller G., Shackel N.A., Ramm G.A., McCaughan G.W., Elsegood C.L., Olynyk J.K., Tirnitz-Parker J.E.E. (2016). Divergent Inflammatory, Fibrogenic, and Liver Progenitor Cell Dynamics in Two Common Mouse Models of Chronic Liver Injury. *American Journal of Pathology*, **186**: 1762-1774.

Muller M., Wetzel S., Köhn-Gaone J., Chalupsky K., Lullmann-Rauch R., Barikbin R., Bergmann J., Wohner B., Zbodakova O., Leuschner I., Martin G., Tiegs G., Rose-John S., Sedlacek R., Tirnitz-Parker J.E.E., Saftig P., Schmidt-Arras D. (2016). A disintegrin and metalloprotease 10 (ADAM10) is a central regulator of murine liver tissue homeostasis. *Oncotarget*, **7**: 17431-17441.

ABSTRACTS

Dwyer B.J., Köhn-Gaone J., Olynyk J. K., Grzelak C. A., Shackel N. A., McCaughan G. W., Tirnitz-Parker J.E.E. (2013).

Dynamics of inflammatory, fibrogenic and liver progenitor cell responses during early thioacetomide-induced chronic liver injury in mice.

Oral presentation at the Australian Liver Association meeting 2013, Queensland, Australia.

Köhn-Gaone J., Dwyer B. J., Elsegood C. L., Tirnitz-Parker J. E. E. (2014).

Differential inflammatory, fibrogenic and liver progenitor cell response dynamics in mouse models of progressive chronic liver injury.

Poster presentation at the 24th Annual Combined Biological Sciences Meeting 2014, Perth, Australia.

Köhn-Gaone J., Dwyer B. J., Elsegood C. L., Tirnitz-Parker J. E. E. (2014).

Differential inflammatory, fibrogenic and liver progenitor cell response dynamics in mouse models of progressive chronic liver injury.

Poster presentation at the Mark Liveris Research Student Seminar 2014, Perth, Australia.

TABLE OF CONTENTS

TABLE OF FIGURES

LIST OF TABLES

ABBREVIATIONS

A	absorbance
A6	murine LPC marker, epitope unknown
2-AAF	2-acetylaminofluorene
Ac-Me	acetone-methanol
A/E	annealing/extension
AFP	α-fetoprotein
Alb	albumin
ALD	alcoholic liver disease
ALT	alanine transaminase
αSMA	α-smooth muscle actin
BDL	bile duct ligation
BEC	biliary epithelial cell
CC	cholangiocarcinoma
CCl_4	carbon tetrachloride
CD	cluster of differentiation
CDE	choline-deficient, ethionine-supplemented
CK	cytokeratin
c-Kit	CD117, stem cell factor receptor
CLD	chronic liver disease
c-Met	hepatocyte growth factor receptor (HGFR)
CoH	Canals of Hering
Col1	collagen I
CSC	cancer stem cell

Cx	connexion
DAB	3,3’-diaminobenzidine
DDB1	damaged DNA binding protein 1
DDC	3,5-diethoxycarbonyl-1,4-dihydrocollidine
ddH2O	double-deionised H2O
DEN	diethylnitrosamine
D-gal	D-galactosamine
Dlk	delta-like protein
DMAB	4-dimethylaminobenzaldehyde
DNA	deoxyribonucleic acid
DR	ductular reaction
ECM	extracellular matrix
EDTA	ethylene diamine tetraacetic acid
EGF	epidermal growth factor
EpCAM	epithelial cell adhesion molecule
FACS	fluorescence-activated cell sorting
FGF	fibroblast growth factor
Fn14	fibroblast growth factor-inducible 14
Foxl1	forkhead/winged helix-box L1
FOV	field of view
Fwd	forward
Gapdh	glyceraldehyde 3-phosphate dehydrogenase
GGT	γ-glutamyl transpeptidase

HBV	hepatitis B virus
HCC	hepatocellular carcinoma
HCV	hepatitis C virus
Hep	hepatocyte
HGF	hepatocyte growth factor
HRP	horseradish peroxidase
Igf2	insulin-like growth factor 2
HSC	hepatic stellate cell
F	female
IF	immunofluorescence
IFN	interferon
IHC	immunohistochemistry
IL	interleukin
KC	Kupffer cells
LSEC	liver sinusoidal endothelial cell
Lgr5	leucin-rich-repeat-containing G-protein coupled receptor 5
LPC	liver progenitor cell
LPS	lipopolysaccharide
LT	lymphotoxin
LTβR	LTβ receptor
M	male
MIC1-1C3	oval cell marker
MMP	matrix metalloproteinase

M2PK	muscle pyruvate kinase 2
Mu	murine
N/A	not assessed
NAFLD	non-alcoholic fatty liver disease
NASH	non-alcoholic steatohepatitis
NCAM	neuronal cell adhesion molecule
NK	natural killer
NO	nitric oxide
Nope	neighbor of Punc E 11
Nqo1	NAD(P)H quinone oxidoreductase
Nrf1	nuclear factor erythroid-derived 2-related factor 1
NT	non-tumour
OC.2	oval cell antigen 2
OPN	osteopontin
PBS	phosphate buffered saline
PFA	paraformaldehyde
PH	partial hepatectomy
pNAFLD	pediatric NAFLD
π-GST	pi-glutathione-S-transferase
Rev	reverse
RNA	ribonucleic acid
RT	room temperature
RT-PCR	real-time polymerase chain reaction

Sca-1	stem cell antigen-1
SEM	standard error of the mean
Sox9	SRY (sex determining region Y)-related HMG (high mobility group) box 9
SP	side population
STAT	signal transducer and activator of transcription
T	tumour
TAA	thioacetamide
TAM	tumour-associated macrophage
TACE	transcatheter arterial chemoembolisation
Taf	TATA box binding protein associated factor
TGF	transforming growth factor
Thy-1	thymocyte antigen-1
TIMP	tissue inhibitor of metalloproteinase
TNF	tumour necrosis factor
Trop2	tumour-associated calcium signal transducer 2
Tris	tris(hydroxymethyl)aminomethane
TUNEL	Terminal Deoxynucleotidyl Transferase dUTP-biotin Nick End Labelling
TWEAK	TNF-like weak inducer of apoptosis
Txn	thioredoxin

CHAPTER 1

Literature Review

Parts of the literature review have already been published and the article is included in the appendix (Köhn-Gaone *et al.* 2016b)

Köhn-Gaone J., Gogoi-Tiwari J., Ramm G.A., Olynyk J.K., and Tirnitz-Parker J.E. (2016b). The Role of Liver Progenitor Cells During Liver Regeneration, Fibrogenesis, and Carcinogenesis. *Am J Physiol Gastrointest Liver Physiol*, **310**: G143-154.

1.1 The liver

1.1.1 Anatomy and physiology of the liver

The liver is the largest abdominal organ in the body and represents a central organ with highly diverse functions, including the metabolism of proteins, fat and carbohydrates, regulation of the blood-glucose level, bile production, storage of vitamins and nutrients, plasma protein synthesis, detoxification, drug metabolism and host defence.

A healthy adult human liver consists of four lobes including right, left, quadrate and caudate; however, based on vascular and ductal arrangements can be further functionally subdivided into nine segments (Kogure *et al.* 1999). Mouse and rat livers similarly comprise four lobes termed median, left, right and caudate, which are all further subdivided, except the left lobe (Kogure *et al.* 1999; Malarkey *et al.* 2005).

The blood supply of the liver is provided by the portal vein and the hepatic artery, which together with a bile duct represent the portal triad (on average a portal triad contains one to two arteries, one portal vein and one to two bile ducts). Highly nutritious blood from the portal vein drains from the splenic and gastrointestinal veins and carries 70% of the hepatic blood flow (40% of the oxygen), whereas the hepatic artery delivers the remaining 30% of higher oxygenated blood (60% of the oxygen) (Malarkey *et al.* 2005). Upon entry into the portal tract, arterial and venous blood mixes, enters the sinusoidal system through the terminal portal venules, flows towards the central veins (also referred to as hepatic venules) and exits through the hepatic vein and the *inferior vena cava*. Incomplete mixing of portal blood and blood flow alterations can lead to different interlobular responses during liver diseases such as hepatitis C virus (HCV)-derived cirrhosis and carcinogenesis (Solt *et al.* 1977; Richardson *et al.* 1986; Regev *et al.* 2002). Bile is secreted from hepatocytes, moves within bile canaliculi towards the portal tract, in the opposite direction of the blood flow in the liver, and is collected in intrahepatic bile ducts. The cell compartments at the biliary-hepatocytic interface located between the terminal bile ductules and the

first hepatocytes of the hepatic plate are referred to as the Canals of Hering and have been suggested to harbour dormant liver stem cells (Sell 1990; Theise *et al.* 1999).

Cellular components of the epithelial and mesenchymal lineage are organised in multiple repetitive units, which form the characteristic complex three-dimensional structure of the liver. Different concepts have been proposed to describe the smallest hepatic unit. The most common models are the liver lobule and the liver acinus. In 1833 Kiernan described the classical hexagonal lobule as the smallest hepatic unit, which consists of a centric hepatic vein surrounded by portal tracts in the shape of a hexagon (Kierman 1833). Based on functional differences and dependent on the location within the lobule, Rappaport *et al.* introduced the liver acinus, which only focusses on the area between central veins (Rappaport *et al.* 1954). Thus the acinus defines a functional unit, which is divided into a periportal (zone 1), an intermediate (zone 2) and a pericentral area (zone 3). Based on the oxygen and nutritional gradient created by the incoming blood, there is a great functional heterogeneity from periportal towards pericentral hepatocytes (Gebhardt 1992). Characteristic functions of the periportal area include oxidative metabolism, gluconeogenesis, lipid and amino acid metabolism, bile formation and the synthesis of the plasma proteins albumin and fibrinogen, whereas the pericentral area is mainly responsible for glycolysis, fatty acid synthesis, ketogenesis, xenobiotic metabolism and detoxification (Jungermann and Kietzmann 1996; Malarkey *et al.* 2005).

1.1.2 Adult hepatic cell types

1.1.2.1 Hepatocytes

Hepatocytes represent the main cell type in the liver by making up 80% of the volume and numerically accounting for 60% of all hepatic cells (Blouin *et al.* 1977). Their size ranges from 20 - 30 µm and the morphology resembles a characteristic cuboidal epithelial cell. Hepatocytes form a labyrinth-like structure consisting of one cell-thick plates (laminae) radiating out from the central vein, which also determines the sinusoidal architecture since their lumen is formed by neighbouring hepatic plates. Hepatocytes are polarised cells that face different adjacent compartments in

the liver and show three characteristic membrane domains with specialised functions: the basolateral, lateral and apical domain (Treyer and Musch 2013). The basolateral surface or sinusoidal domain is exposed to the perisinusoidal space, also called the Space of Disse, which represents the extracellular space between hepatocytes and the sinusoidal endothelium. Microvilli structures on the surface of the basolateral domain facilitate the exchange of substances between the blood and hepatocytes (Grisham *et al.* 1975). The lateral surface or intercellular membrane domain anchors neighbouring hepatocytes by forming tight junctions, intermediate junctions and desmosomes, as well as gap junctions for communication (Treyer *et al.* 2013). The apical surface or canalicular domain secretes bile acid, and bile canaliculi are formed by the apical membranes of two opposing hepatocytes. Due to their high metabolic activity and numerous functions, hepatocytes contain a large number of mitochondria, free ribosomes, cytoskeleton elements, lysosomes and peroxisomes, as well as smooth and rough endoplasmic reticulum, and furthermore can be mono- or binucleated (di-, tetra- and octoploid), showing increased ploidy primarily towards the central area (Gandillet *et al.* 2003).

1.1.2.2 Cholangiocytes

Cholangiocytes or biliary epithelial cells line the lumen of bile ducts and represent approximately 3-5% of all hepatic cells. They form a branched three-dimensional network of intra- and extrahepatic bile ducts, termed the biliary tree, which drains secreted canalicular bile and mediates its transport from the Canals of Hering towards the intestine. During development, cholangiocytes from the intrahepatic biliary tree originate from bipotential hepatoblasts and thus share the same precursor cell with hepatocytes (Vestentoft *et al.* 2011). According to the diameter of their lumen, rodent intrahepatic bile ducts can be further subdivided into two groups, small and large ducts, which are lined by four to five small or 8-12 large cholangiocytes, respectively, with cell sizes ranging from 6-12 μm (Tabibian *et al.* 2013). In addition to the function of bile transport, cholangiocytes also perform canalicular or primary bile modifications and concentration by coordinated membrane-transport of ions, solutes and water, mediated through numerous transporter proteins on their basolateral and apical surface (Franchitto *et al.* 2013;

LaRusso *et al.* 1991; Alpini *et al.* 1988). Furthermore, it was shown in rats that connexin 43-gap junctions mediate hormonal-controlled intercellular communication (Bode *et al.* 2002).

1.1.2.3 Liver Sinusoidal Endothelial Cells

Combined blood entering through the hepatic artery and portal vein, streams between the hepatocyte plates towards the central vein. Blood flow is coordinated by hepatic sinusoids, which are lined by liver sinusoidal endothelial cells (LSECs) and act as a semi-accessible barrier between the blood and the extracellular Space of Disse, allowing bi-directional transfer of soluble and small substrates with hepatocytes (Wisse 1972). To facilitate this transport, LSECs have specialised characteristics, including the lack of a typical basement membrane and the existence of numerous transcellular pores termed fenestrations, which are clustered in sieve plates (Wisse *et al.* 1983; Svistounov *et al.* 2012). Consequently, their morphology, functions and phenotypes are significantly different from vascular endothelial cells in the liver and other organs. The availability of markers to label LSECs with specific antibodies is somewhat limited, as they also label other types of vascular endothelial cells. Widely used are markers such as von Willebrand factor (also called factor VIII) and platelet-endothelial cell adhesion molecule 1, referred to as cluster of differentiation 31 (CD31). Due to discrepancies in expression patterns in published studies, there is however much controversy regarding their respective expediency (Irving *et al.* 1984; Couvelard *et al.* 1993; Smedsrod *et al.* 1994).

1.1.2.4 Kupffer cells

Kupffer cells (KCs) were first described in 1876 by the anatomist Karl Wilhelm von Kupffer and named accordingly. They are defined as tissue-resident macrophages that reside in the hepatic sinusoids between LSECs, firmly attached to the sinusoid wall and play an important role in liver homeostasis and innate immunity (Smedsrod *et al.* 1994; Parker and Picut 2005). KCs account for approximately 15% of all hepatic cells and 30% of sinusoidal cells. The majority of KCs exist in the periportal area (43%) (Bouwens *et al.* 1986), facilitating the first contact to substances

absorbed from the gastrointestinal tract and transported via the blood entering the hepatic vein. In addition, KCs are found in the intermediate (28%) and pericentral area (29%) of the lobule in rats (Bouwens *et al.* 1986), and importantly might be able to migrate within the sinusoids (MacPhee *et al.* 1992). Their main characteristics are scavenger and phagocytic functions, such as the elimination and detoxification of microorganisms, lipopolysaccharides, apoptotic cells, immune complexes and toxic agents from the blood (Parker *et al.* 2005). A previous study in rats found the distribution of KCs to be in a ratio of 4:3:2 from portal via intermediate towards central areas and showed functional heterogeneity depending on their position within the liver lobe (Sleyster and Knook 1982). Portal KCs were found to be larger and showed higher phagocytic and lysosomal enzyme activity than midzonal and central KCs (Sleyster *et al.* 1982). Initially the identification of KCs was based on their high peroxidase activity (Fahimi 1970; Widmann *et al.* 1972), however nowadays their phenotype can be characterised by immunodetection with markers such as CD68, F4/80 and CRIg (Brown *et al.* 2001; Elsegood *et al.* 2015).

1.1.2.5 Hepatic Stellate Cells

Hepatic stellate cells (HSCs), first described as "Sternzellen" ("star cells" in German) together with KCs by Kupffer in 1876, are located in the Space of Disse between LSECs and hepatocytes, and account for about 5% of all hepatic cells. The term hepatic stellate cell was standardised amongst researchers in 1996, as up to that date several different names were used in the literature including perisinusoidal cell, Ito cell, lipocyte, parasinusoidal cell, and fat-storing cell, causing confusion in the field (Friedman 2008a). In healthy livers, HSCs are quiescent and their main characteristic feature is the cytoplasmic storage of Vitamin A in lipid droplets (Wake 1971). In rodents, desmin was described to represent a reliable marker for HSCs and distinguishes them from other fibroblast populations in the liver (Yokoi *et al.* 1984; Takase *et al.* 1988). The HSC population shows a high heterogeneity and plasticity. In response to liver injury, HSCs assume an activated state and severely change their morphology and phenotype by losing the lipid droplets and transforming into a myofibroblast-like cell type expressing α-smooth muscle actin (αSMA) (Schmitt-Graff *et al.* 1991). These are the main producers of extracellular matrix (ECM)

components and central players in ECM remodelling (Friedman 2008b), and hence fulfil an important role during fibrogenesis in chronic liver injuries.

1.1.2.6 Pit cells

Pit cells were first described in 1976 by Wisse *et al.* and named according to their high characteristic granules in the cytoplasm resembling fruit pits (Wisse *et al.* 1976). They are located in the hepatic sinusoids firmly adhering to KCs and LSECs, and occasionally migrate along the sinusoid wall or penetrate the endothelial fenestrae mediated by microvilli or extending pseudopodia to facilitate contact to hepatocyte microvilli within the Space of Disse (Wisse *et al.* 1976; Kaneda and Wake 1983; Kaneda *et al.* 1984). Originally pit cells were identified as hepatic large granular lymphocytes with natural killer (NK) cell activity, however due to similar morphologies the pit cell population includes liver-associated NK cells and natural killer T cells (Nakatani *et al.* 2004).

1.1.3 Liver tissue homeostasis under healthy conditions

The origin and mechanism of newly generated hepatocytes during normal liver tissue homeostasis is still under debate. An early theory is termed “streaming liver” and claims that hepatocytes proliferate in portal areas with subsequent central-orientated migration and maturation while creating the distinct portal-to-central zonation with different metabolomics and gene expression patterns. (Zajicek *et al.* 1985; Arber *et al.* 1988). However, this model of normal tissue turnover has been disputed. Firstly, there is no evidence of a correlation between gradual maturation and cell function, and it was shown that lobular zonation is not dependent on the hepatocyte lineage maturation stage but rather on oxygen access and metabolic activities (Thurman and Kauffman 1985). Moreover, hepatocyte tracing studies revealed a contribution of all hepatocytes throughout the liver lobule by clonal proliferation (Bralet *et al.* 1994; Kennedy *et al.* 1995).

More recently an albumin-driven lineage tracing study demonstrated the existence of new-born hepatocyte lineages emerging from prehepatocyte albumin-naïve cell

populations in normal healthy livers (Iverson *et al.* 2011). A continuous supply of new hepatocytes was detected under steady-state conditions, which represented 0.076% of all hepatocytes. As hepatocytes are proliferative, they give rise to several new hepatocytes. However, it is not known how many cell divisions they are capable of undergoing and whether they become senescent. The steady-state condition of new-born hepatocytes demonstrated by Iverson *et al.* indicates a finite self-renewing capacity of hepatocyte lineages and their senescence.

A recent study by Wang and colleagues demonstrated the existence of an $Axin2^{+}$ stem cell/progenitor cell compartment adjacent to the central vein, which is active during normal healthy conditions and thus contributes to newly derived hepatocyte lineages (Wang *et al.* 2015). It was shown that this pericentral stem cell niche is maintained via Wnt signalling and is mediated by central vein endothelial cells.

The current literature proposes that hepatocytes might not fuel the generation of new hepatocyte lineages by themselves. Instead there may be different cell sources of "prehepatocytes" contributing to tissue homeostasis. Whether they act in concert with each other or are mutually exclusive remains to be determined.

1.2 Liver regeneration: tissue response in acute vs. chronic liver injury

A unique characteristic of the liver is its great potential to regenerate in response to different injuries. There are two main mechanisms described in the literature, which mediate the regeneration process, depending on the type of injury. Acute liver injury caused by drug, toxin and acute viral exposure as well as resection, activates the hepatocyte-mediated regeneration cascade. However, following severe or chronic liver injury, residual hepatocytes may no longer meet the tissue demand due to cell cycle arrest and senescence, and consequently a progenitor cell compartment takes over and facilitates the replacement of damaged hepatocytes via liver progenitor cell (LPC)-mediated regeneration.

Hepatocyte-mediated liver regeneration has mainly been studied after partial hepatectomy (PH). The protocol used in rats, where two thirds of the liver are resected (Higgins 1931), had to be adjusted for safe performance in mice (Greene

and Puder 2003) due to induced necrosis after removal of the left and median lobes (Fausto *et al.* 2006). However, in both species a PH consistently leads to the expansion of the remaining lobes until the original mass is restored, which is accomplished within five to seven days. The restoration process is mediated by a sequential replication of the residual liver cells including hepatocytes, which represent one of the few fully differentiated cell types capable of performing DNA replication and cell proliferation (Inoue *et al.* 2006). However, differences in hepatocyte proliferation capabilities were reported to be dependent on the location within the liver acinus, showing initial replication in periportal areas and lower activity in central areas (Rabes 1976; Gebhardt 1988). It is commonly accepted that hepatocyte compensation is self-regulated by the metabolic needs and ends when the appropriate liver-body-weight ratio is reached. This regeneration process is regulated by a complex signalling network including cytokines, growth factors and metabolic pathways, which operate simultaneously and/or sequentially (Fausto *et al.* 2006; Riehle *et al.* 2011). Kupffer cells represent at least one initiator of hepatocyte regeneration, since they activate the inflammatory cascade mediated by tumour necrosis factor (TNF)-induced NF-κB signalling and subsequent interleukin 6 (IL6) secretion (Yamada *et al.* 1997; Cressman *et al.* 1996). Downstream signalling in hepatocytes causes nuclear translocation of signal transducer and activator of transcription 3 (STAT3), and promotes cell proliferation in concert with several growth factors, in particular members of the epidermal growth factor (EGF) family such as EGF (Francavilla *et al.* 1986; Raper *et al.* 1987), transforming growth factor (TGF) α (Webber *et al.* 1993) and heparin binding EGF-like growth factor (Kiso *et al.* 2003), as well as hepatocyte growth factor (HGF) (Strain *et al.* 1991; Inoue *et al.* 2006; Natarajan *et al.* 2007) and TNF (Akerman *et al.* 1992; Webber *et al.* 1998). It was shown that full mitogen function of HGF, TGFα and EGF during acute injury is achieved after initial stimulation of hepatocytes with factors including TNF, a process called "hepatocyte priming" (Webber *et al.* 1994; Webber *et al.* 1998). Since HGF is bound to the ECM and requires release before performing mitogen activity (Schuppan *et al.* 1998) and matrix remodelling is associated with liver regeneration, it is not surprising that matrix metalloproteinases (MMPs) play an important role during hepatocyte proliferation (Kim *et al.* 2000; Olle *et al.* 2006; Riehle *et al.* 2011). During the end stage of liver repair these growth-stimulating processes eventually have to be abolished. Suppressor of cytokine signalling 3 is an important

player as it inhibits STAT3 signalling via a negative feedback loop during IL6 signal transduction, and thus helps to mediate the end of hepatocyte compensatory proliferation (Campbell *et al.* 2001; Fausto *et al.* 2006).

On the other hand, activation of the LPC compartment is associated with chronic liver injuries such as hepatitis B virus (HBV) and HCV infections, alcoholic liver disease (ALD), non-alcoholic fatty liver disease (NAFLD) and haemochromatosis. It was shown that inflammatory cytokines and growth factors play a key role in the LPC response (Knight *et al.* 2005b; Bird *et al.* 2008; Riehle *et al.* 2011). Several *in vitro* and *in vivo* studies have reported the relevance of numerous signalling molecules including TNF superfamily members such as TNF (Knight *et al.* 2000), lymphotoxin (LT) α (Knight and Yeoh 2005c), LTβ (Akhurst *et al.* 2005) and TNF-like weak inducer of apoptosis (TWEAK) (Tirnitz-Parker *et al.* 2010), as well as interferon γ (IFNγ) (Akhurst *et al.* 2005), TGFβ (Nguyen *et al.* 2007), HGF (Ishikawa *et al.* 2012) and fibroblast growth factor (FGF) (Kaneko *et al.* 2015). Within this complex signalling network, the mitogens TWEAK and FGF, in particular, represent molecules which are active in the primary induction phase of LPCs since their expression was sufficient to induce a LPC response in uninjured livers (Jakubowski *et al.* 2005; Takase *et al.* 2013). Besides its proliferative effect on LPCs, HGF signalling through its receptor c-Met is also involved in LPC migration and parenchymal invasion (Suarez-Causado *et al.* 2015). Further details on the biology of LPCs are discussed in the following paragraphs.

During the process of regeneration, hepatocytes and LPCs do not act in a mutually exclusive manner and have been reported to function simultaneously (Dabeva and Shafritz 1993; Thorgeirsson 1996; Ochoa *et al.* 2010), which is consistent with the fact that several factors act as growth factors for both cell types. A human study by Katoonizadeh *et al.* showed that LPC activation occurs in response to PH when at least 50% of hepatocytes are lost and the remaining hepatocytes show decreased proliferation activity (Katoonizadeh *et al.* 2006). However, dependent on the severity of the injury and the degree of hepatocyte inhibition, the liver favours one of the two pathways. Even though several signalling molecules have an impact on both hepatocytes and LPCs, opposing effects may result from different responses to specific cytokines, mediated by divergent downstream pathways. Candidates which promote opposing effects and thus potentially mediate the switch from hepatocyte-

towards LPC-mediated regeneration, include TGFβ and IFNγ. TGFβ signalling is induced in chronic liver disease (CLD) (Dooley and ten Dijke 2012) and is capable of inhibiting proliferation in both cell types (Moustakas and Kardassis 1998; Thenappan *et al.* 2010). However lower inhibitory activity in LPCs was demonstrated to be potentially due to the expression of the TGFβ inhibitor Sma- and Mad-related protein 6 (Nguyen *et al.* 2007). Moreover in hepatocytes, TGFβ signalling was linked to dedifferentiation and the treatment of LPCs *in vitro* resulted in tumour-initiating potential (Wu *et al.* 2012a), which further highlights different responses in the two cell types. Similar results were obtained when investigating the role of IFNγ signalling, which is involved in promoting the LPC response during chronic injury (Knight *et al.* 2007b). *In vitro* studies showed an inhibitory effect of IFNγ signalling on TNF-stimulated hepatocyte proliferation mediated by nitric oxide (NO) formation, whereas LPC proliferation was not affected due to a lack in NO production (Brooling *et al.* 2005). Furthermore, data generated with the LPC line PIL-2 even suggest a pro-proliferative effect of IFNγ via STAT3 signalling activation (Akhurst *et al.* 2005).

1.3 Liver progenitor cell-mediated regeneration

1.3.1 Discovery and characteristics of liver progenitor cells

In contrast to the haematopoietic system, the somatic stem cells in the liver have not been isolated or even identified yet (Reya *et al.* 2001; Spangrude *et al.* 1988) and thus only a potential progenitor cell population has been extensively studied up-to-date. In rodents, LPCs were originally identified by Kinosita in rats treated with the azo dye and former food additive "Butter Yellow" (Kinosita 1937) and later introduced by Farber as "ovoid cells", describing their cytologic appearance following treatment with carcinogenic agents (Farber 1956). Since then a variety of different terminologies have been used to describe this extremely heterogeneous cell population, including hepatic stem-like/progenitor cells, oval cells (mainly used in rodent models) or transit-amplifying ductular cells. In addition, they are described as a component of so-called ductular reactions (DRs) (mainly used in human pathologies, detailed further below). They are defined as small cells (7-10 μm in

diameter) featuring a high nuclear-to-cytoplasmic ratio, a small ovoid nucleus, a basophilic character, and variably express both biliary and hepatocytic as well as haematopoietic markers (see Table 1.1 and Table 1.2). Common markers used in the literature to identify LPCs are cytokeratin (CK) 7, CK19, CD24, CD133, epithelial cell adhesion molecule (EpCAM), oval cell marker (MIC1-1C3), and SRY (sex determining region Y)-related HMG (high mobility group) box 9 (Sox9) (Dorrell *et al.* 2008; Dorrell *et al.* 2011; Okabe *et al.* 2009; Qiu *et al.* 2011; Sackett *et al.* 2009; Schievenbusch *et al.* 2012; Shin *et al.* 2011; Suzuki *et al.* 2008; Lu *et al.* 2015; Kim *et al.* 2014). These markers do not differentiate between cholangiocytes and LPCs, however a study by Okabe *et al.* proposed tumour-associated calcium signal transducer 2 (Trop2) to be a marker that distinguishes between activated proliferative LPCs and cholangiocytes as well as potential dormant LPCs during liver injury response. Trop2 expression was detected in EpCAM-positive LPCs following a 3,5-diethoxycarbonyl-1,4-dihydro-collidine (DDC) diet but not in normal mouse livers (Okabe *et al.* 2009) indicating its potential value as a specific LPC marker. However, its exclusive expression profile has not been confirmed in other experimental models.

1.3.2 Origin of liver progenitor cells

The origin of LPCs remains highly controversial. The multi-lineage phenotype of LPCs provoked the debate of their cellular origin and many theories were proposed. Some studies were based on marker co-expression and the fact that LPCs express common cell surface markers, which they share with haematopoietic stem cells, such as CD34, c-Kit, stem cell antigen-1 (Sca-1) and Thy-1 (CD90), suggesting that they might originate from the bone marrow (Petersen *et al.* 1998; Petersen *et al.* 1999; Petersen *et al.* 2003).

Mouse and Rat					
Marker	**LPC**	**Hepatocyte**	**Cholangiocyte**	**Model**	**Reference**
A6	+	-	+	AAF/PH, DDC, CDE. DDB1 deletion	(Petersen *et al.* 2003; Ueberham *et al.* 2007; Tirnitz-Parker *et al.* 2007; Tonkin *et al.* 2008; Endo *et al.* 2012; Schievenbusch *et al.* 2012)
AFP	+	fetal	-	AAF/PH, DEN, CDE	(Sell 1978; Evarts *et al.* 1987; Smith *et al.* 1996; Jelnes *et al.* 2007)
Alb	+	+	-	CDE, AAF	(Sell 1978; Tian *et al.* 1997)
CD13	+	-	?		(Kamiya *et al.* 2009)
CD24	+	-	+	AAF/PH, DDC	(Yovchev *et al.* 2007; Qiu *et al.* 2011; Schievenbusch *et al.* 2012)
CD34	+	-	+	AAF/PH, DDC	(Omori *et al.* 1997; Petersen *et al.* 2003)
CD44	low	-	?	AAF/PH	(Ueberham *et al.* 2007)
	+ (intermediate state)		-	D-gal	(Kon *et al.* 2006)Kon 2006
CD133	+	-	+	AAF/PH, DDC	(Rountree *et al.* 2007; Suzuki *et al.* 2008; Kamiya *et al.* 2009)
CK7	+	-	+	AAF/PH	(Sarraf *et al.* 1994; Paku *et al.* 2005; Clouston *et al.* 2005)
CK8	+	+	(+)	AAF/PH	(Sarraf *et al.* 1994; Sasaki *et al.* 2008)
CK18	+	low	(+)	AAF/PH	(Sarraf *et al.* 1994; Golding *et al.* 1995)
CK19	+	-	+	AAF/CCl_4, AAF/PH, DDC, CDE	(Sarraf *et al.* 1994; Petersen *et al.* 1998; Paku *et al.* 2005; Okabe *et al.* 2009)
c-Kit	+	-	+	AAF/PH, CDE, D-gal	(Fujio *et al.* 1994; Fujio *et al.* 1996; Knight *et al.* 2008)
c-Met	+	-	+	AAF/PH	(Hu *et al.* 1993)
Cx43	+	-	+	AAF/PH	(Zhang and Thorgeirsson 1994; Paku *et al.* 2004; Yovchev *et al.* 2007)
Dlk	+	fetal	-	AAF/PH, CDE, retrorsine	(Jensen *et al.* 2004; Jelnes *et al.* 2007)
E-cadherin	+/high	-/low	+/high	CDE	(Ueberham *et al.* 2007; Tirnitz-Parker *et al.* 2007; Van Hul *et al.* 2009)
EpCAM	+	-	+	AAF/PH, DDB1 deletion, DDC, D-gal	(Yovchev *et al.* 2007; Okabe *et al.* 2009; Endo *et al.* 2012; Schievenbusch *et al.* 2012)
Foxl1	+	-	+	DDC, CDE, BDL	(Sackett *et al.* 2009; Shin *et al.* 2011)
GGT	+	-	+	AAF/CCl_4, AAF/PH, D-gal	(Petersen *et al.* 1998; Holic *et al.* 2000)
Integrin αvβ6	+	-	+	MDR2 deletion	(Peng *et al.* 2015)
Lgr5	+	-	-	CCl_4	(Huch *et al.* 2013)
MIC1-1C3	+	-	+	DDC	(Dorrell *et al.* 2008; Dorrell *et al.* 2011)

Table 1.1: Adult LPC marker expression in different cell lineages in liver injury-induced and non-injured settings. To be continued on following page.

Mouse and Rat					
Marker	**LPC**	**Hepatocyte**	**Cholangiocyte**	**Model**	**Reference**
M_2PK	+	fetal	+	AAF/PH, CDE	(Tee *et al.* 1994; Smith *et al.* 1996; Jelnes *et al.* 2007; Tirnitz-Parker *et al.* 2007)
Nope	+	-	low	DDC	(Schievenbusch *et al.* 2012)
OC.2	+	-	+	AAF, AAF/CCl_4, AAF/PH, CDE	(Hixson and Allison 1985; Petersen *et al.* 1998)
OPN	+	-	+	DDC, CDE, CCl_4	(Carpentier *et al.* 2011; Espanol-Suner *et al.* 2012)
Sox9	+	-	+	DDC, CDE	(Carpentier *et al.* 2011; Furuyama *et al.* 2011)
OV-6	+	-	+	AAF, AAF/CCl_4, AAF/PH, CDE,	(Yang *et al.* 1993; Petersen *et al.* 1998; Paku *et al.* 2004)
π-GST	+	fetal	-	CDE	(Tee *et al.* 1994; Smith *et al.* 1996; Lowes *et al.* 1999; Oliva *et al.* 2010)
Sca-1	+	-	-	DDC	(Petersen *et al.* 2003)
Thy1.1/CD90	+	-	-	AAF/CCl_4, AAF/PH, DDC	(Petersen *et al.* 1998; Petersen *et al.* 2003)
Trop2	+	-	-	DDC, CDE	(Okabe *et al.* 2009; Carpentier *et al.* 2011)
Progenitor cell compartments in non-injured livers					
$CD49f^+CD13^+CD133^+$					(Kamiya *et al.* 2009)
$MIC1\text{-}1C3^+CD133^+$					(Dorrell *et al.* 2011)
EpCAM					(Okabe *et al.* 2009)

Table 1.1: Adult LPC marker expression in different cell lineages in liver injury-induced and non-injured settings. +, positive; -, negative; (+), occasionally expressed; "low" denotes weakly expressed; "high" denotes highly expressed; AAF, 2-acetylaminofluorene; PH, partial hepatectomy; CDE, choline deficiency and ethionine supplementation; DDC, 3,5-diethoxycarbonyl-1,4-dihydrocollidine; DDB1, damaged DNA binding protein 1; D-gal, D-galactosamine; DEN, diethylnitrosamine; MDR2, multidrug resistance protein 2.

Human					
Marker	**LPC**	**Hepatocyte**	**Cholangiocyte**	**Disease**	**Reference**
AFP	+	-	-	Acetaminophen-induced necrosis, acute necrotising hepatitis	(Theise *et al.* 1999; Spee *et al.* 2010)
CD90	+	-	-	HCV	(Villano *et al.* 2014; Li *et al.* 2014)
CD109	+	low	low		(Li *et al.* 2014)
CD133	+	-	(+)	Acute necrotising hepatitis, HBV, HCV, primary biliary cirrhosis	(Porretti *et al.* 2010; Spee *et al.* 2010)
CK7	+	-	+	Alcoholic hepatitis, acute necrotising hepatitis, HCV, pNAFLD, primary biliary cirrhosis	(Spee *et al.* 2010; Nobili *et al.* 2012; Sancho-Bru *et al.* 2012; Villano *et al.* 2014)
CK8	+	low	(-)		(Li *et al.* 2014)
CK18	+	low	(-)		(Li *et al.* 2014)
CK19	+	-	+	Acetaminophen-induced necrosis, ALD, genetic hemochromatosis, HBV, HCV	(Lowes *et al.* 1999; Theise *et al.* 1999; Li *et al.* 2014; Villano *et al.* 2014)
c-Kit	+	-	+/-	Acetaminophen-induced necrosis, acute liver failure, extrahepatic biliary atresia (Cirrhosis)	(Baumann *et al.* 1999; Theise *et al.* 1999; Li *et al.* 2014)
EpCAM	+	-	+	Alcoholic hepatitis, HBV, HCV	(Porretti *et al.* 2010; Sancho-Bru *et al.* 2012; Villano *et al.* 2014)
Jagged 1	+	-	(+)	Acute necrotising hepatitis, HCV, primary Biliary cirrhosis	(Spee *et al.* 2010)
M_2PK	+	(-)	-	Genetic hemochromatosis, ALD, HCV	(Lowes *et al.* 1999)
NCAM	+	-	(-)	Acute necrotising hepatitis, HBV, HCV, primary biliary cirrhosis	(Porretti *et al.* 2010; Spee *et al.* 2010)
Oval-6	+	-	-		(Li *et al.* 2014)

Table 1.2: Adult human LPC marker expression in different cell lineages in liver injury and non-injured settings. +, positive; -, negative; (+), occasionally expressed; "low" denotes weakly expressed; ALD, alcoholic liver disease; BDL, bile duct ligation; pNAFLD, paediatric non-alcoholic fatty liver disease; HBV, hepatitis B virus infection; HCV, hepatitis C virus infection.

However, it was later shown in a cell transplantation model that bone marrow-derived hepatocytes were a result of cell fusion rather than transdifferentiation (Wang *et al.* 2003). Another study identified a LPC population that expresses several mesenchymal markers such as vimentin, mesothelin, bone morphogenic protein and TWEAK receptor (fibroblast growth factor-inducible 14, Fn14) (Yovchev *et al.* 2008) indicating a mixed epithelial/mesenchymal phenotype.

Since their proliferation is always first seen in periportal hepatic regions, the general view has been that they are the progeny of a yet to be identified liver-resident stem cell, residing in the Canals of Hering (Lenzi *et al.* 1992). More evidence for their role as progenitor cell origin was provided by three-dimensional reconstructions in healthy adult tissue and following massive hepatic necrosis secondary to acetaminophen toxicity, where it was demonstrated that LPC proliferation was topographically identified in the Canals of Hering structures (Theise *et al.* 1999). Label retention assays on the basis of bromodeoxyuridine incorporation equally identified the Canals of Hering and in addition intraductal cholangiocytes, periductal "null cells" (lacking expression of hepatobiliary markers) and the first hepatocytes of the hepatic acinus as potential functional stem cell niche locations, and thus suggested a flexible regeneration system with more than one stem cell niche (Kuwahara *et al.* 2008). Additionally, a cell lineage tracing study, following Sox9 expression, demonstrated that embryonic ductal plate cells give rise to adult LPCs and represent at least one of the precursor cell types (Furuyama *et al.* 2011; Carpentier *et al.* 2011).

A recent study using a hepatocyte-chimeric lineage tracing system followed by extensive RNA-sequencing and ultrastructural analysis suggested that mature, fully differentiated hepatocytes can contribute to the LPC pool by undergoing reversible metaplasia to a biliary-like progenitor state during 3,5-diethoxycarbonyl-1-4-dihydrocollidine (DDC)-induced liver injury (Tarlow *et al.* 2014b). Kordes and colleagues demonstrated through HSC transplantation experiments in two chronic liver injury models that HSCs were able to contribute to the regeneration process by transdifferentiation into hepatocytes and cholangiocytes and may therefore represent another candidate cell contributing to the LPC population under certain experimental conditions (Kordes *et al.* 2014). Another lineage tracing study that followed the fate and regenerative capacity of hepatocyte nuclear factor 1 β-positive biliary cells

demonstrated that this population did not contribute to the generation of new hepatocytes in healthy liver or after acute injury. However these cells can differentiate into hepatocytes in certain chronic injury regimes, such as shown using the choline-deficient, ethionine-supplemented (CDE) dietary mouse model (Rodrigo-Torres *et al.* 2014), via an intermediate LPC phenotype.

Taken together, these data suggest that the adult liver may retain a certain level of plasticity and the ability to recruit multiple distinct cellular sources for LPC generation (Fig. 1.1). The term "LPC" could lead to the false assumption of a potential stem cell origin, which has not been established yet. In this thesis, the term LPC will be used without evaluating the source of this cell population induced during CLD.

1.3.3 Function of liver progenitor cells during chronic liver injury

LPCs, defined by their immature stem cell-like marker expression profile, have been shown to differentiate bipotentially into biliary cells and hepatocytes (Forster *et al.* 2011; Sackett *et al.* 2009; Shin *et al.* 2011; Suzuki *et al.* 2008; Tirnitz-Parker *et al.* 2007) and in some models have demonstrated multipotentiality by differentiation into pancreatic and intestinal lineages (Leite *et al.* 2007; Tatematsu *et al.* 1985; Yang *et al.* 2002).

However, the actual regenerative capacity of LPCs has been highly debated. A recent genetic lineage tracing study used yellow fluorescent protein-osteopontin (OPN)-marked cholangiocytes and LPCs to study their role during (i) PH, (ii) carbon tetrachloride (CCl_4)-induced acute injury, or (iii) chronic injury following administration of either a CDE or DDC diet (Espanol-Suner *et al.* 2012). This study revealed that OPN-expressing LPCs only contributed significantly to hepatocellular regeneration in the CDE model of chronic liver injury, highlighting injury context specificity. Further evidence that LPCs might play an important role during liver mass reconstitution comes from experiments using a reporter mouse for the LPC marker forkhead helix-box L1 (Foxl1), establishing that $Foxl1^{+}$ LPCs and their descendants are critically required for hepatocyte generation during recovery from CDE-induced injury (Shin *et al.* 2015).

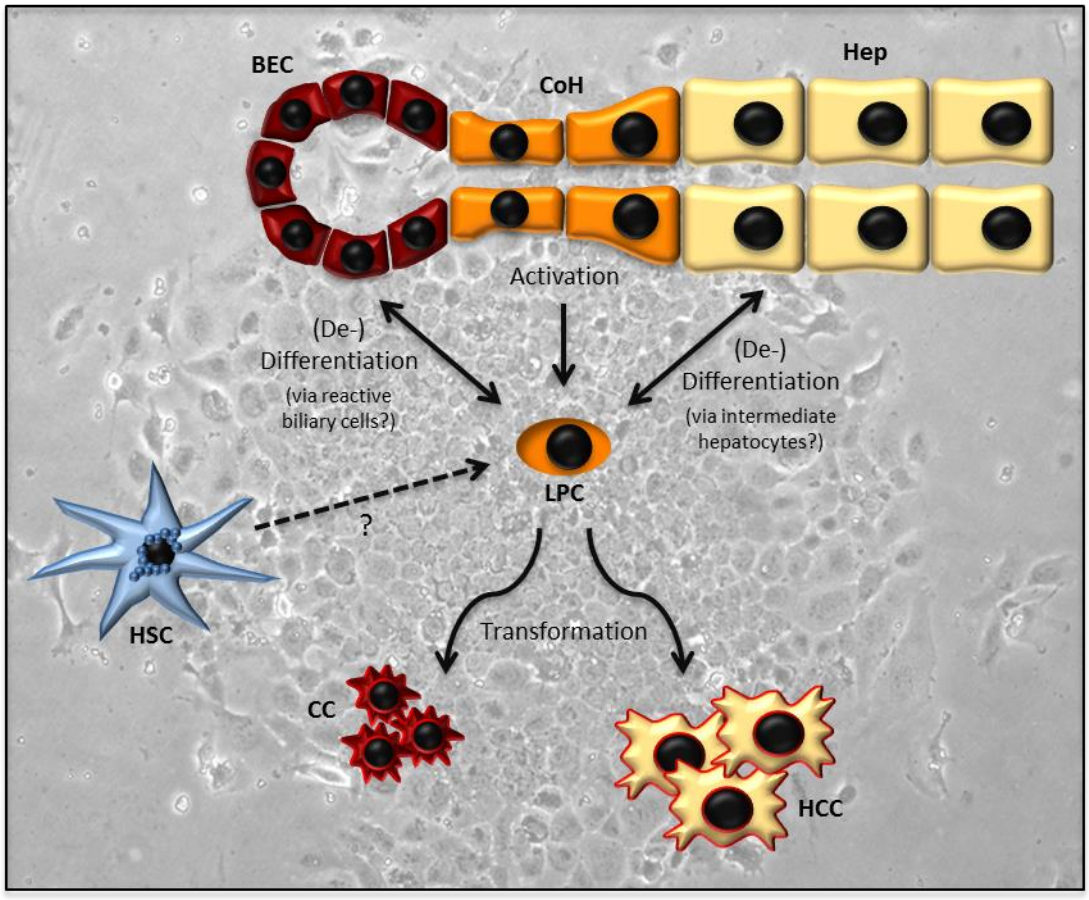

Fig. 1.1: The potential origins and differentiation capabilities of liver progenitor cells. LPCs have been suggested to originate from dormant precursors in the Canals of Hering (CoH), the dedifferentiation of biliary epithelial cells (BEC) or hepatocytes (Hep) or the metaplastic contribution of hepatic stellate cells (HSC). Upon appropriate stimulation, they can differentiate into cholangiocytes and hepatocytes, possibly via transitional phenotypes (reactive biliary cells and intermediate hepatocytes, respectively), and have been suggested as precursor cells for cholangiocarcinoma (CC) and hepatocellular carcinoma (HCC). The background photomicrograph depicts a primary cell culture of LPCs isolated from a chronically injured, CDE-treated mouse liver.

Additionally Huch and colleagues demonstrated that single cells positive for leucine-rich repeat-containing G protein-coupled receptor 5 (Lgr5) can be expanded as epithelial three-dimensional organoids *in vitro*, and can be differentiated towards hepatocytes *in vitro* and form new hepatocytes upon transplantation into CCl_4-retrorsine-treated mice (Huch *et al.* 2015).

Tarlow *et al.* reported conflicting results by showing that LPCs labelled via expression of Sox9 only rarely (<1%) produced new hepatocytes in the CDE model (Tarlow *et al.* 2014a). However, it should be noted that this study used supplementation with only 0.1% ethionine in the drinking water, as opposed to the more common concentration of 0.15% also used by Shin and colleagues (Shin *et al.* 2015), highlighting the fact that observed disparities might be the result of differences in the severity of induced liver injury.

A very recent study defined a population of highly expandable, clonogenic cells negatively sorted for haematopoietic (CD45), endothelial (CD31) and erythroid (Ter119) markers and with the expression profile epithelial cell adhesion molecule $(EpCAM)^+CD24^+CD133^+$, as capable of efficiently repopulating the liver bipotentially. This was observed following repeated rounds of induced hepatocyte senescence in mice lacking functional E3 ubiquitin-protein ligase Mdm2 in hepatocytes (Lu *et al.* 2015). The discrepancies and contradicting results between studies probably stem from a lack of uniformity with regards to the animal model used, the degree of evoked liver injury and differences in the underlying injury and repair mechanisms. However, overall it shows a high degree of plasticity in the liver and LPC-mediated regeneration (see Fig. 1.1).

1.3.4 Isolation strategies for liver progenitor cells

Primary cell culture is of considerable value for LPC research as these cells most closely mimic their *in vivo* status whilst facilitating the study and direct manipulation of cell proliferation, lineage commitment and differentiation. Since LPCs are hardly detectable in healthy liver, most isolation procedures involve an induction protocol, followed by a series of standard isolation steps including tissue perfusion, digestion

and fluorescence-activated cell sorting (FACS) or cell centrifugation and fractionation for further purification.

To establish a mixed culture containing a variety of heterogeneous LPC phenotypes, centrifugal elutriation based on cell size and density (Yaswen *et al.* 1984) can be used to separate LPC populations from other liver cell fractions, followed by growth in LPC-promoting culture conditions (Tirnitz-Parker *et al.* 2007). The generation of clonogenic cell lines for single cell tracing is required to thoroughly characterise these different populations. However, the resultant LPC subpopulation as well as cell quantity, viability and features of LPCs maintained in culture, very much depends on the method of isolation, the surface coating of the culture dish and the combination and concentration of growth factors in the culture medium. These factors vary considerably amongst laboratories, making it difficult to interpret *in vitro* results obtained by different groups, and it is clear that reliable, standardised protocols are urgently required.

Importantly, the term LPC primarily describes a cell's bi-lineage marker expression and ability to differentiate into cholangiocytes and hepatocytes *in vitro* or *in vivo* and does not describe a specific cell origin, cell ontogenesis or predefined lineage fate. In addition, LPCs may continuously change their phenotype, according to their transient proliferation and differentiation status. Consequently the LPC compartment is composed of heterogeneous cell populations including immature, intermediate and more mature or differentiated phenotypes and, so far, no marker is available that is specific for LPCs and able to discriminate between LPCs and other cell types sharing certain markers, such as cholangiocytes, hepatocytes and haematopoietic stem cells (see Table 1.1 for published LPC expression profiles). Thus, a combination of different markers is necessary to identify and isolate specific LPCs using FACS.

1.3.5 Animal models to study liver progenitor cells

Rodent models are commonly used to study CLD and associated processes as rats and mice generally display high levels of genetic similarity to humans, while the ever increasing availability of genetically manipulated mice makes them powerful tools for the mechanistic evaluation of disease development and progression. They are

easy to handle due to their size, easy to breed in captivity and have a relatively short gestational period and life span, allowing cost effective analyses. Nevertheless, no model can be a complete replica of the corresponding human liver disease due to differences in the immune system and metabolic rates during tissue homeostasis as well as the metabolic response to injury stimuli (Liu *et al.* 2013b). Importantly, remarkable heterogeneity with respect to phenotypic disparity has been displayed by LPCs in different models, warranting careful selection and interpretation. Most of the models described below were initially developed to follow hepatocellular carcinoma development and only later adapted to study induction and subsequent biology of LPCs.

1.3.5.1 The D-galactosamine model

The non-carcinogenic agent D-galactosamine has been routinely used to induce LPCs in rats. It is metabolised by centrilobular hepatocytes, where it blocks RNA synthesis, leading to an inhibition of protein synthesis by trapping uridine-nucleotides and uridine diphosphate glucose, and subsequently to the development of necrosis (Farber and El-Mofty 1975). Activation of LPC-like non-parenchymal cells occurs in the periportal area due to impaired hepatocyte proliferation within 48 h of administration of a single dose of D-galactosamine (70 mg/100 g body weight), followed by expansion into the parenchyma forming a network of cells expressing γ-glutamyl transpeptidase (Dabeva *et al.* 1993). D-galactosamine was shown to induce the proliferation of LPCs and small hepatocytes (only up to 16 µm in diameter) that are positive for the fetal form of α-fetoprotein (AFP), which importantly does not seem to be induced in mouse models featuring LPC proliferation (Lemire *et al.* 1991).

1.3.5.2 The Solt-Farber Model and the 2-AAF/PH regimen

This model, which is commonly used in rats and only rarely in mice, is composed of three stages of disease/LPC induction - (i) injection of the ethylating hepatocarcinogen diethylnitrosamine (DEN), which acts as disease initiator, (ii) administration of 0.02% 2-acetylaminofluorene (2-AAF) two weeks later and (iii)

PH, as a growth stimulus, one week into 2-AAF feeding (Solt and Farber 1976). This regimen is frequently modified by omission of the DEN initiation step and 2-AAF is administered four days prior and after PH. Both models induce proliferation of ductular or periductular LPCs, which accelerates when 2-AAF feeding is terminated, indicating that not only hepatocytes but also LPCs are growth-inhibited by 2-AAF, although to a lesser extent. LPCs tend to differentiate more efficiently into hepatocytes at low 2-AAF doses, whereas they undergo apoptosis at higher dosages (Alison *et al.* 1997). As a consequence, the rate of hepatocytic LPC differentiation can be controlled through variation of the 2-AAF dose (Paku *et al.* 2004).

1.3.5.3 The DDC diet model

DDC is a potent xenobiotic hepatotoxin that stimulates robust biliary and LPC proliferation, while inducing mitochondrial stress, hepatocyte ballooning, apoptosis, the formation of cytoplasmic aggregates termed Mallory-Denk bodies that resemble hepatocyte inclusion bodies observed in human alcoholic and non-alcoholic steatohepatitis (NASH), and hepatomegaly (Preisegger *et al.* 1999; Zatloukal *et al.* 2007). Feeding of 0.1% DD

C in chow leads to a DR involving $CK19^{+}$ cells and significantly increased biliary secretion within the first week, which is followed by segmental bile duct obstructions through deposition of porphyrin pigment plugs in the lumina of small bile ducts - a distinct histological feature of this cholestatic liver injury model (see Fig. 1.4.5). At later disease stages, activated periductal myofibroblasts cause progressive biliary liver fibrosis with portal-portal septa, resembling human sclerosing cholangitis (Fickert *et al.* 2007). Interestingly, this model only results in activation of LPC proliferation in mice and not in rats (Jelnes *et al.* 2007) and the liver phenotype, in particular the extent of hepatomegaly and pigment deposition induced by DDC feeding, largely depends on the genetic background of the mouse strain used in the model (Hanada *et al.* 2008).

1.3.5.4 The CDE diet model

Dietary deficiency of the lipotrope choline combined with 0.05 or 0.1% of the methionine-agonist and hepatocarcinogen ethionine was initially developed as a

chronic liver injury model in rats, where it produces alterations in phospholipid metabolism, fatty liver and substantial numbers of proliferating AFP^+ LPCs by three weeks (Shinozuka *et al.* 1978). Due to its high murine morbidity and mortality, an alternative protocol was later developed for use in mice that involved feeding of a choline-deficient diet with separate administration of 0.15% of ethionine dissolved in the drinking water (Akhurst *et al.* 2001). The CDE diet reliably induces steatosis, an inflammatory response, proliferation of hepatocytic and biliary LPCs (see Fig. 1.4.5), portal fibrosis and eventually, hepatocellular carcinoma after 10-12 months (Knight *et al.* 2008; Tirnitz-Parker *et al.* 2007).

1.3.5.5 The thioacetamide (TAA) supplementation model

Prolonged administration of TAA, either via intraperitoneal injection at concentrations of 150-200 mg/kg body weight three times a week, or given orally in the drinking water at 200-300 mg/L, is a well-established rodent model of hepatotoxicity and cirrhosis akin to human cirrhosis (Liedtke *et al.* 2013). TAA is a thiono-sulfur-containing compound that is converted by microsomal flavin-adenine dinucleotide-containing monooxygenase as well as the P450 cytochrome enzyme CYP2E1 through reduction of dioxygen to superoxide anion and subsequent catalysis to hydrogen peroxide, which is responsible for the observed oxidative stress-induced liver injury, lipid peroxidation and centrilobular necrosis (Low *et al.* 2004). TAA administration has been used to induce chronic inflammation, LPC proliferation (see Fig. 1.4.5), fibrosis, cirrhosis, cholangiocarcinoma (CC) as well as hepatocellular carcinoma (HCC) (Boulter *et al.* 2015; Sakurai *et al.* 2013).

1.4 Liver progenitor cells in human chronic liver disease

Most human CLDs are associated with the proliferation of LPCs, either as single cells or strings of cells or as part of DRs. The latter are seen in many acute and CLDs and are commonly composed of a diversity of cellular components, including activated or reactive biliary epithelial cells and LPCs - providing the ductular component of the name - as well as mesenchymal, endothelial, neural, haematopoietic and inflammatory cells. These cellular changes go hand-in-hand with ECM modifications and depositions and there is an enormous range of patterns seen

clinically. The time of appearance after injury induction, the morphology and the relative proportion of DR (cellular) components depend on the aetiology, severity of underlying stimuli and the respective disease progression state (for reviews see (Gouw *et al.* 2011; Williams *et al.* 2014)). A study by Lunz and colleagues in a mouse model of decompensated biliary cirrhosis demonstrated that DRs and LPC proliferation are induced when mitochondria-rich hepatocytes are targeted by oxidative stress and undergo replicative arrest through upregulation of the cyclin-dependent kinase inhibitor p21 (Lunz *et al.* 2005). Oxidative stress plays a major role during ALD and NAFLD, which alongside chronic hepatitis represent the most prevalent risk factors for the development of hepatocellular carcinoma in the Western World. All of these conditions feature DRs and LPC proliferation and the magnitude of this response directly correlates with the progression of fibrosis and the severity of the underlying disease (Clouston *et al.* 2005; Lowes *et al.* 1999; Roskams *et al.* 2003b). In addition, continuous iron loading of hepatocytes leading to impaired hepatocyte replication in hereditary haemochromatosis has been linked to LPC proliferation and the DR, with both the presence of the DR and portal inflammation strongly associated with hepatic fibrosis progression (Lowes *et al.* 1999; Tirnitz-Parker *et al.* 2013; Wood *et al.* 2014). A recent retrospective cohort study on HCV-infected patients demonstrated that inflammatory, fibrogenic and LPC-associated responses are intricately linked and co-regulated during disease progression as well as during HCV recurrence after orthotopic liver transplantation (Prakoso *et al.* 2014).

1.5 Liver progenitor cells and the extracellular matrix

The ECM represents an important component of the LPC niche. This structural network contains different types of collagens, proteoglycans and glycoproteins such as laminin and plays an essential role in the regulation of LPC proliferation, migration and differentiation (Katoonizadeh and Poustchi 2014). In healthy livers and chronic liver injury models, ductular structures and LPCs are surrounded by the ECM component laminin which promotes LPC and biliary gene expression and thus supports a progenitor phenotype, whereas hepatocyte-specific gene expression is inhibited (Lorenzini *et al.* 2010). With the use of a AAF/PH-induced hepatic injury model, Paku and colleagues demonstrated in rats that LPC-mediated regeneration and hepatic differentiation is associated with downregulation of laminin-receptor

integrin α6 and subsequent loss of contact with this basement membrane component (Paku *et al.* 2004). Furthermore, *in vitro* studies have shown that collagen I and IV, and fibronectin on the other hand had no impact on LPC and biliary gene expression, however fibronectin drove gene expression of factors regulating the early hepatocyte lineage such as CCAAT/enhancer-binding protein α (C/EBP-α) (Lorenzini *et al.* 2010). Thus, the composition of the surrounding ECM and its interactions with LPCs play an important role during CLD regeneration by regulating the LPC fate.

1.6 Liver progenitor cells and hepatic fibrosis

Matrix remodelling is a key mechanism during wound healing and tissue regeneration in CLD. However, an uncontrolled and inappropriate process can lead to complications such cirrhosis and HCC. Remodelling of the ECM in response to tissue injury is mediated by activated HSCs and portal fibroblasts, which transdifferentiate into collagen-producing myofibroblasts. The transformation from a quiescent state to an activated profibrogenic myofibroblast is mediated by growth factors and cytokines produced by other resident and infiltrating cells in response to tissue injury (Bataller and Brenner 2005; Ramm 2009). A variety of studies have proposed that HSCs are influenced by their hepatic paracrine environment (Dwyer *et al.* 2014; Tirnitz-Parker *et al.* 2014; Williams *et al.* 2014), mediated by the local production of soluble mediators as well as by direct cell-cell contact with LPCs, inflammatory cells and other parenchymal cells (Ramm *et al.* 2009; Ruddell *et al.* 2009; Tirnitz-Parker *et al.* 2010).

As mentioned earlier, the LPC phenotype and their expansion is closely related to ECM remodelling. Parenchymal infiltration of LPCs occurs in close temporal and spatial association with activated HSCs, which support the cell migration process by matrix degradation and the maintenance of the liver architecture by forming a collagen-scaffold structure (Tirnitz-Parker *et al.* 2012). Several studies demonstrated a co-dependent relationship between the two cell populations. The lack of T helper type 1 immune signalling in mice caused a significantly reduced LPC response as well as a decrease in fibrosis when exposed to a CDE diet (Knight *et al.* 2007a). On the other hand, mice receiving IFNγ administration in combination with CDE treatment showed an increased LPC response and a simultaneous acceleration of

HSC activation and fibrogenesis (Knight *et al.* 2007b). Moreover, Patsenker and colleagues demonstrated that integrin αvβ6 is induced in $CK19^+$ proliferating bile duct epithelial cells (and possibly LPCs) in bile duct-ligated rats and that its inhibition significantly impedes fibrosis progression (Patsenker *et al.* 2008).

It has been proposed that communication between HSCs and LPCs may be mediated via direct cell-cell contact (Ruddell *et al.* 2009; Tirnitz-Parker *et al.* 2014). One potential coordinating pathway that may control fibrogenesis is LTβ signalling. This pathway is upregulated in CLD caused by CDE treatment and bile duct ligation in rodents (Akhurst *et al.* 2005; Knight *et al.* 2005a; Lee *et al.* 2005), and in HCV patients (Lowes *et al.* 2003), showing correlating LTβ mRNA and fibrosis levels. Mice lacking LTβ receptor (LTβR) showed reduced LPC and activated HSC numbers, as well as decreased hepatic fibrosis in response to CDE treatment (Akhurst *et al.* 2005; Ruddell *et al.* 2009). More evidence for the potential cross-talk between $LT\beta^+$ LPCs and $LT\beta R^+$ HSCs was provided by Ruddell and colleages (Ruddell *et al.* 2009). Their study demonstrated a LTβ-induced expression of chemotaxis-associated factors in HSCs (intercellular adhesion molecule 1 (ICAM-1) and regulated upon activation, normal T cell expressed and secreted (RANTES)), suggesting that paracrine LTβ/LTβR signalling plays a role in recruiting LPCs, HSCs and leukocytes, which are essential cellular players during liver regeneration.

Even though there is a strong correlation between LPC-mediated regeneration, HSC activation and fibrosis, as well as a potential direct interaction between the two cell populations during fibrogenesis, the question of the successive order of activation still remains. In CDE-fed mice, it was demonstrated that HSC activation and ECM deposition represent initial steps before parenchymal infiltration of LPCs, as these events happen in the early injury phase prior to an evident LPC response (Van Hul *et al.* 2009). Hence, this study suggests that HSCs may be activated first and then regulate the LPC response by establishing the required niche. However, another accepted theory is that LPC expansion and the DR are contemporaneous key drivers of periportal fibrosis (Clouston *et al.* 2005). These opposing patterns are not mutually exclusive and the order of events may depend on the injury cause, the hepatic target area and the induced signalling pathways. Williams *et al.* suggested that both the cellular heterogeneity and polarity of the DR allow for the promotion of

different responses with regards to LPC biology and collagen deposition (Williams *et al.* 2014).

One pathway which may influence both LPC proliferation and fibrogenesis is TWEAK/Fn14 signalling. A study in primary cell isolates from CDE-injured livers observed that LPCs and a subpopulation of activated HSCs express Fn14, the cognate receptor for TWEAK (Tirnitz-Parker *et al.* 2010). While it is well-established that TWEAK represents a mitogen for LPCs, the knowledge of its effects on HSC biology is still limited. Tirnitz-Parker *et al.* first demonstrated a potential link between TWEAK-regulated LPC and fibrogenic responses in Fn14-deficient mice subjected to a CDE diet, showing decreased LPC proliferation in addition to reduced tissue inhibitor of metalloproteinases (TIMP) 1 and 2 mRNA expression and alleviated collagen deposition (Tirnitz-Parker *et al.* 2010). More recently, Kuramitsu and colleagues performed a 70% PH prior to injecting recombinant TWEAK in mice, which resulted in increased numbers of $A6^{+}$ duct-like structures and LPCs, and simultaneously upregulated expression levels of fibrosis-enhancing mediators after five days. On the other hand, mice receiving a neutralising TWEAK antibody showed significant inhibition of the LPC response and associated fibrogenic factors (Kuramitsu *et al.* 2013). Taken together this further suggests a functional contribution of LPCs during hepatic wound healing by modulating the profibrogenic response. However, the underlying mechanism remains elusive. Indeed, fibrosis inhibition following TWEAK pathway manipulation could mean that either TWEAK acts directly on HSCs, or TWEAK-induced LPC expansion may indirectly control fibrogenesis via LPC/HSC cross-talk, i.e. via Notch or LTβ signalling (Tirnitz-Parker *et al.* 2014). Even though investigations on TWEAK signalling in other organs suggested a direct effect on the active state of myofibroblasts and collagen production, there is no evidence of similar effects in liver disease to date (Dohi and Burkly 2012; Novoyatleva *et al.* 2013).

1.7 Liver cancer and liver progenitor cells

1.7.1 Liver cancer and its risk factors

Liver cancer is one of the most common solid cancers worldwide and the global incidence, disease burden and mortality rate are steadily increasing. HCC embodies its major subtype (Jemal *et al.* 2011), accounting for up to 90% of all liver cancers, with major risk factors being represented by chronic HBV and HCV infection, continuous excessive alcohol consumption, NAFLD and other metabolic disorders (Llovet *et al.* 2015). A study by Paradis and colleagues established that in patients with metabolic syndrome as the only risk factor HCC may develop from malignant transformation of pre-existing liver cell adenomas in the absence of significant liver fibrosis and cirrhosis (Paradis *et al.* 2009). Due to the increasing prevalence of obesity and type 2 diabetes worldwide, which significantly predispose to the development of metabolic fatty liver disorders, NAFLD has been of particular concern. Currently, surgical resection, radio-frequency ablation, orthotopic liver transplantion, transcatheter arterial chemoembolisation (TACE) and administration of the small molecule tyrosine kinase inhibitor sorafenib are the treatments of choice for HCC (Llovet *et al.* 2015).

The second most common primary liver cancer, CC, accounts for 10-25% of primary hepatobiliary malignancies worldwide, with the greatest incidence being recorded in Southeast Asian regions, due to higher prevalence of risk factors such as parasitic infections with the hepatobiliary flukes *Opisthorchis viverrini* and *Clonorchis sinensis* as well as hepatolithiasis (gall stones). In the Western World, the most common CC risk factor is primary sclerosing cholangitis, with other less-established risk factors including inflammatory bowel disease, HBV and HCV infection, cirrhosis, chronic alcohol consumption, diabetes and obesity (Tyson and El-Serag 2011). While the global CC incidence has been rising rapidly, this malignancy remains untreatable due to its multifocal nature and chemoresistant profile, signifying a very poor prognosis and survival rate of only 5-10% at five years post-diagnosis (Shaib and El-Serag 2004).

Cancer in general is caused by sequential gene mutations leading to either sequence alterations or changes in the epigenetic signature of regulators including oncogenes and tumour suppressor genes (Hahn *et al.* 1999; Hahn and Weinberg 2002). The most affected genes play key roles in cell cycle control mechanisms, cell proliferation, self-renewal and differentiation. Both HCC and CC develop from focal precursor lesions, reflecting the multistep process of hepatic carcinogenesis (Libbrecht *et al.* 2005).

1.7.2 Tumour microenvironment and the role of cytokines in hepatocellular carcinoma

Alterations in the stromal cell composition and the stromal compounds play a key role in orchestrating tumour growth, invasion and metastasis in HCC. The cellular compounds of the microenvironment consist of carcinoma-associated fibroblasts, HSCs, tumour-associated macrophages (TAMs) and tumour-associated endothelial cells that are wrapped around pericytes (vascular smooth muscle cells). The stromal cell composition, the ECM (Yang *et al.* 2011), and the cellular cross-talk are changed in the tumour environment (Coulouarn *et al.* 2012; Wu *et al.* 2012b). There is evidence that the local inflammatory microenvironment plays a key role in orchestrating cancer development (Budhu and Wang 2006). Several cytokines and their associated signalling pathways have been linked to HCC as well as to LPC proliferation. Elevated expression levels of LTα, LTβ, TNF, and their receptors LTβR and TNFR1, respectively, have been detected in HCC and tumour formation was shown to be mediated through factors such as nuclear factor (NF)-κB signalling (Haybaeck *et al.* 2009). TNF is expressed in inflammatory cells during CDE diet-induced chronic liver injury and is required for LPC proliferation. Impaired TNF signalling through TNFR1 was shown to inhibit LPC proliferation and reduce tumour development (Knight *et al.* 2000). Additional studies in chronically injured livers targeting inflammatory signalling such as mediated by LTβ showed a subsequent decrease in tumour development (Haybaeck *et al.* 2009). NF-κB and STAT3 signalling play major roles in liver inflammation and HCC by regulating genes involved in cell survival, proliferation, invasion and angiogenesis which promote tumour progression upon activation (Nakagawa and Maeda 2012). However,

cytokine expression levels greatly vary between different studies and may depend on the nature of the underlying pathology and its progression. Consequently, the signalling networks are not completely understood and require further investigations.

1.7.3 Hepatocarcinogenesis: dedifferentiation theory versus maturation arrest theory

Considering cell transformation is caused by accumulated gene mutations (Hahn *et al.* 1999; Hahn *et al.* 2002), long-living cells such as stem cells and highly proliferating cells such as transit amplifying progenitor cells are likely targets for transformation. In addition to LPCs, hepatocytes represent the other major target population for cell transformation in HCC; a hypothesis which is based on the dedifferentiation theory versus the maturation arrest theory (Roskams 2006). According to the dedifferentiation theory, hepatocytes undergo clonal proliferation during carcinogenesis, dedifferentiate and gain a high proliferative capacity due to a newly acquired immature phenotype (Bralet *et al.* 1996). Fan *et al.* demonstrated Notch-mediated reprogramming of fully differentiated hepatocytes into CC precursors via atypical biliary cells (Fan *et al.* 2012). In addition, Dubois-Pot-Schneider and colleagues 'retrodifferentiated' hepatocyte-like cells, derived from HCV-induced HCC, into bipotential LPCs through crosstalk of TGFβ1, TNF and IL6, proposing that the proinflammatory microenvironment frequently associated with most CLDs may trigger this pathogenic mechanism (Dubois-Pot-Schneider *et al.* 2014).

On the other hand the maturation arrest theory is based on a combination of proliferation and blocked ontogeny in progenitor cells (Potter 1978). In the case of malignant LPC transformation during carcinogenesis, terminal differentiation is suppressed and an accumulation of maturation-arrested cells occurs due to a lack of apoptosis, making them prone to genetic alterations. Many laboratories worldwide support a precursor-product relationship between LPCs and HCCs, which is discussed more in detail in the following paragraph.

1.7.4 Liver progenitor cells as candidates for the cell of origin during hepatocarcinogenesis

Phenotypical tumour features give a hint for the cell of origin in HCCs, as most tumours still share characteristics with their precursor cell. Several studies based on immunohistochemical analysis of HCCs detected the expression of LPC markers such as CK7, CK19, oval cell marker (OV)-6 and EpCAM (Hixson *et al.* 2000; Libbrecht *et al.* 2000b) with CK19 positivity denoting a particularly poor prognosis for HCC patients (Durnez *et al.* 2006; Roskams 2006).

A prospective study of 242 HCC samples, including resection as well as biopsy material, confirmed the prognostic value of CK19 in a Caucasian cohort, regardless of the underlying aetiology. The data revealed that HCC cells with a $CK19^+$ LPC-like phenotype featured higher invasive or metastatic capacity and chemoresistant properties than $CK19^-$ counterparts (Govaere *et al.* 2014). Consistent with results demonstrating that proliferating, immature LPCs are generally surrounded by the glycoprotein laminin (Lorenzini *et al.* 2010), Govaere and collegues also showed a strong correlation of cytoplasmic laminin and CK19 expression in more aggressive HCCs, suggesting that laminin secretion by $CK19^+$ tumour cells might represent an effective autocrine mechanism to maintain stemness (Govaere *et al.* 2014).

Based on immunohistochemical and microarray studies using several HCCs, different subtypes can be clustered according to their expression profiles (Andrisani *et al.* 2011). Yamashita and colleagues classified HCCs based on their expression levels of EpCAM and AFP and proposed that different stages of hepatic cell lineages may be involved in the transformation process: (i) hepatic stem-cell like HCC, (ii) bile duct epithelium-like HCC, (iii) hepatocytic LPC-like HCC and (iv) hepatocyte-like HCC, where (i) and (iii) were associated with a particularly poor prognosis. They further demonstrated that $EpCAM^+$ HCCs downregulate hepatocyte-specific genes, whilst upregulating the Wnt/β-catenin pathway (Yamashita *et al.* 2008). This profile has been implicated in the maintenance of stemness and stem cell self-renewal and was demonstrated to represent a major regulator of the LPC response in rodents (Apte *et al.* 2008). Furthermore a study by Lee *et al.* analysed the gene expression pattern of HCC in mice and human models and proposed a link between

poor prognosis and LPC marker expression by integrating expression profiles of fetal hepatoblasts and adult hepatocytes (Lee *et al.* 2006).

A study by He *et al.* based on cell isolation and functional characterisation further supports the hypothesis of a precursor-product relationship between LPCs and HCC. They identified a progenitor cell in premalignant dysplastic foci in HCC and showed that isolated HCC progenitor cell aggregates were able to progress to cancer when exposed to a tumorigenic microenvironment induced by chronic liver damage and compensatory proliferation. A comparison to LPCs revealed similarities in the gene expression pattern and some cells were positive for markers shared by LPCs such as CK19, A6, EpCAM and Sox9 (He *et al.* 2013).

Immunohistochemical phenotyping of cirrhotic human livers revealed that at least half of the earliest premalignant precursor lesions or small dysplastic foci consist of immature LPC phenotypes and intermediate hepatocytes, consistent with a progenitor cell origin (Roskams 2006). Moreover, studies targeting LPC proliferation in chronically injured livers correlate LPC inhibition with reduced tumour development (Davies *et al.* 2006; Knight *et al.* 2008; Knight *et al.* 2000; Lee *et al.* 2010b; Lee *et al.* 2010a) potentially linking LPC activation and proliferation with HCC development. Importantly, various studies have demonstrated that only a few mutations are necessary for the transformation of LPCs. For instance, the loss of the tumour suppressor gene p53 enables LPCs to immortalise in culture and to form poorly differentiated HCCs after transplantation into nude mice (Dumble *et al.* 2002; Suzuki *et al.* 2008), demonstrating that dysregulated LPCs may play an important role in early steps of carcinogenesis. Finally, the existence of tumours of a combined hepatocellular-cholangiocarcinoma (HCC-CC) phenotype with characteristics of both hepatocytes and cholangiocytes further suggests the bipotential LPC as a potential tumour-initiating cell (Theise *et al.* 2003; Cai *et al.* 2012; Robrechts *et al.* 1998).

More recently a cell lineage tracing study tracking CK19 expression revealed the existence of cholangiocyte lineage tumours following TAA-induced CLD (Guest *et al.* 2014). Consequently, cholangiocytes and/ or LPCs represent one cell of origin in intrahepatic CC. These results stand in contrast to an earlier study proposing that the appearance of these tumours relies exclusively on the dedifferentiation process of

mature hepatocytes, induced by Notch and AKT signalling activation (Sekiya and Suzuki 2012).

1.8 Cancer stem cells in the liver

1.8.1 Cancer stem cell theory

The cancer stem cell (CSC) theory was proposed decades ago, based on the haematopoietic cancer acute myeloid leukaemia (Bonnet and Dick 1997; Lapidot *et al.* 1994). Several studies have addressed this hypothesis and the existence of CSCs has later also been proposed in solid tumours, such as HCC (Visvader and Lindeman 2008; Chiba *et al.* 2009). There is an overall agreement that tumours are composed of heterogeneous cell populations and the hierarchical hypothesis postulates the existence of a small subpopulation of stem-like cells (Reya *et al.* 2001). They share phenotypic characteristics with tissue-specific multipotential stem cells as well as general features such as self-renewing capacity and low proliferation activity. Their differentiation potential enables the formation of a hierarchical tumour structure and thus the promotion of tumour growth (Liu *et al.* 2013a). The hierarchical hypothesis is supported by the fact that radiation therapy and chemotherapy only target the major tumour cell population featuring a highly active cell cycle progression and very often cannot cure the disease completely. The resistance of a cancer subpopulation, such as CSCs, could be explained by differentially expressed signalling pathways active in stem cells as compared to mature, differentiated cells (Boniver and Herfs 2011).

A widely used strategy to investigate the tumorigenic potential of cells to identify CSC populations in different cancer subtypes is their transplantation into immunodeficient mice and the subsequent monitoring of tumour development. Using this method, several isolated cell subpopulations from cancer tissues or cancer cell lines (including HCC) have been referred to as CSCs according to their properties (Chiba *et al.* 2006; Zhu *et al.* 2010). Recently an orthotopic tumour model as alternative approach to subcutaneous injection has been described, which allows studying the tumour-initiating potential under pathologic host microenvironments

(Reiberger *et al.* 2015). As all of these studies are based on tumour cell isolation and transplantation, they do not represent tumour development in its native environment. However, further support for the CSC theory in solid tumours came from studies that identified CSCs *in vivo* using lineage tracing experiments that genetically labelled individual tumour cells (Chen *et al.* 2012; Driessens *et al.* 2012; Schepers *et al.* 2012). Here, recurrence after tumour treatment has been attributed to clonal cell origins most likely represented by CSCs.

There is a discrepancy in the literature about the term "cancer stem cell" and it has been debated whether it may be more appropriate to name this cell population "tumour-initiating cells". Tumours most likely arise from a single progenitor cell with enhanced growth and survival capabilities due to genetic and epigenetic changes (Hahn *et al.* 2002; Marquardt *et al.* 2010). Thus, the definition CSC in that context is not necessarily valid as they do not maintain and renew already established tumours (Visvader *et al.* 2008) but following mutations in response to selective pressure may establish premalignant lesions. However regardless of any terminology disputes, the "stem-like" characteristics and functions remain the same in this cell population. The term CSC is used throughout this thesis.

1.8.2 Cancer stem cells in hepatocellular carcinoma and a potential link to LPCs

In HCC, high levels of metastasis, recurrence as well as mortality after treatment of the primary tumour have been reported, suggesting the potential involvement of CSCs. Support for the existence of a potential liver CSC has been provided by Mishra and colleagues who reported alterations in signalling pathways that are known to regulate stem cell maintenance and self-renewing in HCC, such as altered Wnt, sonic hedgehog homologue and Notch pathways (Mishra *et al.* 2009). This suggests a key role for CSCs in promoting tumour development and inducing molecular changes in HCCs. It was also shown that poor HCC prognosis is associated with LPC marker expression and an immature phenotype (Lee *et al.* 2006). Moreover CK19 expression in HCCs was linked to postoperative recurrence and metastasis (Ding *et al.* 2004; Uenishi *et al.* 2003). This further supports the theory that CSCs exist and originate from less differentiated cells, such as LPCs, capable of forming a more aggressive hierarchical tumour structure.

In addition to the concept of LPCs playing a role during carcinogenesis as a potential cell of origin, it has been debated if they might even represent CSCs. As mentioned above, poor prognosis and recurrence is highly associated with tumours featuring a LPC phenotype. Moreover, Zhang and colleagues identified LPC characteristics in a cell population obtained from human resected non-tumorous tissue samples adjacent to HCC. The authors confirmed their tumorigenic potential *in vitro* and *in vivo* using an anchorage-independent growth assay (soft agar assay) and transplantation into immunodeficient mice (Zhang *et al.* 2010a). This population might represent dormant tumour-initiating cells in the tumour-surrounding tissue, which are responsible for a high rate of recurrence in HCC patients. Further support is provided by a study from Cai *et al.* who showed a strong correlation between background LPC proliferation, as part of the non-tumour DR, and tumour recurrence (Cai *et al.* 2012). The Wnt/β-catenin signalling pathway is generally involved in normal stem cell regulation including self-renewing, cell growth, development and differentiation but has also been associated with the process of carcinogenesis (Nusse 2008; Polakis 2012). In HCC, OV-6^+ cells represent a subpopulation of less differentiated progenitor-like cells with active Wnt/β-catenin signalling. This subpopulation was increased following Wnt pathway activation and decreased after inhibition of β-catenin signalling, and has been referred to as CSCs, due to their high tumorigenic potential *in vivo* and a remarkable resistance to chemotherapy (Yang *et al.* 2008a).

Moreover, it was shown that Notch-induced hepatocarcinogenesis in mice is accompanied by panCK$^+$ progenitor cell expansion and Notch target gene activation including *insulin-like growth factor 2* (*Igf2*) and *Sox*9 (Villanueva *et al.* 2012). IGF2 is a critical player in Nanog-mediated self-renewal of CSCs (Shan 2012 Hepatology) and Sox9 expression is associated with regulation of the progenitor cell fate (Furuyama *et al.* 2011). These findings suggest that Notch signalling might drive LPC-mediated development into HCC via LPC expansion or dedifferentiation.

1.8.3 Identification of liver CSCs

In general, there are two different applications to identify and isolate CSCs from cancer tissues or cell lines: (i) the functional approach takes advantage of the CSC characteristics and (ii) isolation strategies include the side population (SP) assay,

which is based on the exclusion of Hoechst dye (Chiba *et al.* 2006; Haraguchi *et al.* 2006; Shi *et al.* 2008), and the aldehyde dehydrogenase activity assay (Ma *et al.* 2008a). The so-called SP only represents a small subpopulation of cells featuring high proliferative as well as tumour-initiating potential compared to non-SP cells. The majority of SP cells display characteristics of LPCs and upon transplantation are able to provide the heterogeneity of the cancer structure. Importantly, dissociation of SP-derived tumours and separation into SP and non-SP cells emphasises their plasticity and CSC phenotype (Chiba *et al.* 2006).

The antigenic approach is based on the immunogenic properties of a CSC and relies on the detection of cell markers. Ideally, a combination of different markers is used to define a more "homogeneous" CSC population (Marquardt *et al.* 2010). In the literature surface markers such as EpCAM, CD13, CD24, CD44, CD47, CD90, CD133 and OV-6 are used for the identification as well as isolation of HCC CSCs in primary tumours and cell lines (Ma *et al.* 2007; Yamashita *et al.* 2009; Yang *et al.* 2008b; Haraguchi *et al.* 2010; Lee *et al.* 2011; Lee *et al.* 2014a). These markers are not specific for CSCs but are also expressed on other cell types in the liver including LPCs, biliary cells or cells from the haematopoietic lineage, which again highlights the importance of using different markers simultaneously.

Evidence for a great heterogeneity within the CSC population comes from a study by Yamashita and colleagues. They reported the existence of cell populations independently expressing CD90 and EpCAM in primary HCCs. The analysis of their gene expression profile suggested that the $CD90^+$ cell population shares characteristics with vascular endothelial cells and $EpCAM^+$ cells have features of epithelial cells. Moreover, $EpCAM^+$ HCC has been demonstrated to be associated with poorly differentiated morphology and high serum levels of AFP, whereas $CD90^+$ HCC was related to a high rate of distant metastasis (Yamashita *et al.* 2013). Furthermore serial xenotransplantation of double positive cells generated both $EpCAM^+$ and $CD90^+$ populations with distinct properties. Additionally, this study suggested a TGFβ-mediated interaction between $EpCAM^+$ and $CD90^+$ cells, which results in enhanced motility of $EpCAM^+$ CSCs.

1.8.3.1 Cancer stem cell markers

CD133

Suetsugu and colleagues used the HCC cell line Huh-7 to introduce the $CD133^+$ subpopulation as a putative pool of CSCs. These cells featured a high proliferative potential *in vitro* and were able to form tumours after subcutaneous injection into immunodeficient mice, showing stem-like characteristics such as self-renewing and differentiation capacity (Suetsugu *et al.* 2006; Kohga *et al.* 2010). A less differentiated phenotype of the $CD133^+$ subpopulation has been indicated by increased AFP expression levels and decreased levels of mature hepatocyte markers (Suetsugu *et al.* 2006). Similar results were obtained with $CD133^+$ cells isolated from the HCC cell line SMMC-7721 demonstrating a high clonogenicity *in vitro* and tumorigenic potential *in vivo* (Yin *et al.* 2007). Moreover, analogous properties to normal stem/progenitor cells such as the expression of "stemness" genes, the ability to self-renew, the potential to differentiate into non-hepatocyte lineages and a resistance to chemotherapeutic agents as well to radiotherapy have been detected in CD133-expressing cells (Ma *et al.* 2007; Ma *et al.* 2008b; Piao *et al.* 2012). The relevance of therapeutic intervention targeting the $CD133^+$ cell population has been demonstrated to be beneficial, since an anti-human CD133 antibody (AC133) conjugate linked to the cytotoxic drug monomethyl auristatin F showed a significant delay in tumour xenograft development in immunodeficient mice (Smith *et al.* 2008). The number of cells expressing CD133 differed from 1% up to 90% within several HCC cell lineages, whereas stem cells are thought to only represent a minor subpopulation (Ma *et al.* 2008a; Zhu *et al.* 2010). Consequently, even though they are highly enriched for tumour-initiating cells, $CD133^+$ cells might be composed of heterogeneous subpopulations with different tumorigenic potentials and thus single CD133 marker expression is insufficient to identify the CSC population in HCC.

EpCAM

A gene expression analysis by Kim and colleagues introduced EpCAM as a potential early biomarker of HCC due to significantly increased expression levels in preneoplastic tissue from CLD patients as well as in a subset of HCC specimens

(Kim *et al.* 2004). Furthermore, isolation and clonal analysis of the $EpCAM^+$ subpopulation in HCC cell lines demonstrated their CSC characteristics such as enhanced sphere formation, self-renewing and differentiation capacity *in vitro* as well as a high tumour-initiating potential *in vivo* (Yamashita *et al.* 2009; Kimura *et al.* 2010). Moreover, based on the expression profile and immunohistochemical analysis of HCC tissues, two subtypes were classified; (i) $EpCAM^+$ HCCs shared features with LPCs such as CK19, c-Kit and EpCAM expression as well as active Wnt signalling, and correlated to a poor prognosis when co-expressing AFP, whereas (ii) $EpCAM^-$ HCCs showed characteristics of mature hepatocytes (Yamashita *et al.* 2008). A study by Yamashita *et al.* suggested that EpCAM is a downstream target of the Wnt/β-catenin signalling pathway, as EpCAM expressing cells were increased after signal activation, whereas a decreased tumorigenic potential has been observed after blockage of the pathway (Yamashita *et al.* 2007).

CD90

CD90 expression has been demonstrated to discriminate CSCs form the bulk of tumour cells. $CD90^+$ HCC cells isolated from cell lines as well as from tumour tissue were able to form tumour nodules in immunodeficient mice after transplantation and thus featured tumorigenic capacity (Yang *et al.* 2008c). Furthermore, the $CD90^+$ subpopulation has been identified in 91.6% of blood samples from HCC patients showing the same characteristics (Yang *et al.* 2008b) suggesting a reason for the poor prognosis in HCC. Isolated $CD90^+$ CSCs from human HCC displayed enhanced expression of genes contributing in inflammation, drug resistance, and lipid metabolism (Ho *et al.* 2012).

CD44

A knockout study with the HCC cell line SNU-449 revealed that CD44 inhibition was associated with a decreased tumorigenic potential and invasiveness as well as increased apoptosis, necrosis and chemosensitivity to doxorubicin, supposedly mediated through reduced levels of the anti-apoptotic proteins B cell lymphoma 2 and multi drug resistance gene 1 (Xie *et al.* 2008). CD44 expression alone is not

sufficient to discriminate the CSC population in HCC. However, it acts as a marker that defines a more aggressive subpopulation when co-expressed with other CSC markers (Yang *et al.* 2008b; Zhu *et al.* 2010). Within CD90 expressing CSCs, the $CD90^{+}/CD44^{+}$ subpopulations represents a more aggressive phenotype of circulating CSCs (Yang *et al.* 2008b). Furthermore, the CD44-positive subpopulation in CD133-expressing HCC cells defined a cell population featuring higher tumorigenic potential, preferential expression of "stemness" genes and greater resistance to chemotherapeutic agents compared to their $CD133^{+}/CD44^{-}$ counterparts(Zhu *et al.* 2010). This may explain an aggressive tumour growth and even the potential of metastasis in HCC, as CD44 is a cell adhesion molecule contributing to tumour cell invasion, migration and resistance to apoptosis (Lara-Pezzi *et al.* 2001; Park *et al.* 2012).

1.9 Study Aims

The first aim was to characterise and compare two commonly used murine CLD models, CDE and TAA, over a period of six weeks to follow stages of injury induction, establishment and maintenance. Disease parameters such as hepatocyte damage, hepatic fat loading, oxidative stress, inflammation, fibrosis and the LPC response were to be investigated to analyse their dynamics and lobular appearance and potentially correlate them with distinct injury patterns.

The second aim was to thoroughly characterise the CDE- and TAA-induced LPC response in the six-week time course by immunofluorescent assessment of cell proliferation and the expression pattern of common LPC markers.

The third aim was to investigate the response dynamics induced by CDE and TAA long-term treatment, over a period of 7 months, and to analyse model-specific injury patterns during CLD progression and carcinogenesis. This includes the comprehensive analysis of induced tumours and the examination of disease parameters in the surrounding tissue including the inflammatory, fibrogenic and LPC responses.

The fourth aim was to examine the relationship between the LPC response and HCC development in humans by characterising the magnitude and distribution of CK7+ DRs and LPCs in a retrospective study of CLD patients.

CHAPTER 2

Materials and Methods

2.1 Materials

2.1.1 Laboratory Chemicals

All general laboratory chemicals were of analytical research grade or equivalent and were obtained from a range of commercial manufacturers. Supplier information is provided for specialty reagents.

2.1.2 Solutions and Buffers

Water (H_2O)

All general solutions and buffers were prepared with double-deionised H_2O (ddH_2O) generated with a purification system (Aquatec, VIC, Australia). The ddH_2O quality was monitored with the Hydro-Check Systems 414R, Resistivity Monitor-Controller (Hydro-Check Systems, Inc., CA, USA). For molecular techniques involving RNA and for the preparation of real-time polymerase chain reactions (RT-PCR), UltraPure™ DNase/RNase-free water (Life Technologies, VIC, Australia) was utilised.

Acetate Citrate Buffer (hydroxyproline assay)

0.88 M sodium acetate tri-hydrate, 0.24 M citric acid, 0.2 M acetic acid, 0.85 M NaOH; adjusted to pH 6.5 and stored at RT.

Acetone-Methanol Fixative (fixation of frozen tissue sections)

A 1:1 (v/v) ratio of acetone and methanol was prepared and stored at -20°C prior to use.

Alanine transaminase (ALT) Colour Reagent (ALT assay)

For the preparation of 1 mM 2,4-dinitrophenylhydrazine in 1 M HCl, 20 mg of 2,4-dinitrophenylhydrazine were dissolved in 20 ml of 5 M HCl and adjusted to a total volume of 100 ml with ddH_2O.

ALT Substrate Solution (ALT assay)

0.2 M DL-alanine, 1.8 mM α-ketoglutarate in PBS, adjusted to pH 7.5 and stored at 4°C.

Chloramine-T Solution (hydroxyproline assay)

The solution was prepared by adding 127 mg of chloramine-T to 2 ml of 50% n-propanol, and then added up to a total volume of 10 ml using Acetate Citrate Buffer. The solution was prepared freshly prior to use.

Citrate Buffer (antigen retrieval)

A 10x stock solution of 100 mM citrate was prepared, adjusted to pH 6 and stored at RT. Prior to use, the stock solution was diluted 1:10 in ddH_2O.

EDTA Buffer (antigen retrieval)

A 10x stock solution of 1 M EDTA was prepared, adjusted to pH 8 and stored at RT. The stock solution was diluted 1:1000 in ddH_2O prior to use.

Ehrlich's Reagent - DMAB Solution (hydroxyproline assay)

The solution was prepared by dissolving 1.5 g of 4-dimethylaminobenzaldehyde (DMAB) in a 2:1 (v/v) n-propanol/perchloric acid mix.

Gelatine Mounting Medium (Oil Red O staining)

A gelatine-based aqueous mounting medium was prepared by dissolving 1 g of gelatine (Coles Brand, WA, Australia) in 6 ml of ddH_2O while heating. Then 7 ml of glycerol was added and the glycerine jelly was stored at RT. Prior to use, the Gelatine Mounting Medium was heated until molten.

0.5% Oil Red O Solution (Oil Red O staining)

A small volume of propylene glycol was added to 0.5 g of Oil Red O (Sigma-Aldrich, NSW, Australia) and mixed well. A total volume of 100 ml was gradually adjusted with propylene glycol while stirring and heating the solution up to 95-100°C. The warm solution was filtered through a Whatman® coarse filter paper (GE

Healthcare Life Sciences, NSW, Australia), settled overnight at RT prior to use and long-term stored at RT.

4% PFA Fixative (fixation of frozen tissue sections)

A 4% paraformaldehyde (PFA) solution was prepared by dissolving 10 g PFA (Sigma-Aldrich, NSW, Australia) in 250 ml PBS while heating at 60°C, and stored at -20°C.

Phosphate Buffered Saline (PBS)

137 mM NaCl, 2.7 mM KCl, 4.3 mM Na_2HPO_4, 1.47 mM KH_2PO_4, adjusted to pH 7.4, sterilised by autoclaving and stored at RT.

Silver Solution (reticulin staining)

While continuously stirring, ammonium hydroxide was added drop by drop into 5 ml of 10% aqueous silver nitrate solution until the precipitate was fully dissolved. Then 5 ml of 3% aqueous sodium hydroxide solution was added and the precipitate was re-dissolved with ammonium hydroxide. The solution was filled up to a total volume of 50 ml using ddH_2O and filtered through a Whatman® coarse filter paper (GE Healthcare Life Sciences) when new precipitate was formed.

Tris-EDTA Buffer (antigen retrieval)

A 10x stock solution of 100 mM Tris and 10 mM EDTA was prepared, adjusted to pH 9 and stored at RT. The stock solution was diluted 1:10 in ddH_2O prior to use.

2.1.3 Oligonucleotide Primer

Forward and reverse sequences, annealing/extension (A/E) temperatures of oligonucleotide primers (Sigma-Aldrich, NSW, Australia) as well as product information of QuantiTect Primer Assays (Qiagen, VIC, Australia) utilised in this thesis are listed in Table 2.1.

2.1.4 Antibodies

Primary and secondary antibodies used in this thesis and their optimised experimental conditions are listed in Table 2.2.

Target genes	Primer sequences (5' to 3')	A/E (°C)	QuantiTect Primer Assay
Gapdh	Fwd: AAGGTCGGTGTGAACGGATTTGG Rev: CGTTGAATTTGCCGTGAGTGGAG	68	
Mmp9	Fwd: CTGGACAGCCAGACACTAAAG Rev: CTCGCGGCAAGTCTTCAGAG	62	
Nqo1	Fwd: TATCCTTCCGAGTCATCTCTAGCA Rev: TCTGCAGCTTCCAGCTTCTTG	63	
Nrf1	Fwd: AGCACGGAGTGACCCAAAC Rev: TGTACGTGGCTACATGGACCT	60	
Rn18S	Fwd: CGGCTACCACATCCAAGGAA Rev: GCTGGAATTACCGCGGCT	60	
Tgfβ	Fwd: GCGGACTACTATGCTAAAGAGG Rev: GTAGAGTTCCACATGTTGCTCC	55	
Timp1	Fwd: ATTCAAGGCTGTGGGAAATG Rev: CTCAGAGTACGCCAGGGAAC	62	
Txn	Fwd: GCCAAAATGGTGAAGCTGAT Rev: TGATCATTTTGCAAGGTCCA	60	
Col1α1		60	QT00162204
Hgf		60	QT00158046
Ifnγ		60	QT01038821
Il6		60	QT00098875
Ltβ		60	QT00107443
Mmp2		60	QT00116116
Taf4α		60	QT01060661
Timp2		60	QT00138558
Tnf		60	QT00104006
Tweak		60	QT01743252

Table 2.1: Primer sequences and QuantiTect Primer Assays.

Epitope	Host Species	Reactivity	Clone	Dilution	Conjugate	Fixation	Antigen Retrieval	Supplier details
Primary Antibody								
A6	rat	mu		1/200		Ac-Me		Gift from Dr. Factor, National Cancer Institute, Bethesda, MD, USA
CD11b	rat	mu	M1/70	1/400		Ac-Me		eBioscience, CA, USA
CD31	rat	mu	MEC13.3	1/100	Alexa Fluor 594	Ac-Me		BioLegend, CA, USA
CD31	rat	mu	MEC13.3	1/200		Ac-Me		BioLegend, CA, USA
CD34	rat	mu	RAM34	1/200		Ac-Me		eBioscience, CA, USA
CD44	rat	hu, mu	IM7	1/400		Ac-Me		eBioscience, CA, USA
CD45	rat	mu	30-F11	1/30 IHC, 1/200 IF		Ac-Me	Dako GV805	BD, NSW, Australia
CD90	rat	mu	IBL-6/23	1/300		Ac-Me		Abcam, VIC, Australia
CD133	rat	hu, mu, rat	13A4	1/200		Ac-Me		eBioscience, CA, USA
CK7	rabbit	hu, mu, rat	EPR17078	1/4000			Tris-EDTA	Abcam, VIC, Australia
CK7	mu	hu	OV-TL 12/30	1/50			Tris-EDTA	Dako, NSW, Australia
CK19	rat	mu		1/200 Fr-IF, 1/100 IHC		Ac-Me	Proteinase K	TROMA-III, Developmental Studies Hybridoma Bank, IA, USA
CPS1	rabbit	hu, mu		1/1000			Dako GV805	Abcam, VIC, Australia
E-cadherin	rabbit	hu, mu	24E10	1/200		Ac-Me		Cell Signaling, MA, USA
EpCAM	rabbit	hu, mu,rat		1/200		Ac-Me		Abcam, VIC, Australia
EpCAM	mu	hu	Ber-EP4	1/200			Dako GV805	Dako, NSW, Australia

Table 2.2: List of primary and secondary antibodies. To be continued on following page.

Epitope	Host Species	Reactivity	Clone	Dilution	Conjugate	Fixation	Antigen Retrieval	Supplier details
Primary Antibody								
EpCAM	mu	hu	Ber-EP4	1/200			Dako GV805	Dako, NSW, Australia
F4/80	rat	mouse	BM8	1/80			Proteinase K	eBioscience, CA, USA
HNF4α	goat	mu	C-19	1/400 P-IF, 1/700 Fr-IF		Ac-Me	EDTA	Santa Cruz Biotechnology, TX, USA
Ki67	rabbit	mu	D3B5	1/400		Ac-Me	Dako GV805	Cell Signaling, MA, USA
Oval Cell	rat	mu	MIC1-1C3	1/100		Ac-Me		Novus Biologicals, CO, USA
panCK	mu	hu, mu	AE1/AE3	1/50		Ac-Me	Tris-EDTA	Dako, NSW, Australia
panCK	rabbit	mu		1/300		Ac-Me	Proteinase K	Dako, NSW, Australia
αSMA	mu	mu	1A4	1/2000 IHC, 1/500 IF		Ac-Me	Non	Sigma-Aldrich NSW, Australia
Sox9	rabbit	hu, mu		1/600 P-IF, 1/600 IHC			Tris-EDTA	Merck Millipore, VIC, Australia
Secondary Antibody								
IgG	donkey	rabbit		1/500	Alexa Fluor 488			Life Technologies, VIC, Australia
IgG	donkey	goat		1/500	Alexa Fluor 594			Life Technologies, VIC, Australia
IgG	goat	rabbit		1/500	Alexa Fluor 488			Life Technologies, VIC, Australia
IgG	goat	rabbit		1/500	Alexa Fluor 594			Life Technologies, VIC, Australia
IgG	goat	rat		1/500	Alexa Fluor 488			Life Technologies, VIC, Australia
IgG	goat	rat		1/500	Alexa Fluor 594			Life Technologies, VIC, Australia
IgG	goat	rat		1/500	Alexa Fluor 647			Life Technologies, VIC, Australia

Table 2.2: List of primary and secondary antibodies. To be continued on following page.

Epitope	Host Species	Reactivity	Clone	Dilution	Conjugate	Fixation	Antigen Retrieval	Supplier details
Secondary Antibody								
IgG	goat	mu		1/500	Alexa Fluor 488			Life Technologies, VIC, Australia
IgG	goat	mu		1/500	Alexa Fluor 594			Life Technologies, VIC, Australia
IgG	rabbit	goat		1/500	Alexa Fluor 594			Life Technologies, VIC, Australia
IgG	mu	rat		1/100	Biotin			eBioscience, CA, USA
IgG	goat	rabbit		1/300	Biotin			Dako, NSW, Australia

Table 2.2: List of primary and secondary antibodies. Primary antibodies used for immunohistochemistry and immunofluorescence are listed. Ac-Me; Aceton-Methanol Fixative, hu, human; GV805, Target Retrieval Solution low pH (Dako, NSW, Australia); mu, murine

2.2 General Methods

2.2.1 Animals

2.2.1.1 Animal handling

Animals were housed under pathogen-free conditions on wheaten chaff bedding and kept on 12-hour day/night cycles in individually ventilated cages and in temperature-controlled rooms. A maximum of six mice were grouped together in one cage with *ad libitum* access to food and water. All animal experiments were performed in accordance with the Australian code for the care and use of animals for scientific purposes at Curtin University, Perth, Australia with local Animal Ethics Committee approval.

2.2.1.2 Mouse strains

C57BL/6J mice were purchased from the Animal Resources Centre of Western Australia (Murdoch, WA, Australia).

2.2.1.3 Experimental diets

Mice had free access to either choline-deficient chow (MP Biomedicals, NSW, Australia) and drinking water containing 0.15% DL-ethionine (Sigma-Aldrich, NSW, Australia) (CDE diet) or normal chow and water containing 300 mg/l thioacetamide (Sigma-Aldrich) (TAA). Drinking water under both experimental conditions was changed every alternate day for the initial two weeks and twice a week thereafter. Control animals received normal chow and drinking water.

2.2.1.4 Anaesthesia

Mice were anaesthetised by intraperitoneal injection of ketamine (Provet, WA, Australia) at a dose of 100 mg/kg body weight and xylazine (Provet, WA, Australia) at a dose of 10 mg/kg body weight. The amount of anaesthetics was calculated according to the individual body weight and diluted in PBS (2.1.2) to reach a total volume of approximately 200 µl for injection. Depth of anaesthesia was monitored using the leg withdrawal effect.

2.2.1.5 Serum extraction

Following complete anaesthesia, blood was extracted by cardiac puncture using a 27½ G needle (Terumo®, NSW, Australia) attached to a 1 ml syringe (Terumo®, NSW, Australia). After allowing the blood to clot at RT, serum was separated from cellular components by centrifugation of samples at 16,100 x g for 10 min at 4°C. The serum-containing supernatant was transferred to a new microcentrifuge tube and stored at -80°C.

2.2.1.6 Liver perfusion

The liver was manually perfused by cannulating the portal vein using a 27½ G needle (Terumo®, NSW, Australia) attached to a 10 ml syringe (Terumo®, NSW, Australia), and subsequent flushing with PBS. The heart was cut after visible blanching of the liver, indicating appropriate positioning of the needle, and the liver was flushed with 5 ml of PBS over a period of 1 min while maintaining a consistent flow rate.

2.2.1.7 Liver isolation, preservation and processing

Following perfusion, the liver was excised and the gall bladder removed. To preserve liver tissue for molecular and biochemical analyses, tissue pieces were snap-frozen in liquid nitrogen and stored at -80°C. For immunofluorescent staining experiments and lipid stainings, two liver pieces were embedded in ornithine carbamoyltransferase

(OCT) (Sakura Finetek, South Holland, Netherlands), snap-frozen in liquid nitrogen and stored at -80°C. Sections were cut at 7 µm using a cryostat microtome (Microm HM550, Thermo Fisher Scientific, VIC, Australia) and stored at -80°C.

For histology and immunohistochemistry experiments, one liver lobe was immersed in 10% formalin (Amber Scientific, WA, Australia) and incubated for 24 h at RT before transferring into 70% ethanol. Fixed tissue was processed in the Pathology Laboratory at Fiona Stanley Hospital (Murdoch, WA, Australia) and subsequently manually embedded in paraffin using a tissue embedder (Leica EG1150C, Leica Biosystems, NSW, Australia). Paraffin blocks were cut into 4 µm thick sections using a microtome (Leica RM2235, Leica Biosystems, NSW, Australia) and mounted onto Superfrost®Plus slides (Grale Scientific, VIC, Australia). Sections were dried at 37°C overnight and stored at RT.

2.2.2 Histology Techniques

2.2.2.1 Dewaxing and rehydration of paraffin sections

Sections of formalin-fixed and paraffin-embedded liver tissue (2.2.1.7) were heated at 60°C prior to use. In order to dewax and rehydrate the tissue sections, the following incubations were performed for two min each while gently agitating: three times in xylene, three times in 100% ethanol, once in 70% ethanol and once in 50% ethanol. Slides were then placed in tap water for 10 min prior to further treatment.

2.2.2.2 Fixation of frozen tissue sections

Frozen tissue sections (2.2.1.7) were fixed in ice-cold Acetone-Methanol Fixative (2.1.2) for 2 min and then dried at RT for 1 h. Slides were placed in PBS for 10 min prior to further treatment.

2.2.2.3 Haematoxylin and eosin staining

Haematoxylin and eosin staining was performed in the Pathology Laboratory at Fiona Stanley Hospital (Murdoch, WA, Australia) using a standard protocol and sections of formalin-fixed and paraffin-embedded liver tissue (2.2.1.7).

2.2.2.4 Reticulin staining

Reticulin staining was performed using a Reticulin Stain Kit (Polysciences Inc., PA, USA). The manufacturer's instructions were slightly modified. Following dewaxing and rehydration (2.2.2.1), paraffin sections were oxidised in 1% aqueous potassium permanganate for 5 min, washed in ddH_2O for 1 min and bleached in 1% aqueous oxalic acid until the tissue was colourless. After washing in ddH_2O, sections were sensitised in 2.5% aqueous ferric ammonium sulfate for 15 min, washed in running tap water and rinsed in three changes of ddH_2O. Then silver impregnation of tissue sections was achieved by incubation of slides in Silver Solution (2.1.2) for 2 min and three quick immersions in two changes of ddH_2O each. Incubation of sections in a 10% aqueous formalin solution for 2 min induced a black colour reaction. Slides were then rinsed in ddH_2O, quickly dipped into 0.2% aqueous gold chloride and rinsed well in ddH_2O. Finally, sections were incubated in 5% aqueous sodium thiosulfate, washed in ddH_2O, counterstained with 1% Nuclear Fast Red Stain Solution for 2 min and washed in running tap water prior to dehydration and mounting (2.2.2.9).

2.2.2.5 Sirius Red staining

Collagen fibers were stained using a Picrosirius Red Stain Kit (Polysciences Inc., PA, USA). The manufacturer's instructions were slightly modified. Following dewaxing and rehydration (2.2.2.1), paraffin sections were immersed in Haematoxylin Solution (Dako, NSW, Australia) for 15 sec for nuclear counterstaining and rinsed in ddH_2O. Then slides were incubated for 2 min in phosphomolybdic acid, rinsed in ddH_2O and incubated in Picrosirius Red Solution for 1 h. After immersion in 0.01 N hydrochloric acid for 2 min, tissue sections were

placed in 70% ethanol, further dehydrated and mounted (2.2.3.9). An additional Sirius Red staining was performed for every sample without the haematoxylin counterstaining step for better detection of thin collagen fibres.

2.2.2.6 Apoptosis assay

Apoptotic cells were detected using a DeadEnd^{TM} Fluorimetric Terminal Deoxynucleotidyl Transferase dUTP-biotin Nick End Labelling (TUNEL) assay (Promega, NSW, Australia). Following dewaxing and rehydration (2.2.2.1), paraffin sections were treated according to the manufacturer's instructions. After the staining procedure, tissue sections were mounted with ProLong® Gold Antifade Reagent with DAPI (Life Technologies, VIC, Australia) to counterstain the nuclei. TUNEL^{+} cells were quantitated in five non-overlapping fields of view at x200 total magnification.

2.2.2.7 Antigen retrieval

Epitope unmasking of paraffin sections (2.2.2.1) was achieved either by heat-mediated antigen retrieval using Citrate Buffer (2.1.2), Tris-EDTA Buffer (2.1.2), EDTA-Buffer (2.1.2) or Dako Target Retrieval Solution low pH (Dako, NSW, Australia), proteolytic digestion with proteinase K (Dako, NSW, Australia) or no necessary treatment. Appropriate antigen retrieval was performed according to the respective antibody requirements (Table 2.2).

2.2.2.8 Immunohistochemical detection of antigens

Following dewaxing, rehydration (2.2.2.1) and antigen retrieval (2.2.2.7), paraffin sections were used for immunohistochemical detection of antigens. In order to inactivate tissue endogenous peroxidases, tissue sections were incubated in hydrogen peroxide for 5 min using a Peroxidase Blocking Reagent (Dako, NSW, Australia) and washed in PBS for 5 min. Tissue endogenous biotin was blocked by using a Biotin Blocking System (Dako, NSW, Australia). Therefore tissue sections were first

incubated in Avidin Solution for 10 min, washed in PBS and incubated in Biotin Solution for 10 min before performing a second PBS wash for 5 min. Unspecific antibody binding was blocked by incubating the tissue sections for 30 min in serum-free Protein Blocking Solution (Dako, NSW, Australia). Antibodies were diluted in Antibody Diluent (Dako, NSW, Australia), with optimal concentrations listed in table 2.2. Tissue sections were incubated with the primary antibody either over night at 4°C or for 1 h at room temperature in a humidified chamber, and washed afterwards for 5 min in PBS. The Dako LSAB+ System-HRP (Dako, NSW, Australia) was used to detect primary antibodies raised in mouse and rabbit. Additionally, primary antibodies raised in rat and rabbit were recognised by the secondary antibodies mouse anti-rat-Biotin (eBioscience, CA, USA) and goat anti-rabbit-Biotin (Dako, NSW, Australia), respectively, in combination with the Streptavidin Peroxidase Solution from Dako LSAB+ System-HRP (Dako, NSW, Australia). Slides were washed in PBS before performing the colour detection using the Liquid DAB+ Substrate Chromogen System (Dako, NSW, Australia). Tissue sections were incubated in DAB chromogen until the colour developed and then placed in water. Nuclear counterstaining was performed by dipping the slides in Haematoxylin Solution (Dako, NSW, Australia) for 30 sec. Afterwards sections were rinsed in running tap water for 2 min, dehydrated and mounted (2.2.2.9). Images were taken using the Olympus BX51 microscope and the Olympus camera DP70 (Olympus, VIC, Australia) or whole tissue sections were scanned using the ScanScope XT digital slide scanner (Aperio Technologies, CA, USA). Positive cell counts were performed manually in five non-overlapping fields of view at x200 total magnification.

2.2.2.9 Dehydration of tissue sections

Tissue sections were dehydrated by sequential incubation and gentle agitation in one change of 70% ethanol, two changes of 100% ethanol and three changes of xylene for 1 min each. Afterwards tissue sections were mounted with VectaMount™ Mounting Medium (Vector Laboratories, CA, USA) and covered with a cover slip (Grale Scientific, VIC, Australia) while avoiding any air bubbles.

2.2.2.10 Immunofluorescent detection of antigens

Fixed frozen liver sections (2.2.2.2) or antigen-retrieved paraffin sections (2.2.2.7) were used for immunofluorescent detection of antigens. In order to avoid unspecific antibody binding, tissue sections were blocked for 30 min in serum-free Protein Blocking Solution (Dako, NSW, Australia). Tissue sections were then incubated with primary antibodies diluted in Antibody Diluent (Dako, NSW, Australia) overnight at 4°C in a humidity chamber or for 1 h at RT. After washing the slides for 5 min in PBS, sections were incubated for 30 min at RT in the dark with respective secondary antibodies diluted in Antibody Diluent (Dako, NSW, Australia). Optimal experimental conditions for primary and secondary antibodies are listed in table 2.2. After staining of sections, slides were washed for 5 min in PBS in the dark and briefly dried before adding ProLong Gold Antifade Reagent with DAPI (Life Technologies, VIC, Australia) to counterstain the nuclei. Sections were then covered with a cover slip and dried in the dark. The staining patterns were analysed with a fluorescent microscope (Olympus BX51, Olympus, VIC, Australia) or by using confocal analysis with the Eclipse T*i* inverted microscope system and the NIS Element AR software version 4.1 (Nikon, NSW, Australia). Cells were counted manually for positive staining in five non-overlapping fields of view at x100 total magnification.

2.2.2.11 Oil Red O staining

To assess accumulation of neutral triglycerides and lipids, frozen liver tissue sections (2.2.1.7) were air-dried for 1 h at RT, then fixed for 5 min in ice-cold 4% PFA Fixative (2.1.2) and afterwards dried once more for 1 h at RT. Slides were immersed in 1,2-propanediol for 5 min, then transferred into pre-warmed 0.5% Oil Red O Solution (2.1.2) and heated for 8 min at 55°C in an oven. After incubating in 85% aqueous 1,2-propanediol for 5 min, sections were washed two times in ddH_2O, immersed in Haematoxylin Solution (Dako, NSW, Australia) for 15 sec to counterstain the nuclei and mounted with Gelatine Mounting Medium (2.1.2). Tissue sections were scanned with the ScanScope XT digital slide scanner (Aperio

Technologies, CA, USA) and assessed using an algorithm-based positive pixel count in five non-overlapping fields of view at x400 total magnification.

2.2.3 Molecular Biology Techniques

2.2.3.1 RNA extraction

Total RNA was extracted from snap-frozen liver tissue using 1 ml TRIzol® Reagent (Life Technologies, VIC, Australia) according to the manufacturer's instructions. RNA samples were dissolved in UltraPure™ DNase/RNase-free water (Life Technologies, VIC, Australia) and stored at -80°C. Prior to long-term storage, an aliquot was diluted in UltraPure™ DNase/RNase-free water (Life Technologies, VIC, Australia) and quantitated using the NanoDrop 1000 Spectrophotometer (Thermo Fisher Scientific, VIC, Australia) by measuring the absorbance at 260 nm. The RNA concentration was calculated by correlating the absorbance and the concentration using the *Beer-Lambert law* ($A = \varepsilon c l$; where A is the absorbance, ε is the extinction coefficient, c is the concentration and l is the light path length). Given the extinction coefficient for RNA is 40 (ng-cm/µl), RNA was quantitated as follows: RNA concentration (ng/µl) = A_{260} / l (cm) x 40 (ng-cm/µl) x dilution factor. By measuring the absorbance at 230 and 280 nm, RNA purity was evaluated according to the ratio of A_{260}/A_{230} and A_{260}/A_{280}, respectively. RNA samples with values greater than 1.8 for A_{260}/A_{280} and values between 2.0 and 2.2 for A_{260}/A_{230} ratios were considered to be without significant contamination of proteins, phenol and other compounds.

2.2.3.2 DNase treatment

Contaminating genomic DNA was removed from RNA samples using the RQ1 RNase-free DNase (Promega, NSW, Australia) according to the manufacturer's instructions.

2.2.3.3 Reverse transcription

One microgram of DNase-treated RNA (2.2.4.2) was reverse-transcribed using Random Hexamers (Promega, NSW, Australia) and the Moloney Murine Leukemia Virus Reverse Transcriptase (M-MLV-RT), RNase H Minus, Point Mutant (Promega) according to the manufacturer's instructions. No-RT-controls were prepared as described but without adding enzyme, and thus served as negative controls to assess genomic DNA contamination.

2.2.3.4 Real time polymerase chain reaction (RT PCR)

Gene expression levels were analysed by SYBR Green-based RT PCR using the GoTaq® qPCR Master Mix (Promega, WA, Australia). PCR reactions were performed in a total volume of 10 µl, with 2 µl of template cDNA (2.2.4.3) diluted 1:2 in UltraPure^{TM} DNase/RNase-free water (Life Technologies, VIC, Australia), and 1 µl of 10x primer assays or primer concentrations of 0.5 µM (2.1.3), respectively. Amplification was achieved using the ViiA7 Real-Time PCR System (Life Technologies, VIC, Australia) and a two-step, fast qPCR program with cycling parameters of initial activation for 2 min at 95°C, followed by 40 cycles of denaturation for 3 sec at 95°C and annealing/extension for 30 sec at primer-specific temperatures (2.2.4.3). Data were normalised to the housekeeping genes *18S rRNA*, *TATA box binding protein associated factor* (*Taf) 4α* and *glyceraldehyde 3-phosphate dehydrogenase* (*Gapdh)* to confirm results and presented as normalised to *18S rRNA* throughout the thesis. All transcript levels were expressed relative to control mice. Primer efficiencies were calculated using standard curves generated from a 1:5 dilution series of cDNA and the ViiA7 Real-Time PCR System Software v1.2.1 (Life Technologies, VIC, Australia).

2.2.4 Biochemical Techniques

2.2.4.1 Serum alanine transaminase assay (ALT assay)

Alanine transaminase catalyses the reaction of L-alanine and α-ketoglutarate to pyruvate and L-glutamate. The pyruvate produced in this reaction reacts with the colour reagent 2,4-dinitrophenylhydrazine to form hydrazone, which can be colorimetrically measured at 490 nm. To asses ALT levels, 25 µl of serum were added to 100 µl of ALT Substrate Solution (2.1.2), mixed gently and incubated for 1 h at 37°C. Then 100 µl of ALT Colour Reagent was added followed by a 20 min incubation at RT. The colour reaction was terminated by adding 1 ml of 0.4 M NaOH, mixed by inversion and incubated for 5 min at RT. 200 µl of the reaction were transferred into a clear 96-well plate (Thermo Fisher Scientific, VIC, Australia) and the absorbance was measured at 490 nm (EnSpire® Multimode Plate Reader, Perkin-Elmer Life Sciences, VIC, Australia).

2.2.4.2 Hydroxyproline assay

Approximately 130 mg of snap-frozen liver tissue (2.2.1.7) was used to quantitate tissue collagen deposition. Therefore, tissue was homogenised in 1 ml of 6 M HCl for 20 h at 95°C and then centrifuged at 13,000 x g for 10 min. For further treatment of samples, 40 µl of supernatant was used per reaction. Then 10 µl of 10 M NaOH and 450 µl of Chloramine-T Solution (2.1.2) were added to each sample and incubated for 25 min at RT. Subsequently 500 µl of DMAB Solution were added and samples were incubated for 20 min at 65°C before absorbance measurement at 560 nm (EnSpire® Multimode Plate Reader, Perkin-Elmer Life Sciences, VIC, Australia).

2.2.4.3 Cholesterol assay

Approximately 50 mg of snap-frozen liver tissue was homogenised in 500 ml of 5% NP-40 in ddH_2O by heating the samples at 90°C in a water bath for 3 min until cloudiness was observed. After cooling the samples to RT, the heating process was

repeated once before samples were centrifuged for 2 min at 16,100 x g. The supernatant was used to assess cholesterol levels using the Amplex® Red Cholesterol Assay Kit (Invitrogen, VIC, Australia), as per the manufacturer's instructions.

2.2.5 Statistical Analysis

Quantitative data are presented as mean ± standard error of the mean (SEM). Statistical significance was evaluated by Student's two-tailed, unpaired t test (normal distribution of data), Mann-Whitney U test (no normal distribution of data) and Kruskal-Wallis test (no normal distribution of data and more than two sample groups). Correlation studies were analysed using the Spearman method and SPSS. Results were considered significant for $p < 0.05$.

CHAPTER 3

Comparison of two CLD models, CDE versus TAA, during early stages of injury induction, establishment and maintenance

Parts of this chapter have already been published and the article is included in the appendix (Köhn-Gaone *et al.* 2016a).

Köhn-Gaone J., Dwyer B.J., Grzelak C.A., Miller G., Shackel N.A., Ramm G.A., McCaughan G.W., Elsegood C.L., Olynyk J.K., and Tirnitz-Parker J.E. (2016). Divergent Inflammatory, Fibrogenic, and Liver Progenitor Cell Dynamics in Two Common Mouse Models of Chronic Liver Injury. *Am J Pathol*, **186**: 1762-1774.

3.1 Introduction

Chronic liver diseases including cholestasis, viral hepatitis infection, haemochromatosis, alcoholic and non-alcoholic fatty liver disease or steatohepatitis, are all associated with hepatocyte injury and varying degrees of inflammation and fibrosis that predispose the patient to cirrhosis and eventually HCC development. In the Western World multiple risk factors with potentially additive effects are often encountered, such as a combination of viral hepatitis, diabetes and excessive alcohol consumption - coalesced settings in which the HCC risk can increase by in excess of 100-fold compared to a cirrhotic patient with a single risk factor (Chen *et al.* 2008). Even though treatment of HCC patients with the promising kinase inhibitor Sorafenib has led to a significantly prolonged time to HCC progression (Llovet *et al.* 2008), there are considerable risks for side effects due to its multi-target nature and overall trials have fallen short of expectations. Hence, preventative and curative therapy approaches are still limited and new treatment targets are urgently required. Moreover, patient numbers are steadily increasing in the Western World due to a changing life style, which causes a major public health burden. Therefor it is of great interest to study the mechanisms of chronic injury progression and understand the driving forces behind these processes.

Murine models are commonly used to study a wide variety of processes, which are associated with CLD. Since the injury response in the human liver is caused by different triggers such as viral infections, excessive alcohol consumption, obesity or autoimmune diseases, the pathology of the underlying diseases are not identical even though they share similar patterns (Ferrell 2000). Therefore, it is essential to use appropriate animal models to mimic particular characteristics of human pathologies to be able to link study outcome and clinical relevance, which is important for therapeutic applications. Several murine CLD models have been used in the literature, based on different treatments, such as the usage of CCl_4, DDC, DEN, CDE or TAA (Liu *et al.* 2013b), which vary with regards to intralobular location, severity of tissue damage and disease progression patterns. In our laboratory, the CDE diet is well established for the study of processes, which are associated with CLD. It is

widely used in mice to examine steatosis, chronic inflammation, fibrosis, LPC proliferation, and hepatocellular carcinoma formation if administered long-term (Shin *et al.* 2011; Knight *et al.* 2008; Akhurst *et al.* 2001; Tirnitz-Parker *et al.* 2010; Van Hul *et al.* 2009). Hepatotoxicity is induced through the deficiency of choline, which is critical for the assembly and secretion of very low density lipoproteins (Yao and Vance 1988), combined with the hepatocarcinogen ethionine. A more recently adapted murine model is based on TAA administration, which can be delivered orally or via intraperitoneal injection. TAA is metabolised to thioacetamide sulfine and subsequently activated to the hepatotoxic compound sulfene (Hunter *et al.* 1977). This metabolic transformation is mediated by the microsomal flavin-adenine dinucleotide-containing monooxygenase as well as the P450 cytochrome enzyme CYP2E1 and generates the reactive oxygen species superoxide anion and hydrogen peroxide, resulting in oxidative stress, which in turn leads to lipid peroxidation and centrilobular necrosis (Low *et al.* 2004). TAA supplementation has traditionally been used to study fibrosis, cirrhosis and the development of liver tumours, especially CC, when administered long-term (Grzelak *et al.* 2014; Boulter *et al.* 2015; Guest *et al.* 2014). The introduction of the TAA model as an alternative regimen will enable us to mimic a broader range of human pathologies and to identify model-specific processes.

3.2 Study Aims

The induction, severity and progression of CLD vary greatly between animal models, depending on the underlying mechanisms. It is therefore vital to understand the molecular and histopathological patterns in order to select the most appropriate regimen and time points to mimic a human pathology of interest. Thus, the aim of this chapter was to compare the dynamics of liver injury as well as the inflammatory, fibrogenic, endothelial and progenitor cell responses in two common mouse models of CLD - CDE versus TAA administration.

3.3 Methods

Six-week old male C57BL/6J mice were randomly grouped and subjected to experimental conditions of the CDE and TAA model as well as a control diet. Animal numbers in each experimental group are listed in Table 3.1. Liver tissue and serum were harvested on days 3, 7, 14, 21 and 42 for further investigations. Firstly, overall liver damage was evaluated by body weight loss, histological assessment by haematoxylin and eosin staining, biochemical analyses of serum ALT levels, number of apoptotic cells, lipid accumulation and oxidative stress. Quantitation of apoptotic cells was performed by using the TUNEL assay, lipid accumulation was measured using Oil Red O staining and oxidative stress was evaluated according to gene expression levels of associated factors such as nuclear factor erythroid-derived 2-related factor 1 (Nrf1), thioredoxin (Txn) and NAD(P)H quinone oxidoreductase (Nqo1). The inflammatory response to either of the two dietary models was evaluated by fluorescent-labelling of $CD45^+$ cells and their quantitation, and also more specifically by analysing populations of liver-resident KCs by immunohistochemical analysis of $F4/80^+$ cells as well as infiltrating monocyte-derived macrophages by immunofluorescent detection of $CD11b^+$ cells. The resulting inflammatory microenvironment was assessed by gene expression analysis of cytokines and growth factors such as TWEAK, TNF, LTβ, IL6 and IFNγ, as well as HGF, using real-time PCR. Resulting special, temporal and numerical changes of

LPCs, HSCs and inflammatory cells were evaluated by immunofluorescent stainings using the markers panCK, αSMA and CD45. Furthermore, fibrotic patterns were assessed by analysing gene expression levels of the fibrosis-associated factors TGFβ, Collagen I (Col1), MMP2 and 9, and tissue TIMP1 and 2, and finalised by visualising collagen (I and III) deposition by Sirius Red staining and biochemical analysis of hydroxyproline levels. Changes in the hepatic vasculature were assessed by fluorescent staining of the endothelial markers CD31 and CD34. Disease-related histological findings were confirmed by an expert pathologist.

Time point (days)	**Animal number**		
	Control	*CDE*	*TAA*
3	4	6	6
7	4	7	6
14	4	4	6
21	4	4	6
42	4	4	6

Table 3.1: Number of animals in each experimental group.

3.4 Results

3.4.1 Divergent tissue damage dynamics and mechanisms in CDE- and TAA-induced liver injury.

To establish and compare the dynamics of CDE- and TAA-induced liver injury, alterations to liver architecture, markers of hepatocyte health and body weight, as an indicator of overall animal health, were evaluated. Throughout the study, disease parameters were assessed on days 3 and 7 (induction phase), 14 and 21 (establishment phase) and 42 days (maintenance phase).

Moderate weight loss of 5-10% was observed in TAA-induced injury compared to the CDE regimen, which caused the animals to lose up to 20% of their initial body weight during the induction phase. After this initial adaptation period, body weights of mice on both liver injury protocols recovered, but remained considerably lower than non-injured controls over the time course (Fig. 3.1).

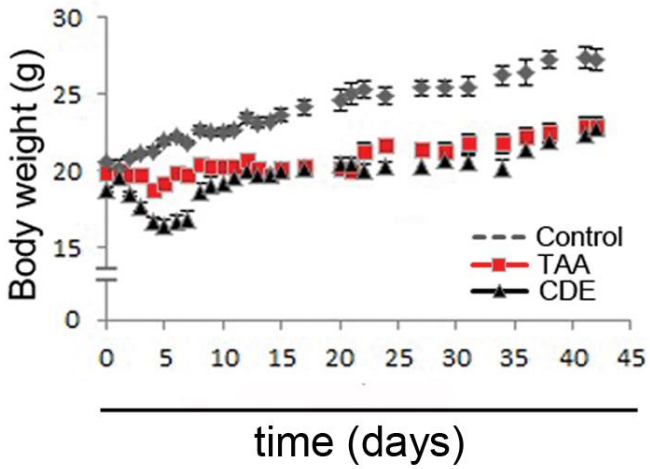

Fig. 3.1: Body weight of mice exposed to CDE, TAA and control diet. The body weight of CDE, TAA and control mice was measured progressively throughout the time course of 0-42 days. All mice from each time point were included in this figure. Data are shown as mean ± SEM and include all animals of each experimental group.

Histological assessment of liver architecture revealed overt differences in morphology associated with CDE or TAA administration. Major tissue damage was seen in CDE mice throughout the liver during the induction phase marked by hepatocyte degeneration, cell enlargement, swelling, rounding and sometimes hepatocyte ballooning. This was accompanied by periportal enrichment of small basophilic cells up to day 14. The liver architecture then returned to normal hepatocyte and general lobular morphology during the maintenance phase (Fig. 3.2). In contrast, TAA provoked centrilobular tissue damage with significant basophilic cell enrichment and formation of eosinophilic bands of hepatocytes as early as day 3, which remained unresolved during the time course (Fig. 3.2).

Dynamic alterations to liver architecture in each liver injury model were reflected in quantitative biochemical assessments of liver damage. Significant increases were observed in serum alanine transaminase (ALT) levels, a reliable indicator of hepatocyte injury, peaking at three days in both injury models (CDE, 64.9 ± 6.6 U/l; TAA, 68.7 ± 0.34 U/l). Serum ALT normalised to control levels after six weeks in CDE-treated mice (22.13 ± 3.6 U/l) but remained elevated in the TAA model (44.5 ± 1.2 U/l, Fig. 3.4.3A). Similarly, the number of $TUNEL^+$ apoptotic cells increased over the first seven days in both regimens but resolved by day 42 in the CDE injury. Conversely, apoptotic cells further increased by day 21 and remained elevated throughout the TAA-injury time course (Fig. 3.3B).

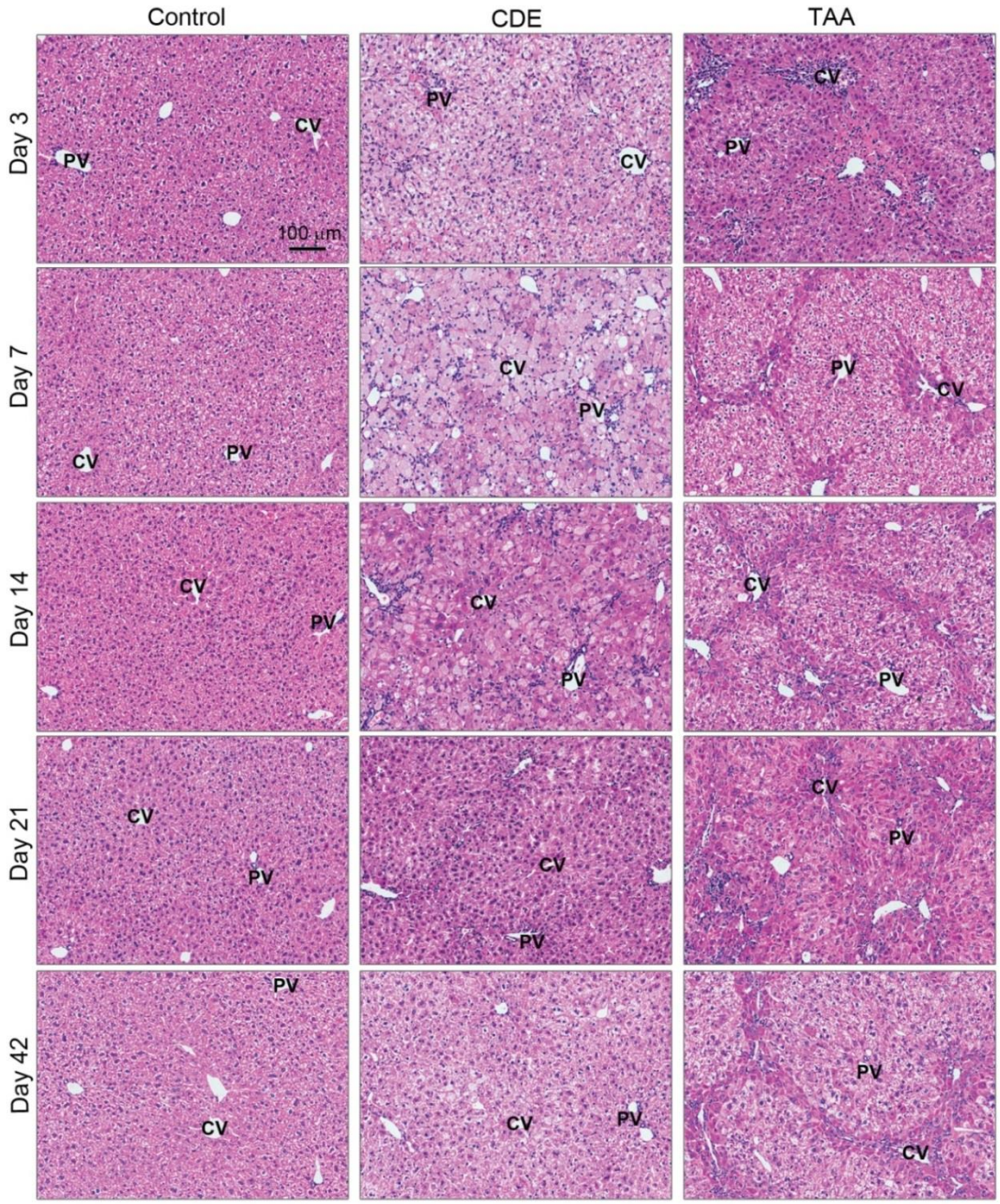

Fig. 3.2: Liver histology changes in response to CDE and TAA treatment. Formalin-fixed, paraffin-embedded liver sections of mice treated for 3, 7, 14, 21 and 42 days and respective controls were used for histological assessment by haematoxylin and eosin staining. The scale bar represents 100 µm, original magnification: x100. *CV*, central vein*; PV*, portal vein.

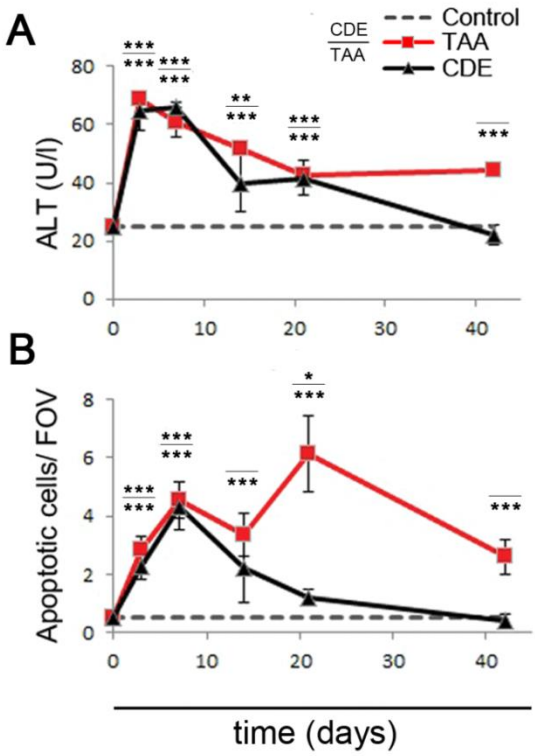

Fig. 3.3: CDE and TAA-induced CLD results in overall liver damage measured by increased ALT levels and enhanced apoptotic cell numbers. (A) Liver damage was assessed biochemically by measuring serum alanine transaminase (ALT) levels of mice exposed to CDE, TAA or control diet. (B) Apoptotic cells were fluorescently labelled and quantified as $TUNEL^{+}$ cell numbers in five fields of view (FOV) per sample. Data are expressed as mean ± SEM (4 to 6 mice per group). *p<0.05, p**<0.01, p***<0.001 compared to control mice.

Since lipid accumulation was observed in hepatocytes, a common histological finding in human CLD biopsies predisposing the patient to further complications, lipid deposition was compared between the two models. Livers were stained with Oil Red O, which detects lipids including mono-, di- and triglycerides, phospholipid and cholesterol. Mice exposed to TAA and CDE quickly induced substantial fatty changes in hepatocytes during the induction phase. The CDE model displayed significantly higher levels of lipid accumulation, resulting in macro- and microvesicular hepatic steatosis throughout the parenchyma and resolving from portal areas over time. Conversely, TAA supplementation induced pericentral hepatic fat deposition with a strong zonal distribution (Fig. 3.4 and 3.5A).

Furthermore, hepatic lipid deposition was examined by biochemically measuring total cholesterol levels as another indicator of steatosis. The hepatic cholesterol levels increased during the induction phase in CDE mice, consistent with the Oil Red O-determined lipid level elevations, then returned to control levels in the establishment and maintenance phases. Surprisingly, and in contrast to Oil Red O-determined steatosis, cholesterol levels were not increased at any time in the TAA regimen (Fig. 3.5B).

Since oxidative stress is implicated in the pathogenesis of CLDs that are associated with steatotic liver changes, oxidative stress markers were measured at the transcript level. Consistent with the detected hepatic lipid changes, expression levels of oxidative stress response mediator Nrf1 (Biswas and Chan 2010) and the anti-oxidant Txn (Okuyama *et al.* 2005) were significantly elevated during the induction phase with a peak at day 3 in CDE mice (Fig. 3.6). As with previously assessed parameters of liver injury, oxidative stress quickly decreased after an early induction phase in CDE-fed mice. In contrast, expression levels of Nrf1 and Txn remained elevated or progressively increased in the TAA model, with additional activation of the sensitive redox indicator Nqo1 (Hardwick *et al.* 2010) (Fig. 3.6).

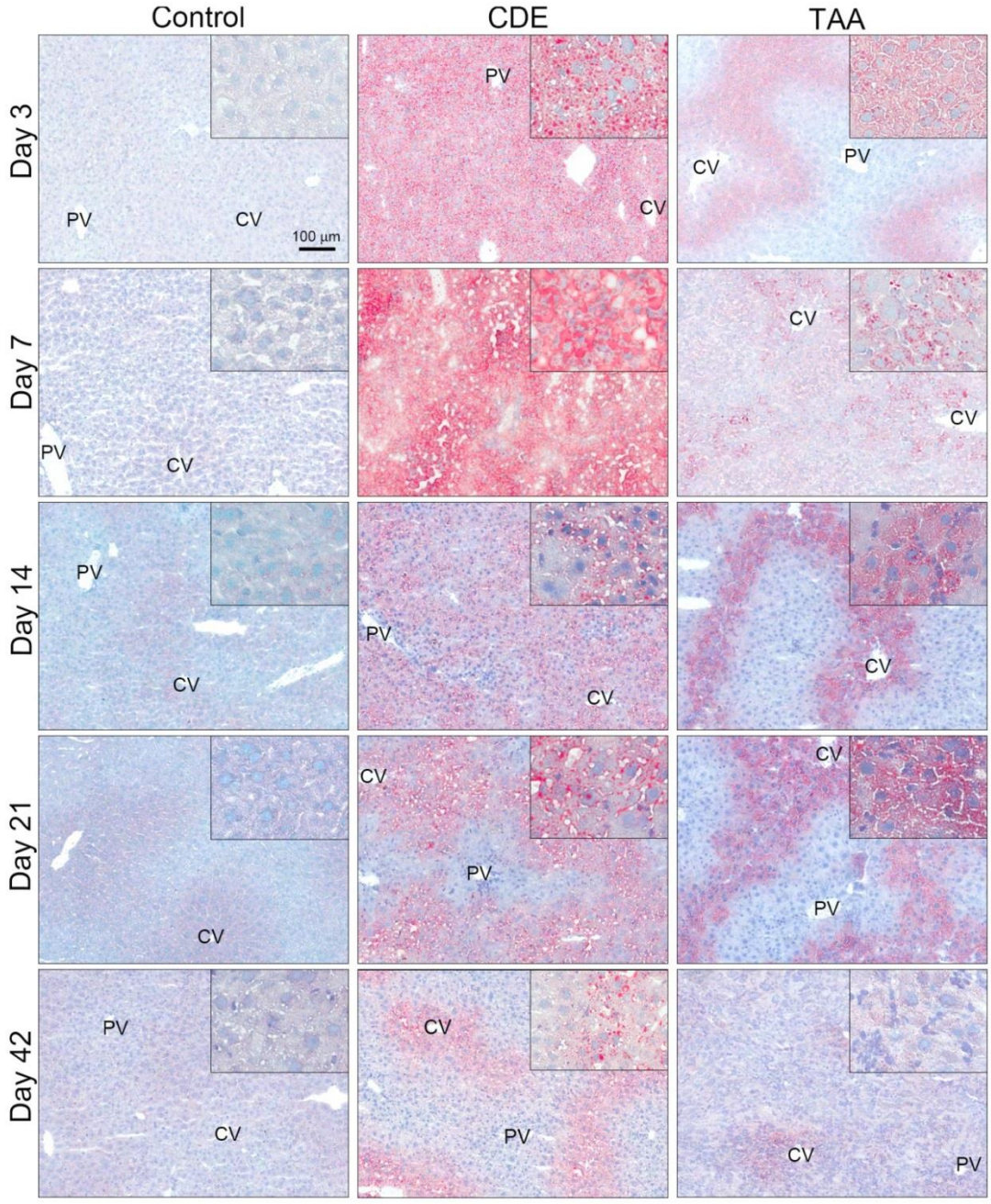

Fig. 3.4: Lipid accumulation and the distinct zonal distribution pattern caused by CDE and TAA exposure. Liver sections of CDE, TAA and control mice were stained for lipids using Oil Red O at day 3, 7, 14, 21 and 42. The scale bar represents 100 µm, original magnification: x100 and x400 for inserts. *CV*, central vein*; PV*, portal vein.

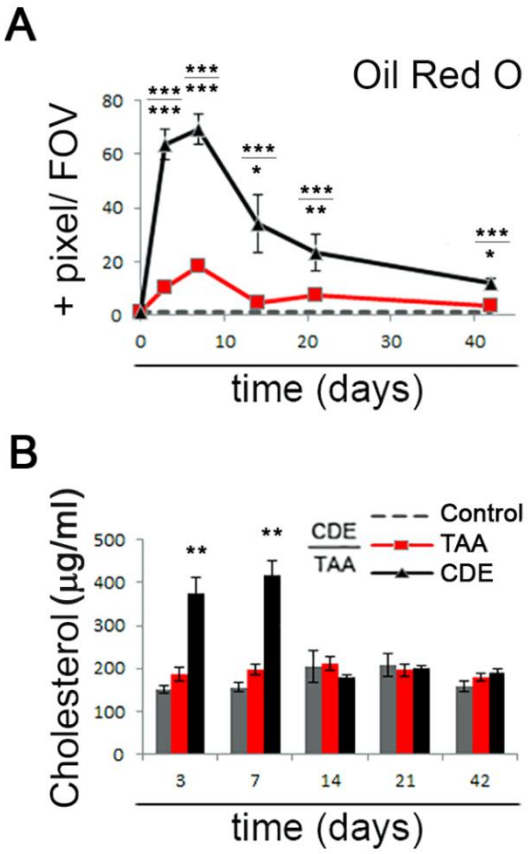

Fig. 3.5: CDE and TAA exposure induces enhanced lipid levels. (A) Liver sections of CDE, TAA and control mice were stained for lipids using Oil Red O at day 3, 7, 14, 21 and 42, (B) and quantified by positive (+) pixel counts (expressed as percentage) in five fields of view (FOV) per sample. Data are shown as mean ± SEM (4 to 6 mice per group). *p<0.05, p**<0.01, p***<0.001 compared to control mice.

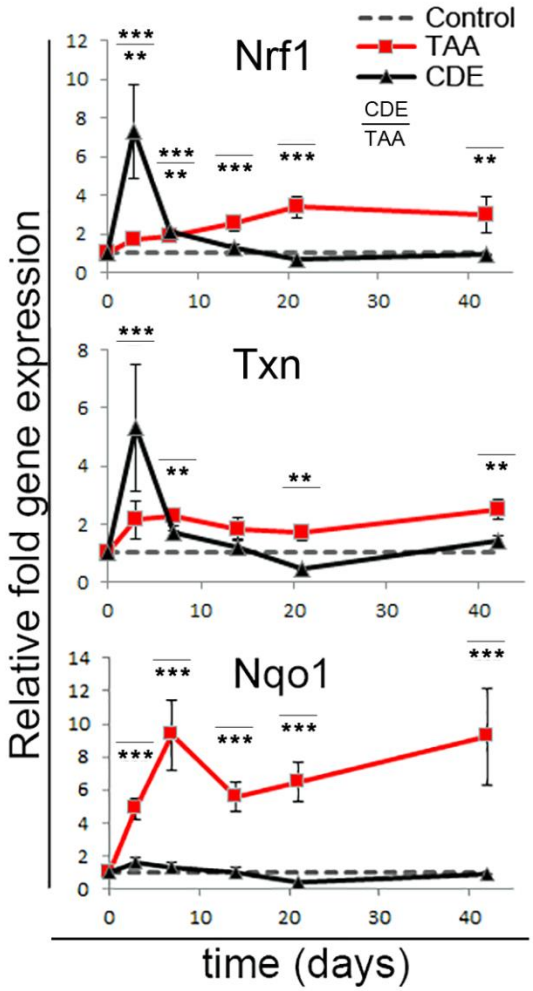

Fig. 3.6: Increased oxidative stress in response to CDE and TAA treatment. Oxidative stress was assessed through transcriptomic analysis of nuclear factor erythroid-derived 2-related factor 1 (Nrf1), thioredoxin (Txn) and NAD(P)H quinone oxidoreductase (Nqo1) expression levels. Data are shown as mean ± SEM (4 to 6 mice per group). *p<0.05, p**<0.01, p***<0.001 compared to control mice.

3.4.2 Injury-specific inflammatory signatures dictate disease progression patterns in the CDE- and TAA-induced liver injury.

The inflammatory response kinetics in these injury models were characterised by comparing the abundance of cells immunofluorescence-positive for the leukocyte common antigen CD45. Furthermore, monocyte-macrophage populations were more specifically examined by immunohistochemically staining for F4/80 (liver-resident macrophages or KCs) and immunofluorescent staining for CD11b (monocyte-derived macrophages) (Elsegood *et al.* 2015). Both regimens induced a rapid inflammatory response with $CD45^+$ (Fig. 3.7A), $CD11b^+$ (Fig. 3.7B and Fig. 3.8) and $F4/80^+$ cell numbers (Fig. 3.7C and Fig. 3.9) peaking at day three in the TAA and day seven in the CDE model. The number of inflammatory cells then slowly returned towards control levels in both regimens but remained significantly elevated in TAA-treated mice. However, Kupffer cell numbers in mice exposed to TAA treatment returned towards control levels similarly to cell numbers in CDE mice. Both models induced increasing cell numbers of liver resident ($F4/80^+$) and infiltrating, monocyte-derived macrophage populations ($CD11b^+$) in damaged lobular regions (CDE, portal; TAA, central). Although this spatial arrangement persisted in the TAA model, the clustered localisation of inflammatory cells reversed to an even lobular distribution from day 14 in CDE-fed mice (Fig. 3.8 and 3.9).

The early expansion of inflammatory cell numbers in both models was accompanied by rapid modulation of the liver microenvironment. An induction or significant increase in transcript expression levels was observed for the proinflammatory cytokines TWEAK, TNF, LTβ, IL6 and IFNγ, as well as HGF, which plays a key role in hepatocyte survival and tissue remodelling during liver injury. Once again, in the CDE model, expression levels normalised, while they remained elevated in TAA-treated mice (Fig. 3.10).

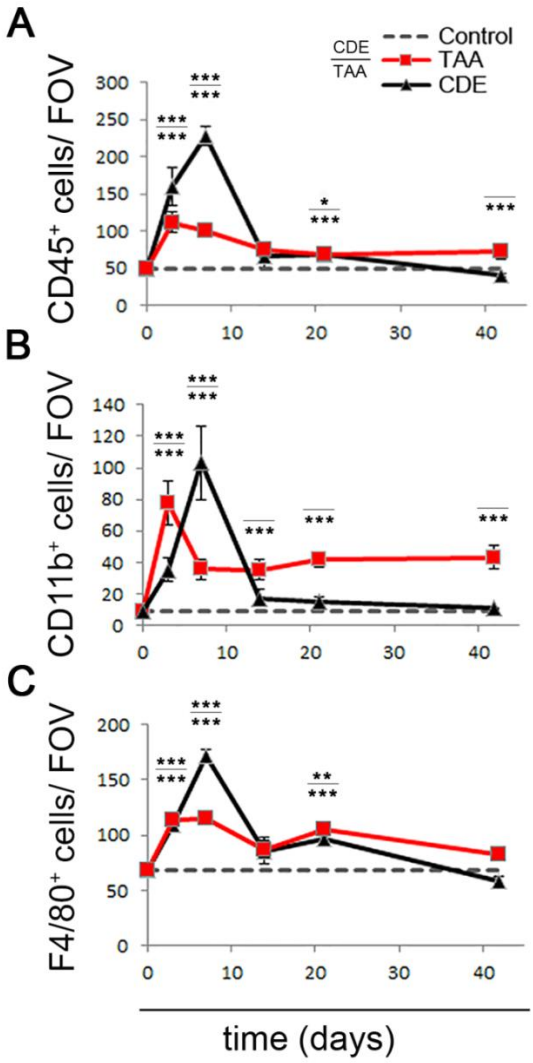

Fig. 3.7: CDE- and TAA-induced CLD results in increased inflammatory cell numbers. Cells positively stained for (A) CD45, (B) the monocyte-derived macrophage marker CD11b and (C) the liver-resident Kupffer cell marker F4/80, respectively, were quantified in five fields of view (FOV) per sample. Data are shown as mean ± SEM (4 to 6 mice per group). *p<0.05, p**<0.01, p***<0.001 compared to control mice.

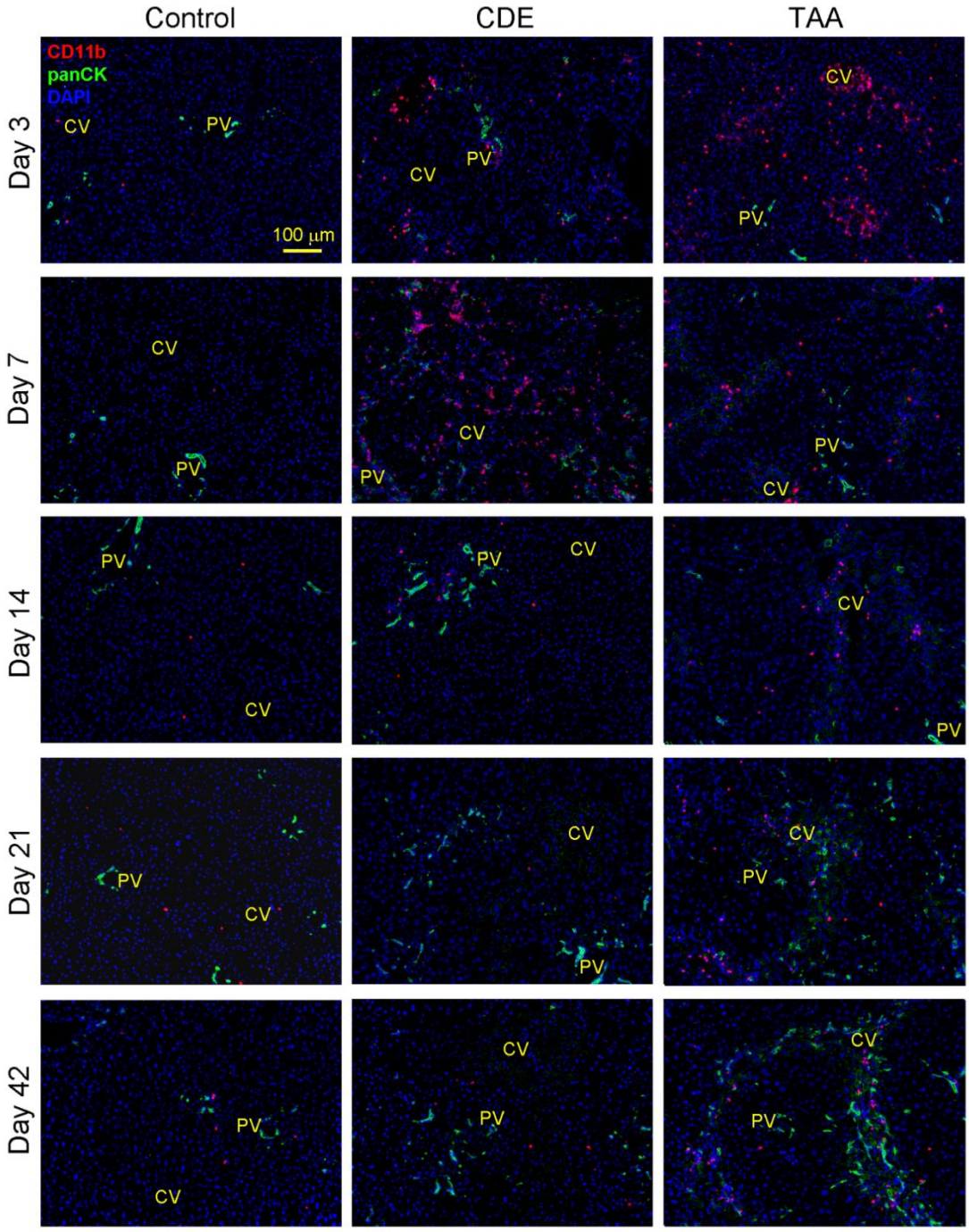

Fig. 3.8: CDE and TAA exposure induce enhanced CD11b$^+$ cell numbers. Frozen liver sections from day 3, 7, 14, 21 and 42 were fluorescently labelled for the monocyte-derived macrophage marker CD11b and the LPC marker pan-cytokeratin (panCK). Nuclei were visualised by DAPI staining. Representative images are shown. The scale bar depicts 100 µm. *CV*, central vein*; PV*, portal vein.

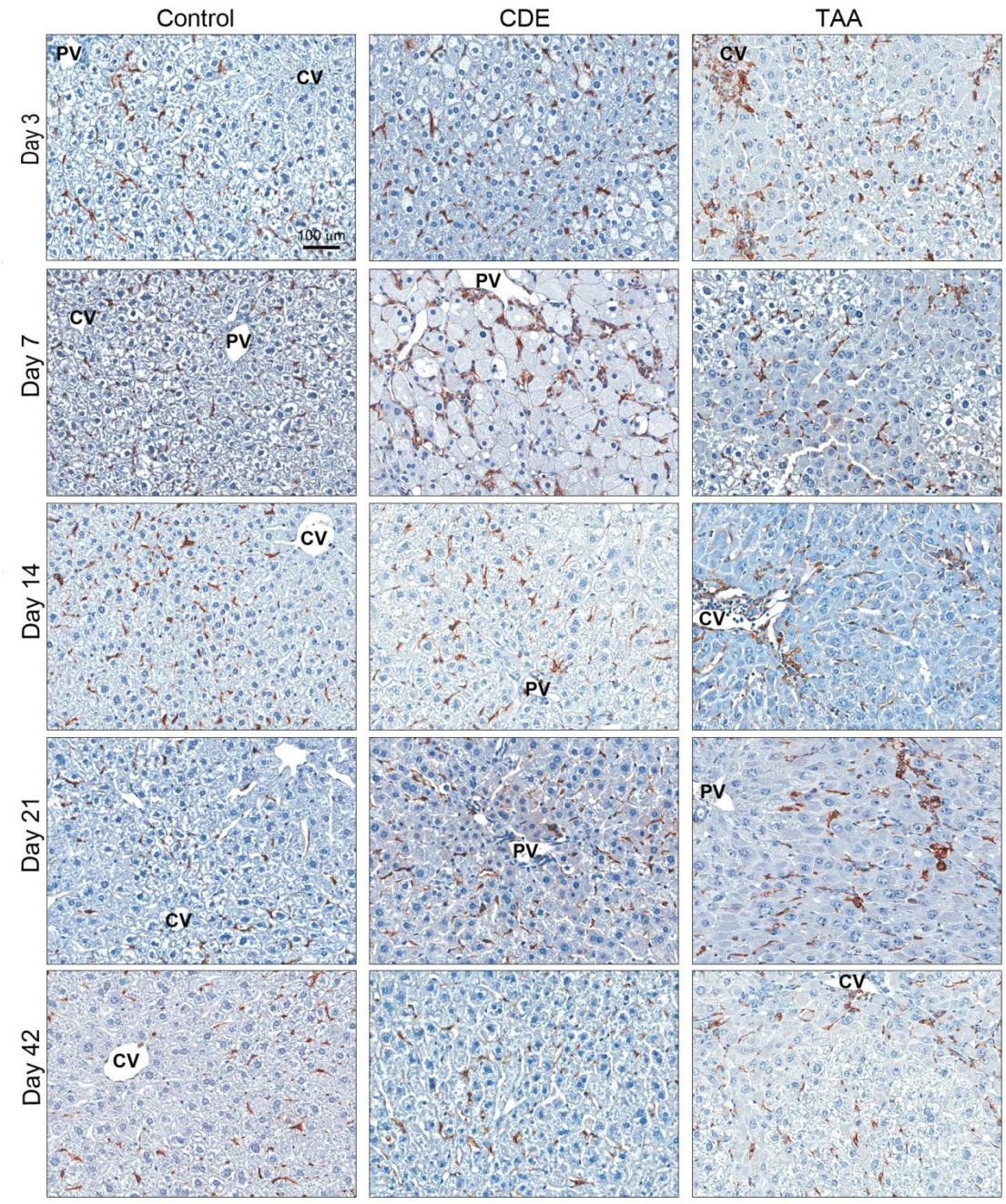

Fig. 3.9: Increased F4/80$^+$ cell numbers following CDE and TAA treatment. Formalin-fixed, paraffin-embedded liver sections of CDE, TAA and control mice were immunohistochemically labelled for the liver-resident KC marker F4/80. Representative images of are shown. The scale bar represents 100 µm. *CV*, central vein*; PV*, portal vein.

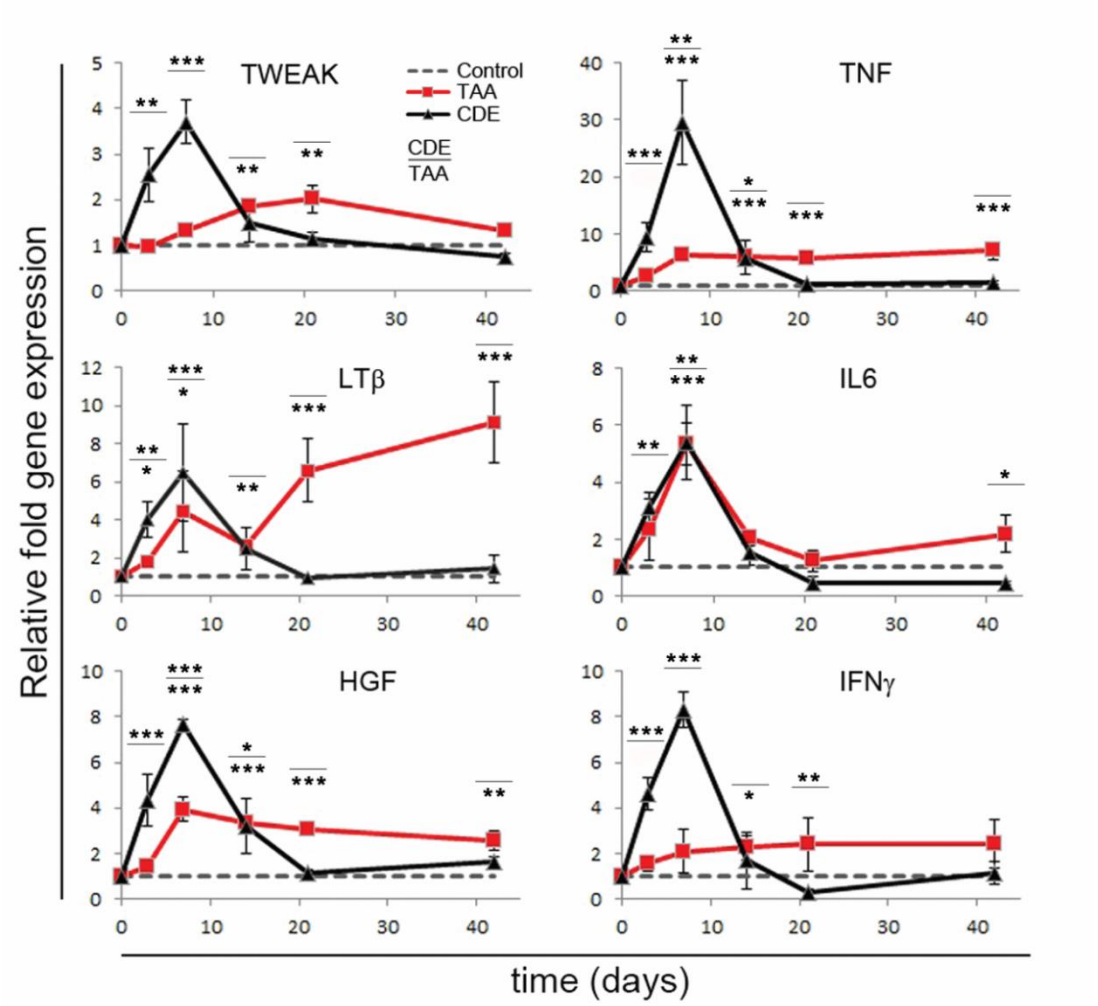

Fig. 3.10: Inflammatory marker expression is increased in CDE- and TAA-induced CLD. Real-time PCR data for mRNA expression levels of tumour necrosis factor (TNF), TNF-like weak inducer of apoptosis (TWEAK), lymphotoxin β (LTβ), interleukin 6 (IL6), interferon γ (IFNγ) and hepatocyte growth factor (HGF) were normalised and expressed as mean ± SEM (4 to 6 mice per group). *p<0.05, p**<0.01, p***<0.001 compared to controls.

3.4.3 Regenerative niches of CDE- and TAA-induced injury display temporal, compositional and spatial differences.

On the background of a significantly altered liver microenvironment, the organisation of the cellular niche, which is proposed to mediate injury, fibrosis and regeneration in most CLDs comprising (i) injury-responsive inflammatory cells, (ii) regenerative LPCs and/or DRs and (iii) fibrosis-driving, activated HSCs (myofibroblasts) was investigated. Immunofluorescent triple staining for CD45, the biliary cell and LPC marker panCK (distinguished by morphology) and the myofibroblast marker αSMA revealed a close spatial and temporal relationship between all three cell populations during the early induction phase in the CDE model. This niche was detected periportally, where numbers of $panCK^+$ cells peaked at 14 days post-induction and maintained a steady-state throughout the remaining four weeks. Strikingly, TAA treatment resulted in niche formation in centrilobular, rather than periportal regions. $PanCK^+$ biliary structures and LPCs, the majority of $CD45^+$ inflammatory cells and αSMA^+ myofibroblasts were only observed in close association from about day 21 onwards. Furthermore, numbers of $panCK^+$ cells progressively increased throughout the time course (Fig. 3.11 and Fig. 3.12).

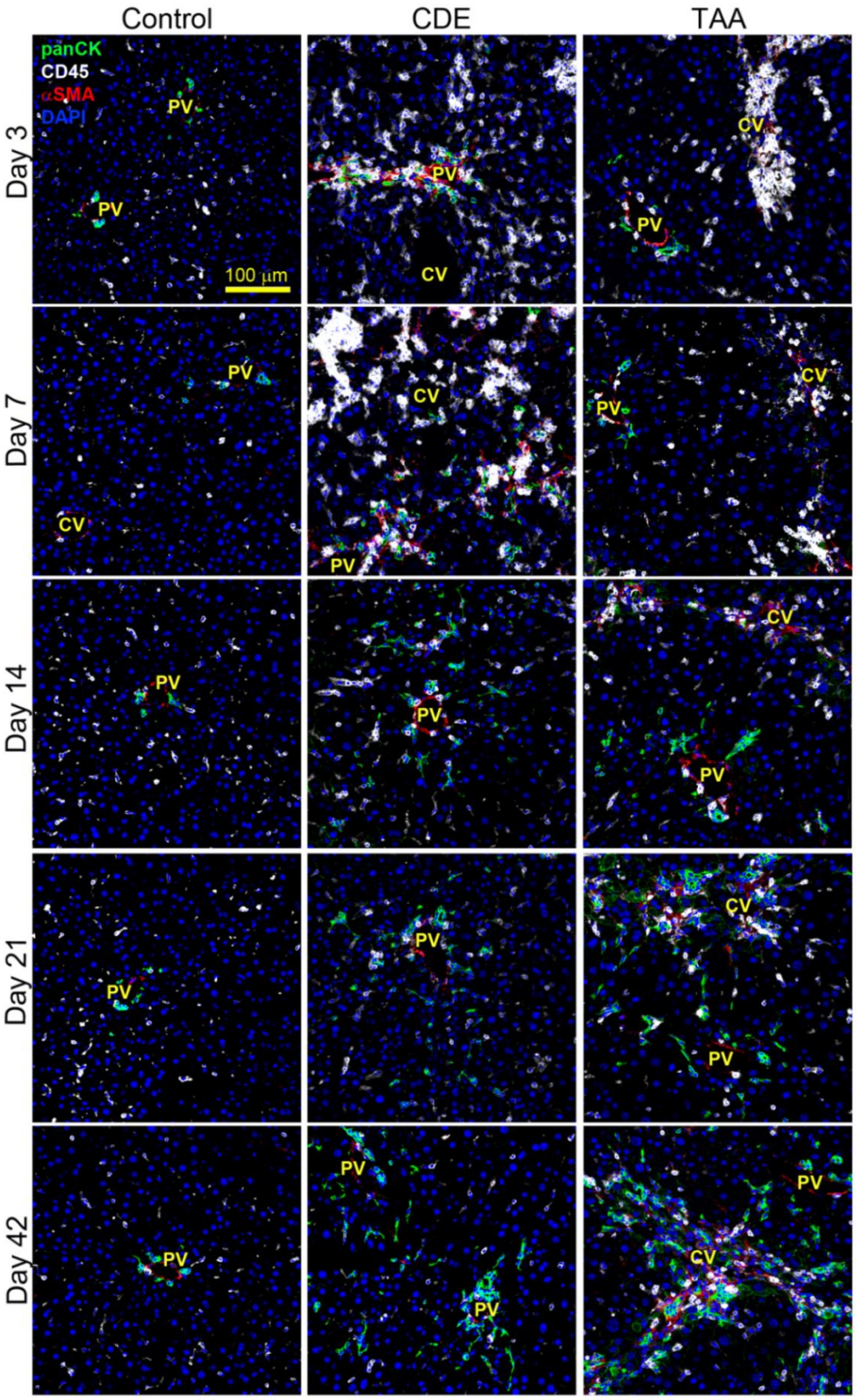

Fig. 3.11: CDE- and TAA-induced tissue regeneration is mediated by the cellular niche hosting LPCs, inflammatory cells and activated HSCs as part of the DR. Please refer to following page for figure legend.

Fig. 3.11: CDE- and TAA-induced tissue regeneration is mediated by the cellular niche hosting LPCs, inflammatory cells and activated HSCs as part of the DR. Control, CDE and TAA liver sections of day 3, 7, 14, 21 and 42 were fluorescently labelled for the biliary cell and LPC marker pan-cytokeratin (panCK), inflammatory cell marker CD45, the activated HSC marker α-smooth muscle actin (αSMA) and DAPI for nuclear quantitation. Representative images are shown and the scale bar depicts 100 µm. Original magnification: x200. *CV*, central vein*; PV*, portal vein.

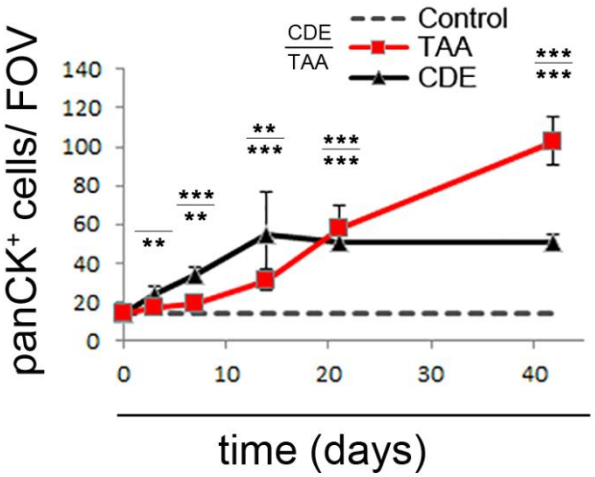

Fig. 3.12: Increased panCK$^+$ cell numbers induced by CDE and TAA. Cells positively stained for panCK were quantified in five fields of view (FOV) per sample. Numbers are expressed as mean ± SEM (4 to 6 mice per group). *p<0.05, p**<0.01, p***<0.001 compared to controls.

3.4.4 CDE- and TAA-induced injuries lead to distinct fibrogenic responses.

Since the progression of most chronic liver injuries is associated with ECM remodelling and the excessive deposition of matrix proteins, it was of particular interest to compare fibrosis-associated processes in both models. These were evaluated in detail by transcriptomic analysis of fibrogenic markers, quantitation of activated HSC numbers, visualisation of collagen deposition by Sirius Red staining, and biochemical hydroxyproline assessment.

Expression levels of the fibrosis-associated factors TGFβ, Col1, MMP 2 and 9, and TIMP 1 and 2 were significantly increased in both injury models. Increased expression of these factors was induced during the initial phase at day 3 and 7, and normalised thereafter in the CDE model. Conversely, consistent with previously investigated injury parameters, a mostly progressive increased expression in fibrosis-associated genes was observed in TAA-fed mice over the course of six weeks (Fig. 3.13).

Since activated HSCs represent the main fibrosis-driving hepatic cell type, the numbers of αSMA^{+} myofibroblasts were assessed in all phases of induced liver injury. Indeed, the quantitation results followed the same trend in both models, with an early peak and subsequent normalisation of activated HSC numbers in CDE mice and a gradual significant increase in the TAA model (Fig. 3.14). While HSCs were mainly activated in periportal regions during the induction phase of CDE treatment, they were localised to central areas in TAA-induced mice, demonstrating a cumulative organisation pattern (Fig. 3.11).

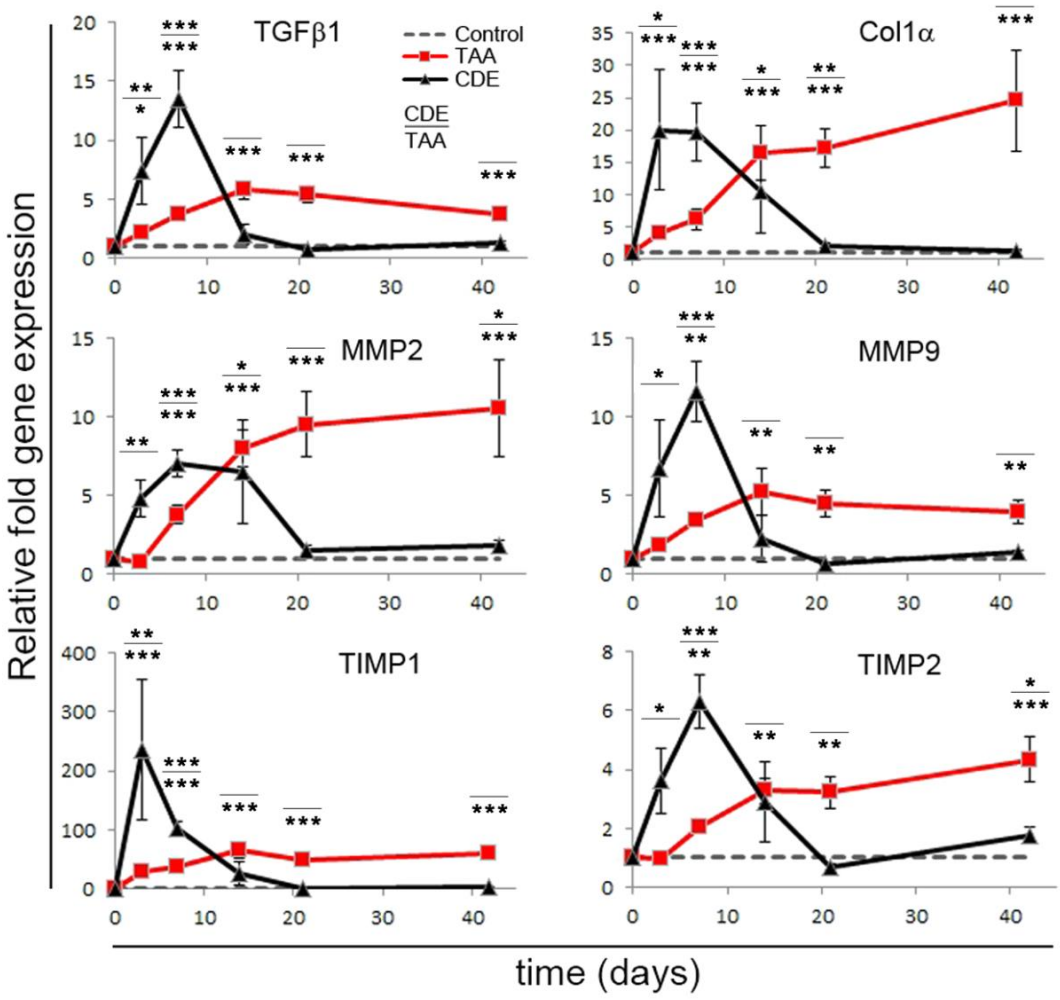

Fig. 3.13: Fibrogenic marker expression is enhanced in CDE- and TAA-induced CLD. Real-time PCR data for mRNA expression levels of transforming growth factor β (TGFβ), Collagen I (Col1), matrix metalloproteinase (MMP) 2 and 9, tissue inhibitor of metalloproteinase (TIMP) 1 and 2 are expressed as mean ± SEM (4 to 6 mice per group). *p<0.05, p**<0.01, p***<0.001 compared to controls. Data are normalised and expressed relative to control levels.

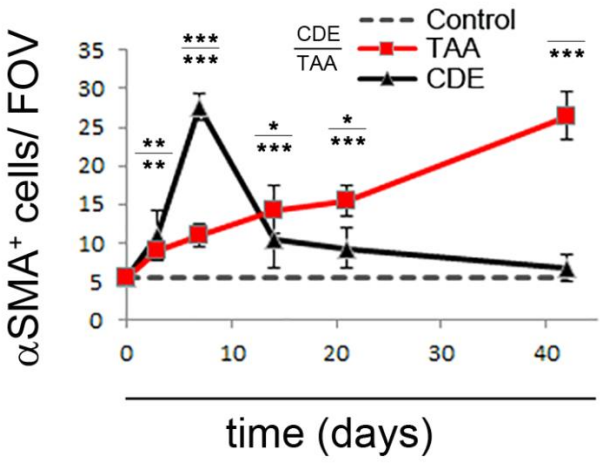

Fig. 3.14: Increased αSMA$^+$ cell numbers induced by CDE and TAA treatment. Cells positively stained for the activated HSC marker α-smooth muscle actin (αSMA) were quantified in five fields of view (FOV) per sample. Cell numbers are expressed as mean ± SEM (4 to 6 mice per group). *p<0.05, p**<0.01, p***<0.001 compared to controls.

Additionally, gross collagen deposition and associated fibrosis patterns were examined using the histopathological stain Sirius Red. Thin layers of collagen surrounded the portal tracts and central veins in control mice, and are a typical feature of a healthy liver. In contrast, both liver injury regimens induced significant collagen accumulation, albeit with very different dynamics and spatial organisation. CDE exposure resulted in early portal fibrosis with 'chicken wire' appearance in the induction phase, and normalisation thereafter. However, TAA-treated livers displayed significant collagen deposition in central areas, as early as day 3 post-induction. The substantial pericentral fibrosis then progressed to form central-central septa in the late establishment and maintenance phase. In addition, portal-to-central bridging fibrosis was occasionally observed when portal and central fields were in close proximity during the later injury phases (Fig. 3.15).

Finally, biochemical examination of hepatic hydroxyproline content confirmed increased collagen deposition, consistent with previously established fibrosis-associated patterns. Thus CDE-mediated collagen deposition peaked at day 7 (225.1 ± 7.4 ng/mg of liver tissue), and then subsequently resolved, whereas the TAA regimen stimulated a progressive collagen accumulation throughout the examined time period, showing the highest level (208.6 ± 25.8 ng/mg of liver tissue) at day 42 of the maintenance phase (Fig. 3.16).

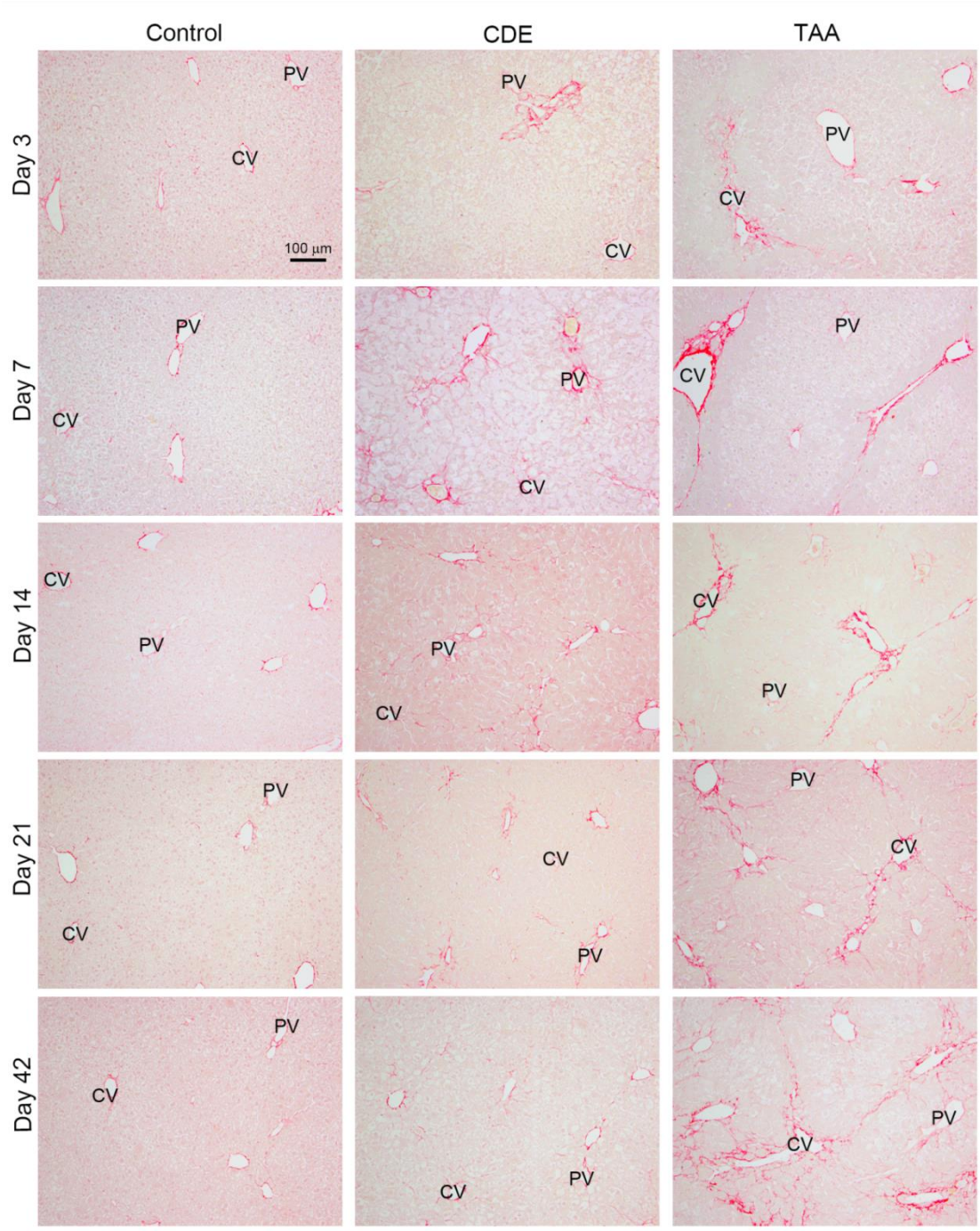

Fig. 3.15: CDE and TAA exposure induces the deposition of collagen and dictates a divergent fibrogenic response. Liver sections of control, CDE and TAA mice were assessed for collagen deposition by Sirius Red staining at days 3, 7, 14, 21 and 42. Representative images are shown. The scale bar represents 100 µm (original magnification: x100). *CV*, central vein*; PV*, portal vein.

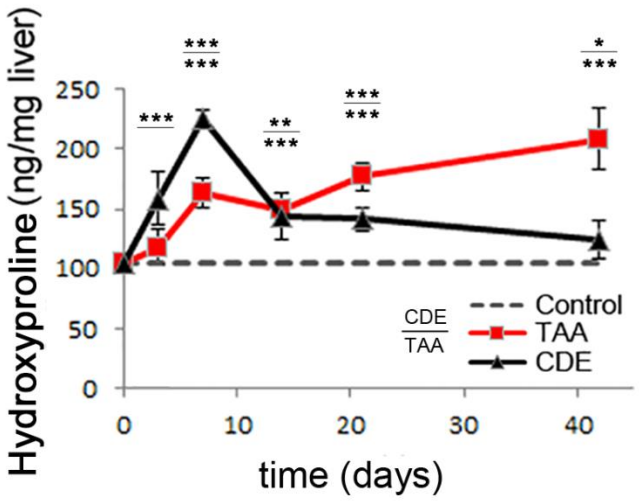

Fig. 3.16: Elevated hydroxyproline levels in response to CDE and TAA treatment. Homogenised liver tissue was used to quantitate collagen deposition by measuring the corresponding hydroxyproline level. Hydroxyproline levels were calculated as µg per mg liver tissue. Data are shown as mean ± SEM (4 to 6 mice per group). *p<0.05, p**<0.01, p***<0.001, compared to control mice.

3.4.5 Hepatic endothelial cell phenotypes in response to CDE- and TAA-induced CLD

Since fibrosis is associated with severe changes in the hepatic vascular system (Iwakiri *et al.* 2014), endothelial phenotypes were investigated by immunofluorescent staining of the endothelial markers CD31 and CD34 in mice subjected to CDE and TAA for 14 and 42 days.

The examination of the CD31 staining pattern revealed universal expression in both models as well as the controls and thus CD31 represents a general marker for hepatic sinusoidal epithelial cells regardless of the treatment status (Fig. 3.17, Fig. 3.18 and Fig. 3.19). The common pattern of CD31 expression showed positive staining in portal vessel-lining cells including portal veins and hepatic arteries, as well as endothelial cells of central veins. Moreover, CD31 expression was seen in the parenchyma, staining sinusoids with a characteristic elongated shape but also rounded LSECs. In contrast to CDE and control mice, the TAA model induced enhanced positivity for CD31 in central areas at day 42 (Fig. 3.19), consistent with injury progression and establishment of the regeneration niche, indicating progressive angiogenesis in response to TAA treatment. In addition, analysis of the location of $CD31^+$ cells and $panCK^+$ LPCs showed no spatial or temporal relationship in CDE-treated mice, however TAA exposure induced close proximity within the regeneration niche at day 42 (Fig. 3.18 and Fig. 3.19).

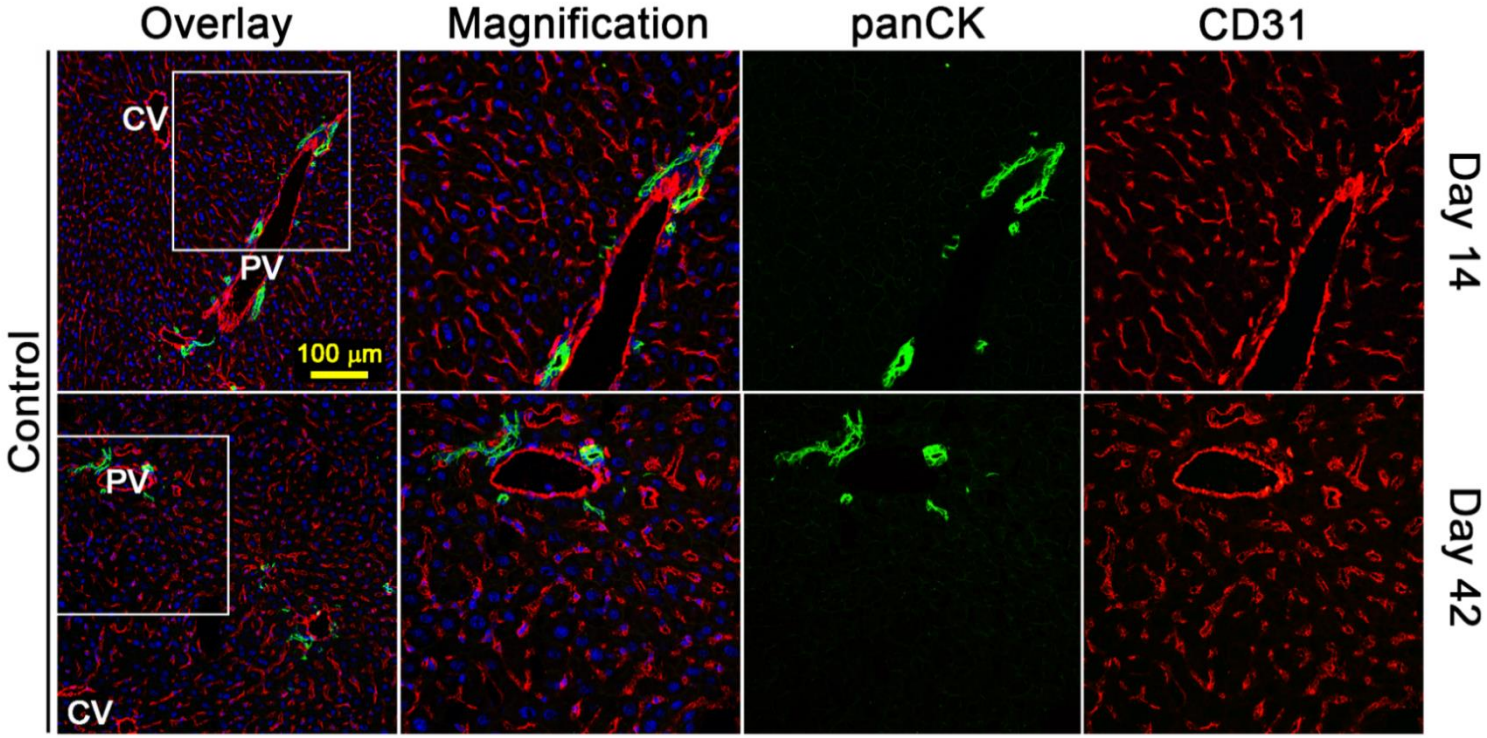

Fig. 3.17: Investigation of the endothelial marker CD31 in control mice. Frozen sections of mice fed a control diet for 14 and 42 days were fluorescently labelled with the endothelial marker CD31 and the LPC/biliary cell marker panCK. Nuclei were visualised by DAPI staining. Representative pictures are shown and the scale bar represents 100 µm. *CV*, central vein*; PV*, portal vein.

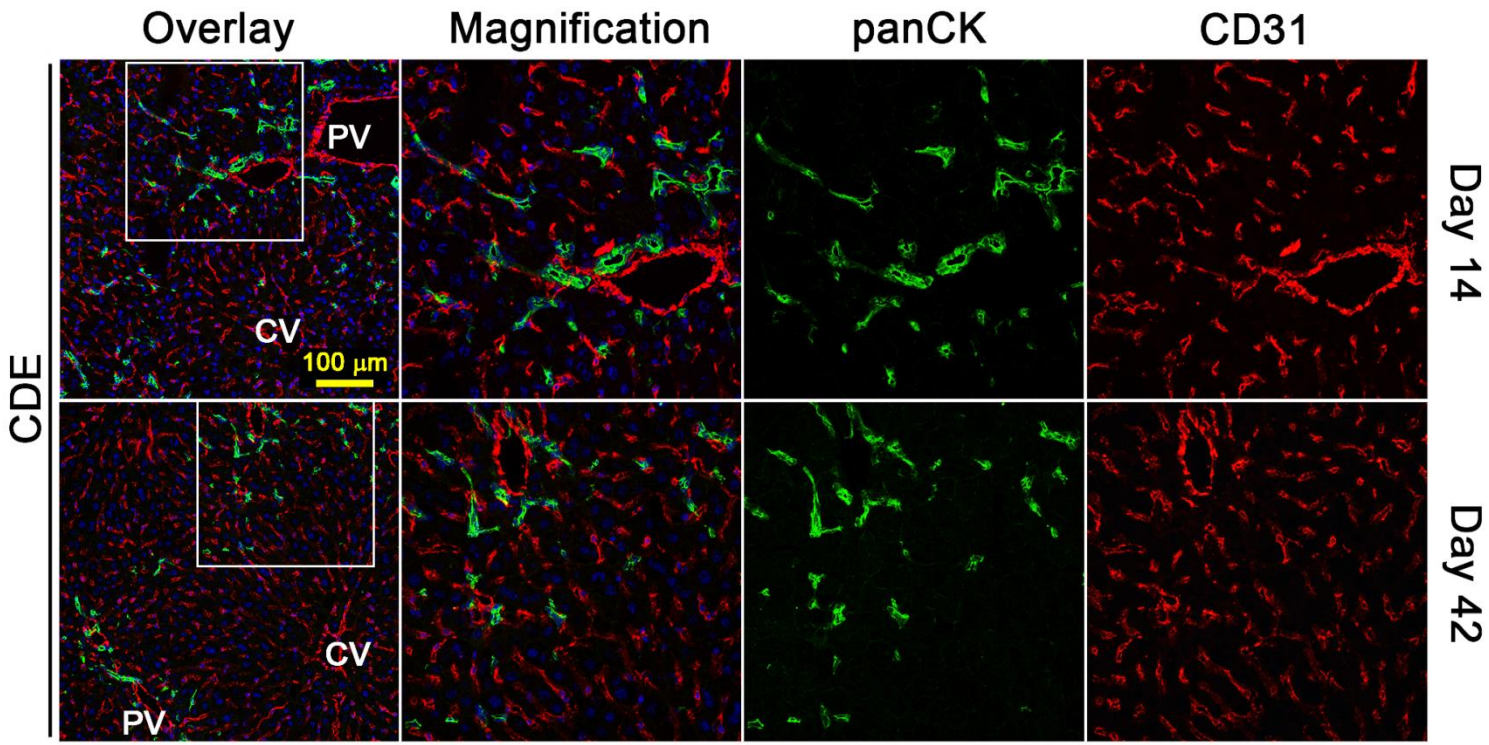

Fig. 3.18: Investigation of the endothelial marker CD31 in CDE-treated mice. Frozen sections of mice exposed to CDE treatment for 14 and 42 days were labelled with the endothelial marker CD31 and the LPC/biliary cell marker panCK using immunofluorescence. Nuclear staining was performed with DAPI. Representative pictures are shown and the scale bar depicts 100 µm. *CV*, central vein*; PV*, portal vein.

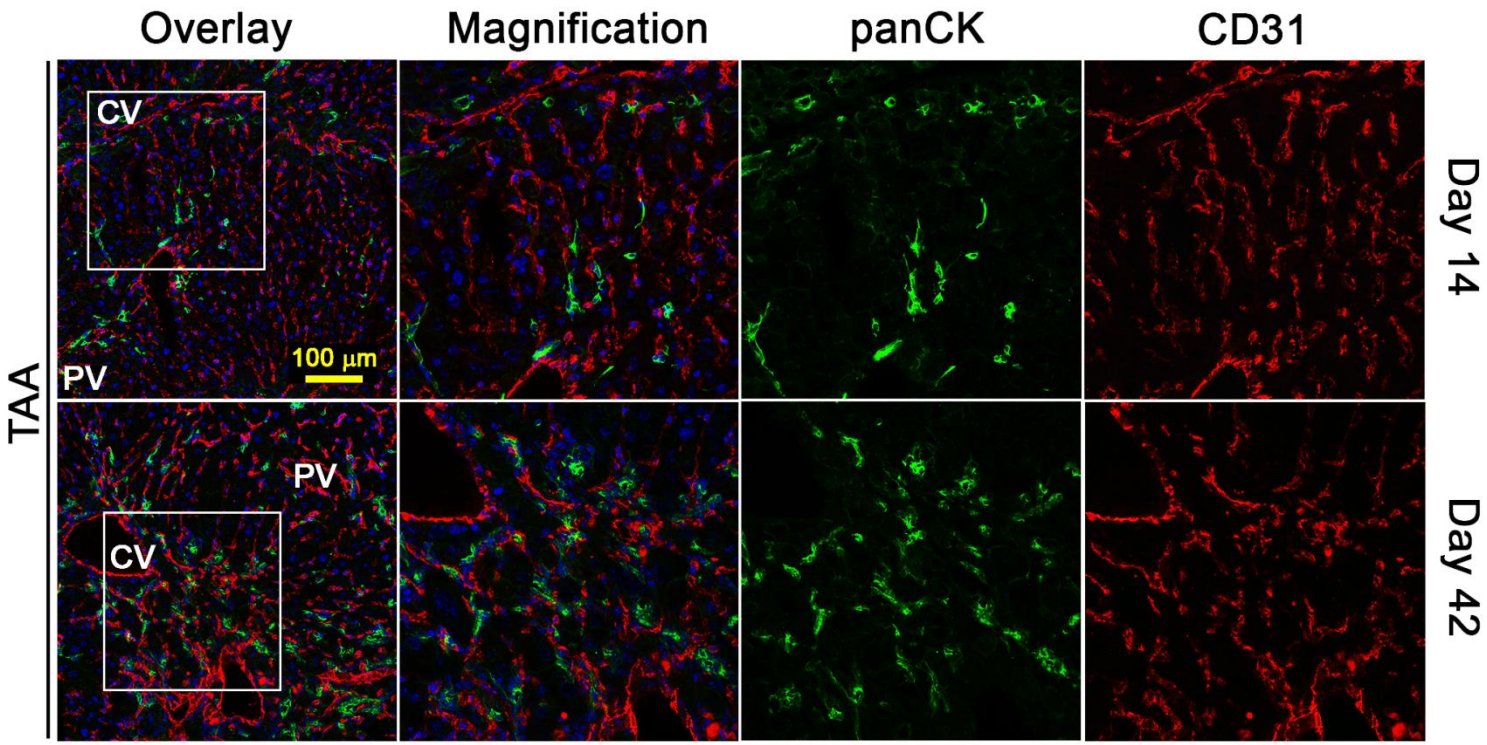

Fig. 3.19: Evaluation of the endothelial marker CD31 in TAA-treated mice. Frozen sections of mice treated with TAA for 14 and 42 days were fluorescently labelled with the endothelial marker CD31 and the LPC/biliary cell marker panCK. Nuclei were counterstained using DAPI staining. Representative pictures are shown and the scale bar represents 100 µm. *CV*, central vein*; PV*, portal vein.

In contrast to CD31 expression, CD34 staining showed model-specific patterns varying greatly between CDE- and TAA-induced CLD. In control mice at day 14 and 42, CD34 expression was limited to portal areas, where $CD34^+$ cells represent portal endothelial cells that line the portal vein and hepatic artery but also surround the $panCK^+$ biliary cells (Fig. 3.20). Similar to controls, CDE mice showed CD34 positivity mainly in portal fields, with occasional appearance of rounded single $CD34^+$ cells in the parenchyma in close proximity to $panCK^+$ LPCs (Fig. 3.21). Significant differences were observed in mice treated with TAA at all investigated time points (Fig. 3.22). Increasing numbers of cells expressing CD34 were found in a time-dependent manner, associated with the LPC response at day 14. On the background of progressive injury, a further increase of CD34 expression was detected centrally in a close spatial relationship with the regeneration niche at day 42 (Fig. 3.22). CD34 expression was not only limited to portal endothelial cells, since $CD34^+/CD31^+$ cells with an elongated shape were also frequently located in the parenchyma displaying sinusoid morphology (Fig. 3.22 and 3.23).

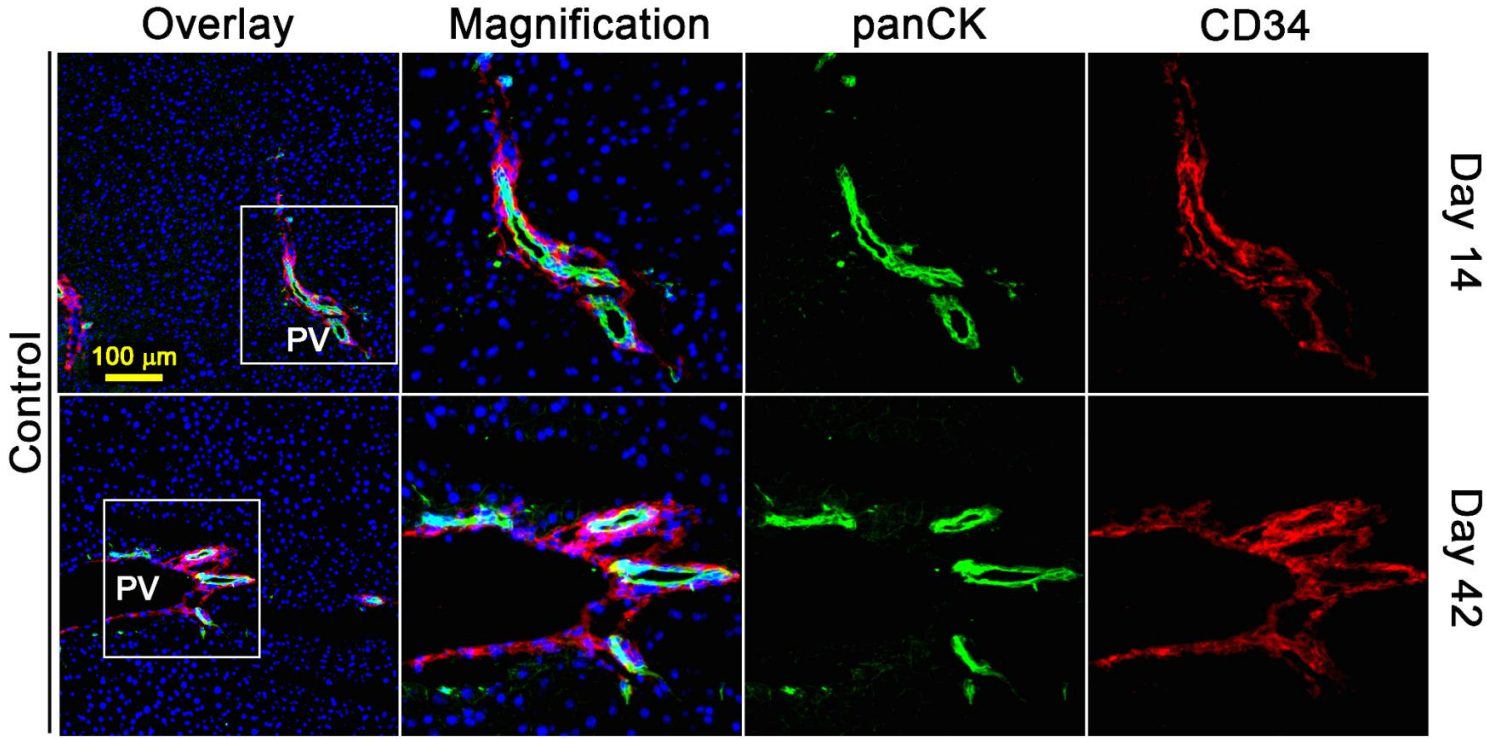

Fig. 3.20: Assessment of CD34 expression in control mice. Frozen sections of mice fed a control diet for 14 and 42 days were labelled with the endothelial marker CD34 and the cholangiocytic LPC marker panCK using immunofluorescence. Nuclei were stained with DAPI. Representative images are shown and the scale bar depicts 100 µm. *PV*, portal vein.

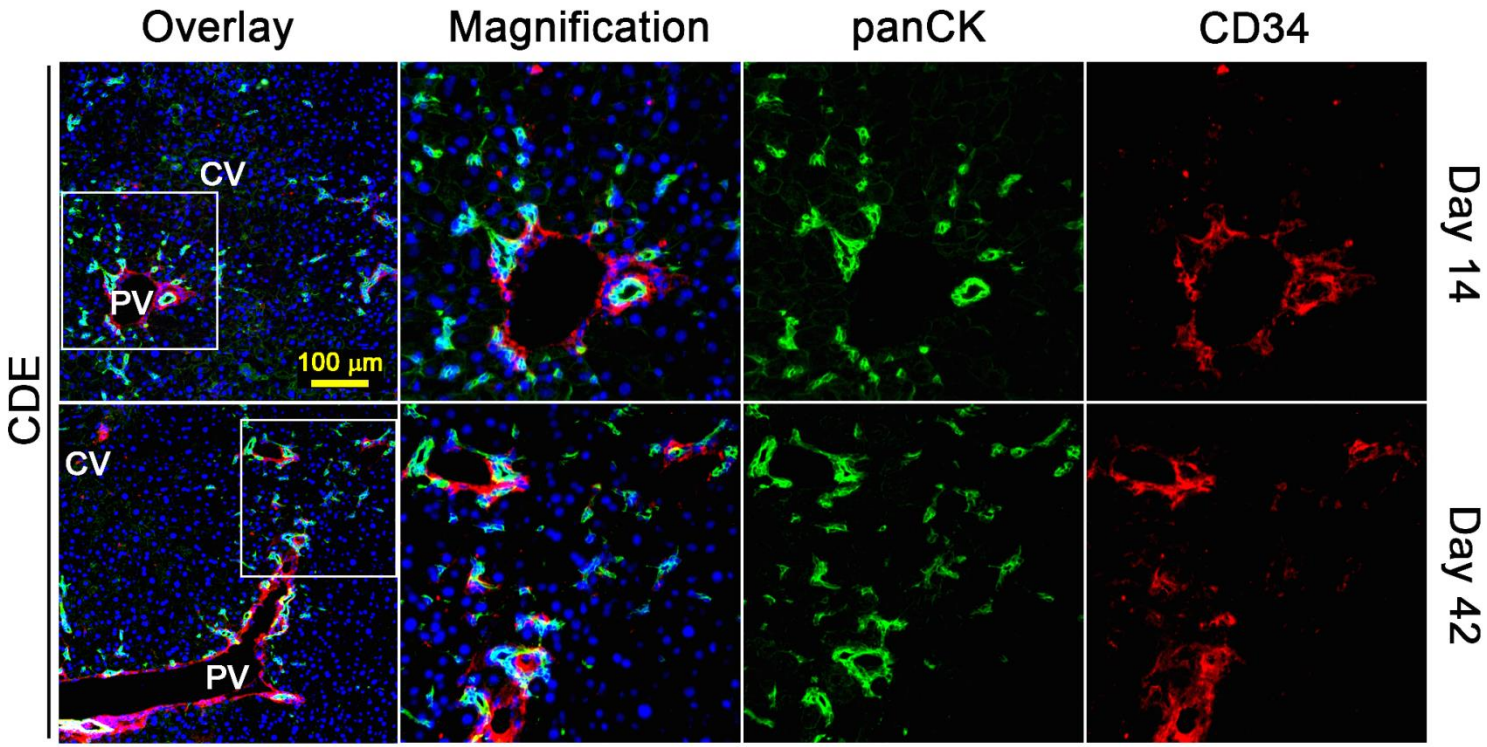

Fig. 3.21: Evaluation of CD34 expression in CDE-induced CLD. Frozen sections of mice treated with CDE for 14 and 42 days were fluorescently labelled with the endothelial marker CD34 and the cholangiocytic LPC marker panCK. Nuclear staining was performed with DAPI. Representative pictures are shown and the scale bar represents 100 µm. *CV*, central vein*; PV*, portal vein.

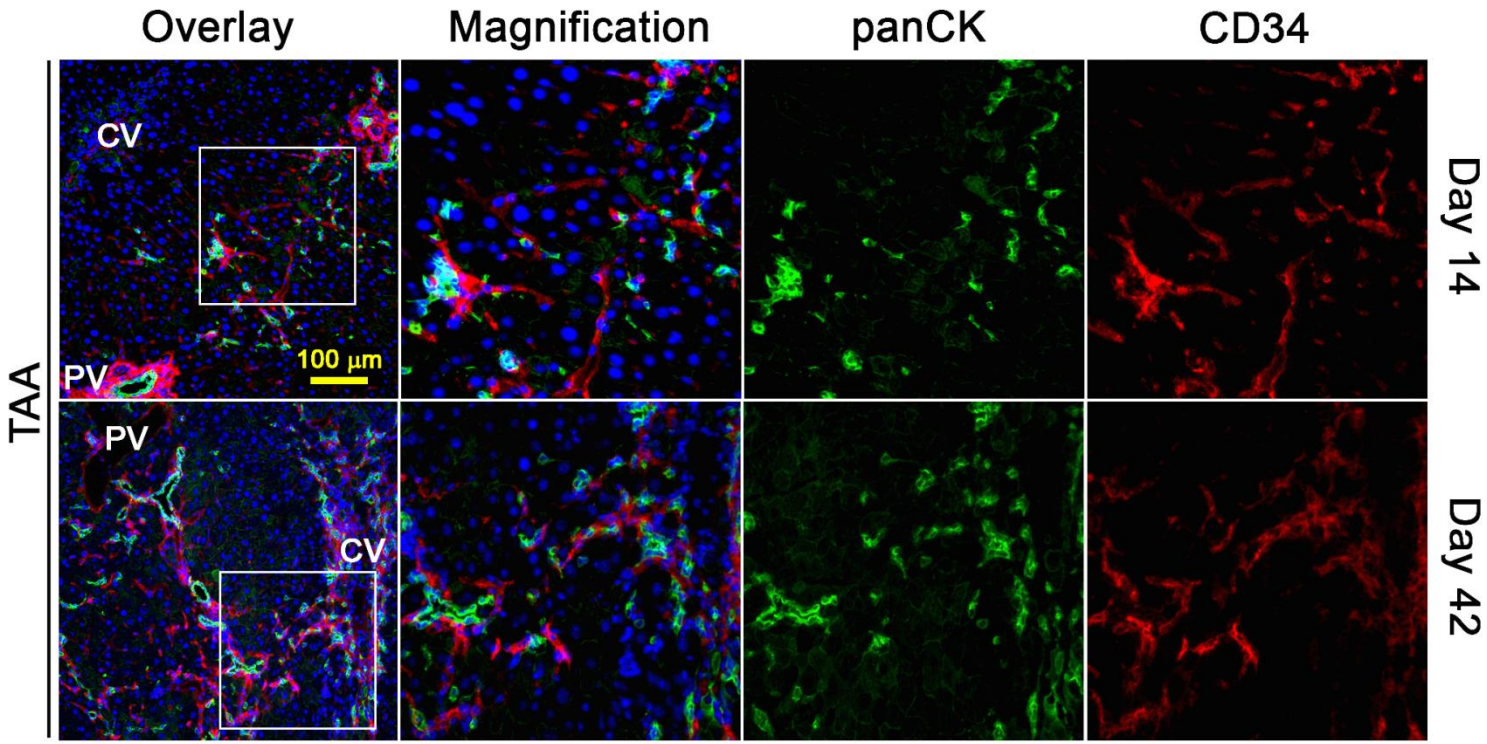

Fig. 3.22: Investigation of CD34 expression in TAA-induced CLD. Frozen sections of mice exposed to TAA treatment for 14 and 42 days were labelled with the endothelial marker CD34 and the cholangiocytic LPC marker panCK using immunofluorescence. Nuclei were counterstained with DAPI. Representative images are shown and the scale bar depicts 100 µm. *CV*, central vein*; PV*, portal vein.

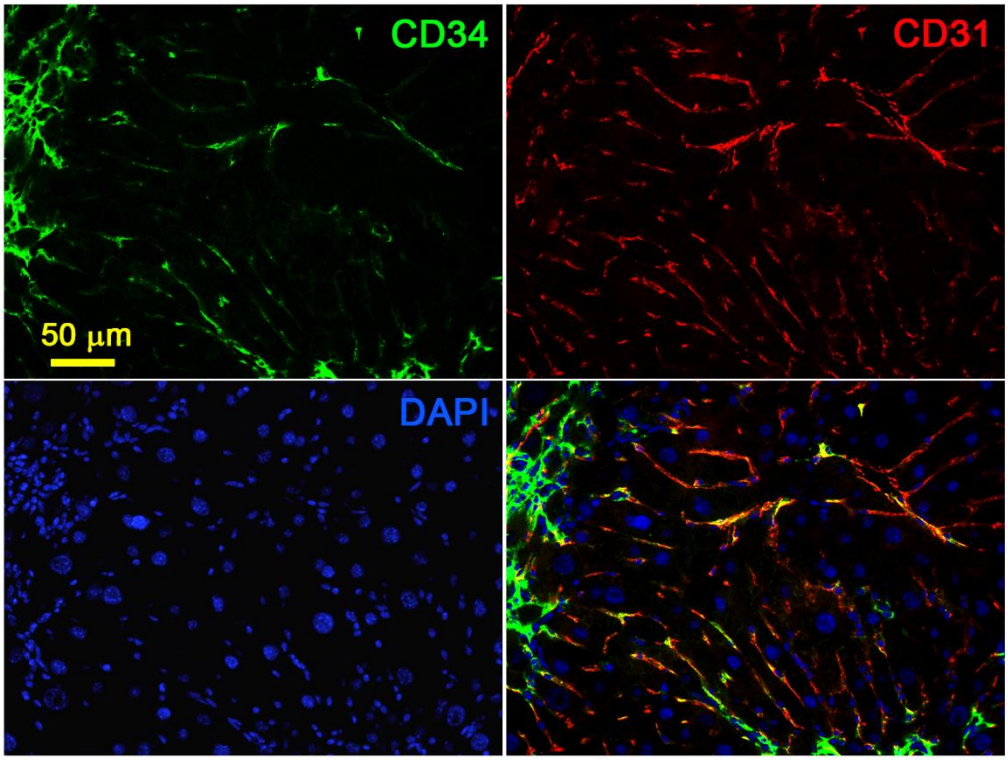

Fig. 3.23: TAA-induced CD34$^+$ cells in the parenchyma co-express the endothelial marker CD31. Frozen tissue sections of mice treated with TAA for 42 days were fluorescently labelled with the endothelial markers CD34 and CD31. DAPI was used for nuclear staining. Representative images are shown and the scale depicts 50 µm.

3.5 Discussion

The CDE diet and TAA supplementation regimens are both commonly used to experimentally induce liver injury and fibrosis (Boulter *et al.* 2015; Darweish *et al.* 2014; Knight *et al.* 2008; Tirnitz-Parker *et al.* 2010; Patsenker *et al.* 2009; Van Hul *et al.* 2009; Grzelak *et al.* 2014). This study now comprehensively compared the two models in a time course over a 42-day period. The injury induction phase was represented by days 3 and 7, the establishment phase by days 14 and 21 and the maintenance phase by day 42. The data clearly indicate that the spatial and temporal kinetics differ significantly between the two CLD regimens. Injury, hepatic fat loading, inflammation and fibrosis all peak during the induction phase of the CDE diet before returning to control levels in the establishment and maintenance phase. This 'flare' is sufficient to orchestrate an LPC response that reaches a steady-state from about two weeks, most likely reflecting an equilibrium of LPC activation and lineage maturation. In contrast, the TAA model produces a more severe, progressive (chronic) phenotype with disease parameters persistently upregulated or gradually increasing throughout the time course. The succession of events is therefore significantly different in both regimens: (i) CDE, liver injury induction – lipid accumulation and inflammation - fibrosis and LPC response - alleviation or regression; and (ii) TAA, liver injury induction - inflammation - fibrosis and LPC response - progressive aggravation.

This study demonstrated that CDE feeding is associated with excessive fat loading in the parenchyma, most likely caused by reduced secretion of very low density lipoproteins, which in turn leads to increased oxidative stress (Aharoni-Simon *et al.* 2011; Yao *et al.* 1988), instigating the molecular and cellular injury cascade emanating from periportal areas. TAA, on the other hand, is a thiono-sulfur-containing hepatotoxin that is converted via dioxygen and superoxide anion to hydrogen peroxide in pericentral regions, thereby directly causing oxidative stress, lipid peroxidation and centrilobular necrosis (Low *et al.* 2004). It is therefore not surprising that CDE-fed mice displayed inflammation in periportal and parenchymal areas, while the TAA regimen induced a persistent pericentral inflammatory

response, reflective of the injury present in this lobular region. The accumulation of inflammatory cells may then orchestrate the initiation of the regeneration process by releasing mediating factors such as cytokines and growth factors that are known to activate and maintain either or both key cellular players, HSCs and LPCs. These include TWEAK (Tirnitz-Parker *et al.* 2010), TNF (Knight *et al.* 2005c), LTβ (Ruddell *et al.* 2009), IL6 (Matthews *et al.* 2004), IFNγ (Brooling *et al.* 2005) and HGF (Ishikawa *et al.* 2012), which were demonstrated to be upregulated in both models, yet with different expression dynamics.

In the CDE model, immune cells and myofibroblasts were present periportally from the induction phase, which has been demonstrated to facilitate LPC activation (Elsegood *et al.* 2015; Tirnitz-Parker *et al.* 2010) and cytokine crosstalk-mediated migration of HSCs and LPCs from portal areas into the hepatic parenchyma (Ruddell *et al.* 2009). In contrast, TAA is known to induce centrilobular damage and immune cells were therefore attracted to central areas, where they, together with sinusoidal endothelial cells and injured hepatocytes, may activate HSCs. The cellular injury and regeneration niche (that is here proposed to consist of closely associated inflammatory cells, LPCs and/or the DR and activated HSCs) was only identified during later injury phases when panCK$^+$ structures were detected pericentrally.

Livers of both the CDE and TAA model displayed deposition of ECM components, however to varying degrees, resulting in divergent degrees and patterns of fibrosis. In the CDE model periportal fibrosis was induced, however fibrosis eventually resolved and returned towards control levels after an initial peak in the induction phase, as demonstrated by immunofluorescent detection of αSMA$^+$ myofibroblasts, mRNA expression of fibrosis mediators as well as Sirius Red-visualised, and hydroxyproline-quantitated collagen deposition. This fibrosis pattern is typically observed in autoimmune or chronic viral hepatitis and chronic biliary diseases or cholestasis (Ferrell 2000). In contrast, investigation of the same parameters in the TAA model revealed gradually increasing fibrosis in central areas, which progressed towards cirrhosis during the injury establishment and maintenance phase, a pattern usually observed in fibrosis resulting from alcoholic or non-alcoholic steatohepatitis (Ferrell 2000). Interestingly, some previous studies using TAA to induce CLD have also reported portal, portal-to-portal bridging or portal-to-central bridging fibrosis, as well as inflammatory cell accumulation in portal areas (Aydin *et al.* 2010; Kornek *et*

al. 2006; Patsenker *et al.* 2009; Wallace *et al.* 2015). It is important to note that TAA induces severe morphological changes in hepatic lobules, including irregular patterns of portal tracts and central veins, DRs and high vascularisation directed to fibrotic areas (Gao *et al.* 2013; Lee *et al.* 2014b; Patsenker *et al.* 2009), providing a rich feeding ground for potential misinterpretation with regards to clear identification of portal as opposed to central areas. It cannot be ruled out that studies from other groups using TAA caused an increased disease activity in periportal areas, since results in experimental CLD greatly depend on the genetic background of the animals, concentration and administration route of the disease-inducing agent, and indeed the point-in-time of experimental design for example. However, the data of this study emphasise that it is fundamental to perform detailed time course analyses instead of snapshot evaluations at later time points when the liver architecture is already well distorted, in order to follow histological changes and thus correctly interpret results. Our immunofluorescent data identifying and following $CD45^+$, $panCK^+$ and αSMA^+ cells over the course of six weeks provide clear evidence that periportal expansion of LPCs is limited in the TAA regimen, and both inflammation and fibrosis are predominantly provoked in the central, toxicity-burdened areas, which in the initial injury phase lack ductular structures characteristic for portal triads. At later stages of TAA-induced injury, $panCK^+$ ductular structures and LPCs also appear in central areas, tempting to misinterpret the local histology as portal instead of central.

Analysis of the vasculature in CLD-induced versus healthy livers revealed no alterations in the CDE model but distinct patterns in mice subjected to TAA. Firstly, it is important to note that hepatic endothelial phenotypes, and accordingly their marker expressions, are controversially discussed due to differences in vessel types and tissue compartments as well as to the underlying experimental models or human pathologies (Pusztaszeri *et al.* 2006; Lalor *et al.* 2006; Scoazec and Feldmann 1991; Couvelard *et al.* 1993; Do *et al.* 1999). The data presented in this chapter showed that CD31 is a marker for LSECs in mice regardless of the investigated injury status. In contrast to the CDE model, the progressive injury pattern in TAA mice was associated with an increased angiogenesis illustrated by increased CD31 expression at the sites of tissue damage, and sinusoidal capillarisation, marked by the $CD31^+/CD34^+$ endothelial subpopulation. Similar results were reported in human

studies, where CD31 expression increased with advancing fibrotic stages in NAFLD patients (Akyol *et al.* 2005), and CD34 expression functioned as indicator of sinusoidal capillarisation and agiogenesis under pathological conditions (Pusztaszeri *et al.* 2006; Ohmori *et al.* 2001; Amarapurkar *et al.* 2007; Di Carlo *et al.* 2002). Moreover, $CD34^+$ LSEC numbers were correlated with a high risk of HCC development in patients with HCV-associated CLD (Ohmori *et al.* 2001). Due to their close spatial relationship to LPCs and the regeneration niche, $CD34^+/CD31^-$ single cells and groups of cells most likely contribute to the regulation of regenerative processes. As CD34 was reported to represent a marker for progenitors of the haematopoietic cell lineage (Kollet *et al.* 2003; Nielsen and McNagny 2008; Sidney *et al.* 2014), positive CD34 staining in the regeneration niche may also be associated with the inflammatory cell response. Overall, this further highlights the value of TAA as an alternative model to study patterns of CLD seen in human pathologies.

Taken together, this detailed comparison of CDE- and TAA-induced liver injury has revealed remarkable differences in the cellular and underlying molecular dynamics, creating distinct disease establishment and progression patterns, and will serve as a valuable basis for future research utilising these two common models of experimental CLD. The data also confirm that both models are suitable for the study of LPC biology.

CHAPTER 4

Characterisation of the LPC response during CDE- and TAA-induced chronic liver disease

Parts of this chapter have already been published and the article is included in the appendix (Köhn-Gaone *et al.* 2016a).

Köhn-Gaone J., Dwyer B.J., Grzelak C.A., Miller G., Shackel N.A., Ramm G.A., McCaughan G.W., Elsegood C.L., Olynyk J.K., and Tirnitz-Parker J.E. (2016). Divergent Inflammatory, Fibrogenic, and Liver Progenitor Cell Dynamics in Two Common Mouse Models of Chronic Liver Injury. *Am J Pathol*, **186**: 1762-1774.

4.1 Introduction

Liver progenitor cells are transit-amplifying cells, committing towards a cell lineage depending on the injury stimulus. Thus they most likely represent a cell pool of different phenotypes depending on their differentiation and maturation status, making this population highly heterogeneous (Jelnes *et al.* 2007). During early investigations, common markers for identifying LPCs included AFP, albumin, OV-6 and a range of different cytokeratins such as CK7, CK8, CK18, CK19 (Sell 1978; Evarts *et al.* 1987; Yang *et al.* 1993; Sarraf *et al.* 1994). Over the last two decades a great variety of markers have emerged in the field and have highlighted the diversity of this cell population. Several LPC markers are described in the literature, which are not specific for LPCs but instead share their expression with other cell types such as hepatocytes, cholangiocytes or haematopoietic cells (see Table 1.1 and 1.2). Nowadays, studies of LPC biology, often comprising lineage tracing and cell isolation strategies, are based on LPC markers of the cholangiocytic lineage such as CD24, CD133, CK19, EpCAM, OPN and Sox9 (Suzuki *et al.* 2008; Espanol-Suner *et al.* 2012; Schievenbusch *et al.* 2012; Guest *et al.* 2014; Tarlow *et al.* 2014a; Lu *et al.* 2015; Mu *et al.* 2015). Some of the more recent markers, such as Foxl1 and Lgr5 (Sackett *et al.* 2009; Shin *et al.* 2011; Huch *et al.* 2015), are not available for antibody detection, instead lineage tracing in genetically modified mice is performed for their study.

Most LPC marker-based studies have in common that they address the question of LPC function, their contribution during tissue repair and their tumorigenic potential. However, it is often problematic to directly compare LPC responses and regeneration outcomes between studies since they often utilise a diverse range of markers. Consequently, it is not clear if the same LPC population is addressed, since despite the accepted feature, the differentiation into hepatic cell lineages such as hepatocytes and cholangiocytes, it is still unresolved whether LPCs represent equivalent cell populations or cells of different stages during lineage commitment. Some evidence that the progenitor pool in the adult liver consists of different LPC phenotypes, and might be context-specific dependent on the stimulus, comes from a study by Jelnes and colleagues. They demonstrated phenotypic discrepancies in the LPC response of mice compared to rats and furthermore identified divergent subpopulations of LPCs

when comparing AAF/PH-, CDE-, DDC- and *N*-acetyl-paraaminophen-induced CLD (Jelnes *et al.* 2007). Thus, it is of great interest to analyse LPC marker expression and characterise the involved subpopulations in different experimental models to set the foundation for studying LPC biology.

This chapter is an extension to the CDE- and TAA-induced injury patterns described in Chapter 3 and characterises the LPC populations that can be observed in both time courses. This study focussed on commonly used LPC markers, which are available for antibody detection. LPCs were discriminated from cholangiocytes by morphology and the relevance of these markers in our experimental models was evaluated.

4.2 Study Aims

This chapter introduces the TAA regime as an experimental model to study LPCs and compares the LPC response following TAA treatment with the well-established induction through CDE exposure. It was shown in Chapter 3 that the DR including the intralobular location and time of niche formation is highly dependent on the underlying model, CDE vs. TAA. Therefore, the experiments in this chapter aimed to provide a detailed characterisation of LPC phenotypes during the injury induction, establishment and maintenance phase of CDE- or TAA-induced chronic liver injury.

4.3 Methods

Mice from the 6-week time course exposed to CDE, TAA or control treatment, which were previously introduced in Chapter 3, were used in this chapter. Liver tissue was further analysed by immunofluorescence to analyse stages of LPC induction and proliferation. Here day 7, 14 and 42 were used since indicated in Chapter 3, these time points represent the progress of changing LPC numbers in both models. LPC proliferation was assessed by labelling A6-positive LPCs with the proliferation marker Ki67. LPC phenotypes were characterised by co-staining of several markers including A6, CD133, CK19, E-cadherin, EpCAM, MIC1-1C3, panCK and Sox9. Pericentral hepatocytes exposed to TAA were evaluated by co-localisation of the hepatocyte marker hepatocyte nuclear factor alpha (HNF4α) and panCK or HNF4α and CK19, respectively. Co-expression analysis of panCK and markers that do not label the bulk of LPCs such as CD44 and CD90 were used to assess the existence of distinct LPCs subpopulations.

4.4 Results

4.4.1 Characterisation of LPC proliferation in response to CDE and TAA treatment

The pro-inflammatory factors TWEAK, TNF, LTβ, IL6 and IFNγ, as well as HGF, which were demonstrated to be increased in the induction phase of the CDE and TAA model (see 3.4.2), do not only perpetuate the inflammatory response but also provide critical mitogens that activate the LPC compartment in a chronically injured liver. Therefore, on the background of elevated mitogen expression levels, LPC proliferation was investigated by identifying $A6^+$ biliary cells/LPCs that express the proliferation marker Ki67. In control mice, A6 staining was restricted to the bile ducts, as expected, and Ki67 expression was limited to only a few non-biliary cells (Fig. 4.1). Following CDE treatment, $A6^+$ biliary structures and single LPCs proliferated from portal regions into the liver parenchyma, with $A6^+/Ki67^+$ cells mainly being observed in the dynamic early phase of the LPC response shown for day 7. During the entire CDE time course, only a few hepatocytes expressed Ki67, as judged by cell and nucleus morphology and lack of A6 expression (Fig. 4.2). In contrast, with TAA supplementation $A6^+/Ki67^+$ structures were mainly detected at later time points, in particular on day 42, when the inflammatory/fibrogenic/LPC niche had been well established in pericentral areas (as shown in chapter 3.4.3), leading to substantial centrally localised DRs that included several $A6^+/Ki67^+$ cells. In addition, many mitotically active $Ki67^+$ hepatocytes were observed following TAA exposure (Fig. 4.3).

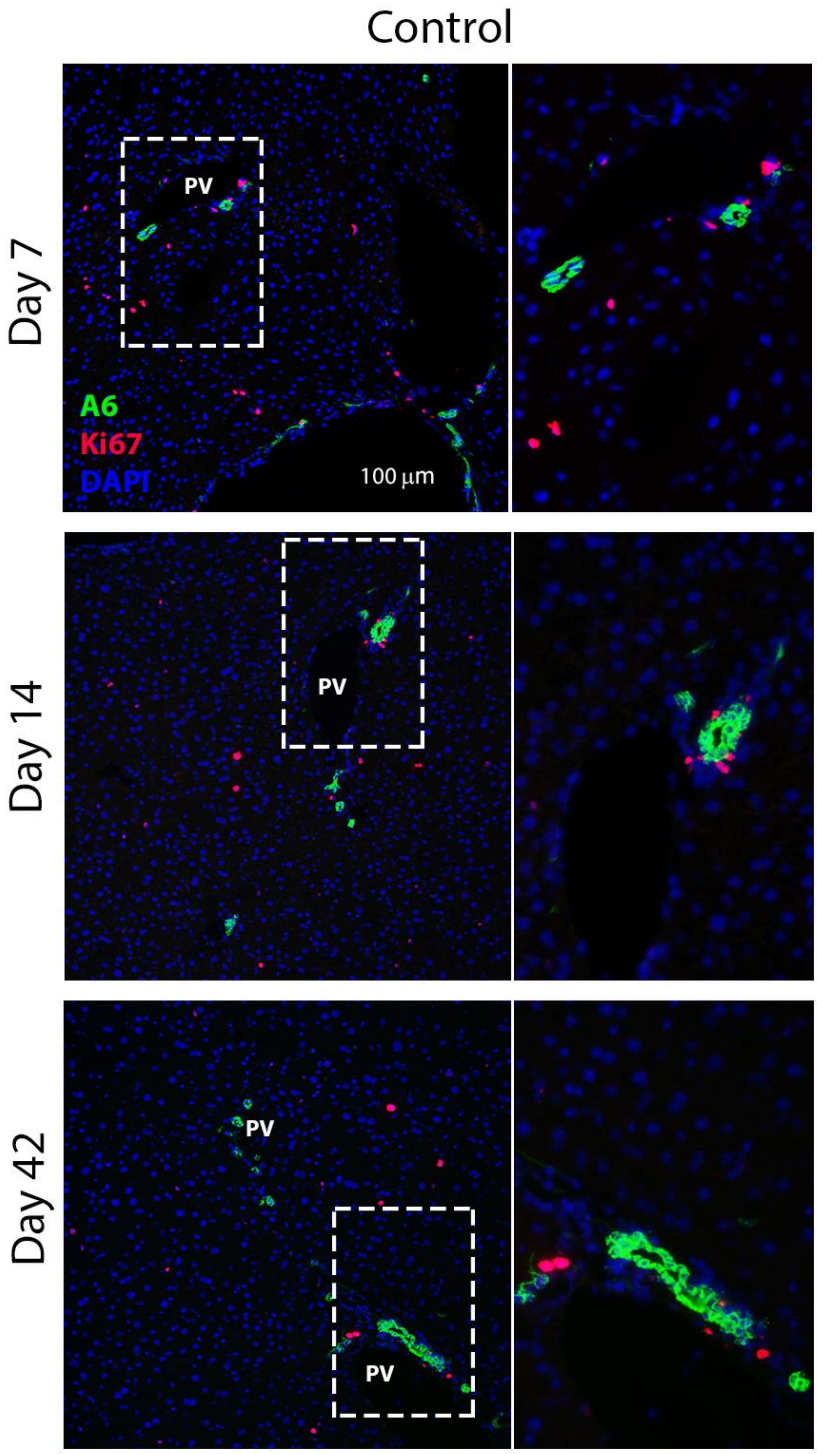

Fig. 4.1: Proliferation and LPC marker expression in control mice. Frozen sections of non-treated control mice were stained for the biliary cell and LPC marker A6 and the proliferation marker Ki67 using immunofluorescence. There were no proliferating biliary cells/LPCs detected on day 7, 14 and 42. The scale bar represents 100 µm and dashed boxes identify the regions of enlarged images *PV*, portal vein.

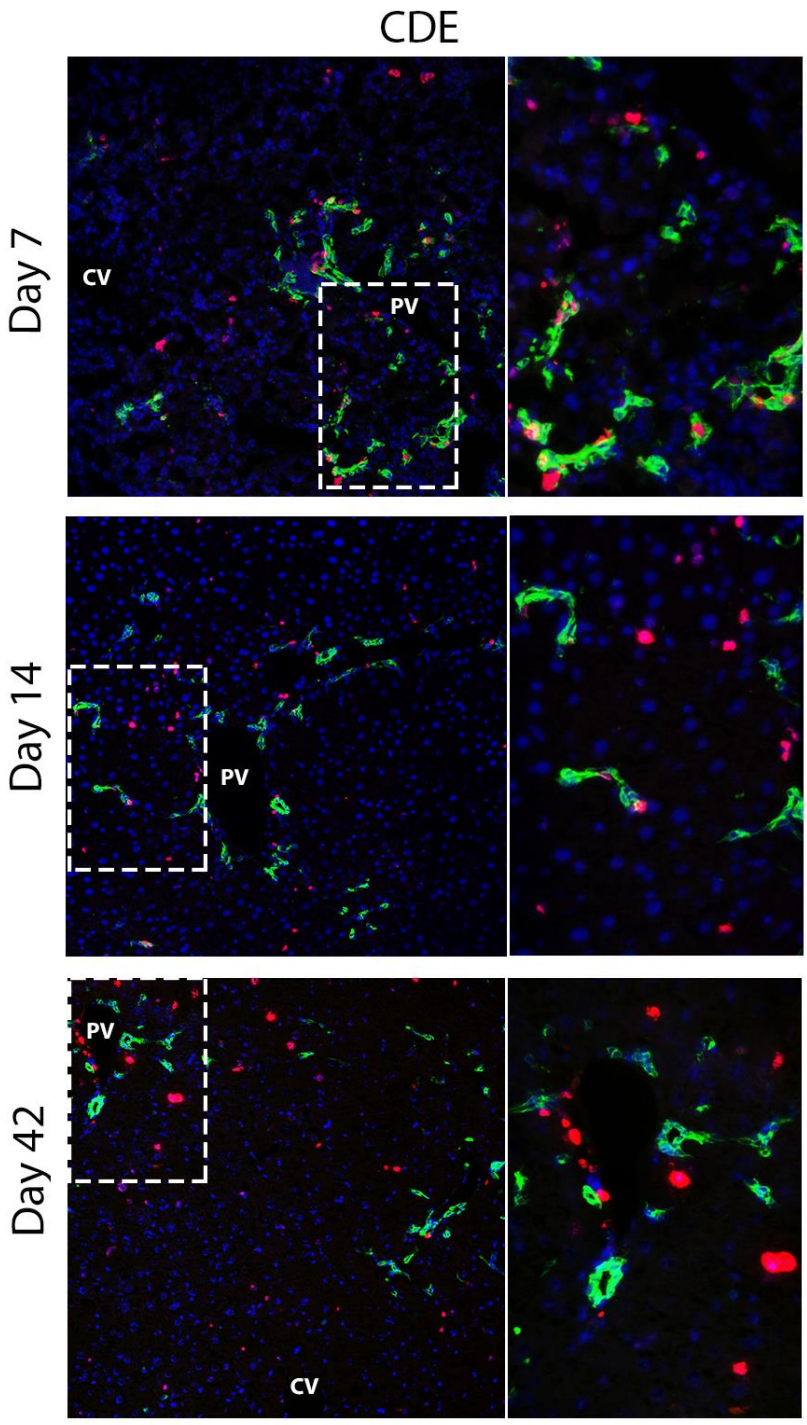

Fig. 4.2: CDE treatment induces LPC proliferation. Liver sections of CDE-treated mice were fluorescently labelled for the biliary cell and LPC marker A6 and the proliferation marker Ki67. CDE exposure predominantly induced $A6^+/Ki67^+$ cells during the induction phase (day 7) where proliferating $A6^+$ biliary structures and single LPCs migrated from periportal areas into the parenchyma. The scale bar depicts 100 µm and dashed boxes highlight the area of magnification. *CV*, central vein*; PV*, portal vein.

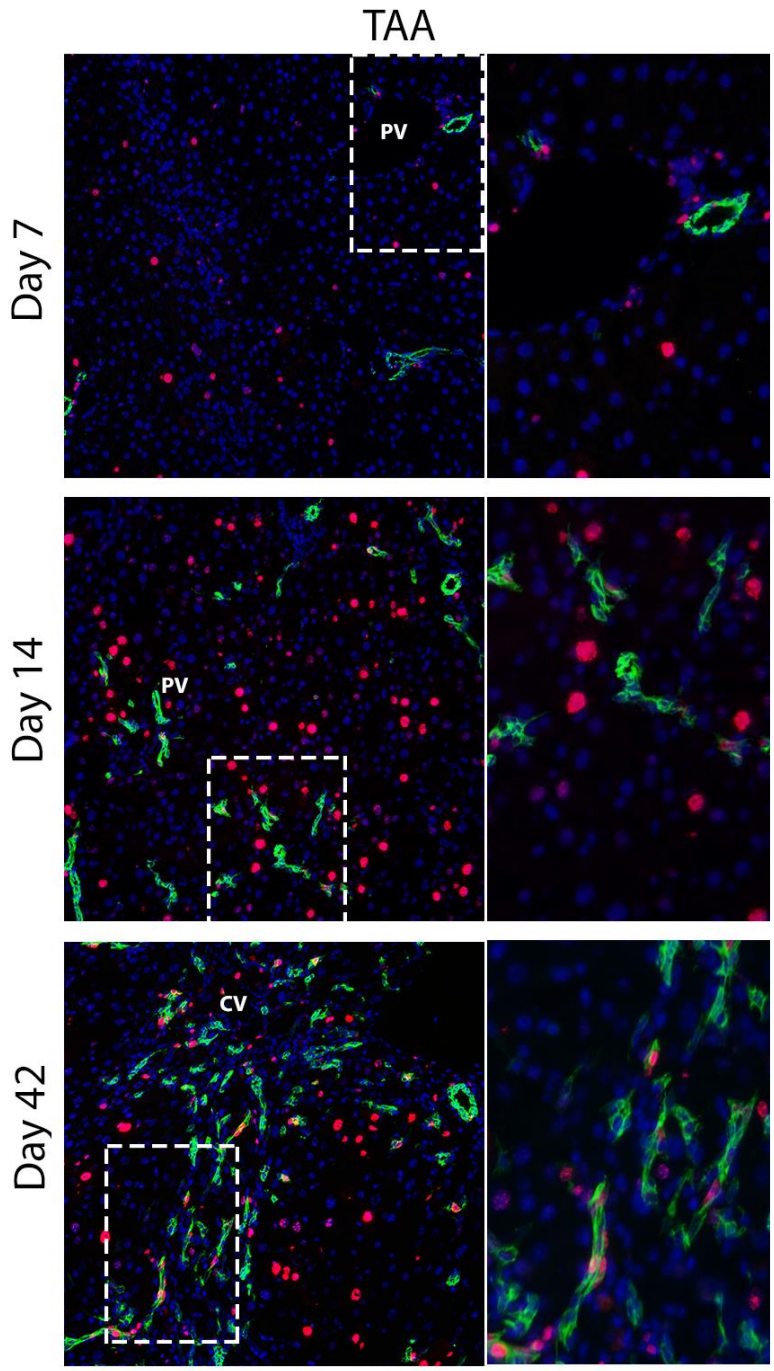

Fig. 4.3: TAA exposure induces LPC proliferation. Liver sections of TAA-treated mice were labelled for the biliary cell and LPC marker A6 and the proliferation marker Ki67 using immunofluorescence. $A6^{+}/Ki67^{+}$ cells were mainly observed at later time points (day 42) as part of the centrally located DR. The scale bar depicts 100 µm and dashed boxes identify the areas of enlarged images. *CV*, central vein*; PV*, portal vein.

4.4.2 CDE and TAA-induced LPC phenotypes

In order to capture the dynamics of a broader ductular cell and LPC population, and to further characterise their corresponding phenotypes induced by CDE and TAA treatment, different co-stainings for commonly used cholangiocytic LPC markers were performed including A6, CD133, CK19, EpCAM, MIC1-1C3, panCK and Sox9, as well as the epithelial cell marker E-cadherin.

Interestingly, when comparing the staining patterns for A6 as the gold standard marker and panCK, previously reported to detect $A6^+$ structures with a sensitivity of >99% in response to *N*-acetyl-paraaminophen (Kofman *et al.* 2005), significant differences were discovered between the CDE and TAA model. In control mice, it was demonstrated that several $A6^-/panCK^+$ cells exist in the cholangiocytic population (Fig. 4.4). There was a substantial overlap of both markers in CDE-treated mice at all investigated time points (shown for day 14 and 42) with occasional appearing single $A6^-/panCK^+$ cells (Fig. 4.5). However, numerous $A6^-/panCK^+$ cells were identified in the TAA regimen (Fig. 4.6). This $A6^-/panCK^+$ cell population comprised slightly larger cells when located at the site of central damage (day 42) resembling intermediate hepatocytes as well as a minor number of small oval-shaped cells in portal areas resembling LPC morphology (day 14). Similar results were obtained for co-labelling cells with the markers CK19 and panCK, MIC1-1C3 and panCK, as well as CD133 and panCK (Fig. 4.7, Fig. 4.8, Fig. 4.9, Fig 4.10, Fig. 4.11 and Fig 4.12). However, stainings in control mice mainly generated a double-positive cholangiocyte population (Fig. 4.) A great overlap of the markers CK19 and EpCAM was observed in both CDE- and TAA-induced LPC populations (Fig. 4.13 and Fig 4.14) with only rare cases of $CK19^+/EpCAM^-$ cells at all investigated time points (shown for day 14 and 42).

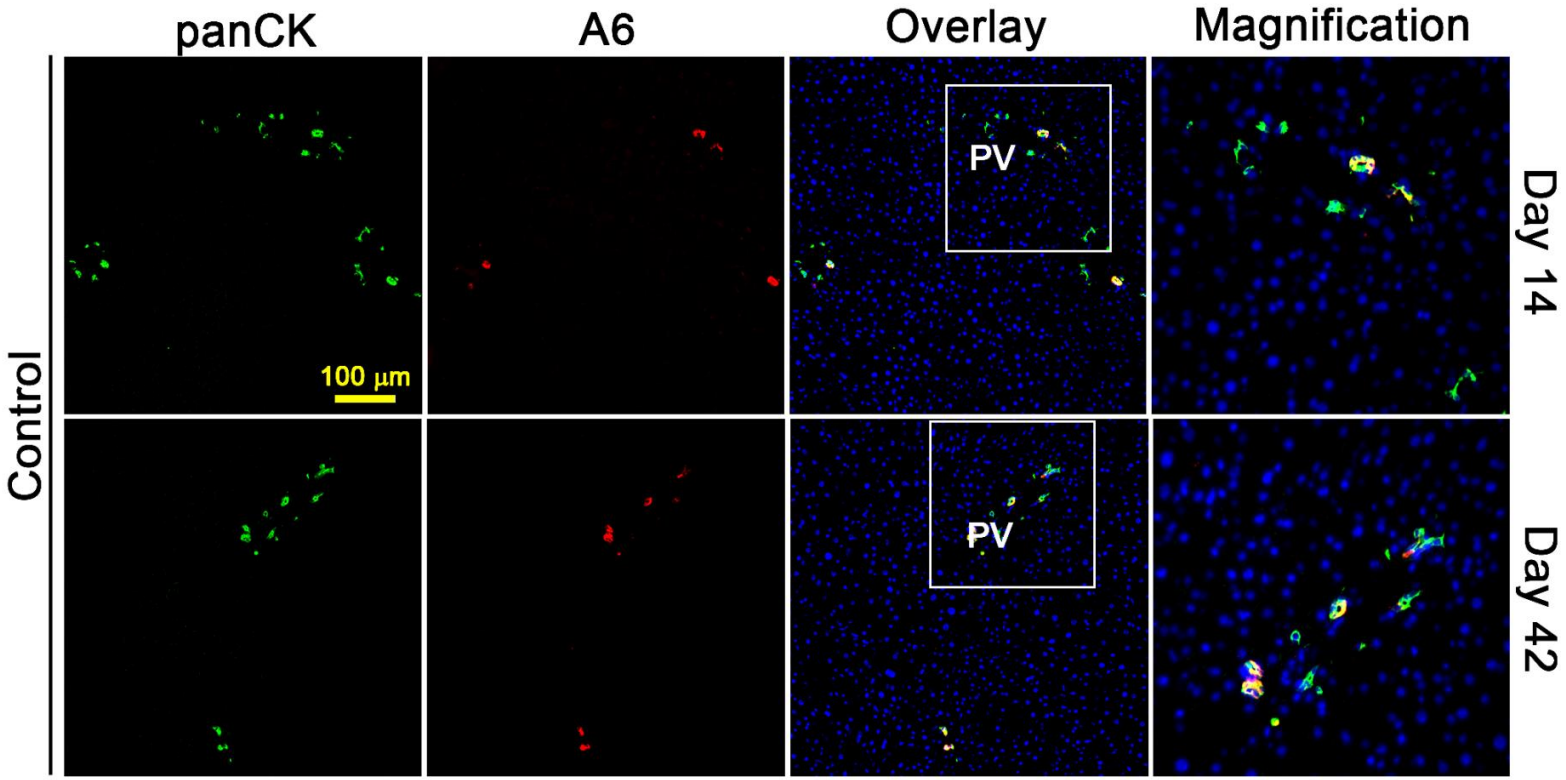

Fig. 4.4: Assessment of the LPC markers A6 and panCK in control mice. Frozen liver sections of control mice at day 14 and 42 were fluorescently labelled for the two biliary cell and LPC markers A6 and panCK. Representative images are shown and inserted boxes identify the regions of enlarged images. The scale bar represents 100 µm. Original magnification x100 and x200 for inserts. *PV*, portal vein.

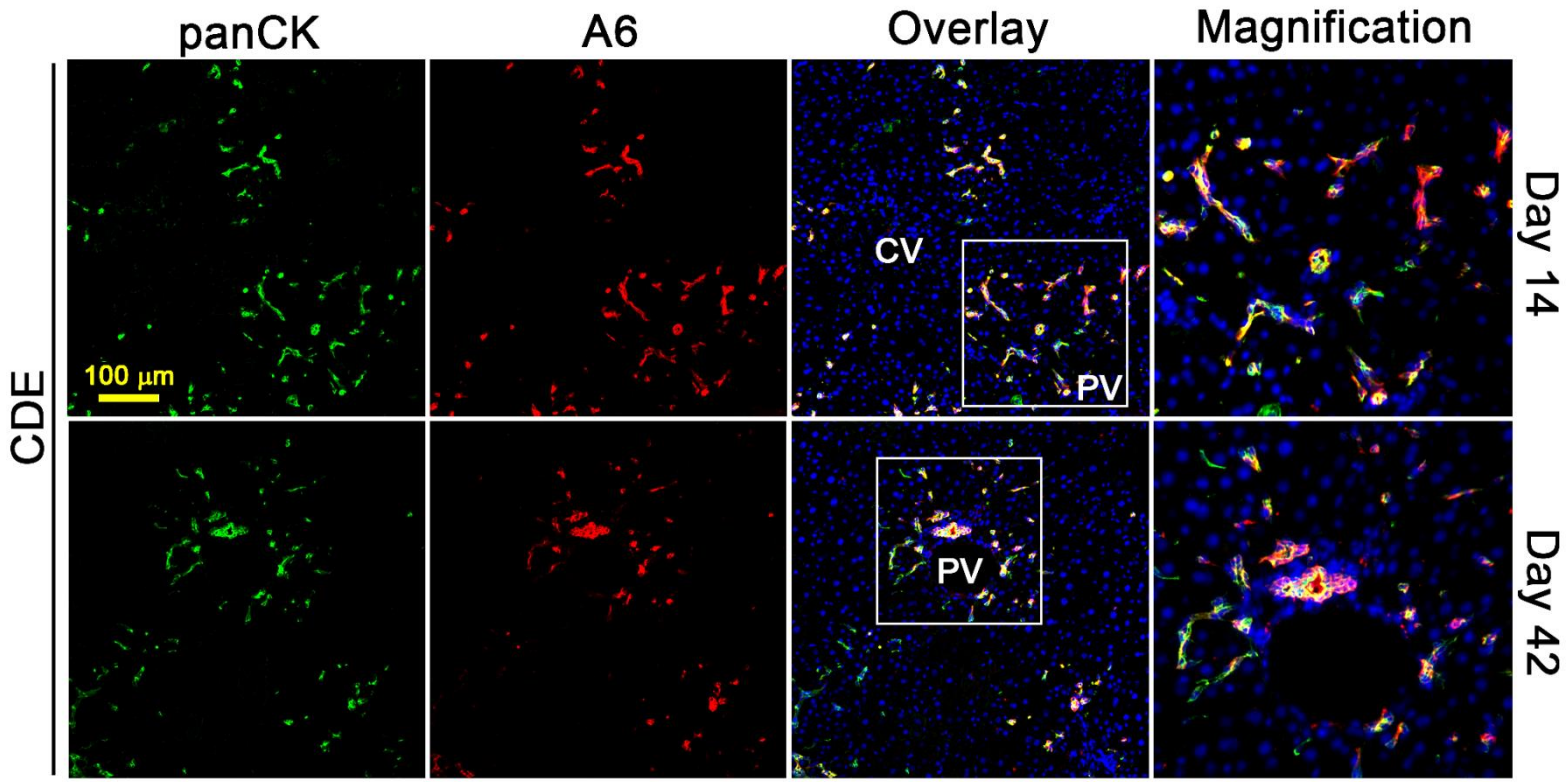

Fig. 4.5: CDE-induced LPC populations defined by the markers A6 and panCK. Frozen liver sections of mice fed a CDE diet for 14 and 42 days were fluorescently labelled for the two biliary cell and LPC markers A6 and panCK. Representative images are shown and inserted boxes identify the regions of enlarged images. The scale bar represents 100 µm. Original magnification x100 and x200 for inserts. *CV*, central vein*; PV*, portal vein.

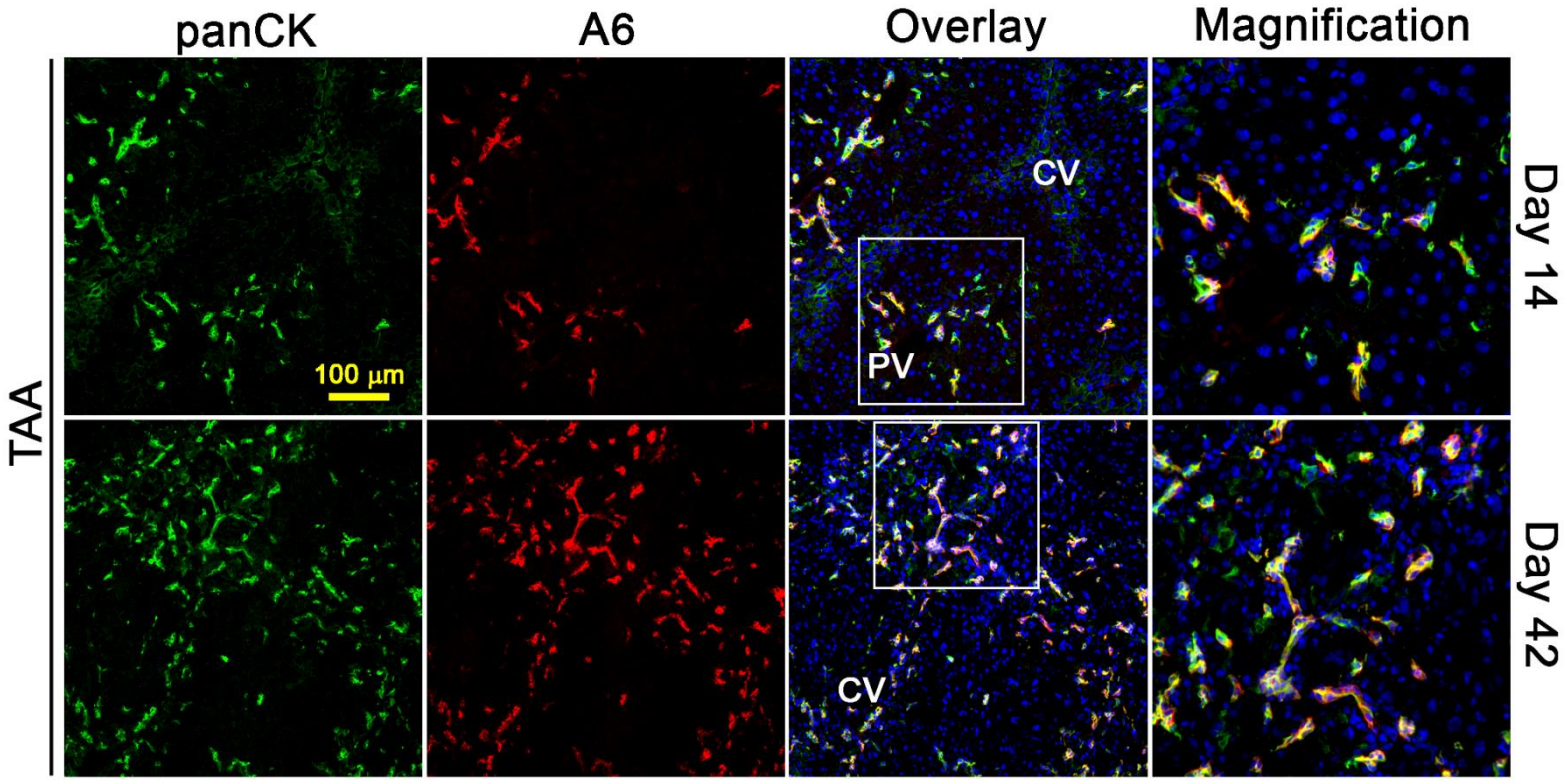

Fig. 4.6: TAA-induced LPC populations defined by A6 and panCK expression. Liver sections of mice exposed to TAA for 14 and 42 days were labelled for the two biliary cell and LPC markers A6 and panCK using immunofluorescence. Representative images are shown and inserted boxes identify the regions of magnification. The scale bar represents 100 µm. Original magnification x100 and x200 for inserts. *CV*, central vein*; PV*, portal vein.

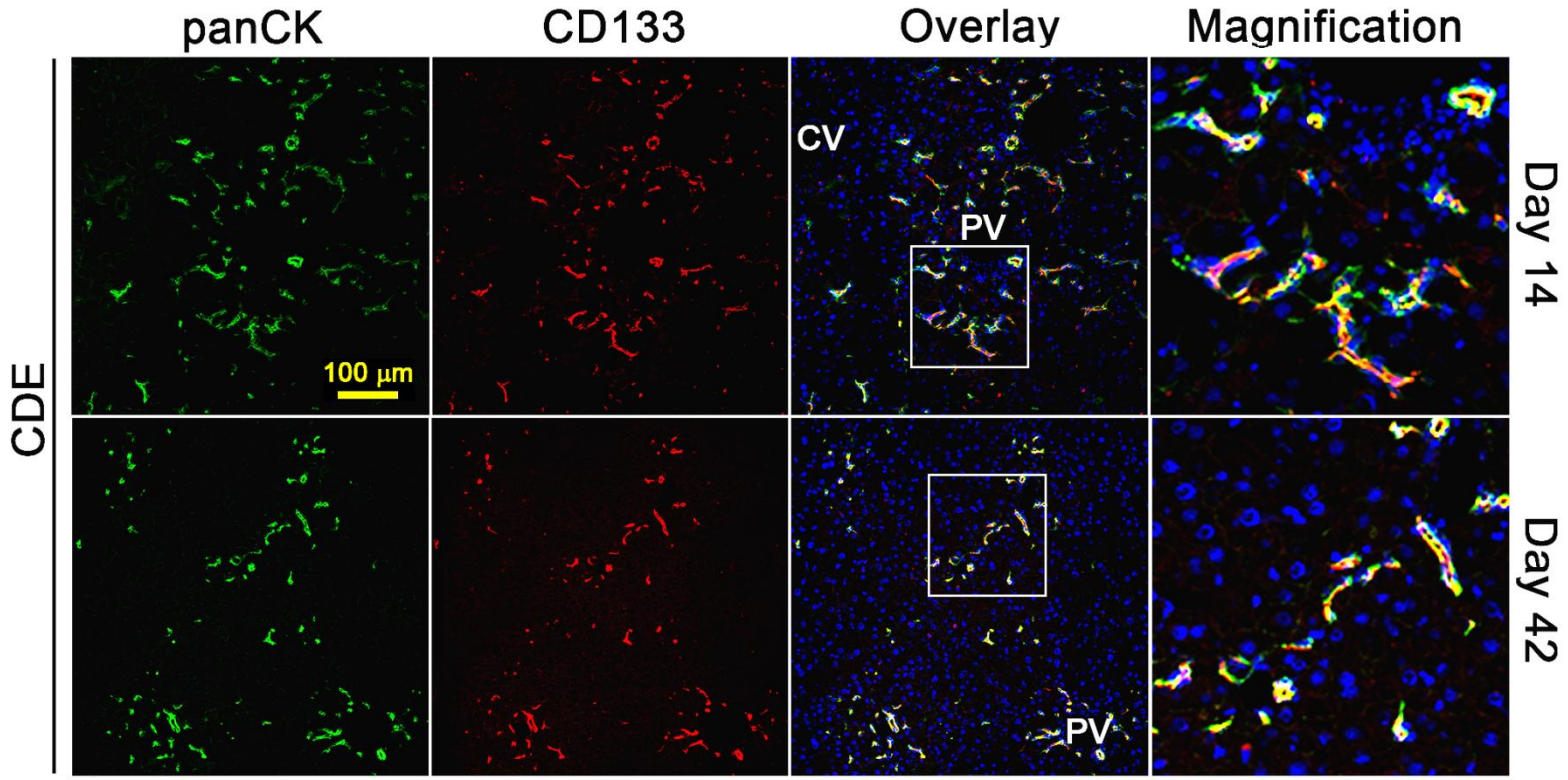

Fig 4.7: Immunofluorescent staining of panCK$^+$ and CD133$^+$ LPCs following CDE exposure. Frozen liver sections of mice exposed to CDE treatment for 14 and 42 days were labelled with the biliary cell and LPC markers panCK and CD133. The scale bar depicts 100 μm and the inserts identify the field of magnification. *CV*, central vein*; PV*, portal vein.

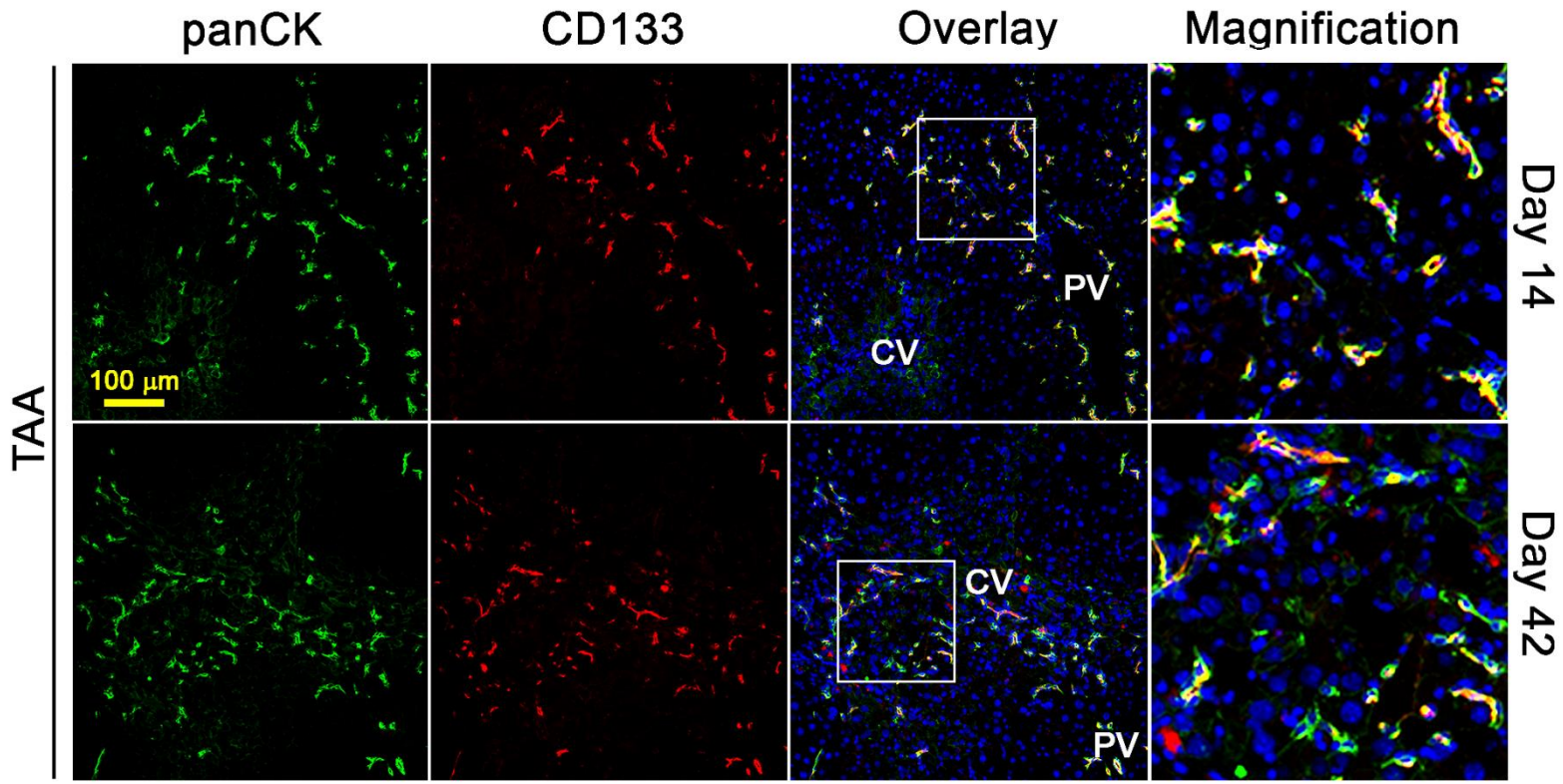

Fig 4.8: Immunofluorescent staining of panCK$^+$ and CD133$^+$ LPCs in TAA-treated mice. Frozen liver sections of mice exposed to TAA treatment for 14 and 42 days were labelled with the cholangiocytic LPC markers panCK and CD133. The scale bar represents 100 µm and the inserts identify the area of magnification. *CV*, central vein*; PV*, portal vein.

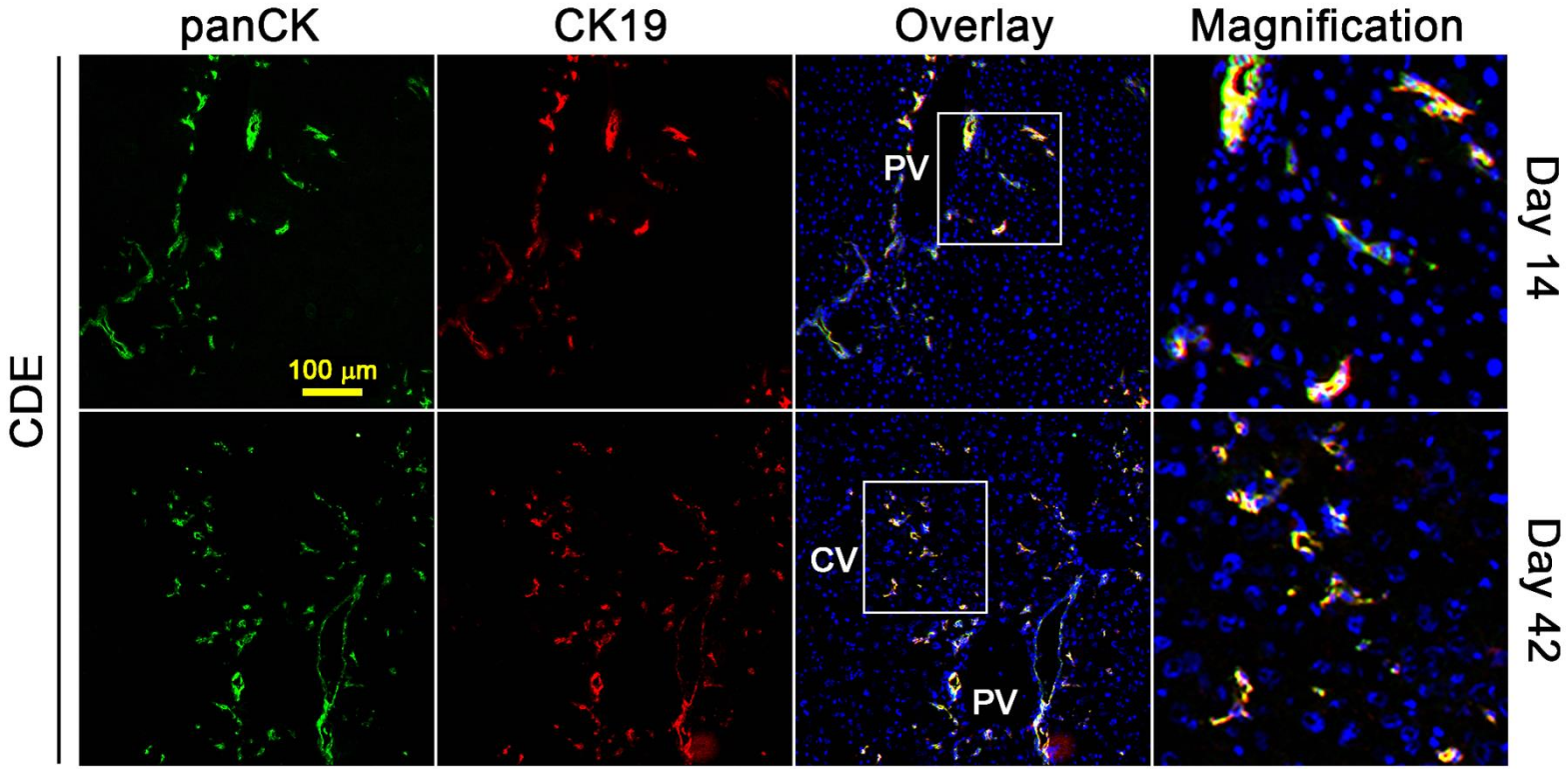

Fig. 4.9: Co-localisation of panCK and CK19 in CDE-induced CLD. Frozen liver sections of CDE-treated mice at day 14 and 42 were fluorescently labelled with the biliary cell and LPC markers panCK and CK19. The scale bar represents 100 µm and the inserted boxes highlight the field of magnification. *CV*, central vein*; PV*, portal vein.

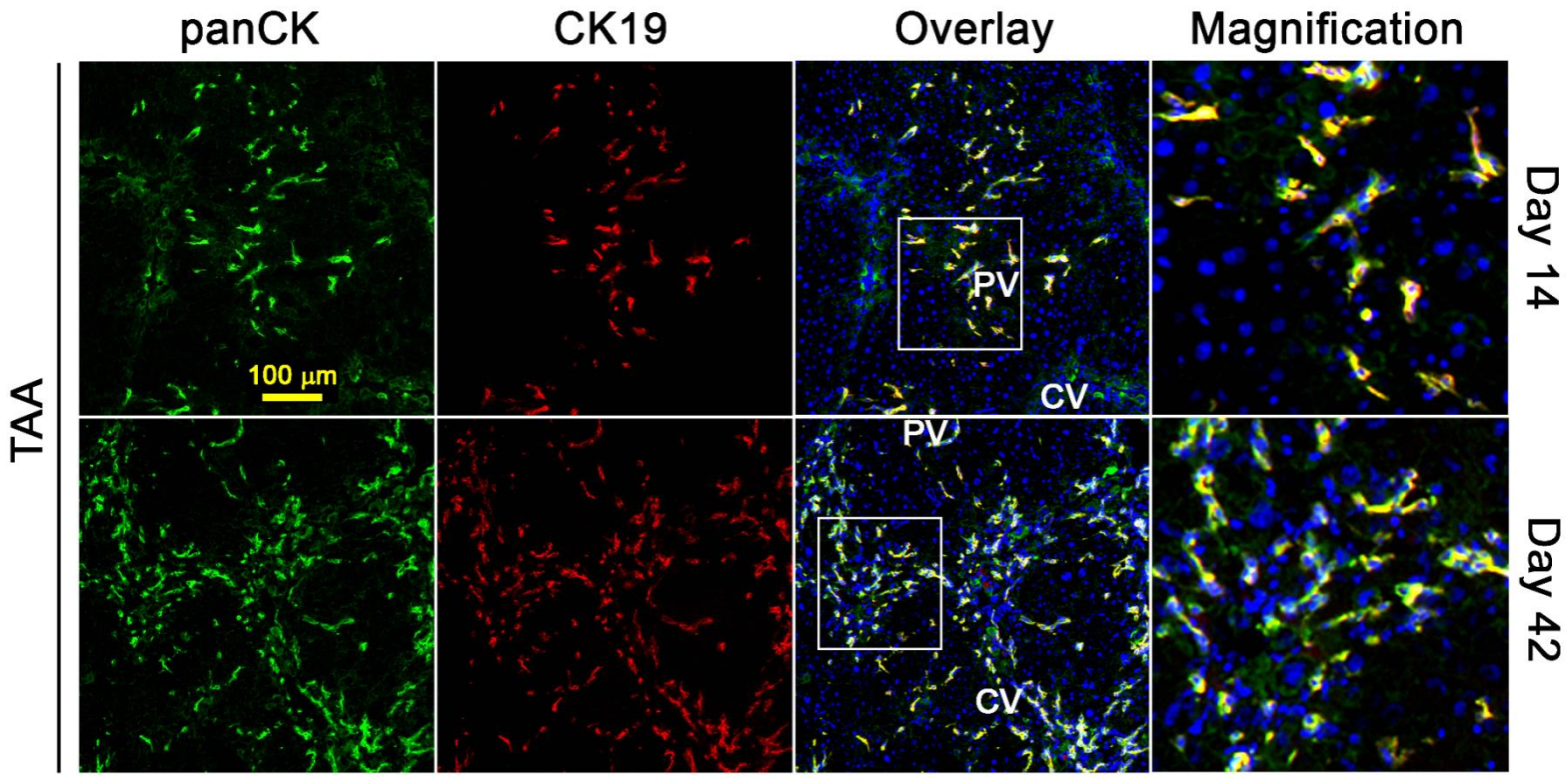

Fig. 4.10: Co-localisation of panCK and CK19 in TAA-induced CLD. Frozen liver sections of mice exposed to TAA for 14 and 42 days were fluorescently labelled with the cholangiocytic LPC markers panCK and CK19. The scale bar depicts 100 µm and the inserts highlight the area of magnification. *CV*, central vein*; PV*, portal vein.

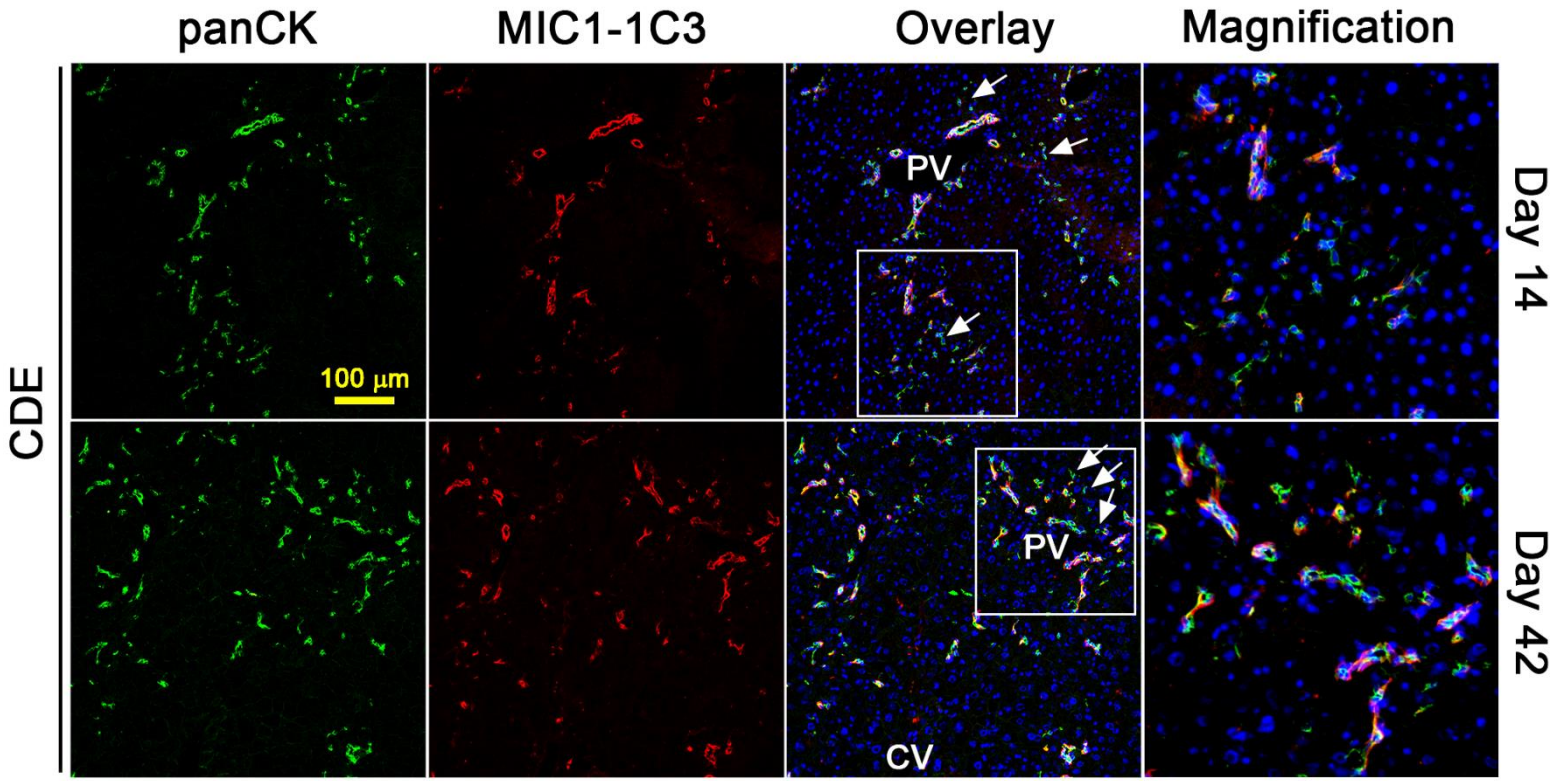

Fig 4.11: Immunofluorescent staining of panCK$^+$ and MIC1-1C3$^+$ LPCs in the CDE model. Frozen liver sections of mice fed a CDE diet for 14 and 42 days were labelled with the biliary cell and LPC markers panCK and MIC1-1C3. The scale bar represents 100 μm and the inserts highlight the field of magnification. Arrows highlight examples of panCK$^+$/MIC1-1C3$^-$ cells. *CV*, central vein*; PV*, portal vein.

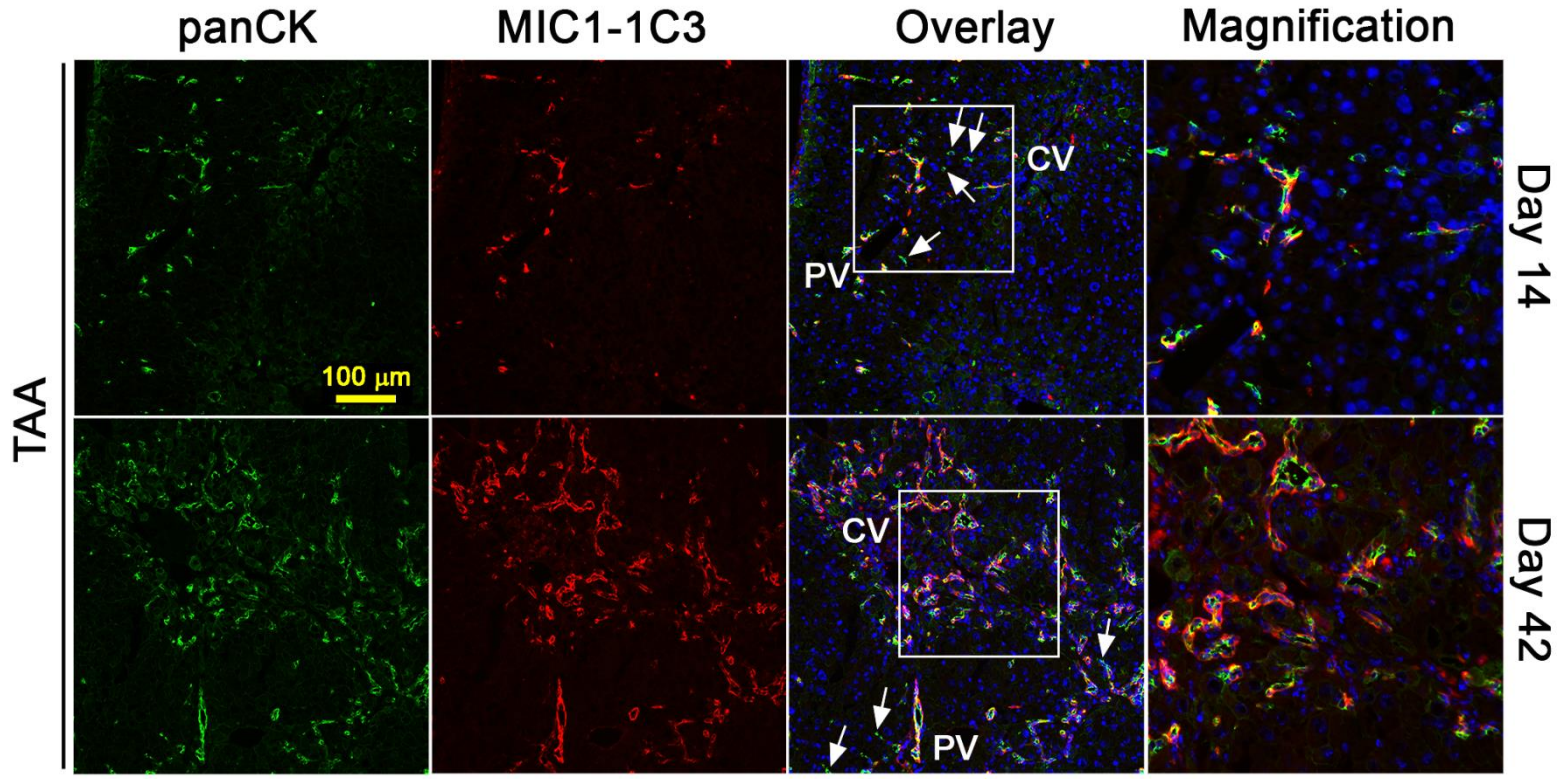

Fig 4.12: Immunofluorescent staining of panCK$^+$ and MIC1-1C3$^+$ LPCs in the TAA model. Frozen liver sections of mice exposed to TAA treatment for 14 and 42 days were labelled with the cholangiocytic LPC markers panCK and MIC1-1C3. The scale bar depicts 100 µm and the inserted boxes highlight the area of magnification. Arrows highlight examples of panCK$^+$/MIC1-1C3$^-$ cells. *CV*, central vein*; PV*, portal vein.

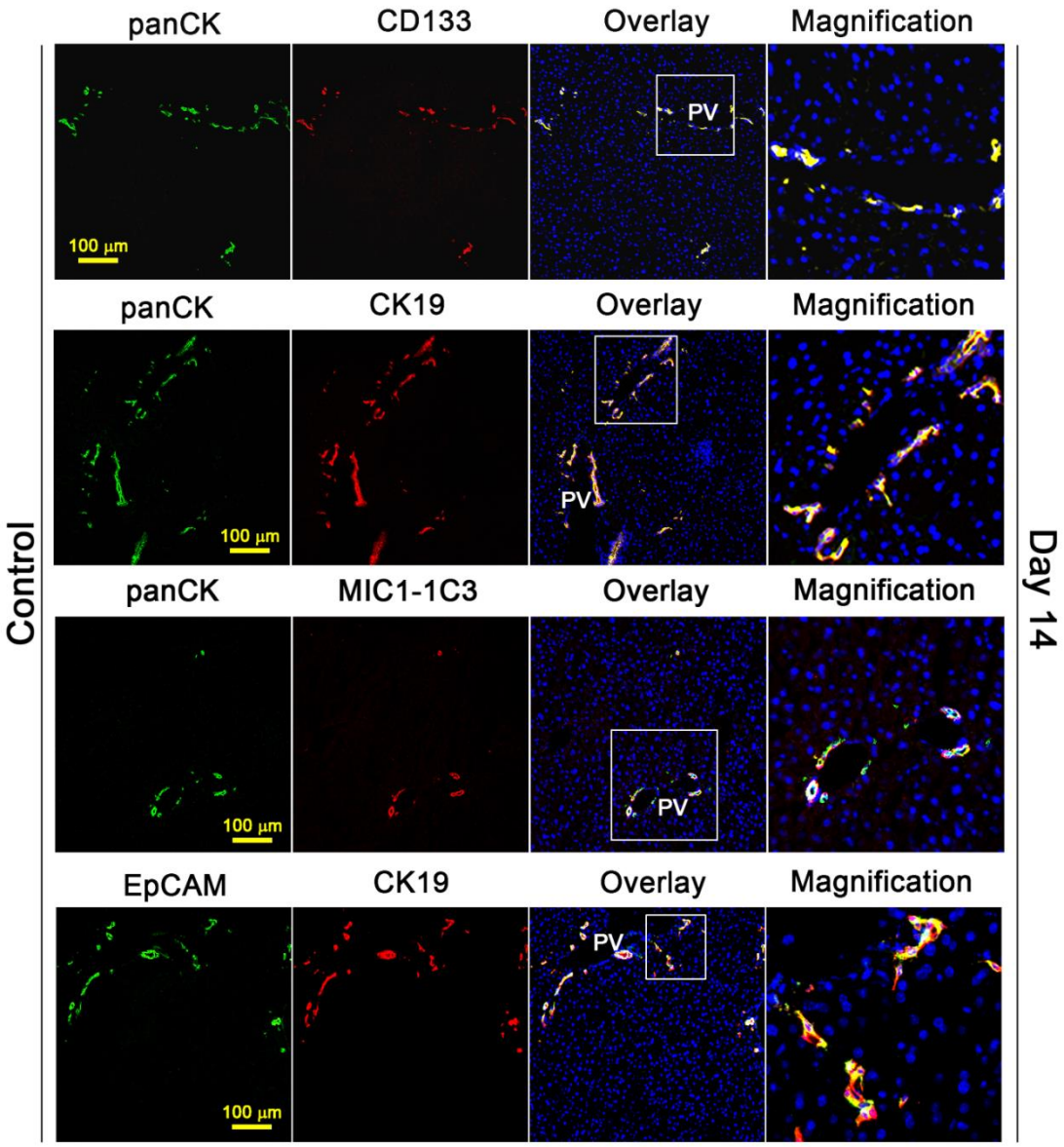

Fig. 4.13: Immunofluorecent staining of panCK, CD133, CK19, MIC1-1C3 and EpCAM in control mice. Frozen liver sections of control mice at day 14 were labelled with the cholangiocytic LPC markers panCK, CD133, CK19, MIC1-1C3 and EpCAM. The scale bar represents 100 µm and the inserted boxes highlight the field of magnification. *PV*, portal vein.

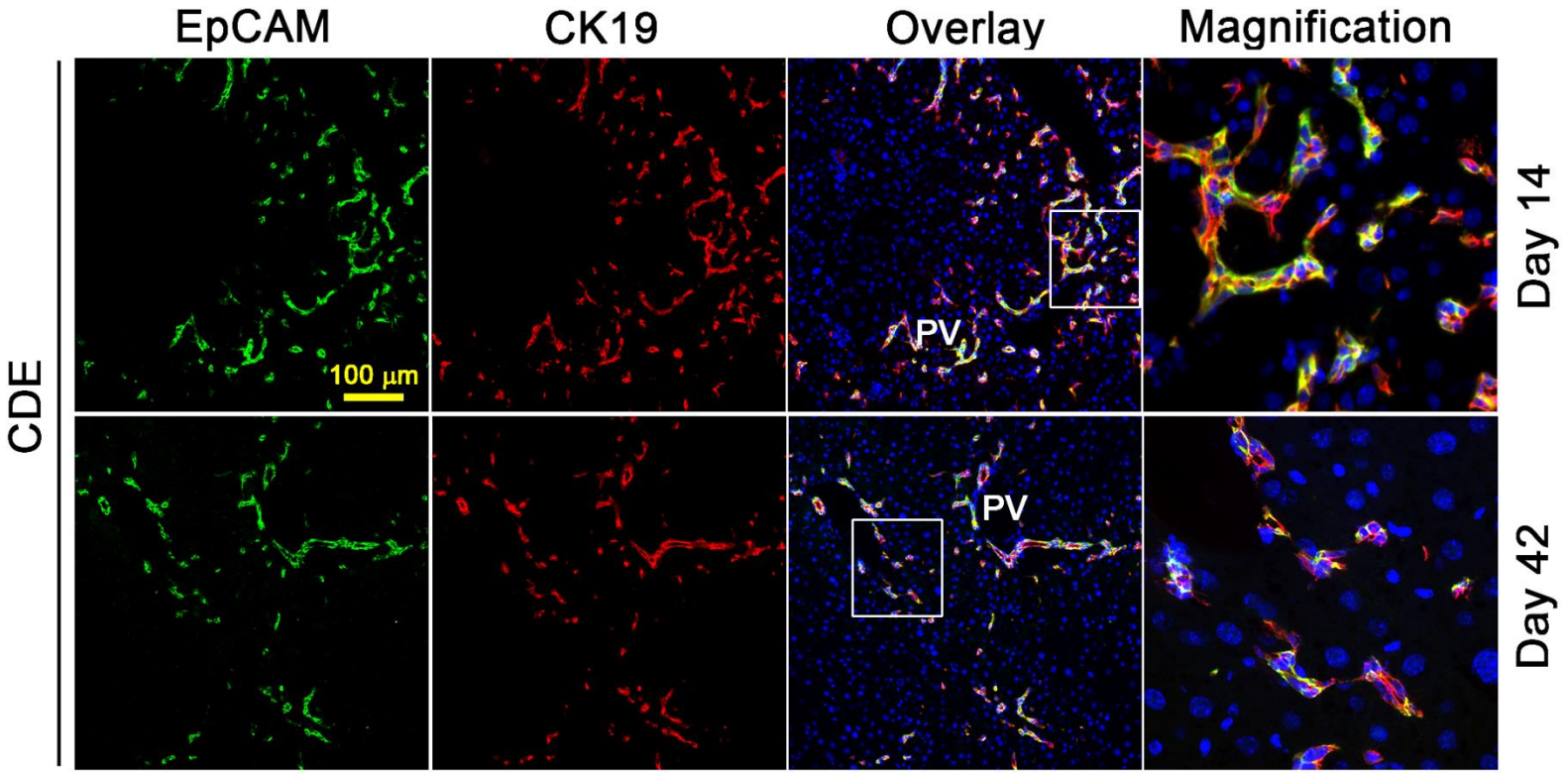

Fig. 4.14: Co-localisation of CK19 and EpCAM in CDE-treated mice. Frozen liver sections of mice treated with CDE for 14 and 42 days were fluorescently labelled with the biliary cell and LPC markers CK19 and EpCAM. The scale bar depicts 100 µm and the inserts identify the area of magnification. *PV*, portal vein.

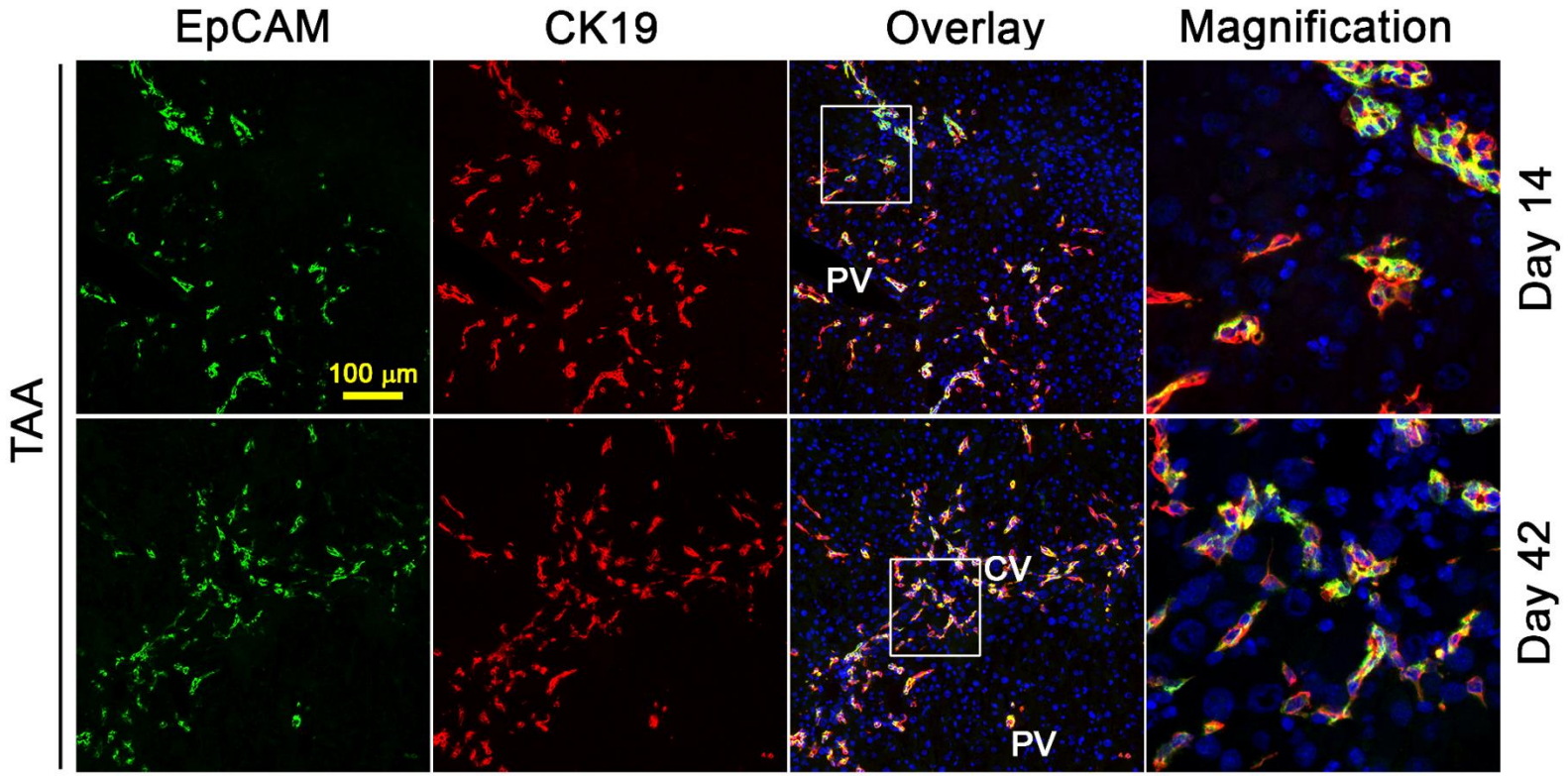

Fig. 4.15: Co-localisation of CK19 and EpCAM following TAA treatment. Frozen liver sections of mice exposed to TAA for 14 and 42 days were fluorescently labelled with the cholangiocytic LPC markers CK19 and EpCAM. The scale bar represents 100 µm and the inserted boxes highlight the area of magnification. *CV*, central vein*; PV*, portal vein.

Interestingly, the staining patterns of the markers panCK and Sox9 revealed the existence of a panCK$^-$/Sox9$^+$ cell population in close proximity to the portal area in CDE- and TAA-treated mice as well as in control mice at day 14 and 42 (Fig. 4.16, Fig. 4.17 and Fig. 4.18). This portal panCK$^-$/Sox9$^+$ cell population had larger nuclei than LPCs without the characteristic oval shape. Additionally, in TAA-induced CLD, the previously observed cell population single-positive for panCK was detected mainly central at 14 and 42 days post treatment (Fig. 4.18).

Hepatocyte loss and the expansion of CLD-induced cellular components involve the reorganisation of cell-cell contacts. Cadherins mediate contacts between adjacent cells by interactions of the extracellular domains and the formation of adherens junctions (Shapiro and Weis 2009). E-cadherin was found to be expressed in biliary cells and LPCs in healthy and injured livers, as well as in periportal hepatocytes in uninjured livers (Ueberham *et al.* 2007; Van Hul *et al.* 2009). The staining pattern demonstrated by Ueberham and colleagues (Ueberham *et al.* 2007) was confirmed in control mice, in which E-cadherin expression was restricted to hepatocytes in the periportal areas and a stronger staining was observed in cholangiocytes that co-expressed CK19 (Fig. 4.19). There was a great overlap of CK19 and E-cadherin expression in CDE-induced LPCs and decreasing E-cadherin staining intensities were observed in hepatocytes from day 14 to day 42 (Fig. 4.20). In contrast to the study from Ueberham *et al.* a weak hepatocytic staining remained in the area of LPC expansion. Similarly, TAA-induced CK19$^+$ LPCs mainly co-expressed E-cadherin (Fig. 4.21). However, hepatocytic E-cadherin staining has been observed in damaged central instead of periportal areas at day 14 and positively stained hepatocytes were detected in the DR surrounding parenchyma at day 42.

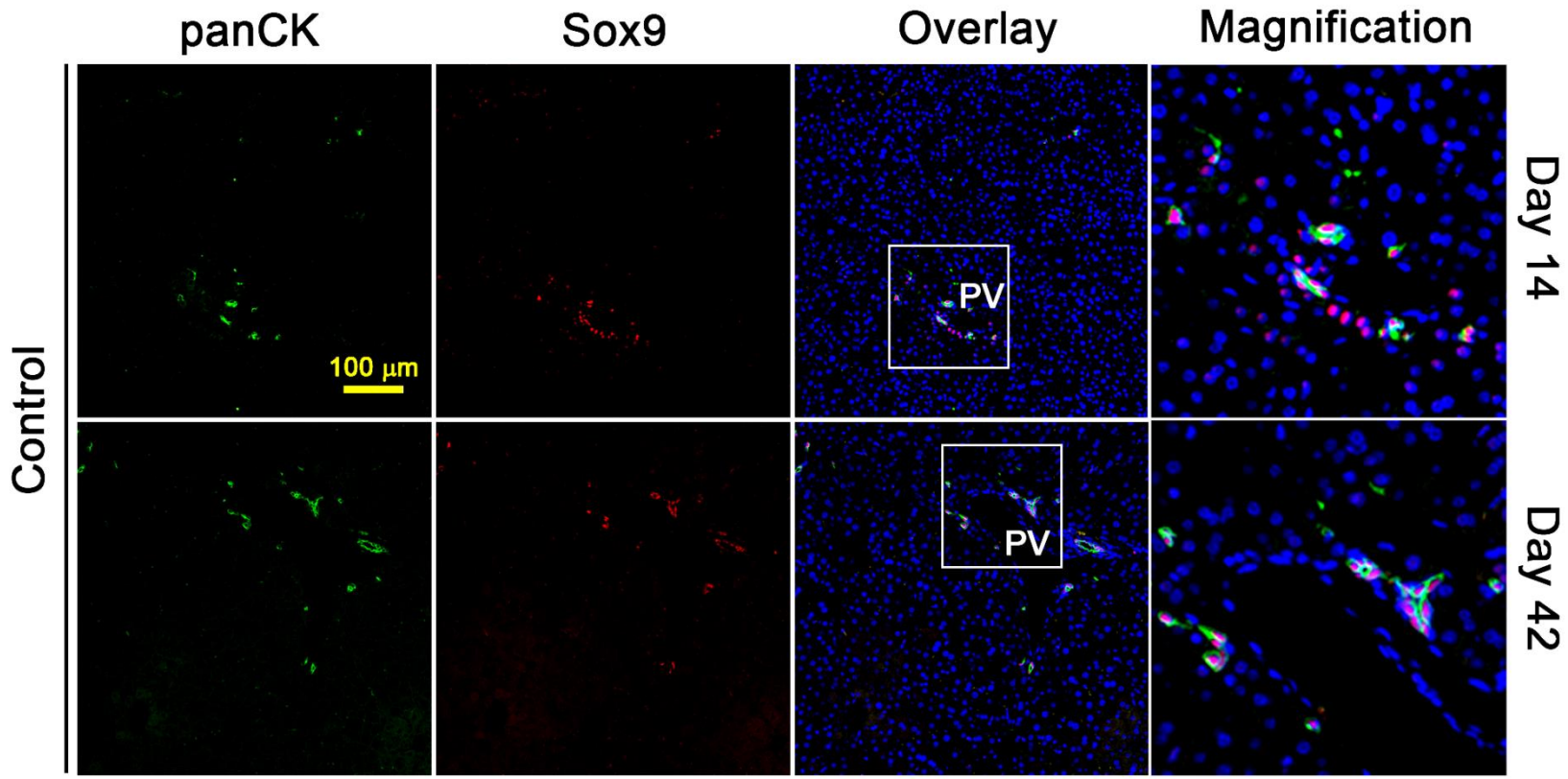

Fig. 4.16: Co-localisation of panCK and Sox9 in control mice. Formalin-fixed, paraffin-embedded liver sections of mice fed with control diet for 14 and 42 days were fluorescently labelled with the cholangiocytic LPC markers panCK and Sox9. The scale bar represents 100 µm and the inserts specify the field of magnification. *PV*, portal vein.

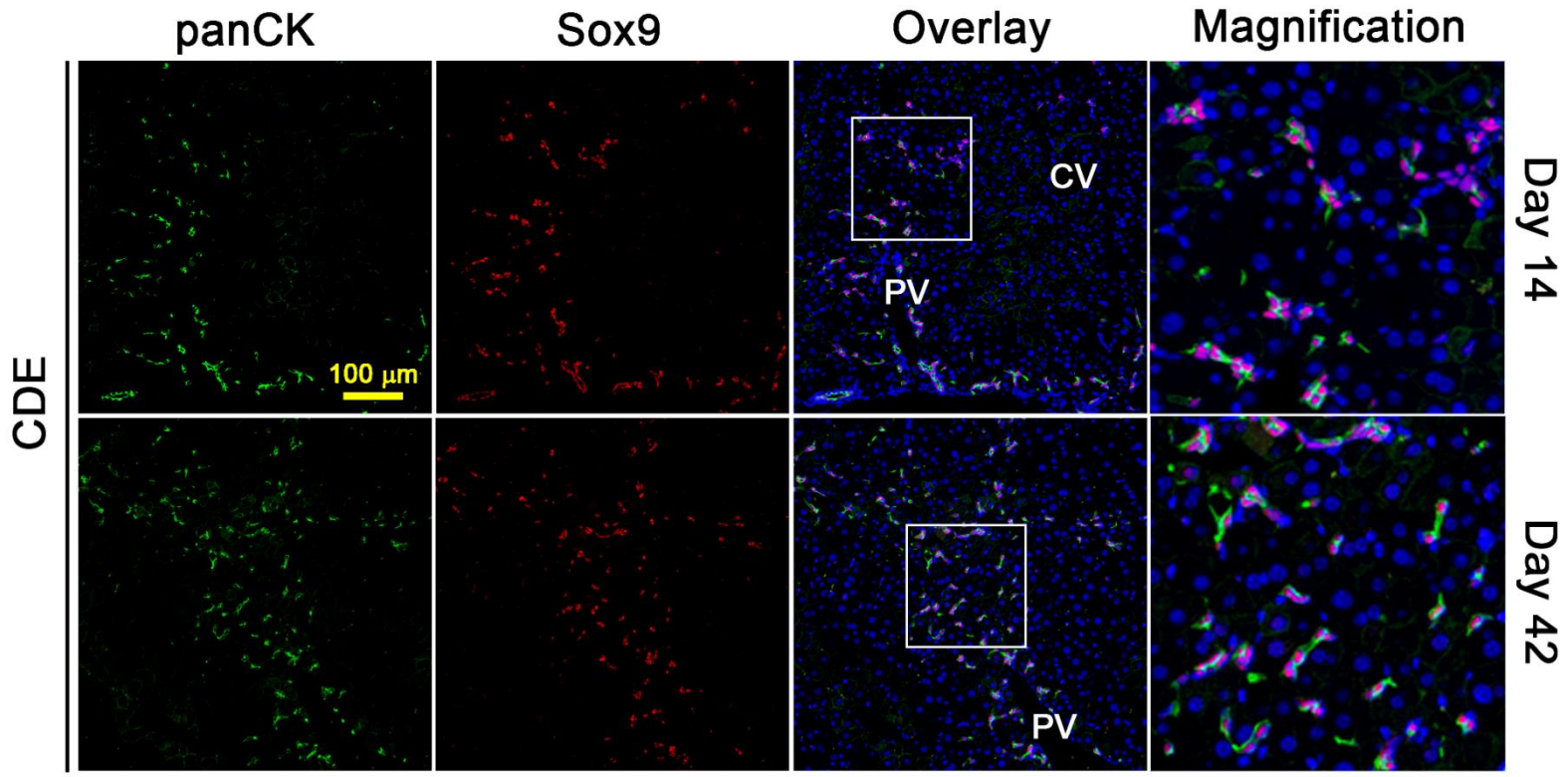

Fig. 4.17: Co-localisation of panCK and Sox9 in the CDE model. Formalin-fixed, paraffin-embedded liver sections of CDE-treated mice for 14 and 42 days were fluorescently labelled with cholangiocytic LPC markers panCK and Sox9. The scale bar represents 100 μm and the inserts highlight the area of magnification. *CV*, central vein*; PV*, portal vein.

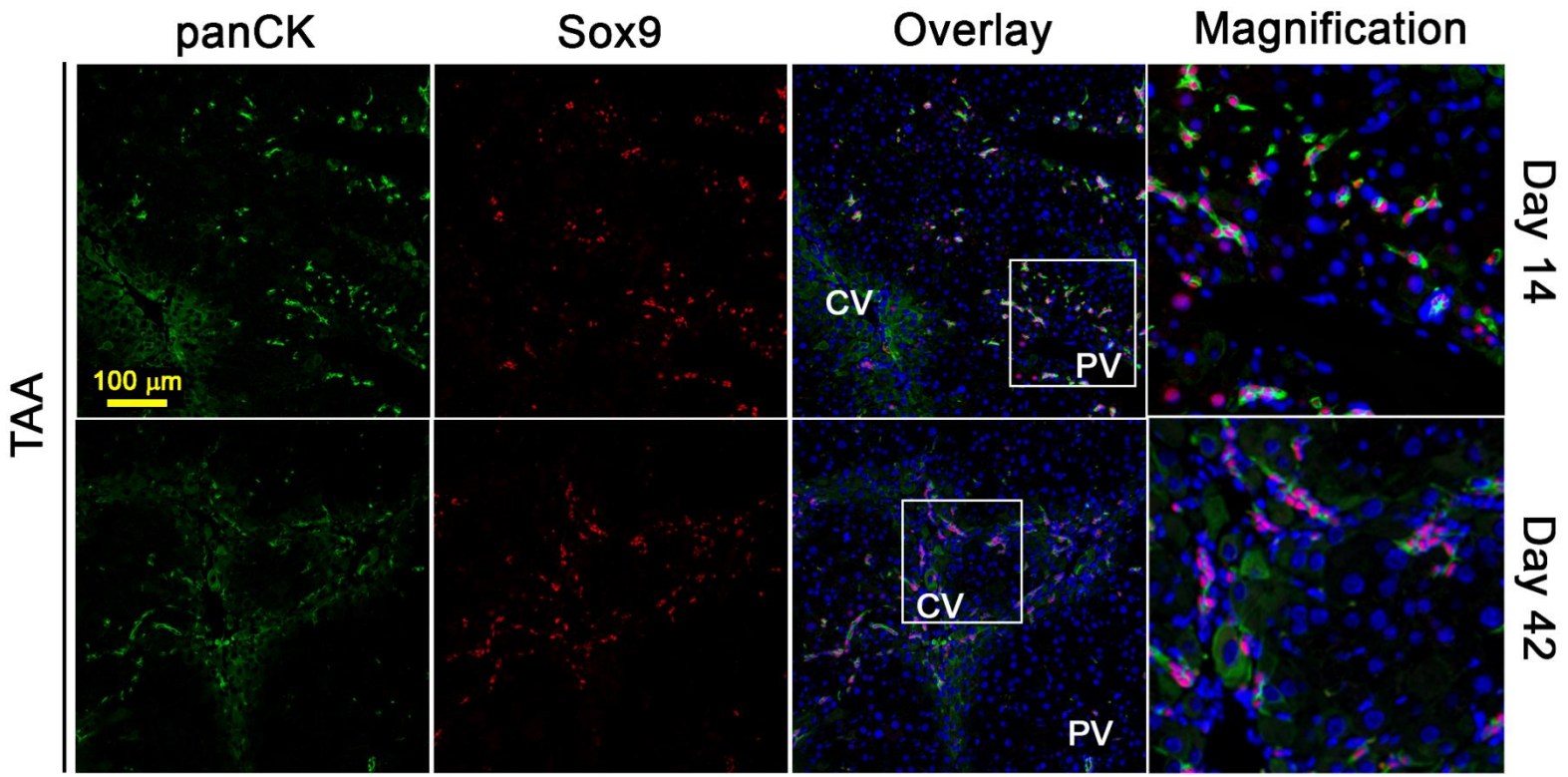

Fig. 4.18: Co-localisation of panCK and Sox9 in the TAA model. Formalin-fixed, paraffin-embedded liver sections of mice exposed to TAA for 14 and 42 days were labelled with the biliary cell and LPC markers panCK and Sox9 using immunofluorescence. The scale bar represents 100 μm and the inserts identify the field of magnification. *CV*, central vein*; PV*, portal vein.

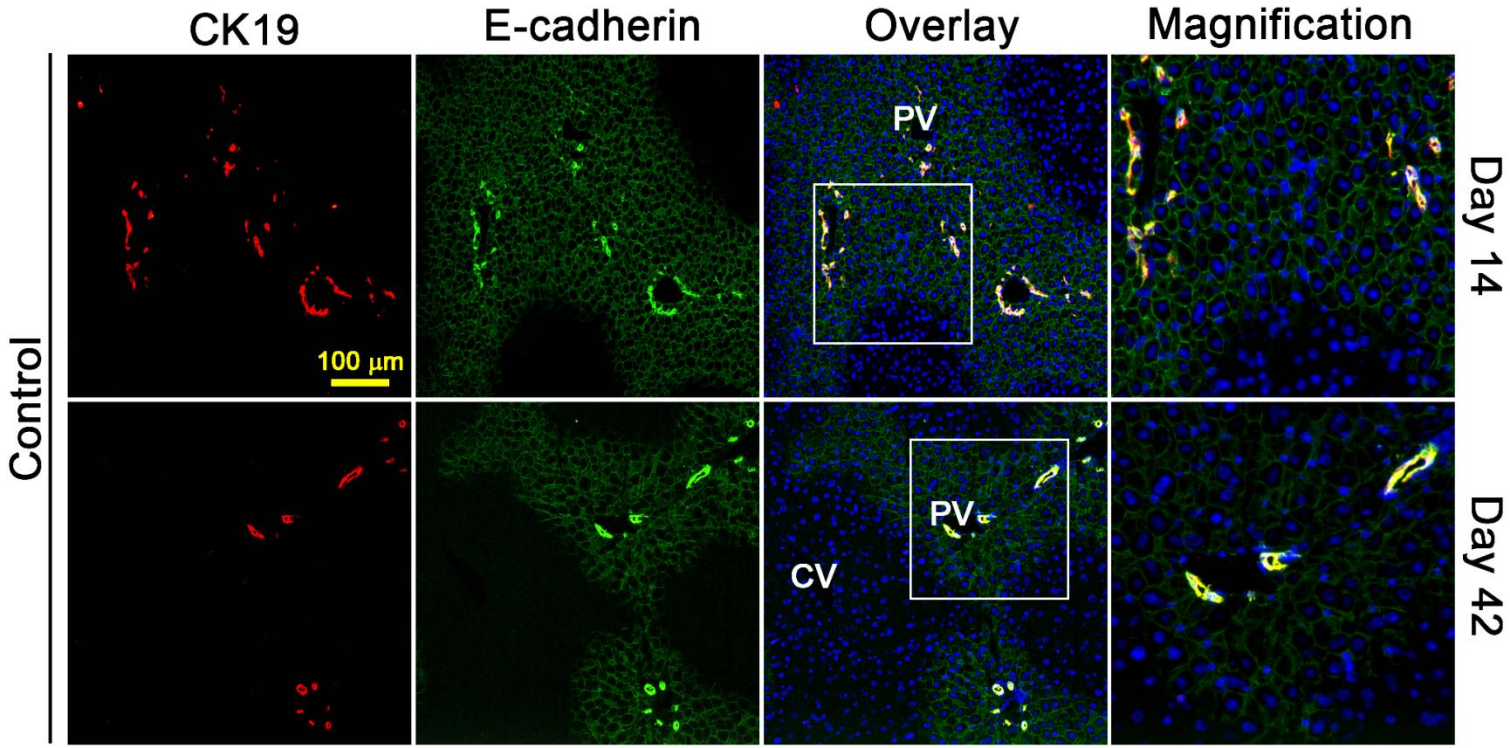

Fig 4.19: Immunofluorescent staining of CK19 and E-cadherin in control mice. Frozen liver sections of mice fed a control diet for 14 and 42 days were labelled with the cholangiocytic LPC markers CK19 and E-cadherin. The scale bar depicts 100 µm and the inserted boxes highlight the area of magnification. *CV*, central vein*; PV*, portal vein.

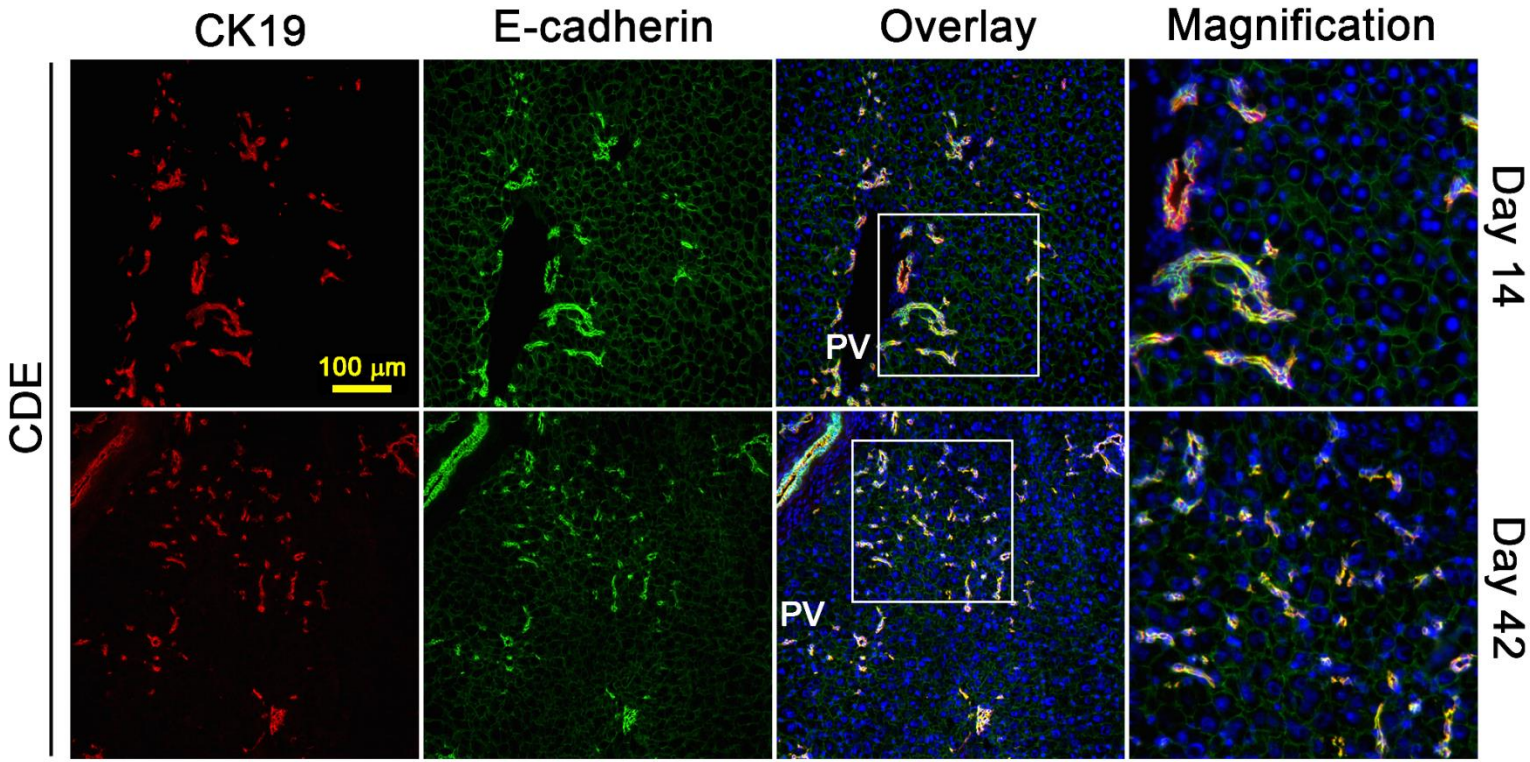

Fig 4.20: Immunofluorescent staining of CK19 and E-cadherin following CDE treatment. Frozen liver sections of mice exposed to CDE treatment for 14 and 42 days were labelled with the biliary cell and LPC markers CK19 and E-cadherin. The scale bar represents 100 µm and the inserts identify the field of magnification. *CV*, central vein*; PV*, portal vein.

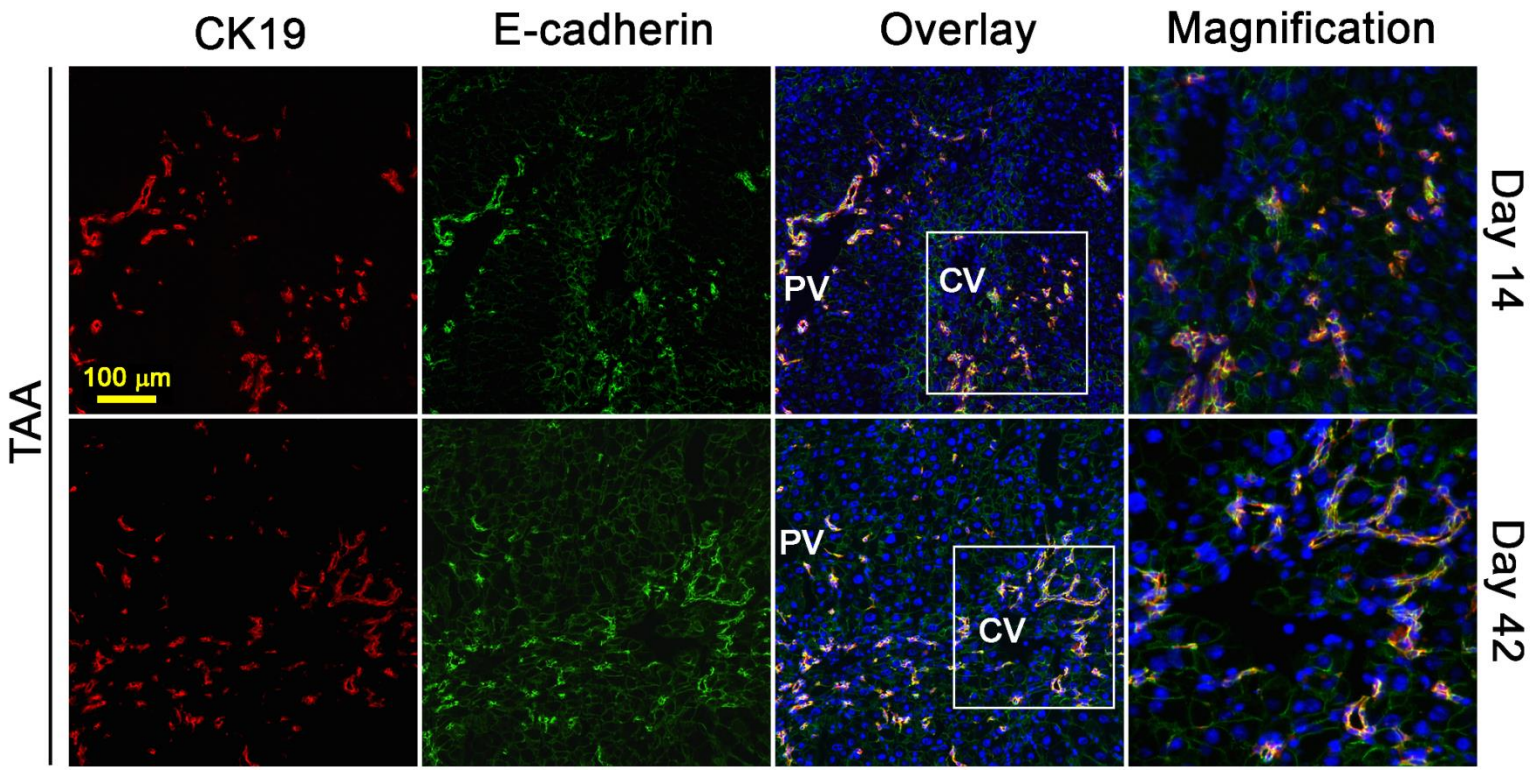

Fig 4.21: Immunofluorescent staining of CK19 and E-cadherin in TAA-induced CLD. Frozen liver sections of mice treated with TAA for 14 and 42 days were labelled with the cholangiocytic LPC markers CK19 and E-cadherin. The scale bar depicts 100 µm and the inserted boxes highlight the area of magnification. *CV*, central vein*; PV*, portal vein.

4.4.3 TAA-induced pericentral HNF4α$^+$ hepatocytes co-express the LPC marker panCK but not CK19

As shown earlier (see 4.4.2), the TAA model induced several A6$^-$/panCK$^+$ after 14 and 42 days of treatment. Since some of these single-positive cells had the morphology of small intermediate hepatocytes or damaged necrotic hepatocytes, their phenotype was further assessed using the hepatocyte lineage marker HNF4α. Co-labelling revealed that several panCK$^+$ cells in pericentral areas expressed HNF4α (Fig. 4.22). To further investigate this panCK$^+$/HNF4α$^+$ cell population in central TAA-damaged areas, a co-staining with the additional LPC marker, CK19, and HNF4α was performed. The data show that CK19 only captures LPCs/biliary structures and there was no overlap with HNF4α-expressing cells (Fig. 4.23).

4.4.4 CLD-induced LPCs comprise small cell subpopulations

In addition to chapter 4.4.2 where LPC populations were labelled using cholangiocytic LPC markers, this paragraph analyses the co-expression of markers which do not label a bulk of LPCs but rather are expressed in other cell populations present in the liver and when co-existent in LPCs may define smaller subpopulations with distinct features. Therefore, to further characterise CDE- and TAA-induced LPC populations, the broad LPC marker panCK (as shown in 4.4.2) was used in co-expression analyses with the markers CD44 and CD90, which have been associated with LPCs in earlier studies (Petersen *et al.* 1998; Petersen *et al.* 2003; Ueberham *et al.* 2007).

The expression pattern of CD44 in control mice showed several positively stained single cells and small cell groups around portal areas and throughout the parenchyma, most likely representing KCs since CD44 has been demonstrated to mark macrophages (Shi *et al.* 2006). However, there were no cells positive for both markers panCK and CD44 (Fig. 4.24). Similar results were obtained when staining liver sections from mice treated with CDE for 14 and 42 days (Fig. 4.25).

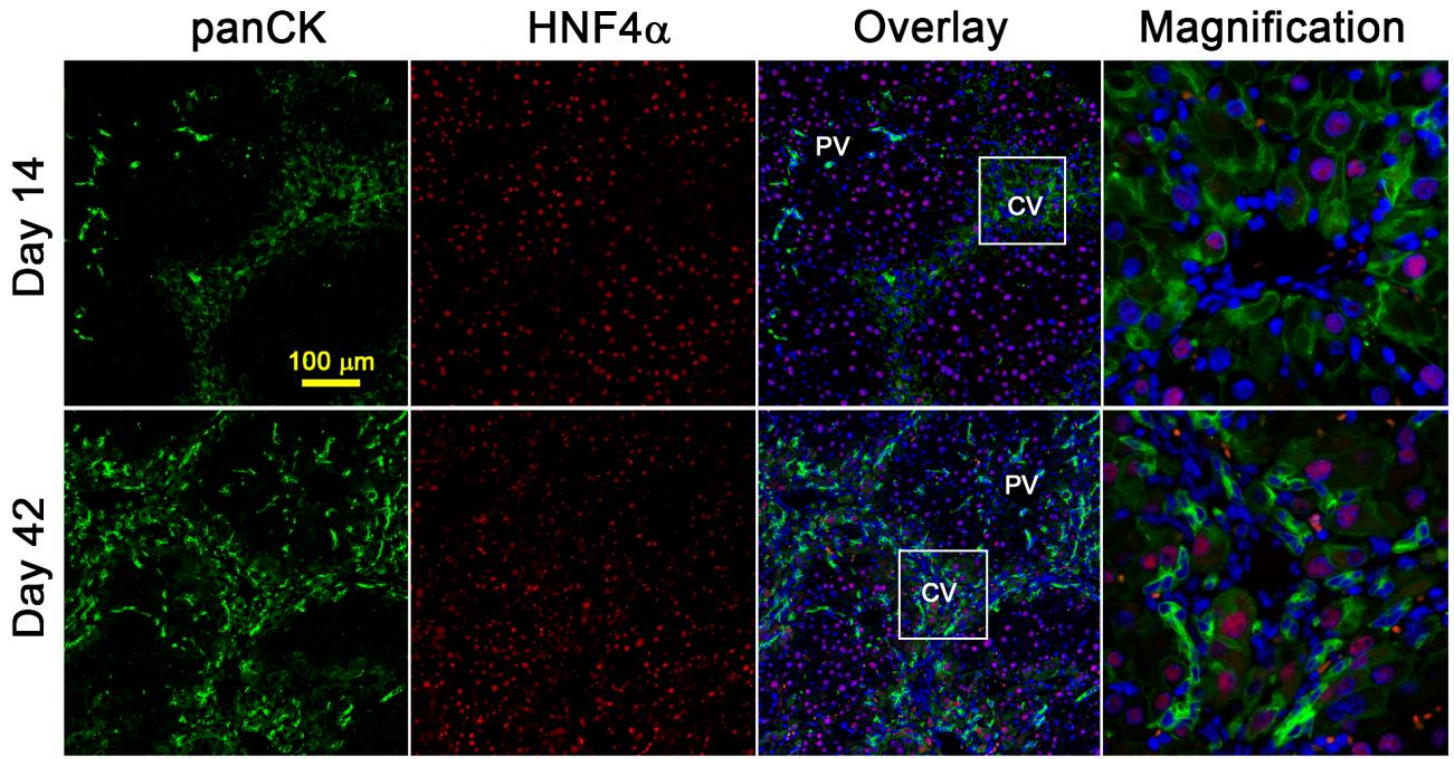

Fig. 4.22: TAA induces a centrally located panCK$^+$/HNF4α$^+$ cell population. Formalin-fixed, paraffin-embedded liver sections were fluorescently labelled for the biliary cell/LPC marker panCK and the hepatocyte marker HNF4α. Nuclei were stained using DAPI. Representative images are shown and the scale bar represents 100 μm. The inserts highlight the area of magnification. *CV*, central vein*; PV*, portal vein.

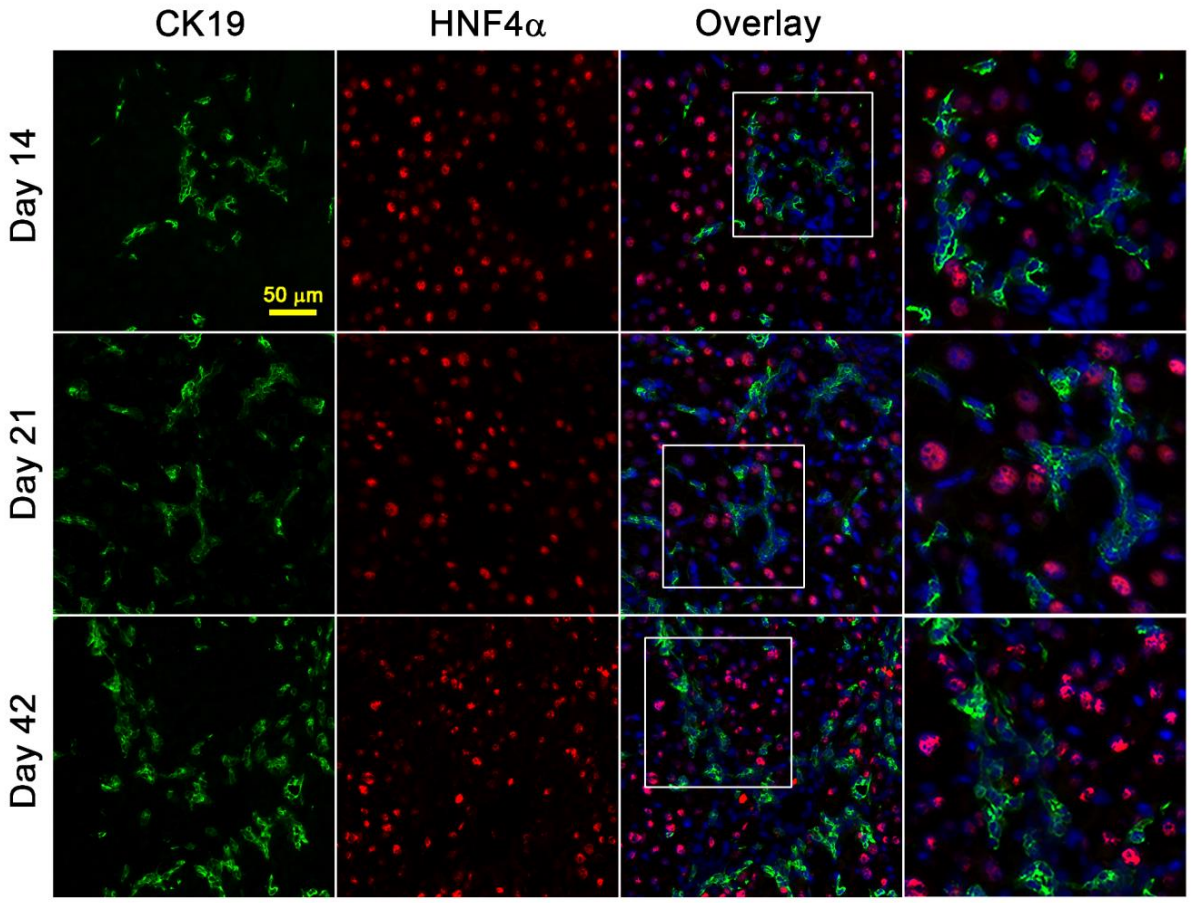

Fig. 4.23: TAA-induced CK19-positive cells do not co-express HNF4α. Frozen sections were fluorescently labelled for the biliary cell/LPC marker CK19 and the hepatocyte marker HNF4α. Representative images are shown and the scale bar depicts 50 µm. The inserted boxes identify the region of enlarged images.

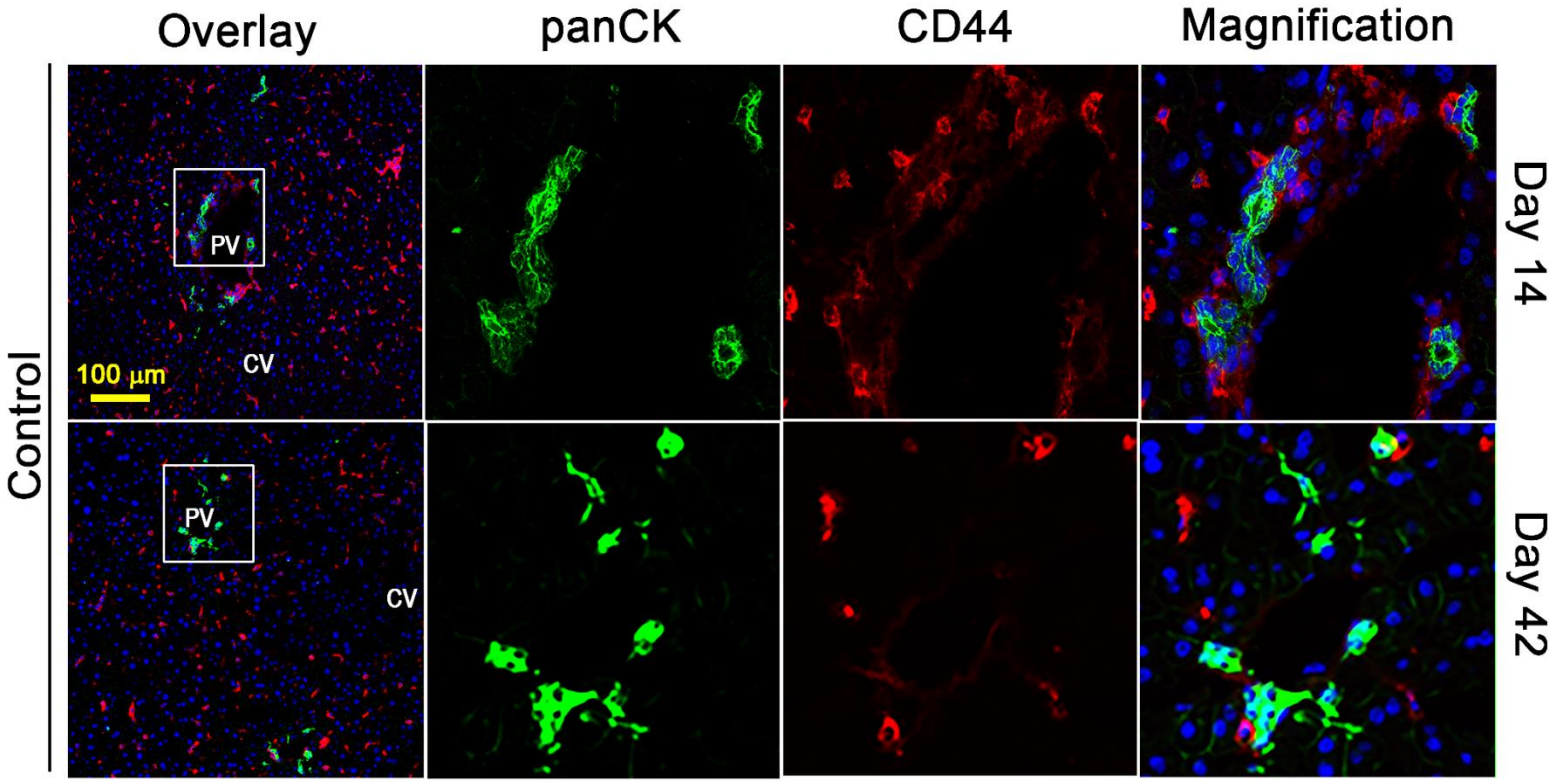

Fig. 4.24: Immunofluorescent staining of panCK and CD44 in control mice. Frozen liver sections of control mice at day 14 and 42 were labelled with the cholangiocytic LPC marker panCK and the marker CD44. The scale bar represents 100 µm and the inserts highlight the area of magnification. *CV*, central vein*; PV*, portal vein.

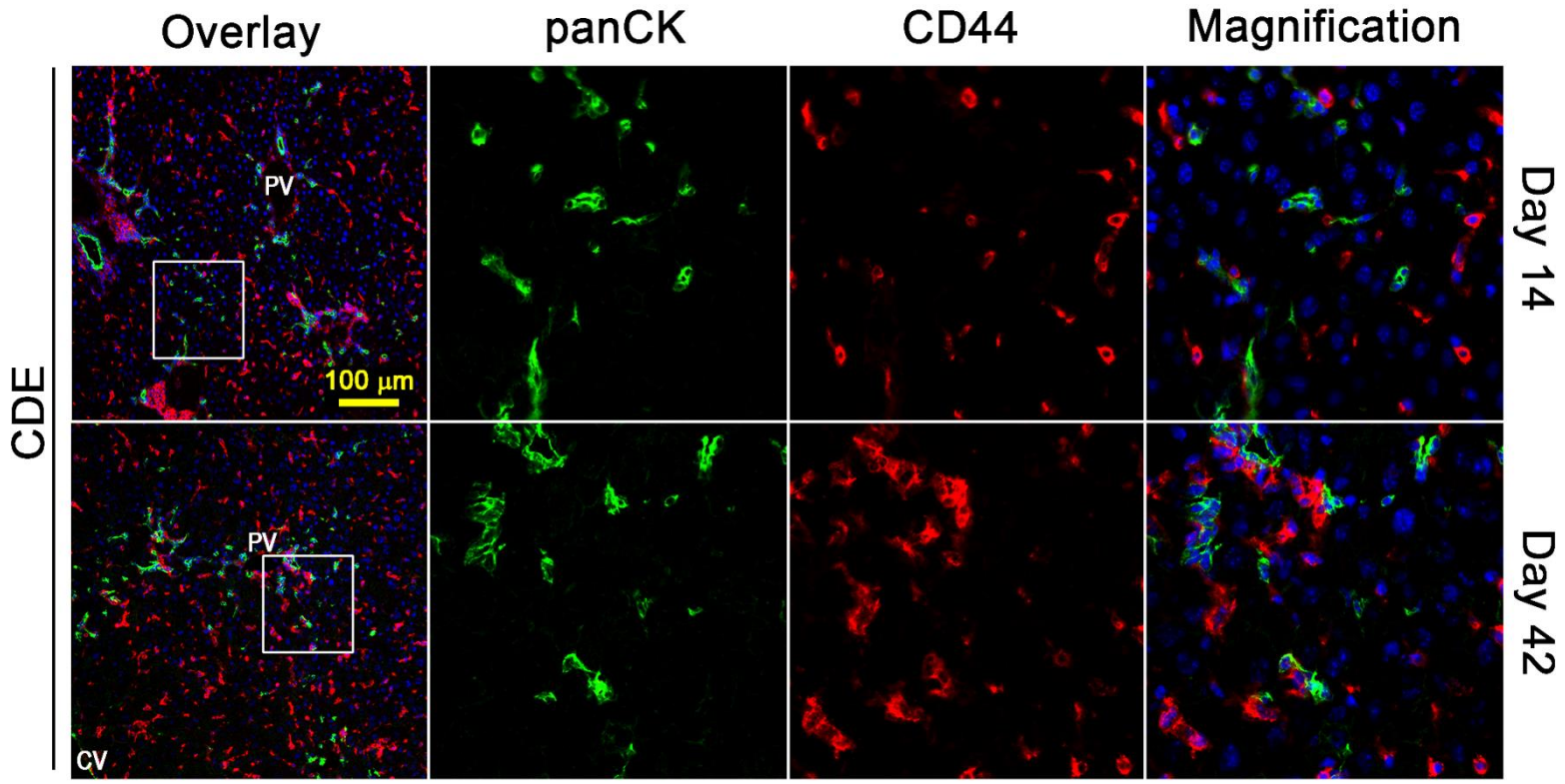

Fig. 4.25: Immunofluorescent staining of panCK and CD44 in CDE-induced CLD. Frozen liver sections of mice fed a CDE for 14 and 42 days were labelled with the biliary cell/LPC marker panCK and the marker CD44. The scale bar depicts 100 µm and the inserted boxes highlight the area of magnification. *CV*, central vein*; PV*, portal vein.

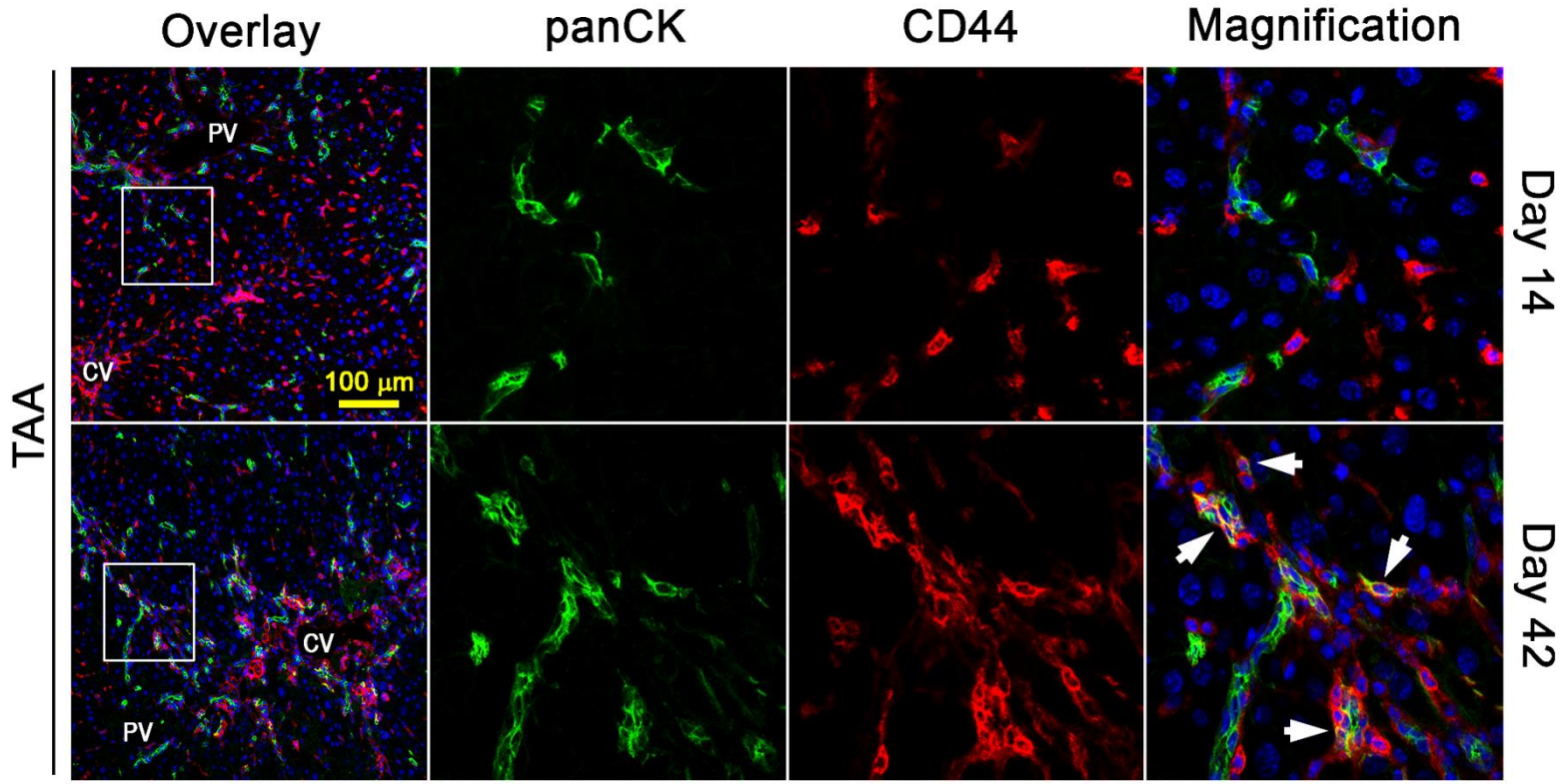

Fig. 4.26: Co-localisation of panCK and CD44 in TAA-induced CLD. Frozen liver sections of mice exposed to TAA treatment for 14 and 42 days were fluorescently labelled with the cholangiocytic LPC marker panCK and CD44. The scale bar represents 100 µm and the inserts highlight the field of magnification. Arrows show examples of panCK^{+}/CD44^{+} cells. *CV*, central vein*; PV*, portal vein.

In contrast to control and CDE mice, TAA exposure for 42 days resulted in several panCK$^+$/CD44$^+$ single cells and small strings of cells in damage burden areas (Fig. 4.26). CD90 expression in control mice was found in cells lining the portal vessels and a few single cells were detected in the parenchyma (Fig. 4.27). Interestingly, in CDE-treated mice, CD90$^+$ cells became more frequent around portal areas and occasionally co-expressed panCK following treatment for 14 and 42 days (Fig. 2.28). However, in response to TAA exposure, no panCK$^+$/CD90$^+$ cells were detected (Fig. 4.29).

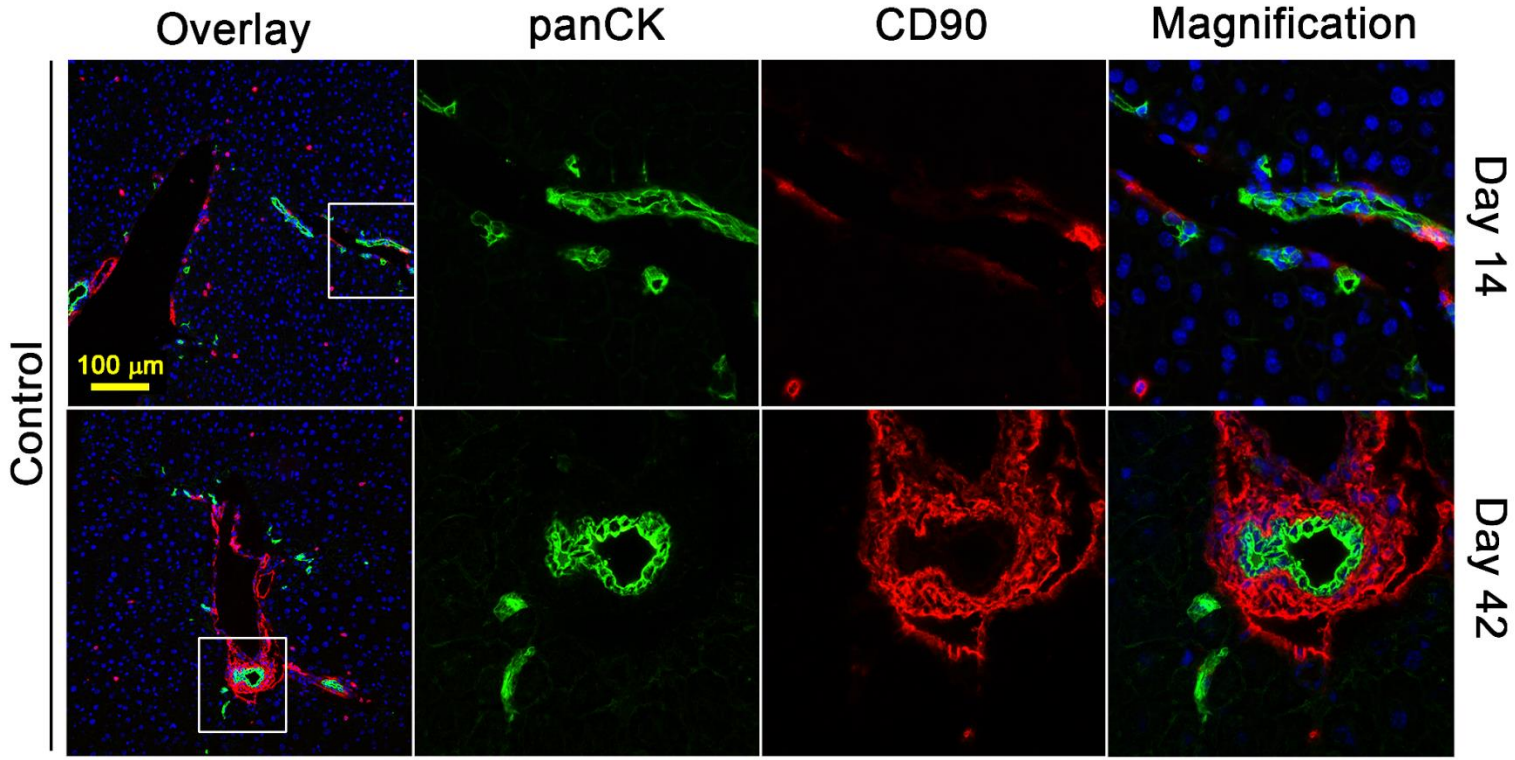

Fig. 4.27: Immunofluorescent staining of panCK and CD90 in control mice. Frozen liver sections of control mice at day 14 and 42 were labelled with the cholangiocytic LPC marker panCK and CD90. The scale bar depicts 100 µm and the inserted boxes highlight the area of magnification.

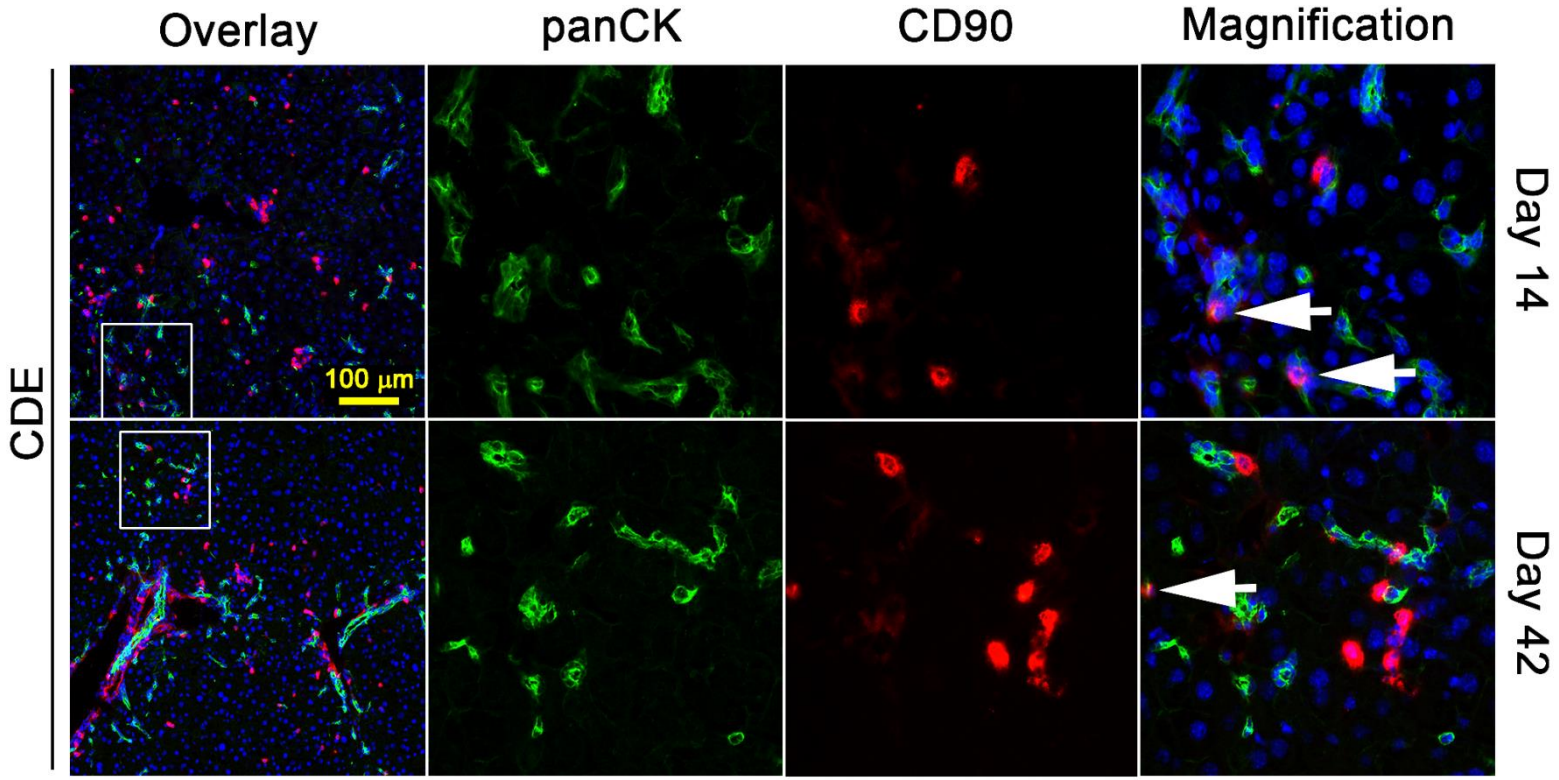

Fig. 4.28: Immunofluorescent staining of panCK and CD90 induced by CDE treatment. Frozen liver sections of mice exposed to CDE treatment for 14 and 42 days were labelled with the biliary cell/LPC marker panCK and the marker CD90. The scale bar represents 100 µm and the inserts highlight the area of magnification. Arrows show examples of $panCK^{+}/CD90^{+}$ cells.

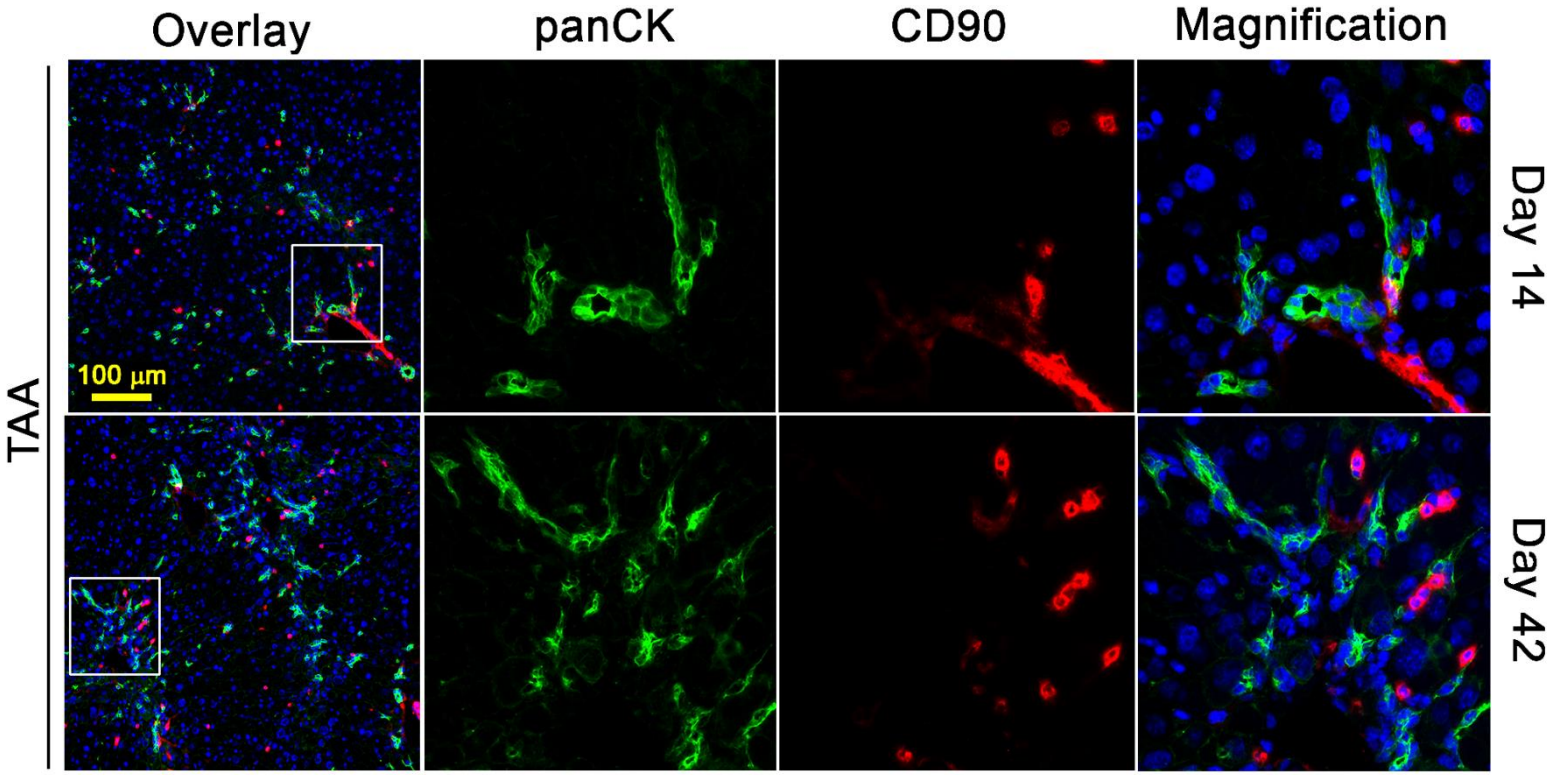

Fig. 4.29: Immunofluorescent staining of panCK and CD90 induced by TAA treatment. Frozen liver sections of mice treated with TAA for 14 and 42 days were labelled with the cholangiocytic LPC marker panCK and the marker CD90. The scale bar depicts 100 µm and the inserts highlight the field of magnification.

4.5 Discussion

The studies in this chapter provide a detailed characterisation of the LPC response in CDE- versus TAA-induced CLD during injury induction (day 7), establishment (day 14) and maintenance (day 42). As already shown in the previous chapter (chapter 3), both CDE and TAA treatments induce biliary cell/LPC expansion as part of the DR. This chapter focuses in more detail on the proliferation status and different phenotypes of LPCs using immunofluorescent staining techniques.

On the background of an LPC-stimulating environment, showing increased mitotic cytokine levels (as documented in Chapter 3), both models induced biliary cell/LPC proliferation, however the timing and location differed between the two regimens. In the CDE model the highest number of proliferating $A6^{+}/Ki67^{+}$ cells was induced in portal areas during early injury induction at day 7, whereas TAA treatment caused increased proliferation of this cell population during injury progression at day 42 in central areas within the well-established regeneration niche. Hepatocyte proliferation was increased in TAA- compared to CDE-induced injury, indicating that TAA induces more severe hepatocyte injury and consequently requires more compensatory regeneration, or CDE more effectively inhibits the mitotic activity of hepatocytes. Consistent with these results, a 30-week TAA treatment in rats caused alterations in cell cycle-related proteins with increasing pro-mitotic protein expression in hepatocytes and the ductular cell compartment but also increased expression levels of the cell-cycle inhibitor cyclin-dependent kinase inhibitor p21 (Jeong *et al.* 2001). Consequently, TAA exposure in mice led to a combination of cell cycle arrest in damaged cells and compensatory proliferation of healthy cells including both hepatocytes and biliary/LPC structures. As demonstrated in Chapter 3, it was clear that in the CDE model at day 7, the LPC response was initiated periportally and further expanded into the parenchyma. In contrast, in the TAA model the expansion of biliary structures and the LPC compartment had shifted from the initial periportal localisation in the induction phase to an accumulation in central areas at later time points consistent with the location of the regeneration niche.

Interestingly, immunofluorescent co-localisation analysis of panCK with other LPC markers such as A6, CD133, MIC1-1C3 and CK19 revealed that CDE feeding

mainly induced double-positive populations. TAA treatment on the other hand produced a population of single panCK$^+$ cells that do not co-express other investigated LPC markers, morphologically resembled an intermediate hepatocyte and were mainly seen in central areas, co-existing in the injury and regeneration niche with double-positive cells. It is tempting to speculate that the double-positive populations represent LPCs with a biliary origin, such as seen for lineage-traced CK19$^+$ CC cells on a TAA background (Guest *et al.* 2014). On the other hand, expression of the hepatocyte marker HNF4α in the panCK$^+$ cell population suggests that they might be a result of hepatocytic dedifferentiation, which has been demonstrated to occur after Notch-mediated conversion of TAA-targeted hepatocytes into biliary cells (Sekiya *et al.* 2012). Since co-staining with the LPC marker CK19 and HNF4α showed no overlap in the expression profile, it is more likely that the single-positive panCK population represents damaged hepatocytes in toxicity-burdened central areas that have changed their cytokeratin phenotype. The pan marker for cytokeratins recognises a cocktail of multiple low and high molecular weight cytokeratins and thus detects a wide range of cytoskeletal changes. Previous studies have demonstrated that hepatocytes can express biliary cell specific cytokeratins under chronic liver injury conditions (Van Eyken *et al.* 1988; Yabushita *et al.* 2001; Bateman and Hubscher 2010).

In general, the investigated markers showed a great overlap in their expression profile regardless of CDE, TAA or control treatment. However, consistent with previous studies (Ueberham *et al.* 2007), co-staining of liver tissue with two markers revealed the existence of many single-positive LPC populations. These included phenotypes such as panCK$^+$/A6$^-$, panCK$^+$/CD133$^-$, panCK$^+$/MIC1-1C3$^-$, CK19$^+$/EpCAM$^-$ and CK19$^+$/E-cadherin. Interestingly, investigations of the cholangiocytic LPCs markers panCK and Sox9 demonstrated several panCK$^-$/Sox9$^+$ cells existing in close proximity to portal areas. Most likely, single Sox9$^+$ cells represent “hybrid hepatocytes” which were recently described by Font-Burgada and colleagues (Font-Burgada *et al.* 2015). In this study the Sox9$^+$/CK19$^-$/HNF4α$^+$ population was capable of replacing damaged hepatocytes by expanding from portal triads into the parenchyma under certain injury conditions.

Furthermore, some LPCs co-expressed the marker CD44, which also marks macrophages and represents the signalling component of the macrophage migration

inhibitory complex CD74-receptor complex (Shi *et al.* 2006). Another LPC subpopulation co-expressed CD90, which is expressed in activated endothelial cells and involved in binding ligand-positive leucocytes (Saalbach *et al.* 2000) as well as in cells of the haematopoietic lineage (Baum *et al.* 1992). Therefore, these markers can be used to further define a smaller LPC population with potentially distinct features. However, the expression patterns were model specific, as TAA induced several panCK$^+$/CD44$^+$ LPCs at day 42 and CDE-treated mice presented a rare panCK$^+$/CD90$^+$ cell population after 14 and 42 on the diet.

Taken together all the investigated LPC markers were suitable to define a broad population of LPCs in CDE- and TAA-induced CLD. Moreover, co-localisation studies further described the heterogeneity of LPC populations by identifying different subpopulations. A detailed multichannel flow cytometry analysis is planned to investigate all LPC markers used in this thesis with additional markers including Fn14, Integrin α5β6 and OPN (Dorrell *et al.* 2008; Tirnitz-Parker *et al.* 2010; Carpentier *et al.* 2011). This will provide insight into the abundance of different LPC subpopulations induced by CDE or TAA treatment. Distinct subpopulations will then be isolated and characterised according to their function (differentiation potential) and gene expression profile, which might be useful to generate a "developmental tree" of LPCs and to identify the role of these subpopulations during CLD.

CHAPTER 5

Characterisation of LPC populations and tumour formation following long-term CDE and TAA exposure

5.1 Introduction

To understand the pathogenesis of liver cancer, several mouse models are utilised in the literature, including the use of transgenic mice and chemical or dietary induction (Newell *et al.* 2008; Bakiri and Wagner 2013). None of these represents an ideal animal model that meets all the criteria necessary to perfectly reflect all stages of hepatocarcinogenesis. Instead adequate experimental conditions are provided to induce the pathology and disease state of interest, depending on the research question. Thus, a thorough characterisation of all steps of carcinogenesis in the experimental models is fundamental to be able to select appropriate time points and settings for individual study designs. Moreover, since the differential diagnostic of nodules in humans highly depends on the non-tumorous tissue background (Brunt 2012), a detailed description of injury-induced tissue dynamics in the liver environment, in addition to the histopathology of neoplasms, is inevitable. Most discussed parameters associated with tumour development include fibrosis, inflammation and LPC expansion (Berasain *et al.* 2009; Cai *et al.* 2012; Zhang and Friedman 2012).

The earlier introduced CLD models, CDE and TAA, represent promising regimens to mimic a wide spectrum of human pathological conditions associated with liver cancer. The progressive fibrosis pattern in the TAA model has been demonstrated to resemble the injury dynamics of chronic viral hepatitis (Ferrell 2000), which is one of the most common risk factors for HCC developing on the background of liver cirrhosis (Gomaa *et al.* 2008; Hoshida 2012; Toshikuni *et al.* 2014). The dietary CDE model, on the other hand, induces changes similar to those seen in NAFLD patients. This regime gained importance in recent years since a worldwide dietary change has led to an increase in numbers of patients suffering from obesity and diabetes - conditions that have been associated with NAFLD, NASH and HCC (Nair *et al.* 2002; Regimbeau *et al.* 2004; Sun and Karin 2012; Pocha *et al.* 2015). In contrast to viral hepatitis-induced carcinogenesis in the liver (McGivern and Lemon 2011), the knowledge of mechanisms leading to NAFLD-related cancer in humans is very limited (Yeh and Brunt 2014). Cohort studies suggest that steatosis represents

an independent predictor for HCC, regardless of the presence of cirrhosis (Pekow *et al.* 2007; Alexander *et al.* 2013).

In chapter 3, the induction, establishment and maintenance phase of CLD, induced through CDE and TAA administration, respectively, have been explicitly described. Liver tumour development has been demonstrated in both models (Becker 1983; Knight *et al.* 2008). While the CDE diet is more frequently used in mice to study HCC development, the TAA regimen has been utilised in the context of CC formation (Guest *et al.* 2014). To date no systematic study has been published characterising the sequential changes leading to neoplastic lesions and tumour development, including the injury-related tissue environment. Therefore, two detailed time courses of CDE and TAA treatment were performed in mice over the period of 7 months to (a) thoroughly characterise the molecular and cellular changes and to (b) compare the two models with regard to histopathological differences. Due to time constraints, this chapter provides a preliminary analysis including a limited number of mice at selected time points. The generated material will be further analysed in future experiments.

5.2 Study Aims

Since liver tumours comprise several phenotypes and arise on the background of different injury conditions, a thorough description of experimental models is necessary to be able to mimic distinct human pathologies and choose the right settings and time points for particular research questions. The studies in this chapter characterise the response dynamics induced by CDE and TAA long-term treatment and analyse model-specific injury patterns during CLD progression and carcinogenesis. This includes a detailed characterisation of induced tumours - phenotype assessment of HCC vs CC - as well as the examination of tissue injury parameters in the surrounding environment such as inflammation, LPC expansion and fibrosis.

5.3 Methods

Liver tissue and serum of 5 to 7 week-old, male C57BL/6J mice that had been subjected to CDE, TAA and control treatment (see Chapter 3), were harvested after 3, 5 and 7 months for further investigations. Due to the expected high diversity of tissue responses at later time points, animal numbers were increased to 8 to 12 mice per experimental group compared to the short-term experiments. Overall animal health was evaluated by body weight changes and liver weight to body weight ratios. Serum ALT levels informed about liver damage. Tumour formation was investigated by assessing gross liver morphology and neoplastic changes were analysed using Reticulin staining and immunohistochemical studies of the HCC marker CPS1 (HepPar 1 antigen) (Butler *et al.* 2008) and the CC marker CK7 and CK19. Tumours and non-tumorous tissue (referred to as background injury) were further characterised during injury progression and carcinogenesis through examination of liver histology and lipid accumulation by haematoxylin and eosin and Oil Red O staining, respectively. Magnitude and pattern of the model-specific inflammatory response was investigated by labelling $CD45^+$ inflammatory cells and $F4/80^+$ resident KCs using immunohistochemistry, as well as fluorescent labelling of $CD11b^+$ monocyte-derived macrophages. The expansion of LPC subpopulations was examined by immunohistochemical and fluorescent detection of the markers panCK, CK19, CD133, EpCAM and CD44. Evaluation of the injury-associated fibrogenic patterns was performed by Sirius Red staining. The regeneration niche was assessed by immunofluorescent staining of $panCK^+$ LPCs, $CD45^+$ inflammatory cells and SMA^+ activated HSCs.

5.4 Results

5.4.1 Overall health of animals exposed to long-term CDE and TAA treatment

Overall animal health in response to long-term CDE and TAA treatment was evaluated throughout the time course of seven months by measuring the body weight and the liver-to-body weight ratios of mice. Furthermore, overall liver damage was assessed by serum ALT levels, reflecting hepatocyte health.

The initial body weight loss induced by TAA and CDE within the first week of treatment was documented in Chapter 3 and was confirmed in this study (not shown). In response to further TAA treatment beyond six weeks, body weights of mice remained significantly lower than the corresponding controls at all investigated time points ($p \leq 0.05$, not shown in graph) (Fig. 5.1). In contrast, CDE exposure caused significantly lower body weights in mice up to eight weeks of treatment ($p \leq 0.05$, not shown in graph) with normalisation towards non-injured mice thereafter (Fig. 5.1).

In rats, there is a correlation between the liver-to-body weight ratio and the time of TAA exposure, reflecting an increase in liver mass relative to body weight as the injury progresses (Jeong *et al.* 2001). These findings were confirmed in mice after 5 and 7 months of TAA treatment and were due to reduced body weight gain and increasing liver weights (Fig. 5.2). Similar results were observed in CDE-fed mice after seven months on the diet. However, since body weights in CDE-treated mice were comparable to controls at later time points, the increased liver-to-body weight ratio reflects a significant increase in liver mass rather than a decrease in body weight.

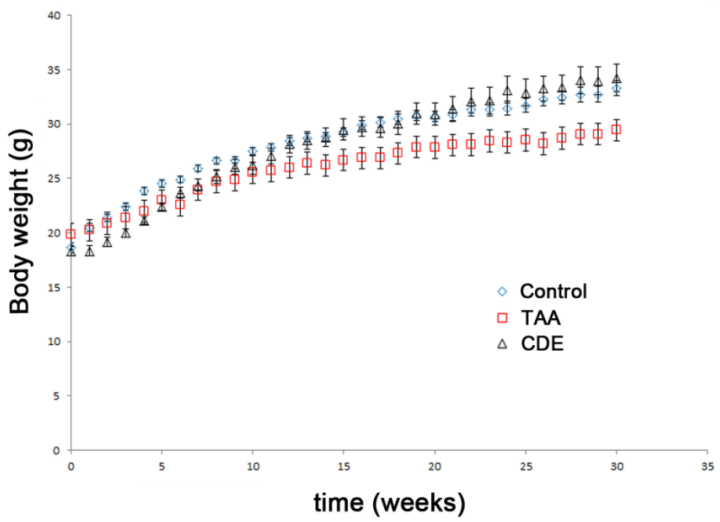

Fig. 5.1: Body weight dynamics in response to CDE and TAA treatment. Body weights of mice treated with CDE, TAA or control diet were measured throughout the time course of seven months.

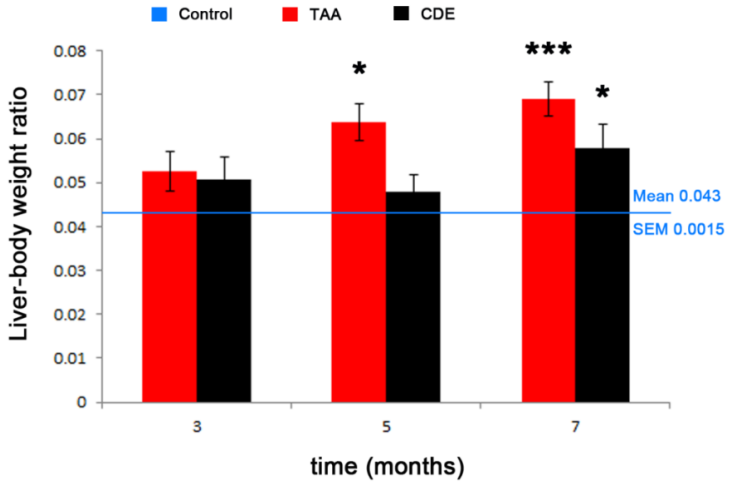

Fig. 5.2 Liver-to-body weight ratios of mice exposed to CDE and TAA treatment. Liver-to-body weight ratios were calculated in mice treated with CDE or TAA for 3, 5 and 7 months, as well as in controls. Ratios are expressed as mean ± SEM (4 to 12 mice per group). *p<0.05, p**<0.01, p***<0.001 compared to controls.

The biochemical assessment of serum ALT activity revealed a continuous liver damage induced by CDE and TAA treatment at all investigated time points (Fig. 5.3). However, different dynamics were observed since ALT levels in TAA mice showed only minor fluctuations (46.9 ± 3.5 U/l, 47.1 ± 1.2 U/l and 43.2 ± 3.1 U/l) whereas CDE exposure provoked a progressive increase from three (39.3 ± 3.7 U/l) to seven months (63.9 ± 4.6 U/l).

5.4.2 Gross liver morphology following long-term CDE and TAA treatment

To assess liver tumour development on the background of CDE- and TAA-induced CLD, the gross liver morphology of mice exposed to experimental conditions were evaluated at the time of sacrifice and compared to uninjured control livers of the same age (Fig. 5.4A). Both treatments induced substantial gross morphological changes ranging from one to numerous neoplastic lesions of 1-12 mm in diameter that appeared as white or brown/yellow nodules. According to their size, these subcapsular nodules were grouped into different categories (Fig. 5.4). Single or multiple neoplasms with a diameter of < 1 mm, distinguished by their white appearance within the liver lobe, most likely represent precursor lesions (Fig 5.4B). Outgrowing nodules of 1-5 mm in size were grouped as intermediate tumours (Fig. 5.4C and Fig. 5.4D), whereas nodules with a diameter of > 5 mm were listed as advanced tumours (Fig. 5.4E-H).

Following CDE and TAA treatment, several categories of neoplastic changes were identified as early as three months of CDE feeding (Table 5.1A) and after five months of TAA exposure (Table 5.1B). All detected tumours were primary tumours since no other organs in the body showed any abnormalities.

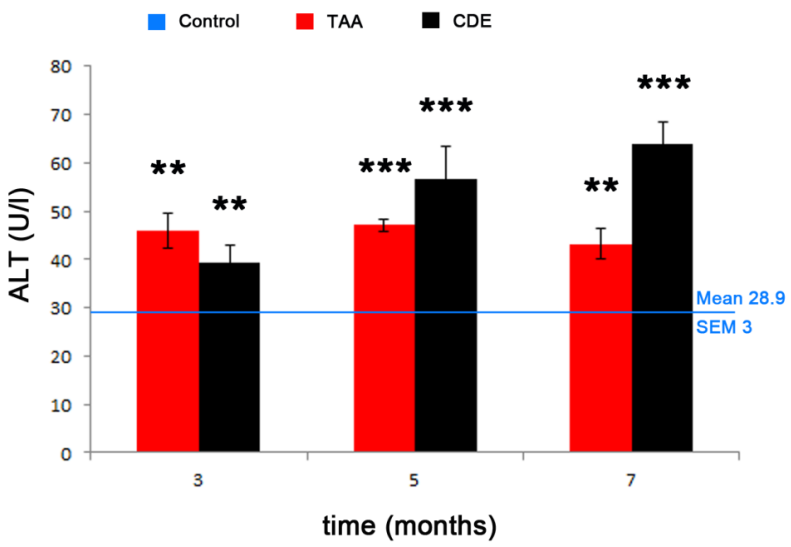

Fig. 5.3: Serum ALT levels were increased in CDE- and TAA-induced CLD. Hepatocyte health was evaluated by biochemically measuring serum alanine transaminase (ALT) levels of mice exposed to CDE, TAA or control treatment for 3, 5 and 7 months.

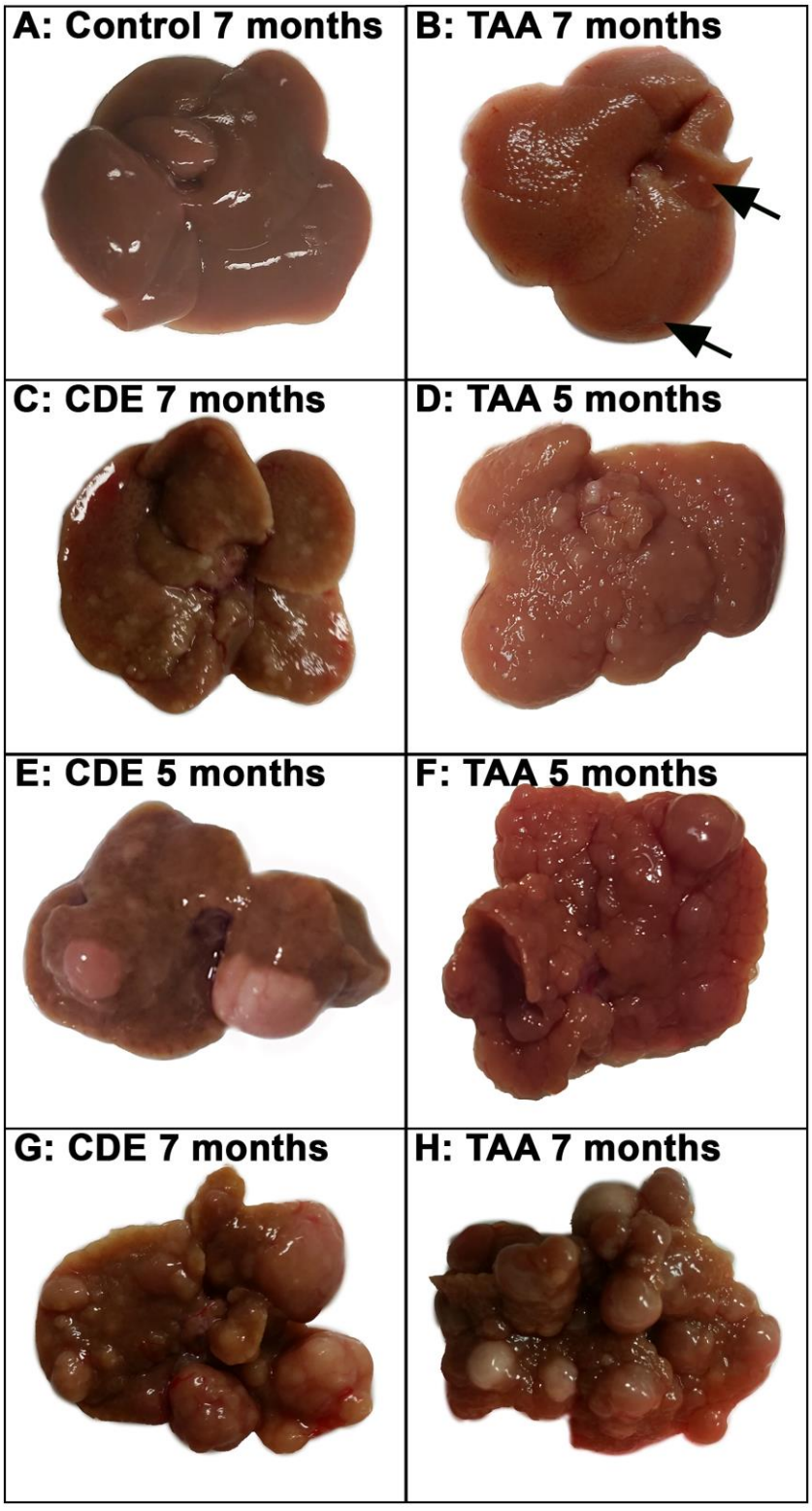

Fig. 5.4: Tumour morphologies induced by CDE and TAA long-term exposure. Gross liver morphologies of CDE-, TAA-treated, and control mice are illustrated. Representative images are shown for (A) a healthy control liver, (B) potential precursor lesions (C, D) intermediate tumours and (E-H) advanced tumours.

A

CDE exposure (months)	Neoplastic changes (%)	Precursor lesions	Intermediate tumours	Advanced tumours
7	11/11 (100)	6	3	2
5	2/7 (29)	1	0	1
3	1/6 (17)	1	0	0

B

TAA exposure (months)	Neoplastic changes (%)	Precursor lesions	Intermediate tumours	Advanced tumours
7	9/13 (69)	3	3	3
5	5/10 (50)	1	1	3
3	0/8 (0)	0	0	0

Table 5.1: Long-term CDE and TAA exposure induced tumour formation in mice. Total animal numbers showing neoplasms after 3, 5 and 7 months of (A) CDE and (B) TAA treatment are listed and further categorised into subgroups according to the gross liver morphology: Precursor lesions: diameter < 1 mm, intermediate tumours: 1-5 mm and advanced tumours: > 5 mm.

5.4.3 CDE- and TAA-induced background injury of non-tumorous tissue

The following paragraphs characterise and compare the injury dynamics in non-tumorous liver tissue in mice treated with CDE or TAA and describe the background settings during disease progression and carcinogenesis. This enables the correlation of tumour occurrence and different response dynamics including histological changes, the DR and fibrogenic patterns.

5.4.3.1 Histological evaluation of tissue damage

Histological assessment of liver sections after long-term treatment revealed distinct CDE- and TAA-induced morphological changes when compared to controls (Fig 5.5, Fig. 5.6 and Fig. 5.7). Moderate tissue damage was detected in livers after three months of CDE treatment, based on infiltrating small basophilic cells in periportal areas and parenchymal foci as well as pale appearing swollen or enlarged hepatocytes - ballooning - with granulated cytoplasm situated around central veins. Prolonged treatment for five and seven months resulted in liver damage progression as hepatocyte degeneration, enrichment of basophilic cells and their parenchymal infiltration was detected in agreement with corresponding increased serum ALT levels assessed earlier (see 5.4.1) (Fig. 5.6). In contrast, TAA long-term exposure provoked a progressive injury pattern following the maintenance phase introduced in Chapter 3.4.1 (Fig. 5.7). Eosinophilic hepatocytes were seen in pericentral areas and were connected by eosinophilic bands of hepatocytes, which were both associated with increasing small basophilic cell infiltrates during injury progression and carcinogenesis.

Since there is a high risk for HCC development on the background of hepatic steatosis (Baffy *et al.* 2012) and the CDE diet induced excessive lipid accumulation in hepatocytes during early time points of the 6-week time course (see 3.4.1), effects of long-term CDE in comparison to long-term TAA treatment were investigated. Therefore, lipid deposition was visualised using Oil Red O staining (Fig. 5.8). In the CDE model, high levels of macrovesicular and microvesicular lipid accumulation were detected at all investigated time points.

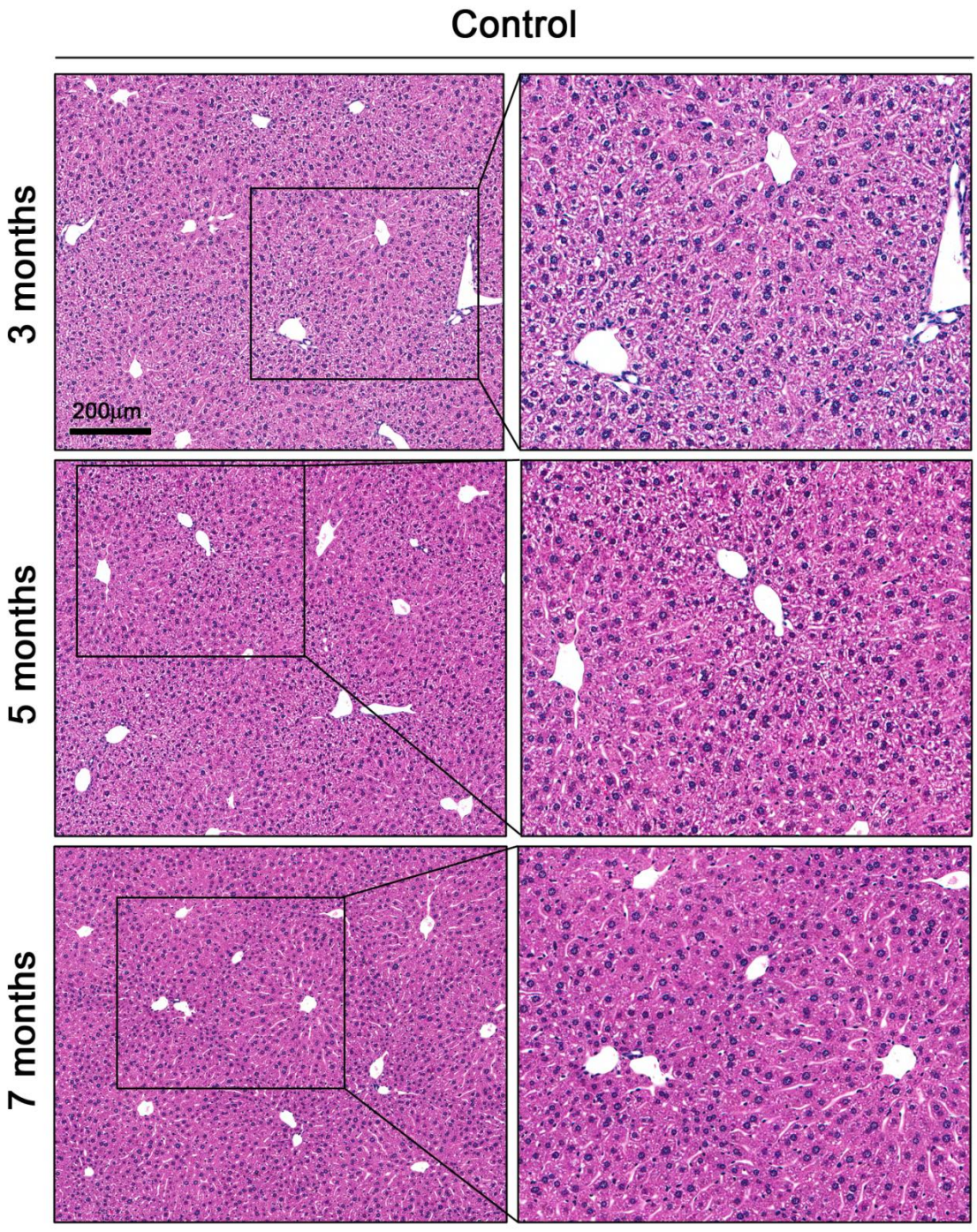

Fig. 5.5: Liver histology of control mice. Formalin-fixed, paraffin-embedded liver sections of mice fed a control diet for 3, 5 and 7 months were stained with haematoxylin and eosin. Representative images are shown for each time point and the inserted boxes highlight the area of magnification. The scale bar represents 200 µm. *CV*, central vein*; PV*, portal vein.

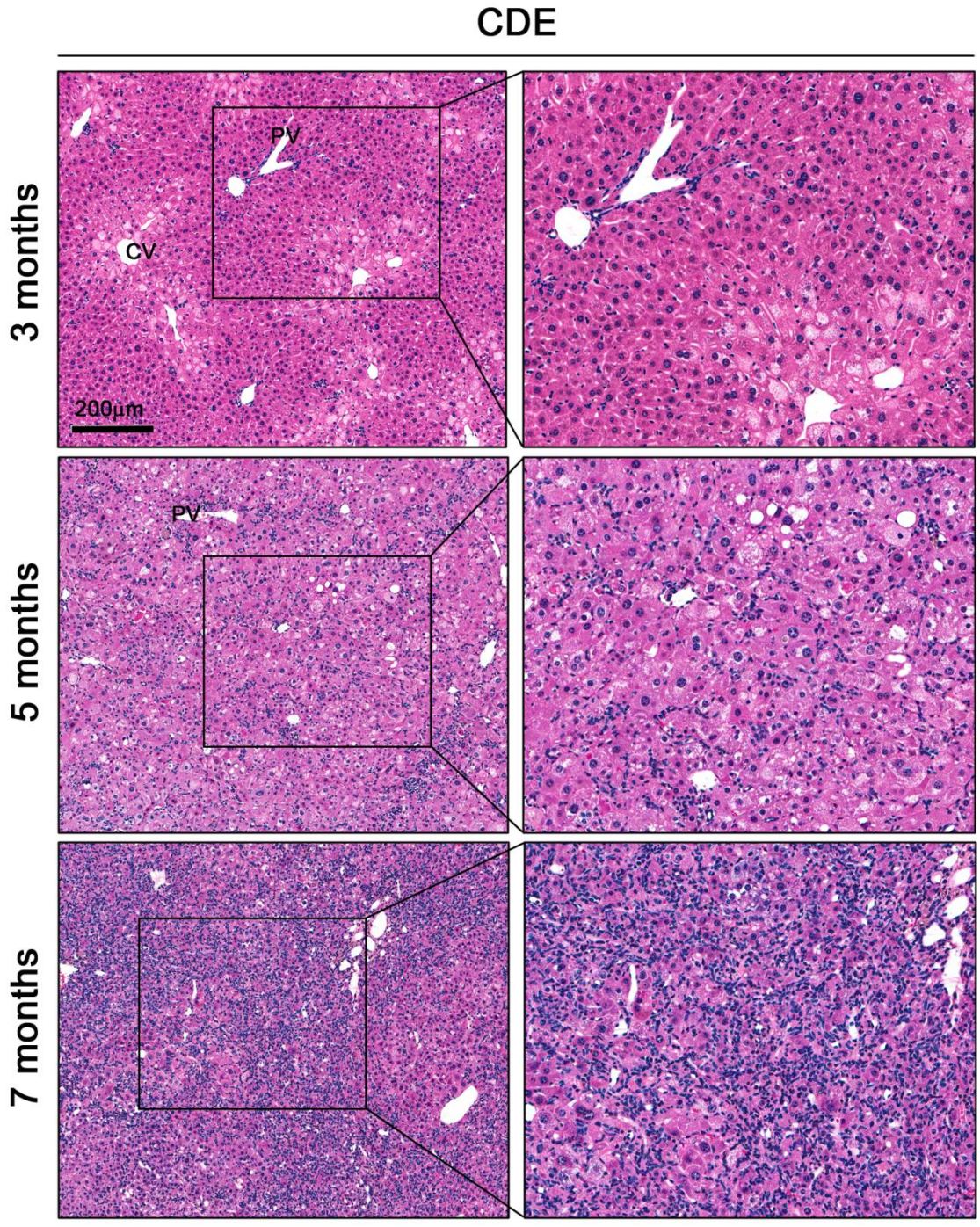

Fig. 5.6: CDE-induced morphological changes of the liver after long-term treatment. Formalin-fixed, paraffin-embedded liver sections of mice treated with CDE for 3, 5 and 7 months were histologically assessed using haematoxylin and eosin staining. Representative images of experimental groups are illustrated. The inserted boxes identify the field of enlarged images and the scale bar depicts 200 µm. *CV*, central vein*; PV*, portal vein.

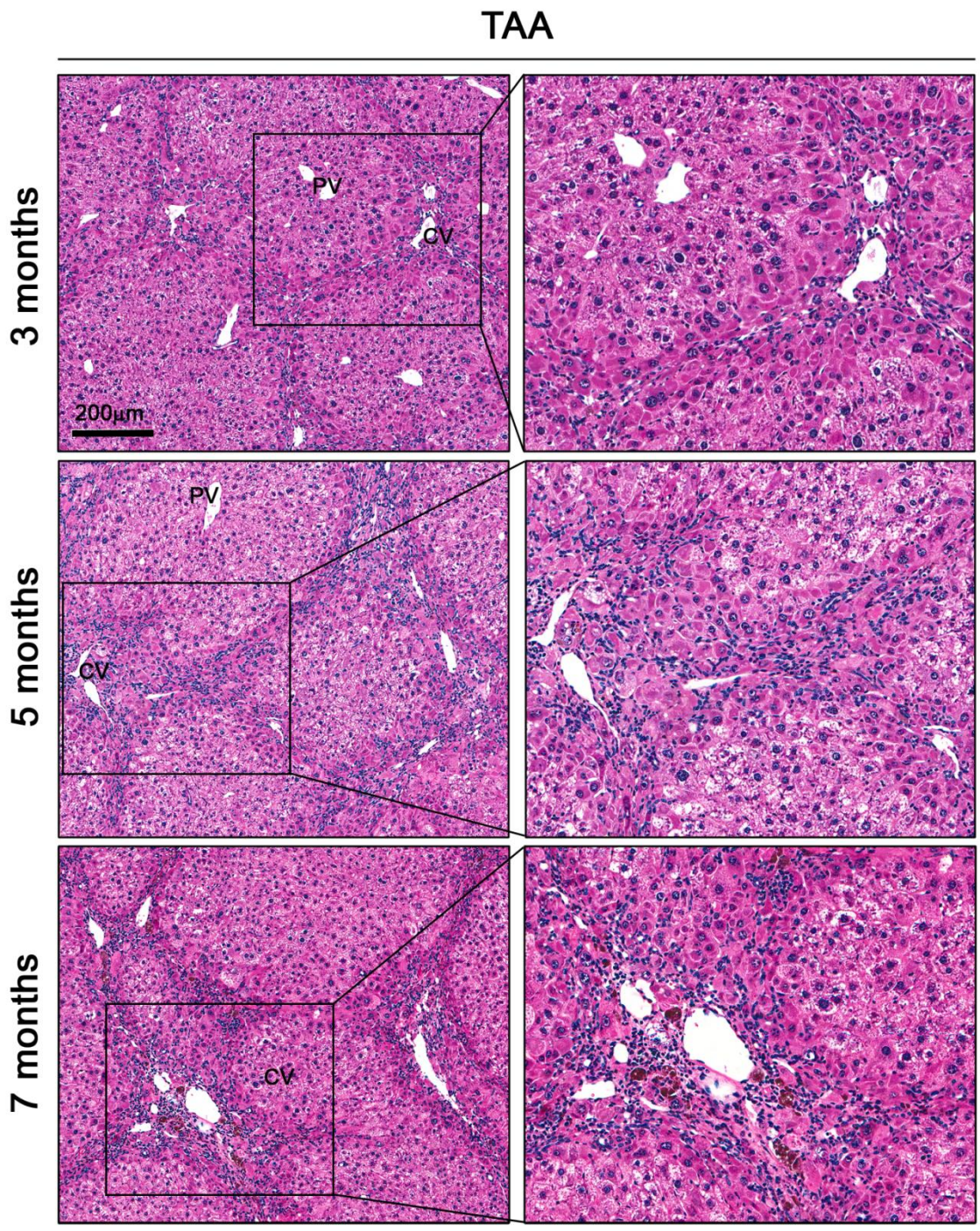

Fig. 5.7: TAA-induced morphological changes of the liver after long-term treatment. The morphology of formalin-fixed, paraffin-embedded liver sections of mice exposed to TAA treatment for 3, 5 and 7 months were was assessed by haematoxylin and eosin staining. Representative images of experimental groups are demonstrated and the inserted boxes identify the enlarged areas. The scale bar represents 200 µm. *CV*, central vein*; PV*, portal vein.

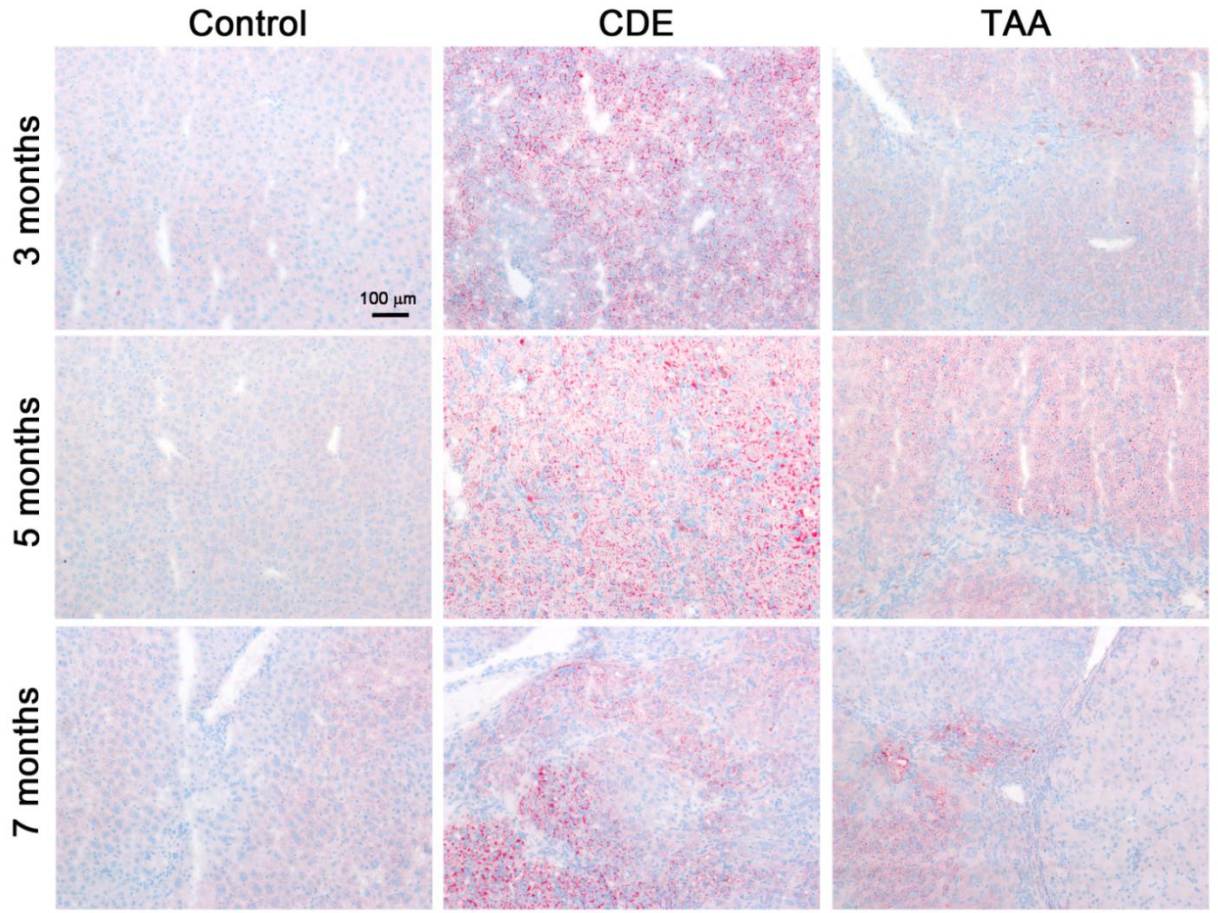

Fig. 5.8: Lipid accumulation in CDE- and TAA-induced CLD. Frozen liver sections of mice exposed to CDE and TAA treatment for 3, 5 and 7 months and respective controls were stained with Oil Red O. Representative images of experimental groups are shown. The scale bar depicts 100 µm.

In contrast, the zonal distribution of fatty changes identified at earlier time points of the 6-week time course (see 3.4.1) was no longer detected in long-term TAA-treated livers.

5.4.3.2 Inflammatory response

The associated inflammatory response dynamics in CDE- and TAA-induced CLD were characterised using the inflammatory cell marker CD45. To further define KCs and monocyte-derived macrophages, expression profiles of the markers F4/80 and CD11b were assessed, respectively. Both regimens induced an inflammatory response at all investigated time points, shown by progressively increasing areas of CD45 expression from 3 months (CDE, 5.7 ± 1%; TAA, 7.3 ± 2.3% positive pixel per FOV) towards 7 months of treatment (CDE, 12.5 ± 2.7%; TAA, 9.9 ± 1.8% positive pixel per FOV) (Fig. 5.9 and Fig. 5.10). However, the spatial arrangements of $CD45^+$ inflammatory cells differed in both models. The CDE diet provoked a mainly lobular and milder periportal response, including inflammatory cell foci, whereas TAA-damaged livers displayed a pericentral and central-to-central located response directed to the site of tissue damage (Fig. 5.9). Examination of CD11b expression revealed a corresponding pattern and showed that monocyte-derived macrophages are a part of the $CD45^+$ cell response (Fig. 5.11). Investigations of F4/80 marker expression demonstrated that the KC population is represented by cells with a low CD45 expression. The typical distribution of KCs, mainly present in periportal and intermediate areas, was distorted after five months of CDE treatment. In TAA mice, KCs were located in the damaged lobular regions and the adjacent intermediate zones at all investigated time points (Fig. 5.12).

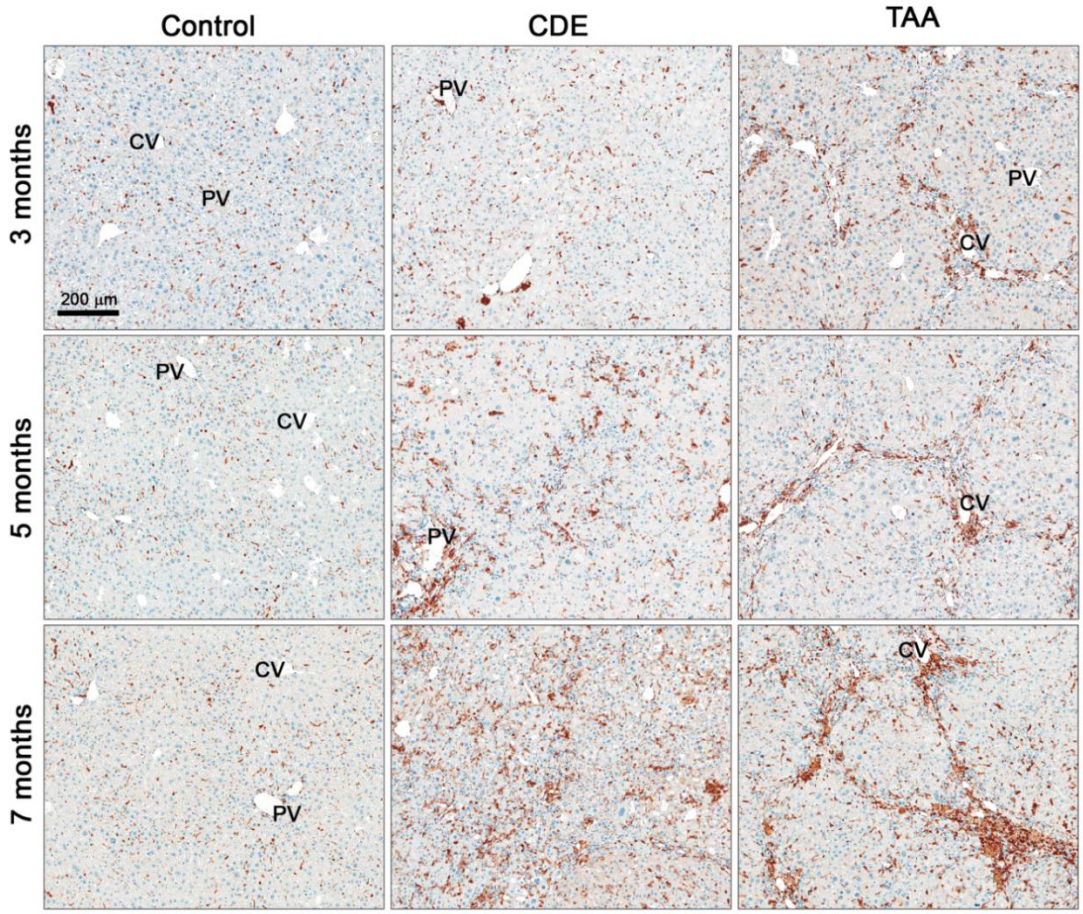

Fig. 5.9: Long-term exposure to CDE and TAA induced a CD45$^+$ cell response. Formalin-fixed, paraffin-embedded liver sections of CDE, TAA and control mice at 3, 5 and 7 months were immunohistochemically labelled for the inflammatory cell marker CD45. Representative images are shown. The scale bar represents 200 µm. *CV*, central vein*; PV*, portal vein.

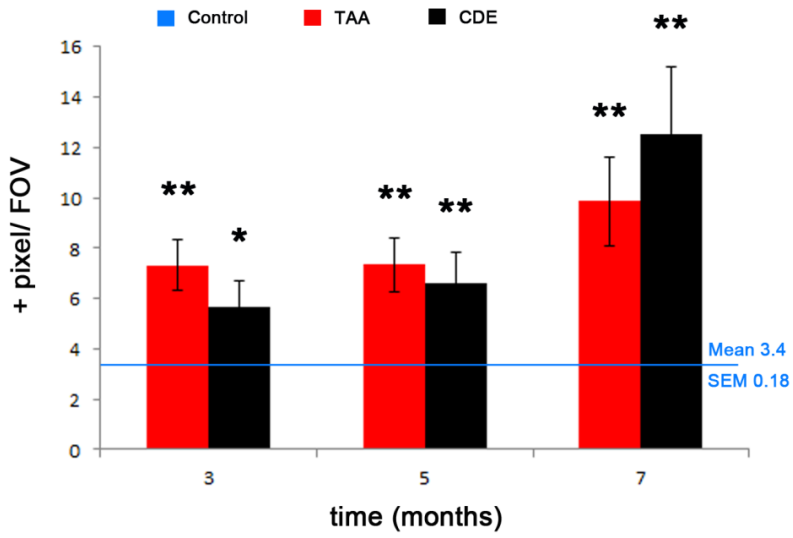

Fig. 5.10: Long-term CDE and TAA treatment induced increased numbers of CD45$^+$ cells. Control, CDE and TAA liver sections of 3, 5 and 7 months were immunohistochemically labelled with the inflammatory cell marker CD45. Positive pixel counts were performed in five non-overlapping fields of view (FOV) per sample. Data are expressed as mean ± SEM. n = 4 to 6 mice per group. * $P < 0.05$, ** $P < 0.01$, *** $P < 0.001$ compared with controls.

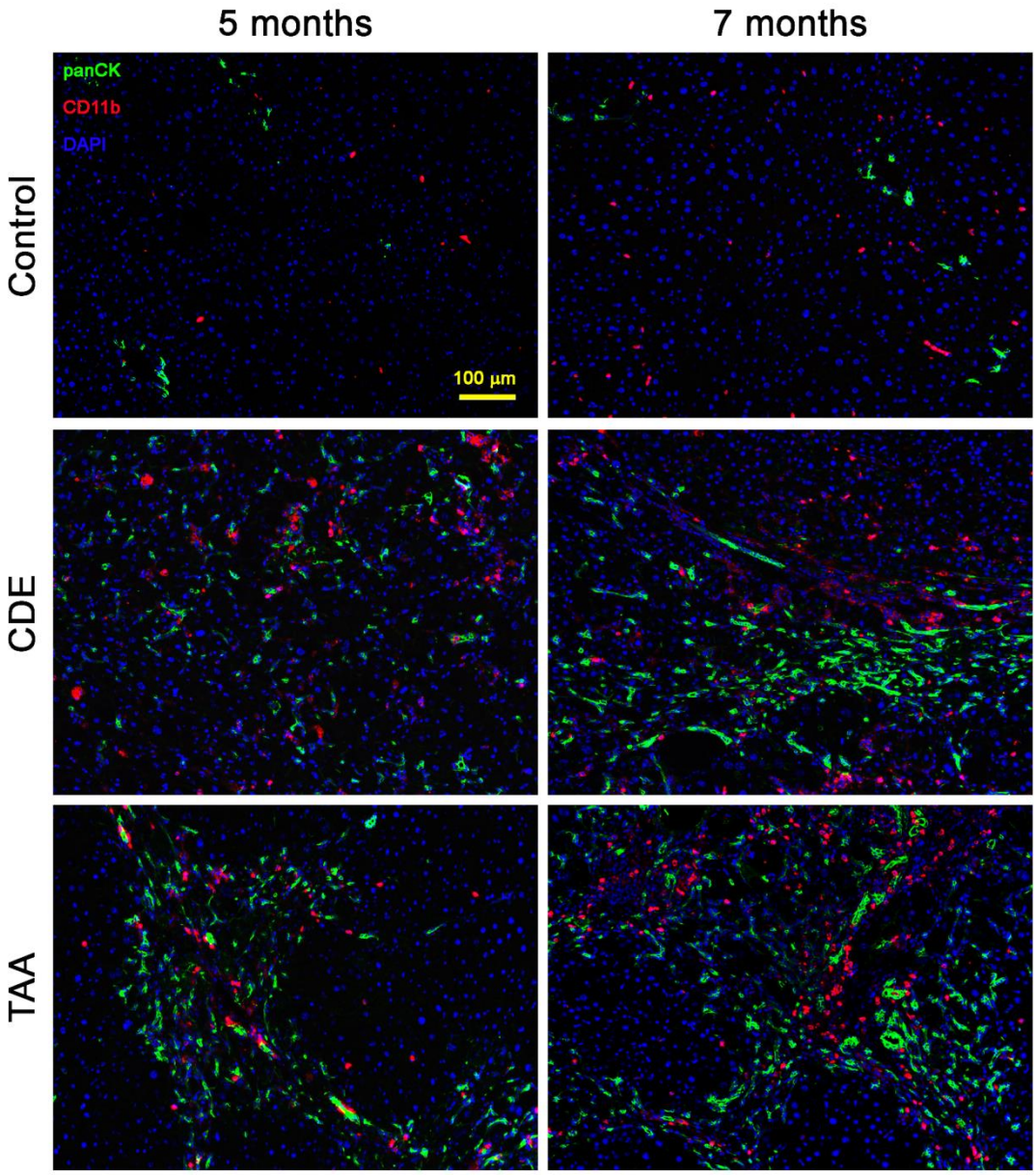

Fig. 5.11: CDE and TAA long-term treatment induce increased CD11b$^+$ cell numbers. Frozen liver sections of mice treated with CDE or TAA for five and seven months and controls were labelled for the cholangiocyte/LPC marker panCK and the monocyte-derived macrophage marker CD11b using immunofluorescence. Representative images are shown. The scale bar depicts 100 µm. *CV*, central vein*; PV*, portal vein.

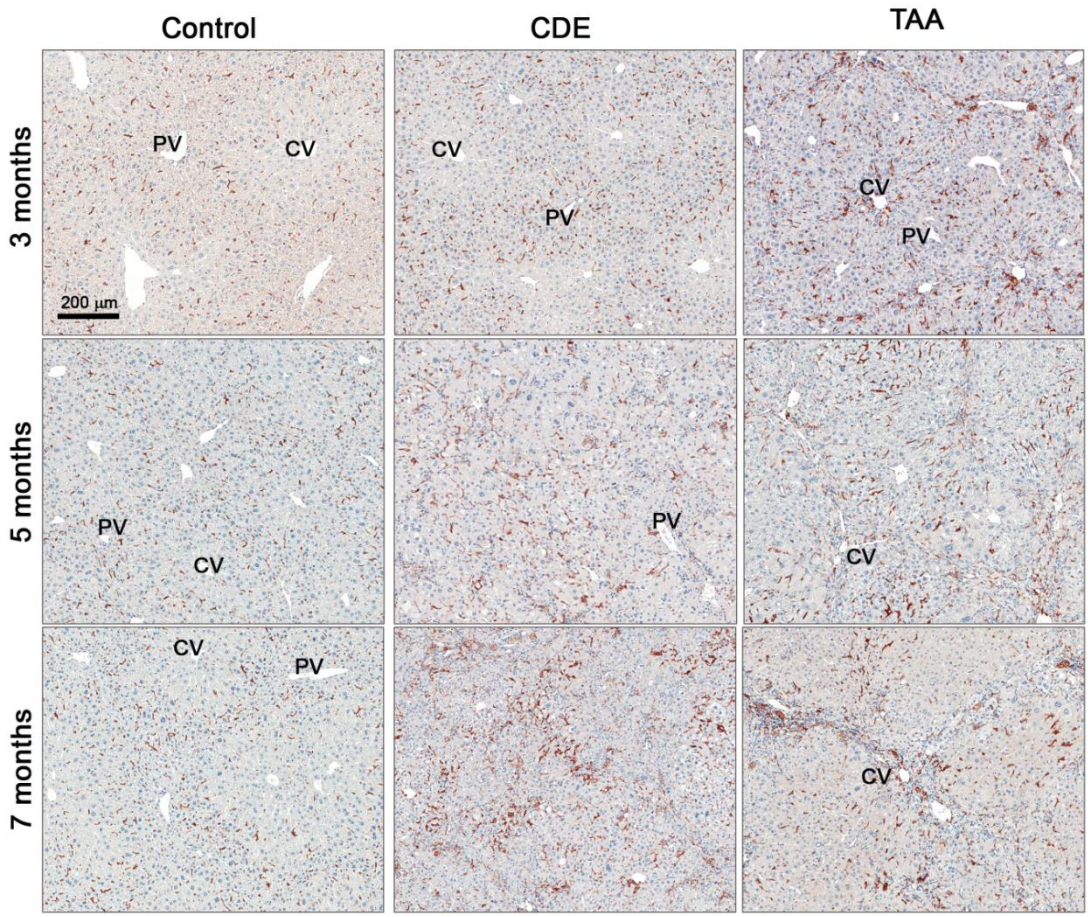

Fig. 5.12: Rearrangement of F4/80$^+$ cells following long-term CDE or TAA treatment. Formalin-fixed, paraffin-embedded liver sections of CDE, TAA and control mice treated for 3, 5 and 7 months were immunohistochemically labelled for the KC marker F4/80. Representative images are shown. The scale bar represents 200 µm. *CV*, central vein; *PV*, portal vein.

5.4.3.3 Liver progenitor cell response

Since LPCs are associated with CLD and carcinogenesis, and both regimens showed their expansion in the first six weeks of treatment (see 3.4.3), the following paragraph investigates the dynamics and different phenotypes of CDE- and TAA-induced LPCs during injury progression and tumour formation. Immunohistochemical staining for the biliary cell and LPC marker panCK revealed a progressive expansion of the LPC response following long-term exposure to either CDE or TAA (Fig. 5.13 and Fig. 5.14A). In the CDE model, panCK$^+$ cells were limited to periportal areas after three months (1.7 ± 0.8 positive pixel per FOV), infiltrated the parenchyma after five months (3.7 ± 1.9% positive pixel per FOV) and further expanded up to seven months of treatment (8.6 ±3.4% positive pixel per FOV) (Fig 5.13 and Fig. 5.14A).

In contrast to TAA, which resulted in minor animal-to-animal variations, CDE treatment caused high discrepancies within experimental groups that increased over time. As a result, mice from the 5- and 7-month time point were further subdivided into groups defined by low and high LPC responses (Fig 5.14B). Despite the relatively low number of animals available for analysis at that stage (5 months, n = 6; 7 months, n = 7), the respective, associated LPC expansions differed significantly between the groups after five (low LPC response group, 1.3 ± 0.2%; high LPC response group, 9 ± 1% positive pixel per FOV) and seven months of treatment (low LPC response group, 0.9 ± 0.02%; high LPC response group, 14.4 ± 3.8% positive pixel per FOV). Furthermore, when correlated to tumour development, the data suggest a positive correlation between the magnitude of the LPC response and tumour formation since only the high LPC group showed severe neoplastic changes. The results in the groups with low versus high LPC numbers were also consistent with a low versus high inflammatory response (Fig. 5.15). Thus, to further investigate the process of tumour formation in the CDE model, only mice of the high LPC response group were used for further characterisations. The distribution of TAA-induced panCK$^+$ cells followed the previously observed pattern in damaged centrilobular regions (3 months, 4.3 ± 0.8%; 5 months, 7.5 ± 0.5%; 7 months, 9 ± 1.4% positive pixel per FOV) and resembled a honeycomb structure with strong central-to-central zonation.

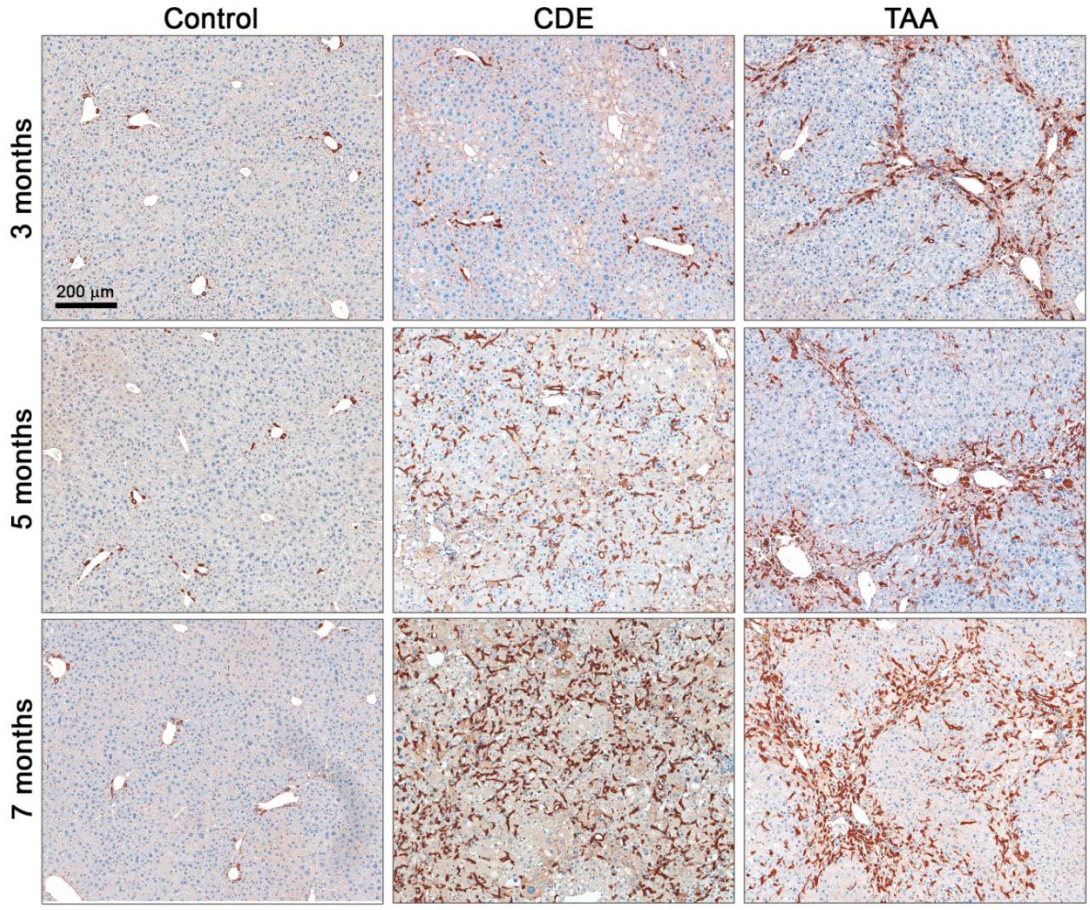

Fig. 5.13: Expansion of panCK$^+$ cells in response to long-term CDE and TAA treatment. Formalin-fixed, paraffin-embedded liver sections of mice exposed to CDE, TAA or control treatment for 3, 5 and 7 months were immunohistochemically labelled for the biliary and LPC marker panCK. Representative images are shown. The scale bar depicts 200 µm. *CV*, central vein*; PV*, portal vein.

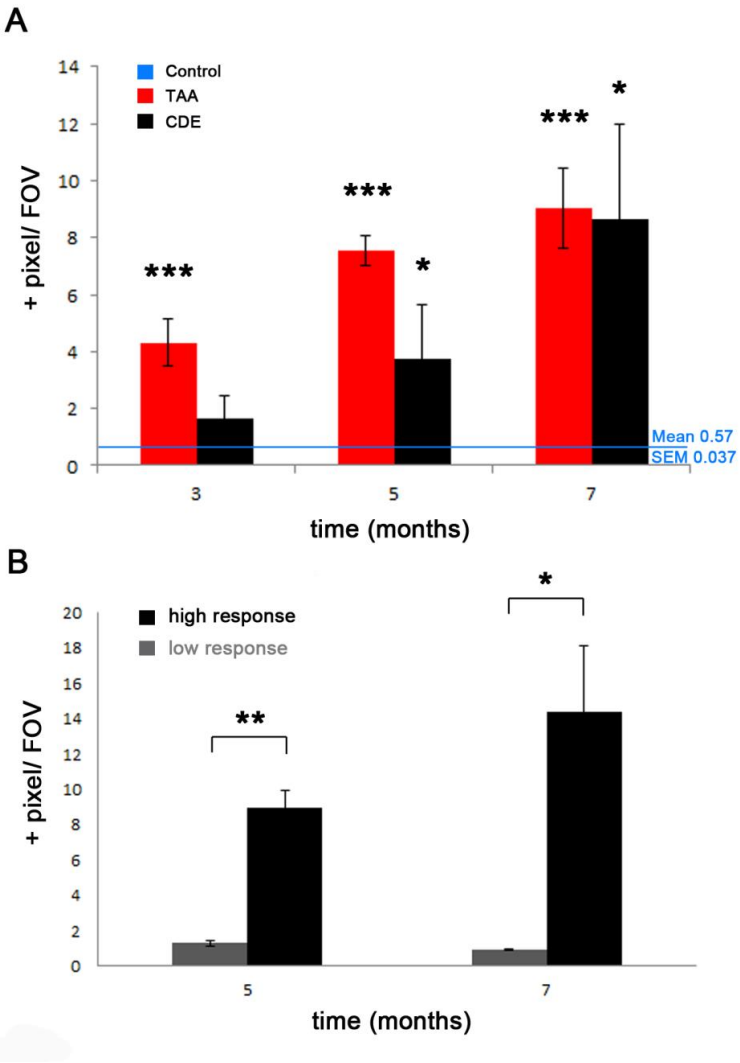

Fig. 5.14: Long-term CDE and TAA treatment induced the expansion of panCK$^+$ cells. Control, CDE and TAA liver sections were immunohistochemically labelled with the biliary cell and LPC marker panCK. (A) Animals of all experimental groups after 3, 5 and 7 months of treatment. (B) CDE mice treated for 5 and 7 months, respectively, further categorised according to their low or high panCK$^+$ LPC response. Positive pixel counts were performed in five non-overlapping fields of view (FOV) per sample. Data are expressed as mean ± SEM. n = 4 to 7 mice per group. * $P < 0.05$, ** $P < 0.01$, *** $P < 0.001$ compared with controls.

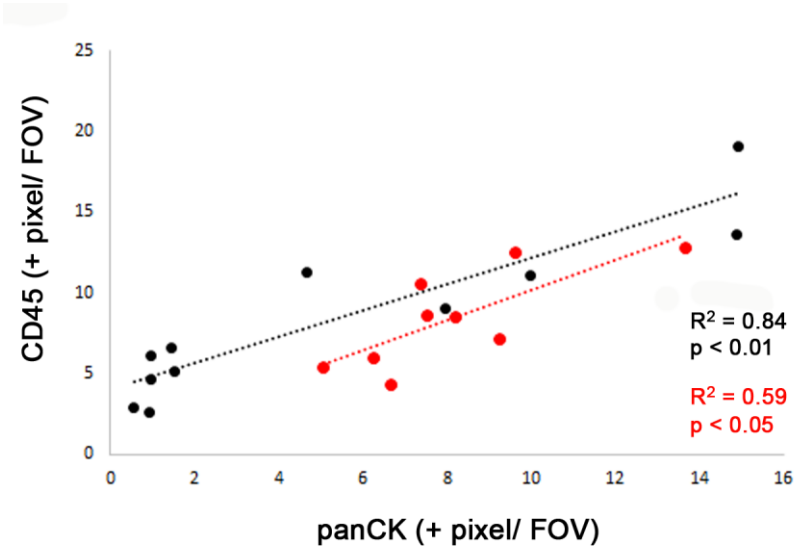

Fig. 5.15: Correlation between the magnitude of panCK and CD45 expression in CDE- and TAA-treated mice. Immunohistochemical analysis of the cholangiocyte and LPC marker panCK and the inflammatory cell marker CD45 in CDE- (black) and TAA-treated (red) mice from the 5- and 7-month time points revealed a positive correlation between the magnitudes of both marker expressions.

As shown in Chapter 4, CDE- and TAA-induced LPCs represented a heterogeneous cell population including several single positive cells in addition to the bulk of double positives when simultaneously staining for different commonly used LPC markers. Therefore, the expression profiles of the markers panCK, CK19, CD133 and EpCAM were further investigated during injury progression and carcinogenesis in order to evaluate distinct LPC phenotypes and the abundance of these subpopulations. Co-localisation studies with the markers panCK and CK19 (Fig. 5.16, Fig. 5.17 and Fig 5.18), CK19 and EpCAM (Fig 5.19, Fig. 5.20 and Fig. 5.21), as well as panCK and CD133 (Fig. 5.19 and Fig. 5.22) revealed a high degree of overlap in expression profiles but also distinct single positive populations in both CDE and TAA mice at all investigated time points. This included phenotypes such as $panCK^+/CK19^-$, $CK19^+/EpCAM^-$, $CK19^-/EpCAM^+$ and $panCK^+/CD133^-$. Moreover, fluorescent labelling with CK19 and Ki67 identified proliferating LPCs after five and seven months of treatment, showing several $CK19^+/Ki67^+$ cells in damaged lobular areas of CDE- and TAA- livers (Fig. 5.23).

As illustrated in Chapter 4.4.4, the TAA maintenance phase induced several $panCK^+$ cells that co-expressed CD44, a marker previously associated with CSCs (Yang *et al.* 2008b; Zhu *et al.* 2010). Since LPCs are discussed as candidates for pre-cancerous cells during carcinogenesis (for review see 1.8.4 and 1.9.2), potentially tumour-initiating phenotypes were investigated in response to long-term CDE and TAA treatment. Assessment of the $panCK^+/CD44^+$ subpopulation revealed that CDE only induced double positive cells starting after 5 months of treatment consistent with increased LPC expansion (Fig. 5.24), whereas in the TAA regimen their presence was observed at all investigated time points (Fig. 5.25). Additional co-localisation of the commonly used hepatic CSC marker EpCAM in $CD44^+$ LPCs further suggested a potential cancer precursor state of $CD44^+/EpCAM^+$ and $panCK^+/CD44^+$ cells (Fig. 5.26).

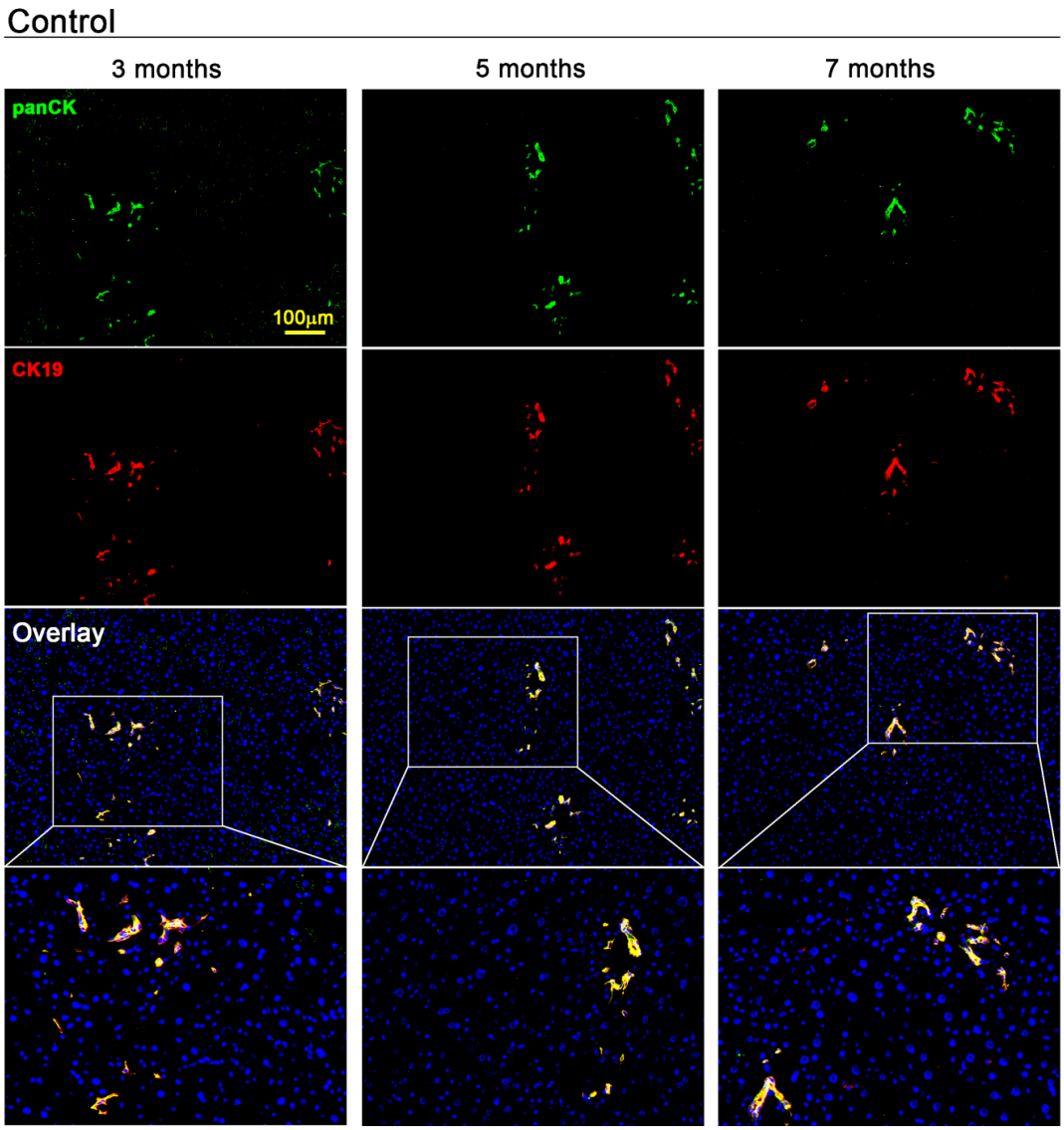

Fig. 5.16: Characterisation of the LPC markers panCK and CK19 in control mice. Frozen liver sections of mice fed a control diet were fluorescently labelled with the biliary and LPC markers panCK and CK19. Representative images are shown. The scale bar represents 100 µm and inserted boxes define the area of magnification.

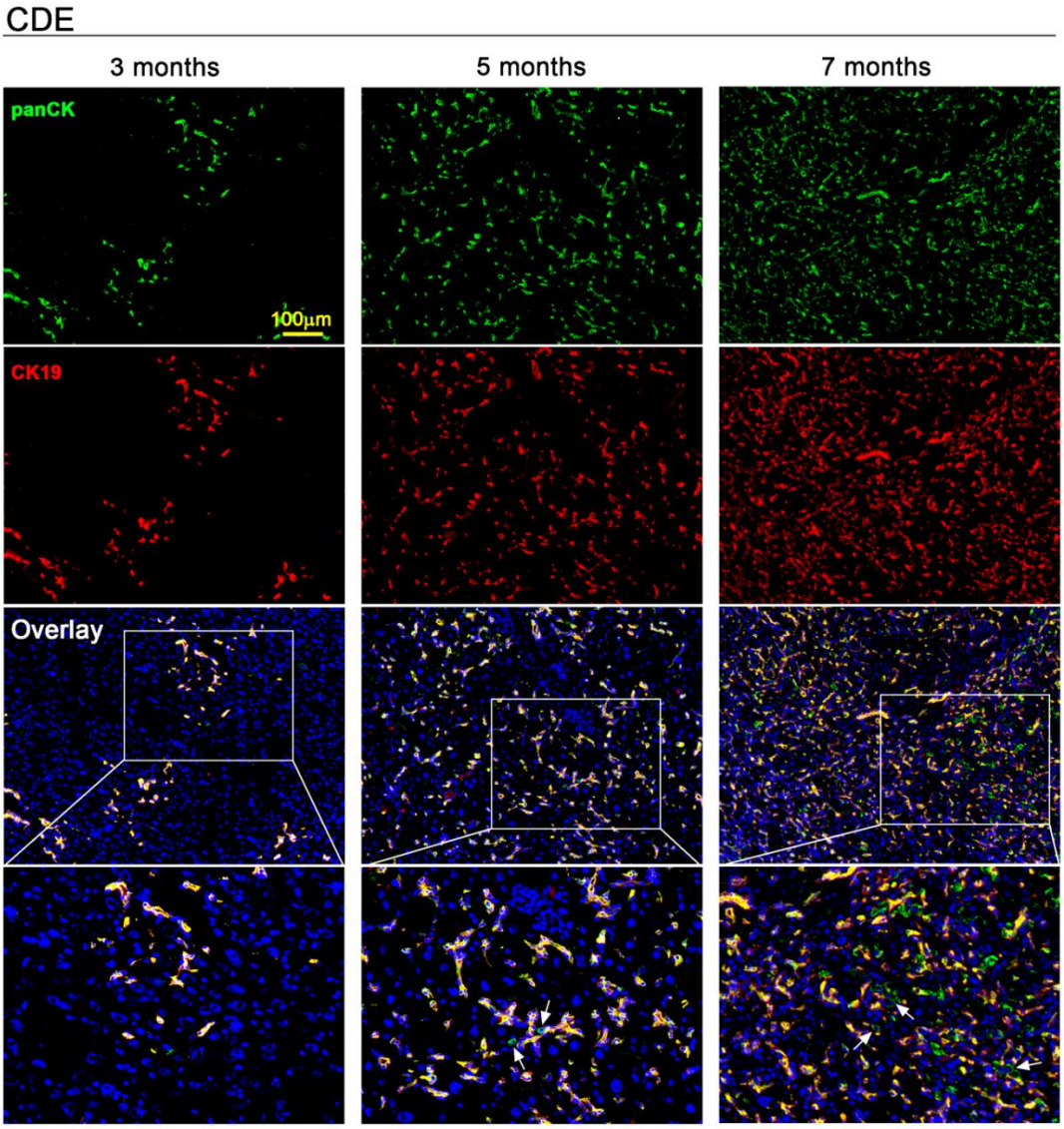

Fig. 5.17: Immunofluorescent staining of panCK$^+$ and CK19$^+$ LPCs following long-term CDE treatment. Frozen liver sections of CDE mice treated for 3, 5 and 7 months were fluorescently labelled with the biliary and LPC markers panCK and CK19. Representative images are shown and the scale bar depicts 100 µm. Inserted boxes highlight the area of magnification. Arrows highlight examples of panCK$^+$/CK19$^-$ cells.

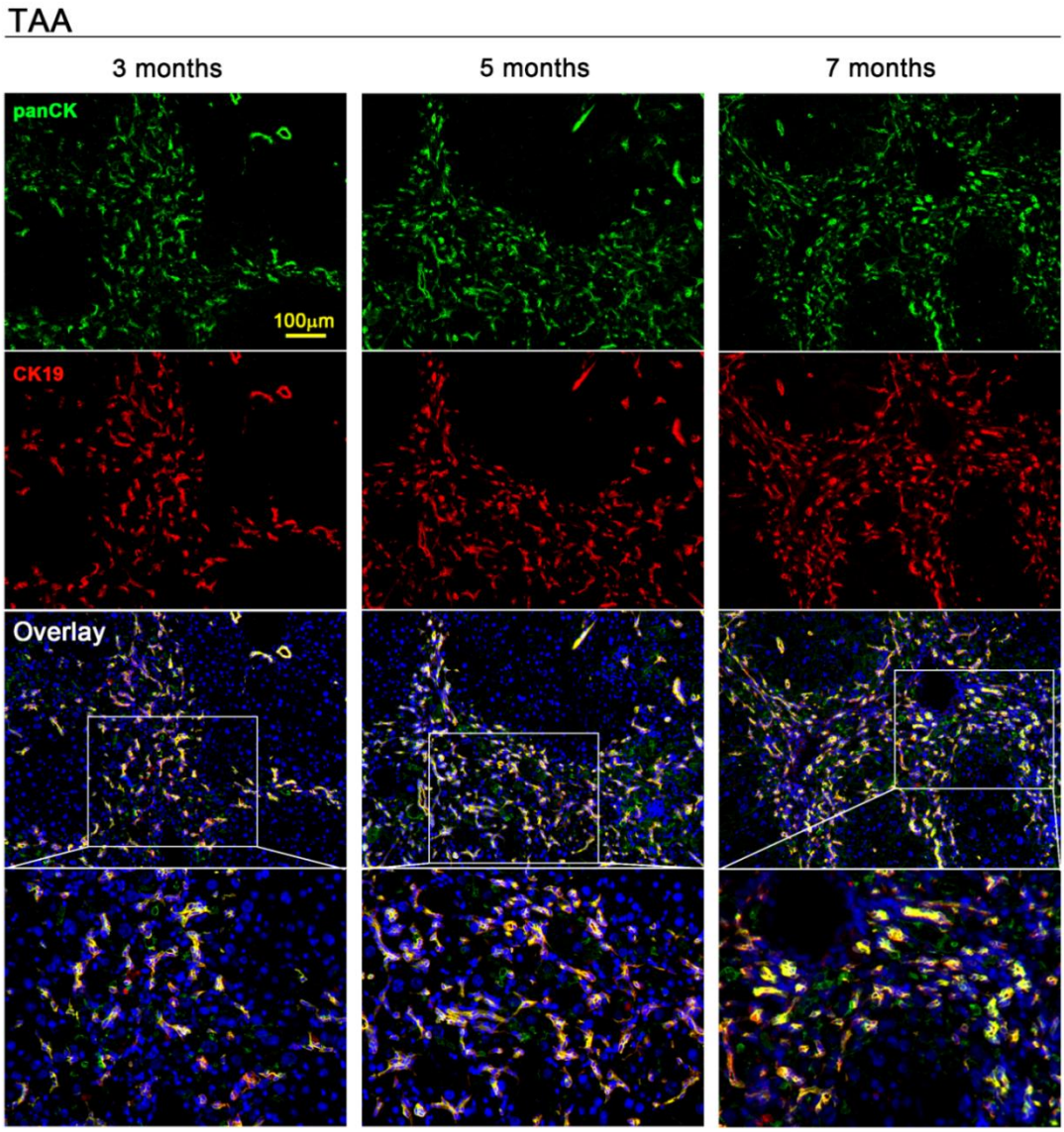

Fig. 5.18: Immunofluorescent staining of panCK$^+$ and CK19$^+$ LPCs following long-term TAA treatment. Frozen liver sections of TAA mice treated for 3, 5 and 7 months were labelled with the biliary and LPC markers panCK and CK19 using immunofluorescence. Representative images are shown. The scale bar represents 100 µm and inserted boxes highlight the field of magnification.

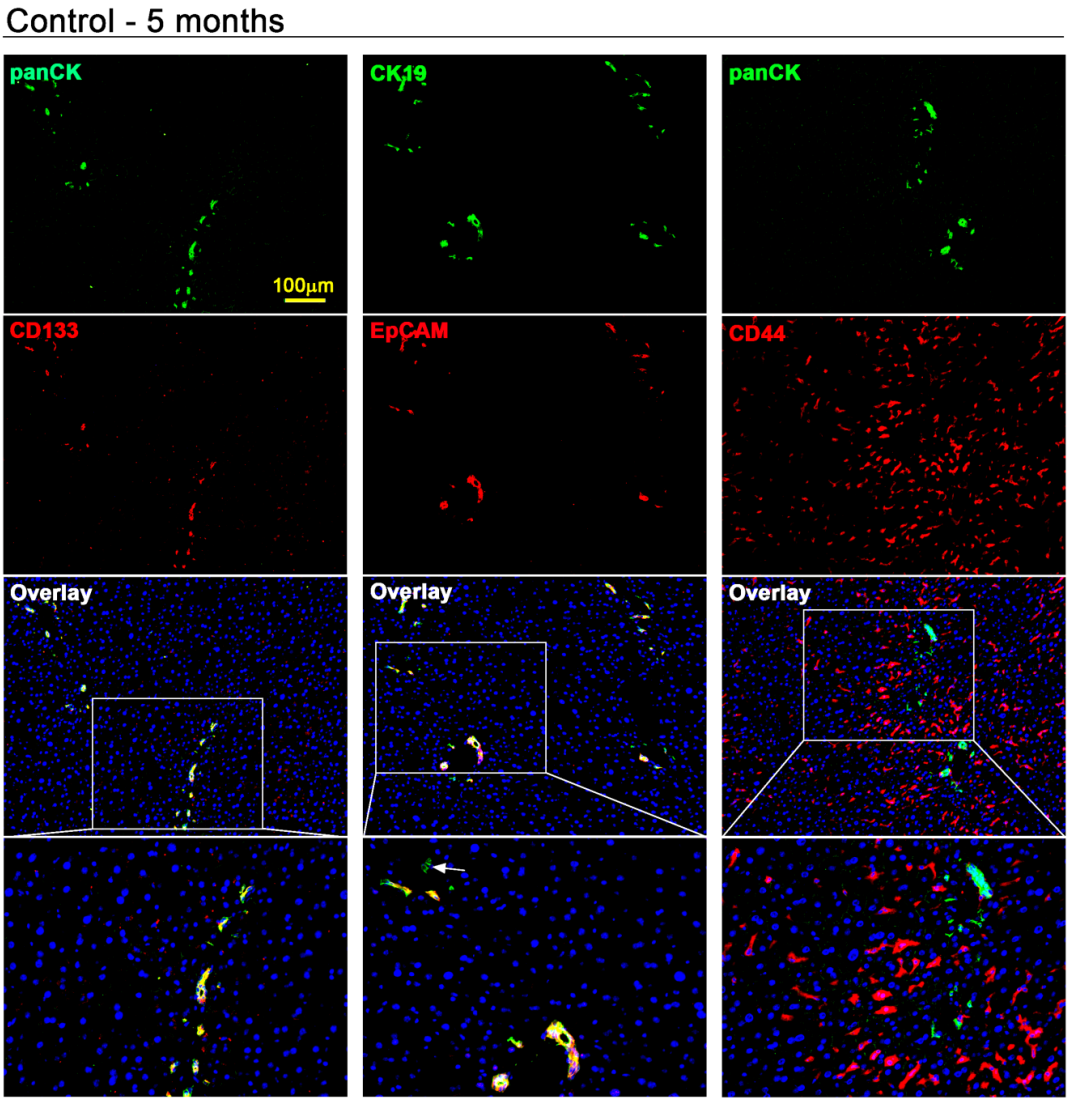

Fig. 5.19: Expression profiles of the markers panCK, CK19, CD133, EpCAM and CD44 in controls. Frozen liver sections of 5-month old mice fed a control diet were fluorescently labelled with the biliary and LPC markers panCK, CD133, CK19 and EpCAM, as well as with the macrophage and CSC marker CD44. Representative images are shown. The scale bar depicts 100 µm and inserted boxes define magnified areas. The arrow in the middle panel highlights an example of $CK19^{+}/EpCAM^{-}$ cells.

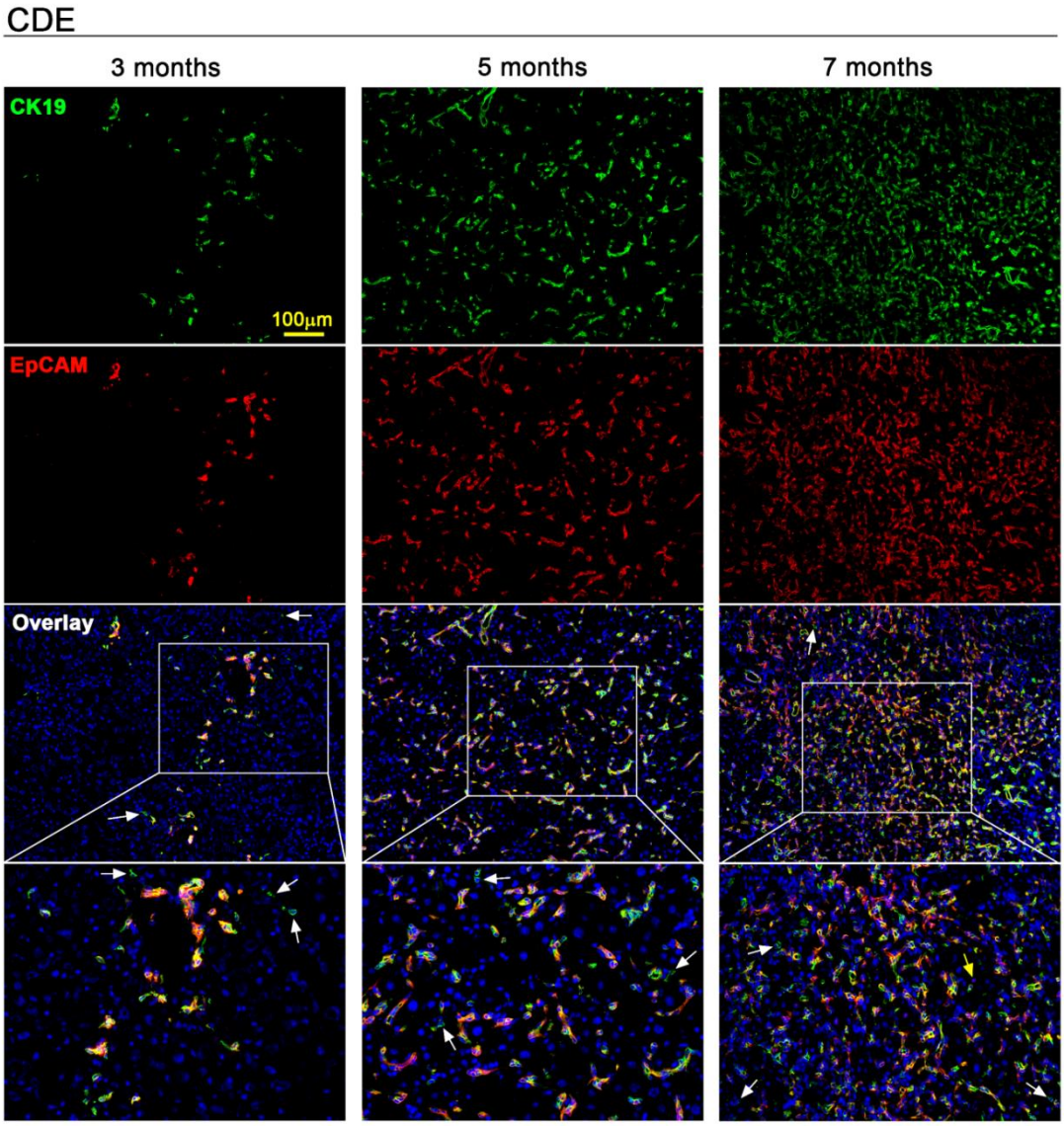

Fig. 5.20: Immunofluorescent staining of CK19$^+$ and EpCAM$^+$ LPCs following long-term CDE exposure. Frozen liver sections of mice treated with CDE for 3, 5 and 7 months were labelled with the biliary cell and LPC markers CK19 and EpCAM using immunofluorescence. The scale bar represents 100 μm and the inserts identify the area of magnification. Arrows highlight examples of CK19$^+$/EpCAM$^-$ (white) and CK19$^-$/EpCAM$^+$ (yellow) cells.

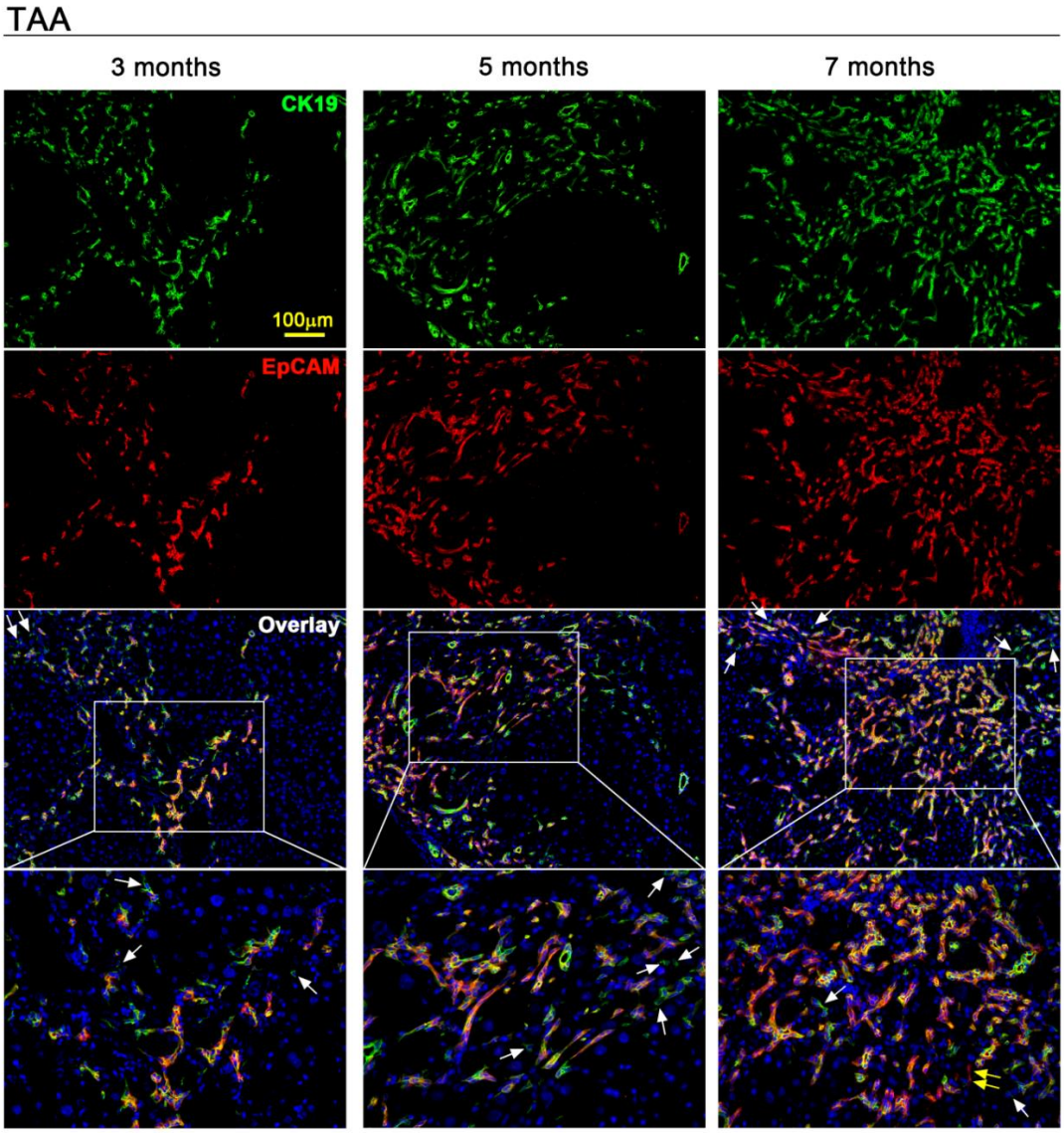

Fig. 5.21: Immunofluorescent staining of CK19$^+$ and EpCAM$^+$ LPCs following long-term TAA exposure. Frozen liver sections of TAA-treated mice of 3, 5 and 7 months were fluorescently labelled with the biliary cell and LPC markers CK19 and EpCAM. The scale bar depicts 100 µm and inserted boxes highlight the field of magnification. Arrows highlight examples of CK19$^+$/EpCAM$^-$ (white) and CK19$^-$/EpCAM$^+$ (yellow) cells.

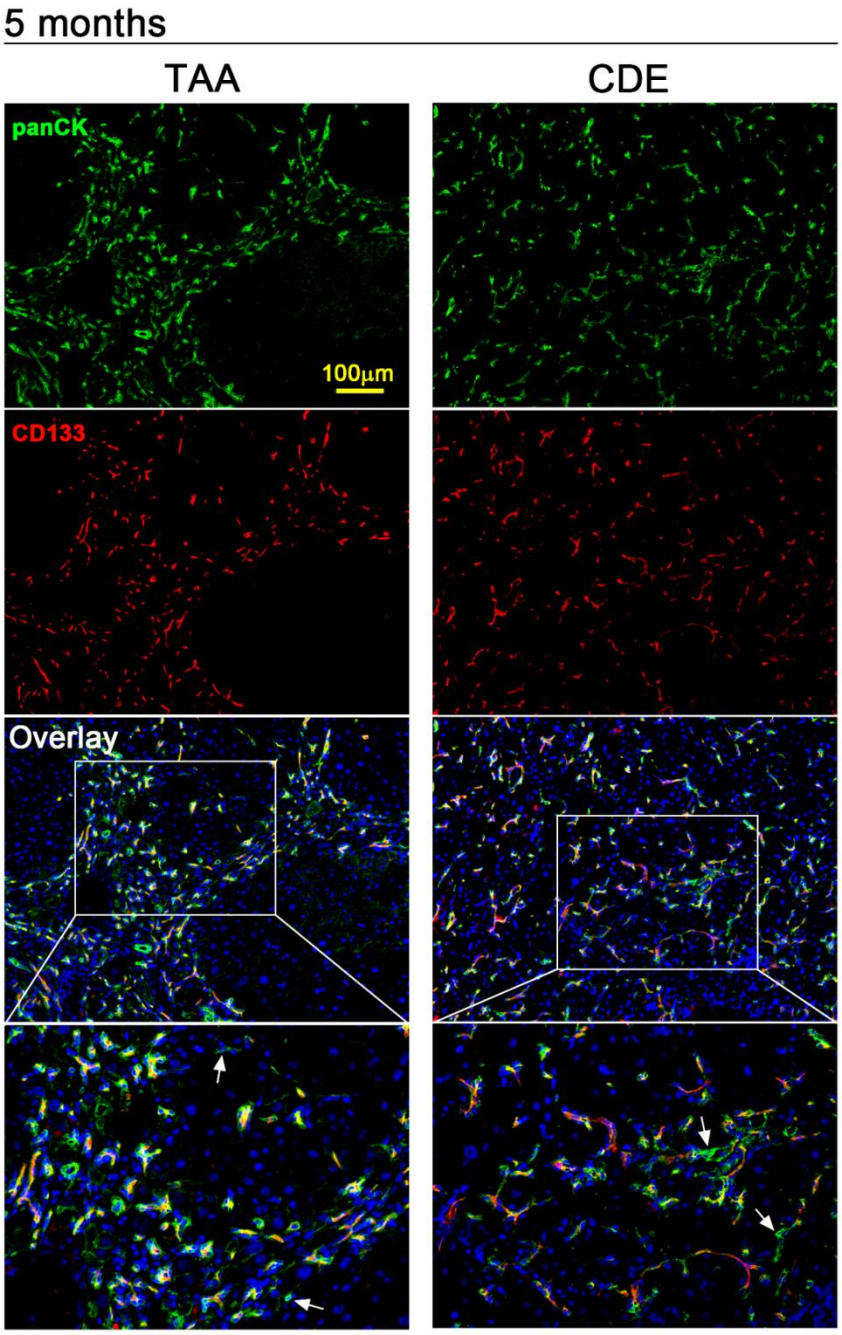

Fig. 5.22: CDE- and TAA-induced LPC populations defined by the markers panCK and CD133. Frozen liver sections of mice treated with CDE and TAA for five months were fluorescently labelled with the biliary cell and LPC markers panCK and CD133. Representative images are shown. The scale bar depicts 100 µm and the inserts identify the enlarged area. Arrows highlight examples of $panCK^{+}/CD133^{-}$ cells.

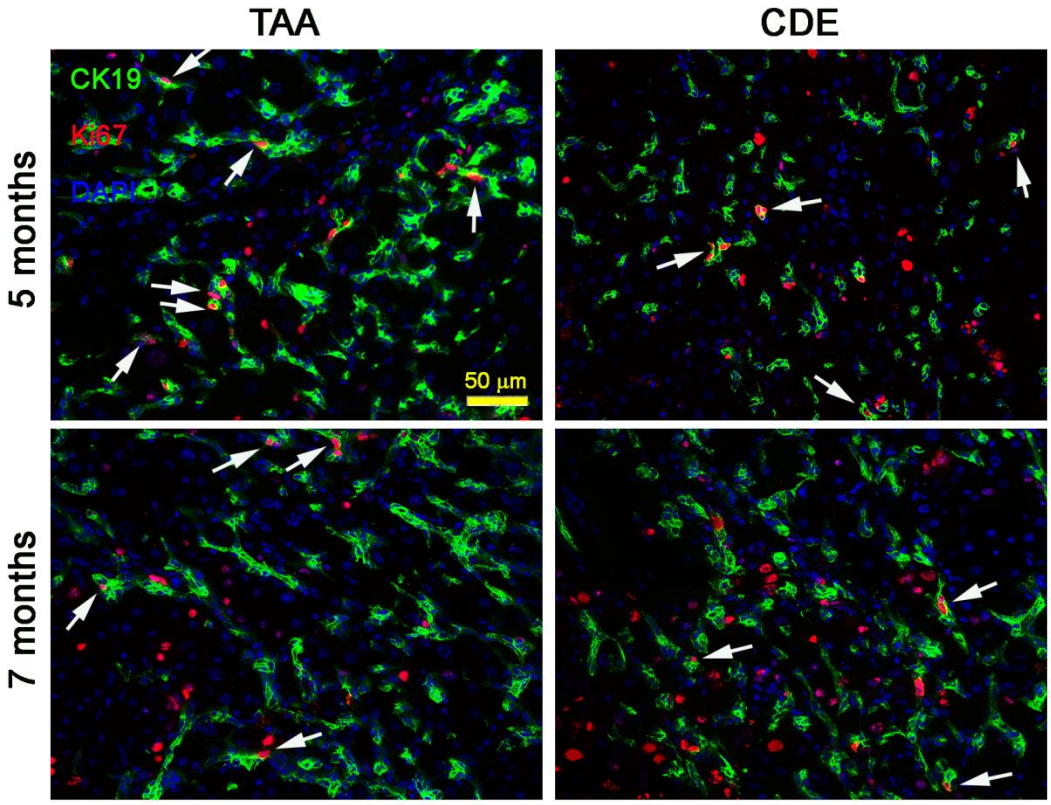

Fig. 5.23: CDE and TAA treatment induce LPC proliferation during CLD progression and carcinogenesis. Frozen liver sections of CDE and TAA mice treated for five and seven months were fluorescently labelled for the biliary cell and LPC marker CK19 and the proliferation marker Ki67. Representative images are shown and the scale bar depicts 100 µm. Arrows highlight examples of proliferating LPCs.

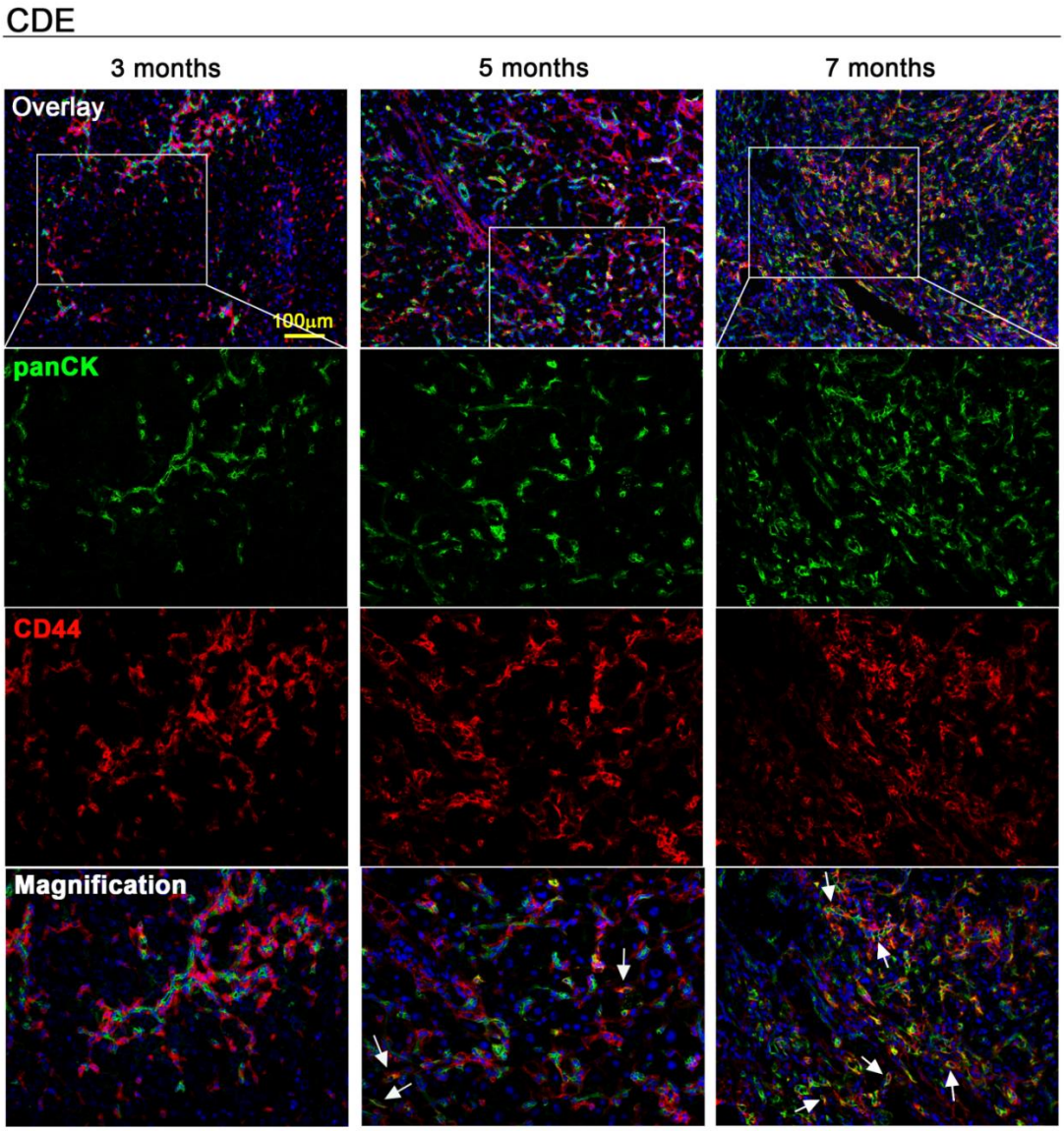

Fig 5.24: Co-localisation of panCK and CD44 in CDE-induced CLD progression and carcinogenesis. Frozen liver sections of CDE mice treated for 3, 5 and 7 months were labelled with the LPC marker panCK and the CSC marker CD44 using immunofluorescence. The scale bar depicts 100 µm and inserted boxes identify enlarges areas. Arrows highlight examples of $panCK^{+}/CD44^{+}$ cells.

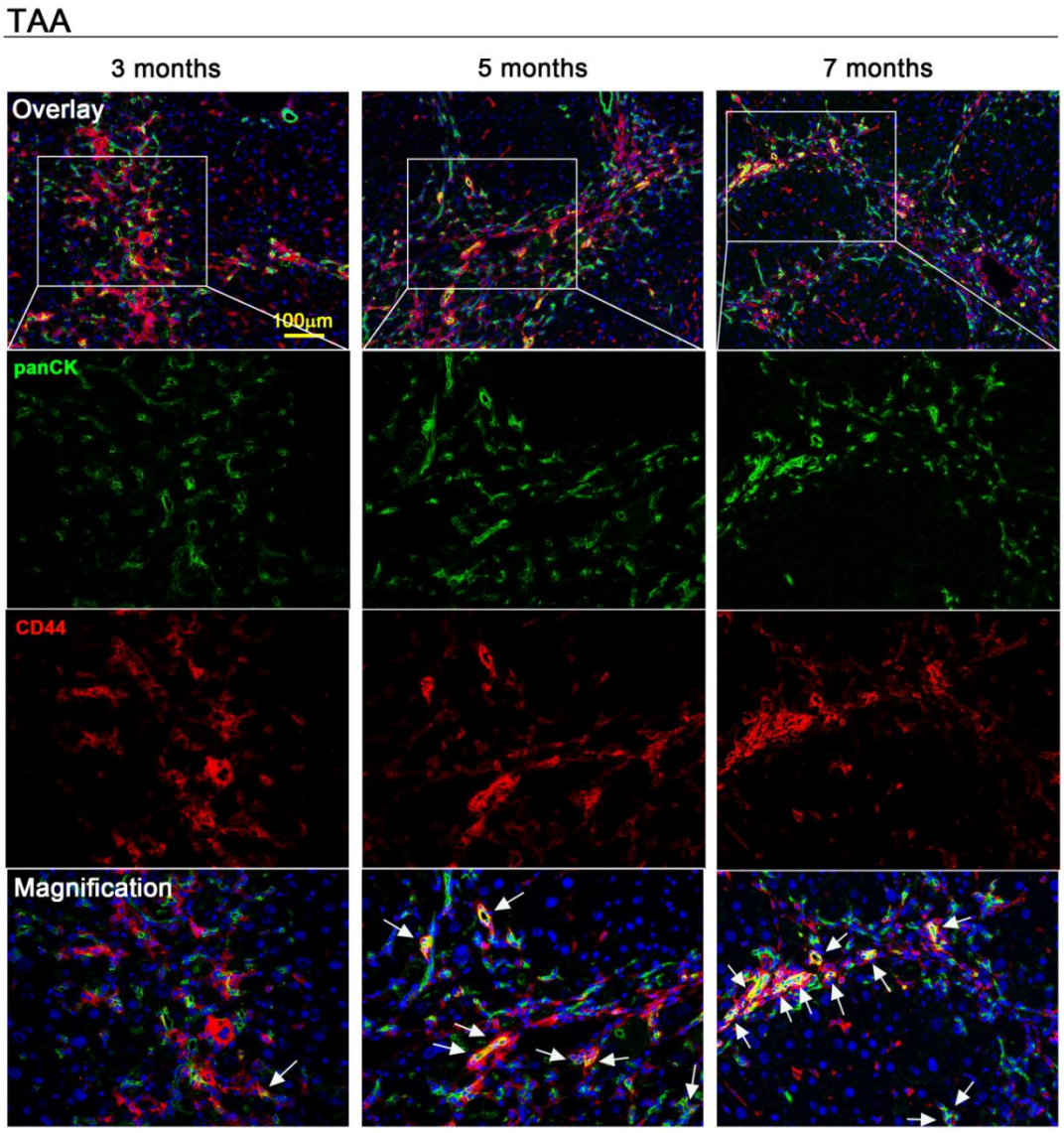

Fig. 5.25: Co-localisation of panCK and CD44 in TAA-induced CLD progression and carcinogenesis. Frozen liver sections of mice treated with TAA for 3, 5 and 7 months were fluorescently labelled with the LPC marker panCK and the CSC marker CD44. The scale bar represents 100 µm and inserted boxes highlight the field of magnification. Arrows highlight examples of $panCK^+/CD44^+$ cells.

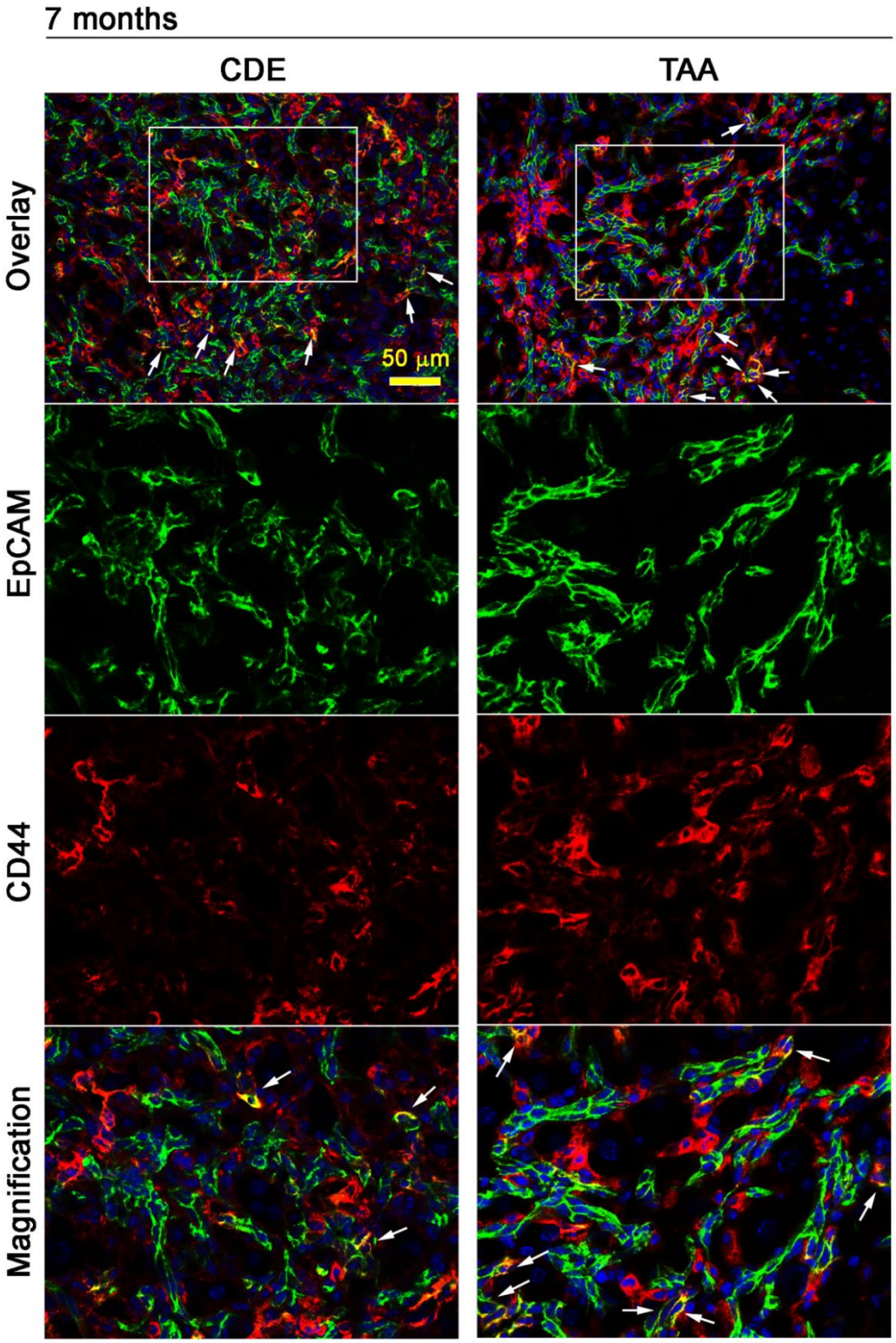

Fig 5.26: Co-localisation of CD44 and EpCAM during CDE- and TAA-induced carcinogenesis. Frozen liver sections of CDE and TAA mice after 7 months of treatment were fluorescently labelled with the LPC and CSC marker EpCAM and the CSC marker CD44. Representative images are shown. The scale bare represents 50 µm and the inserted boxes identify the area of magnification. Arrows highlight examples of $EpCAM^{+}/CD44^{+}$ cells.

5.4.3.4 Fibrosis

Irrespective of the underlying cause of CLD, fibrosis and cirrhosis are the most common risk factors for hepatocarcinogenesis. Assessment of collagen deposition using Sirius Red staining revealed distinct model-specific fibrogenic responses following long-term treatment with CDE and TAA, differing greatly form healthy livers, where thin collagen fibers were primarily detected around portal tracts and central veins (Fig. 5.27). In both regimens, fibrosis increased during the time course. In CDE mice at three months, collagen accumulation was mainly seen in portal and central areas and characterised by a distinct pericellular and "chicken wire" formation. With prolonged time on the diet, the fibrotic response differed greatly between mice of the same time points, which prompted the definition of two different phenotypes. The first group showed mild pericentral fibrosis with chicken wire appearance (zone 3 fibrosis). In the second group fibrosis progressively increased to advanced stages after five and seven months of treatment and was marked by perisinusoidal or pericellular collagen deposition throughout the parenchyma (lobular fibrosis) (Fig. 5.28). Interestingly, only the advanced fibrosis group was associated with tumour formation. In contrast to the CDE model, TAA maintained the previously established fibrogenic pattern (see maintenance phase in 3.4.4) in pericentral areas and bridging central-to-central septa at three months. During injury progression and carcinogenesis, thicker collagen fibres and wider bridging septa were detected, a typical feature for liver cirrhosis (Fig. 5.29). Livers of all experimental groups indicated a strong correlation between the excess of collagen deposition and the degree of LPC expansion and inflammation (data not shown).

5.4.3.5 Tissue regeneration niche hosting LPCs, activated HSCs and inflammatory cells

Fluorescent labelling of the cellular components of the regeneration niche, which hosts panCK$^+$ LPC, αSMA$^+$ HSCs and CD45$^+$ inflammatory cells after 7 months of treatment, illustrated the cells' close spatial relationship in the tumour-surrounding tissue of CDE and TAA mice (Fig. 5.30). However, the zonation provoked by TAA displayed a more distinct pattern and the enhanced accumulation was consistent with previously observed lobular areas of severe tissue damage.

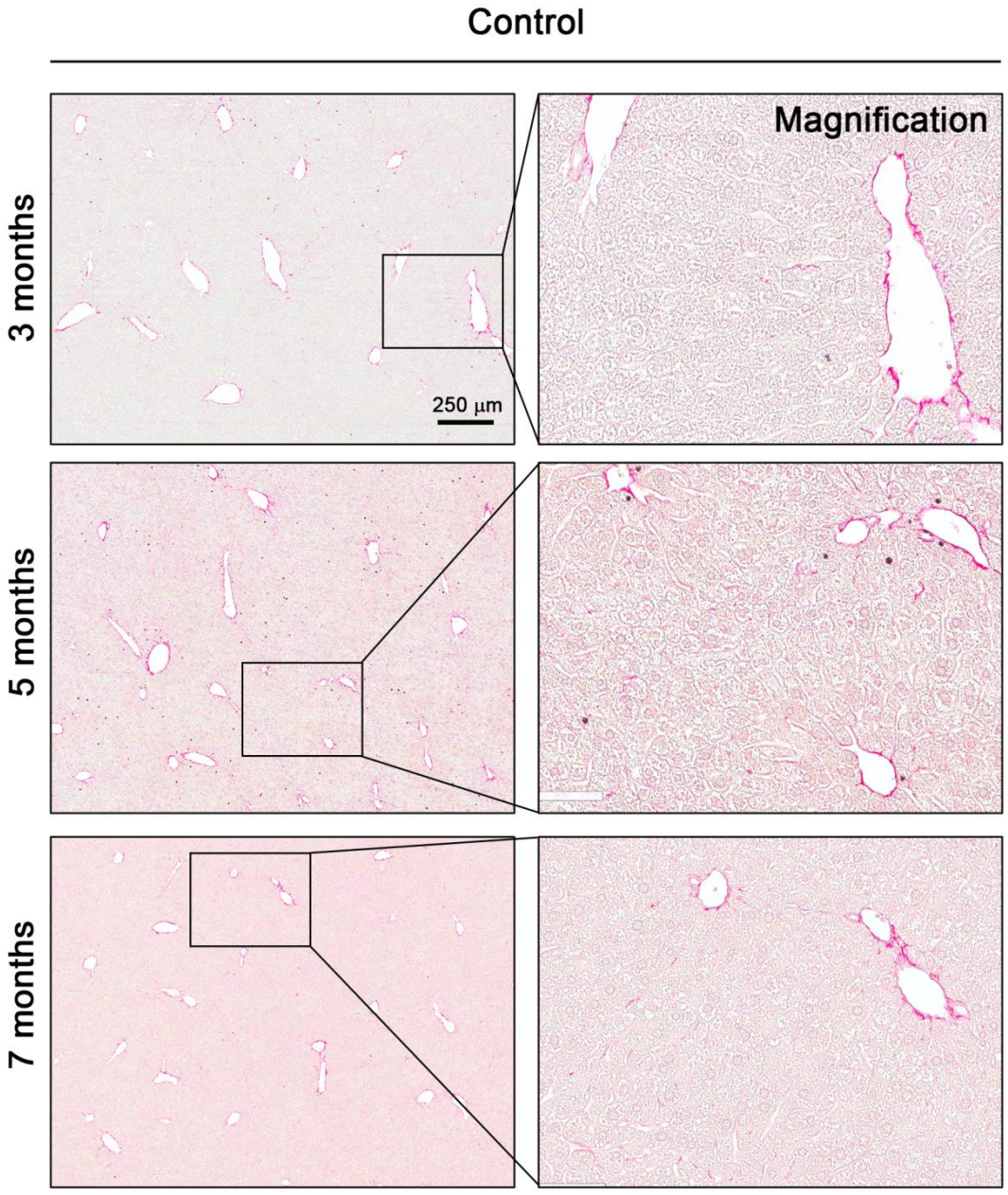

Fig. 5.27: Sirius Red staining of control mice. Formalin-fixed, paraffin-embedded liver sections of 3-, 5- and 7-month old control mice were assessed for collagen accumulation using Sirius Red. Representative images are shown. The scale bar depicts 250 µm and inserted boxes identify the enlarged area.

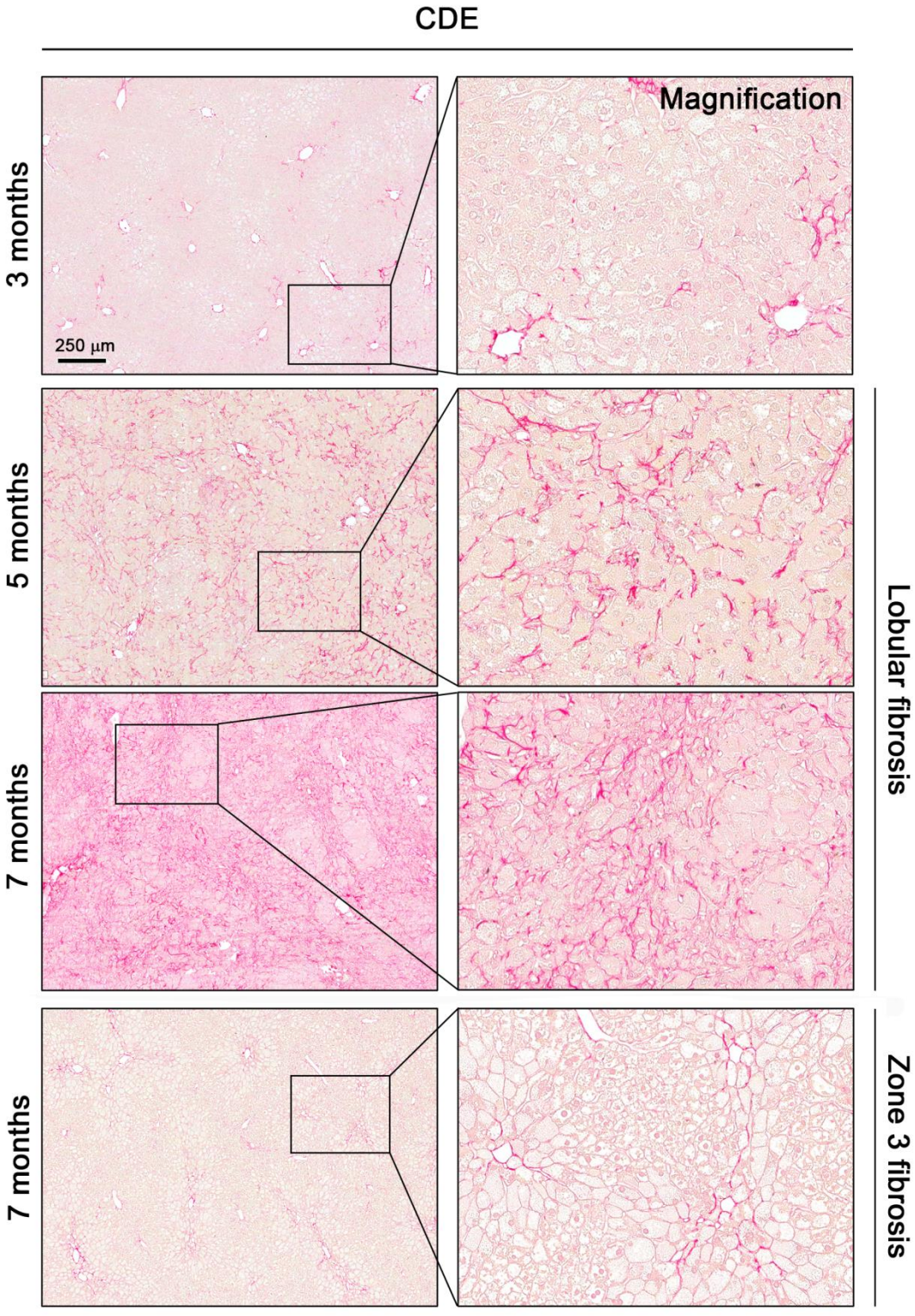

Fig 5.28: Sirius Red staining of CDE-treated mice. Collagen accumulation in formalin-fixed, paraffin-embedded liver sections of CDE mice was assessed by Sirius Red staining after 3, 5 and 7 months of treatment. Representative images are shown. The scale bar represents 250 µm and inserted boxes highlight the area of magnification.

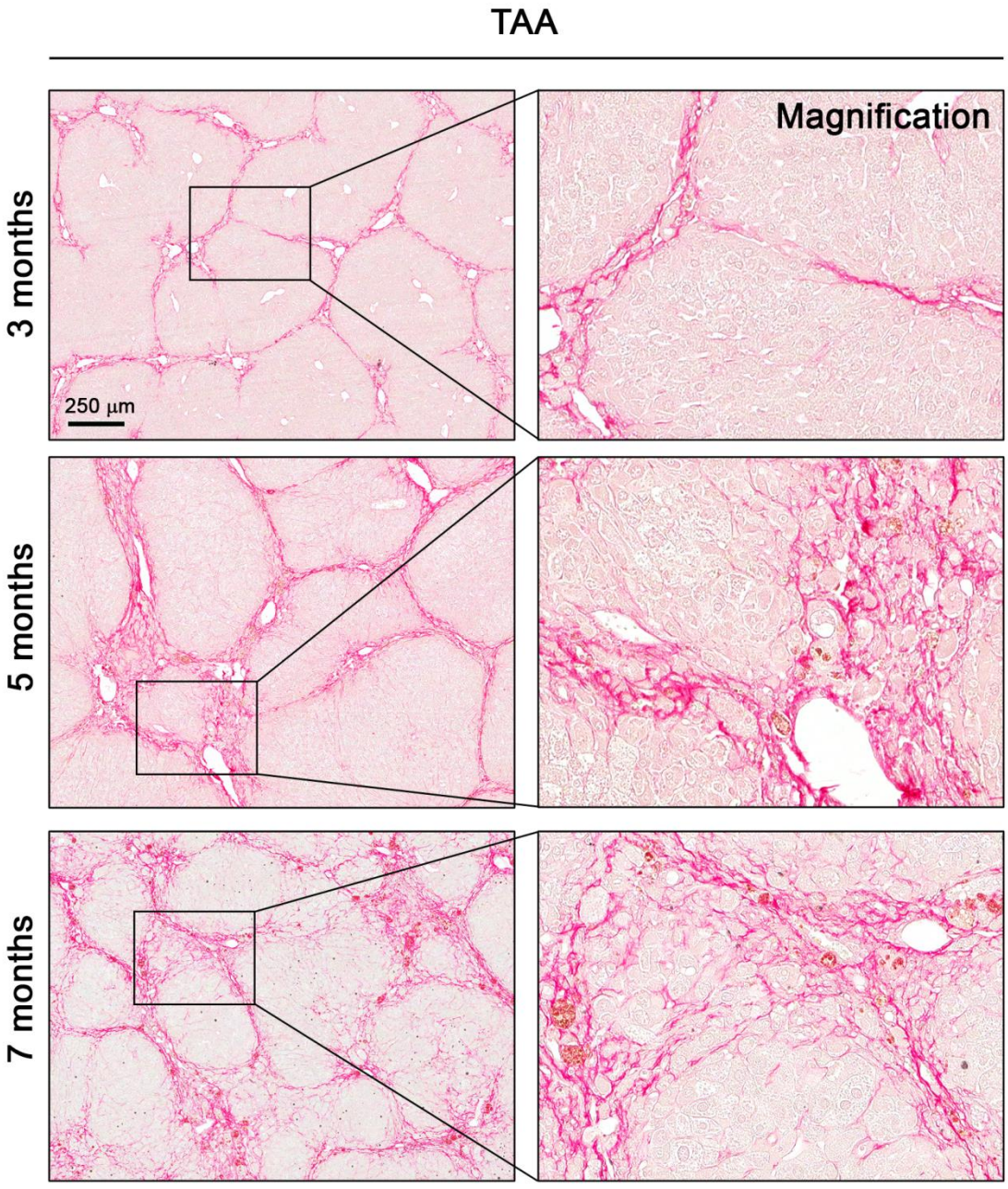

Fig. 5.29: Sirius Red staining of TAA-treated mice. Formalin-fixed, paraffin-embedded liver sections of mice exposed to TAA for 3, 5 and 7 months were assessed for collagen deposition by Sirius Red staining. Representative images are shown. The scale bar depicts 250 µm and inserted boxes define enlarged areas.

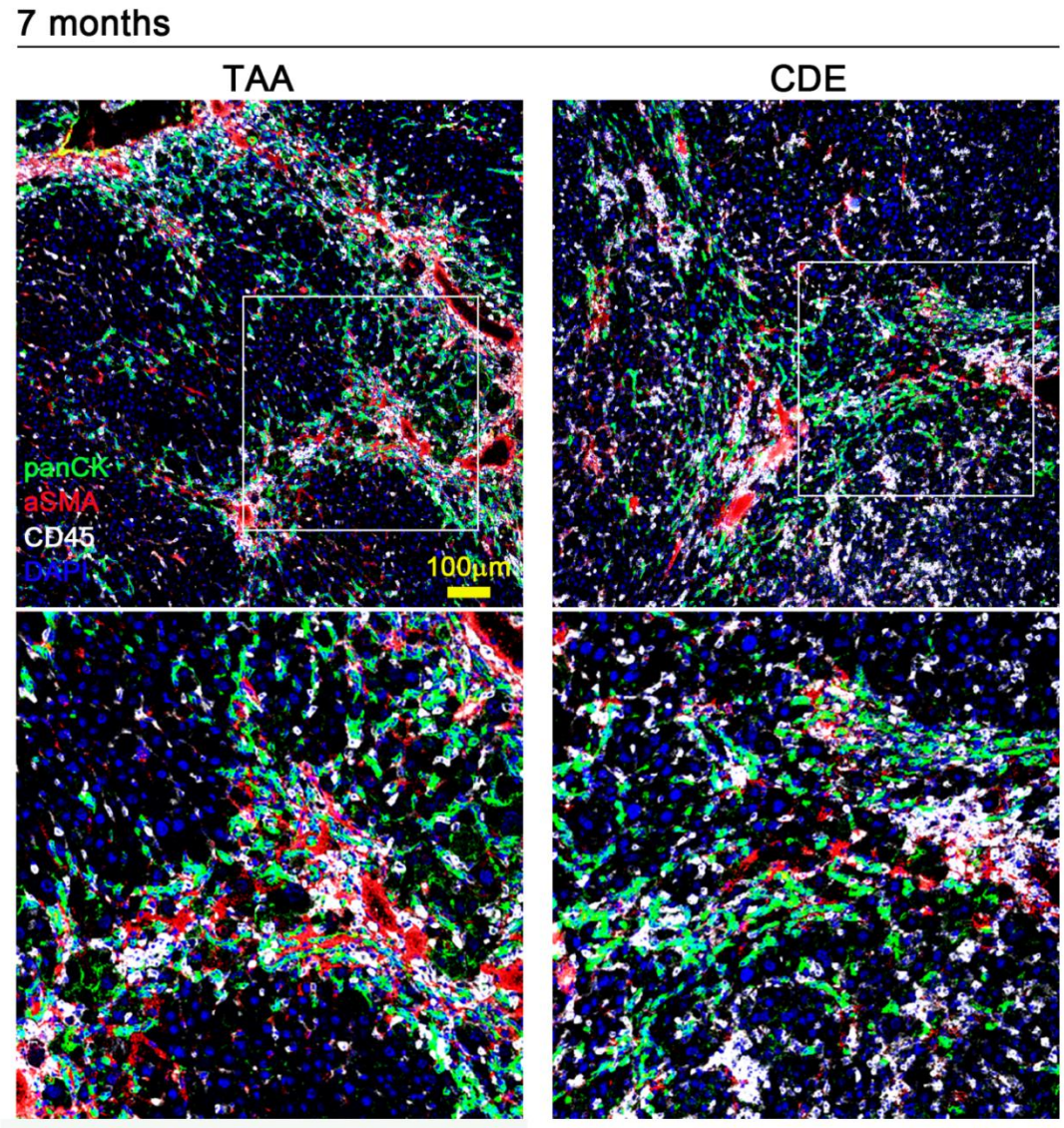

Fig 5.30: CDE- and TAA-induced regeneration niche in tumour-surrounding tissue. CDE and TAA liver sections after seven months of treatment were fluorescently labelled for the cholangiocyte and LPC marker panCK, the inflammatory cell marker CD45, the activated HSC marker αSMA and DAPI for nuclear quantitation. Representative images are illustrated for both experimental groups. The scale bar represents 50 µm and inserted boxes identify areas of magnification.

5.4.4 Characterisation of CDE- and TAA-induced tumours

As a progression from gross liver morphology analyses of CDE- and TAA-treated mice, the studies in this paragraph examine the corresponding histopathology and phenotypes of advanced tumours. The most common method for evaluating characteristics of neoplasms is the use of haematoxylin and eosin stains, which identified a great variety of neoplastic changes and enabled a clear discrimination of nodules from the surrounding tissue in both models. Tumours induced in the TAA regimen comprised large polygonal cells with abundant eosinophilic cytoplasm and atypical stripped nuclei as well as moderate basophilic cell infiltrates (Fig. 5.31). Similar characteristics were identified in CDE-induced tumours, however with weaker eosinophilic cytoplasm and enriched small basophilic cells (Fig. 5.32), and were often marked by steatosis and the presence of Mallory-Denk bodies. Furthermore, tumour-associated ductular structures were occasionally observed in the CDE model (Fig. 5.32C). Reticulin staining revealed an altered stromal network of collagen III-composing fibres in livers of CDE- and TAA-treated mice. Thickening of hepatic cell plates and diffuse reticulin structures were detected within tumours, and reticulin crowding at the interface of tumorous and non-tumorous tissue indicated invasive tumour growth into the surrounding tissue (Fig. 5.31 and Fig. 5.32).

Morphological analyses suggested a HCC phenotype for both CDE and TAA tumours; however, reports in the literature have mainly associated TAA treatment with CC development. Therefore, immunohistochemical staining for the markers CK7, CK19 and CPS1 was performed to further assess the tumour phenotypes. In both models, CK7 and CK19 expression was limited to cholangiocytes and LPCs, mainly detected in the tumour-surrounding tissue. The tumour itself was negative for both markers but positive for CPS1, consistent with an HCC phenotype (Fig. 5.33). Additionally, CDE tumours showed rare incidences of $CK7^{+}$ bile-like structures within the tumour (Fig. 5.33).

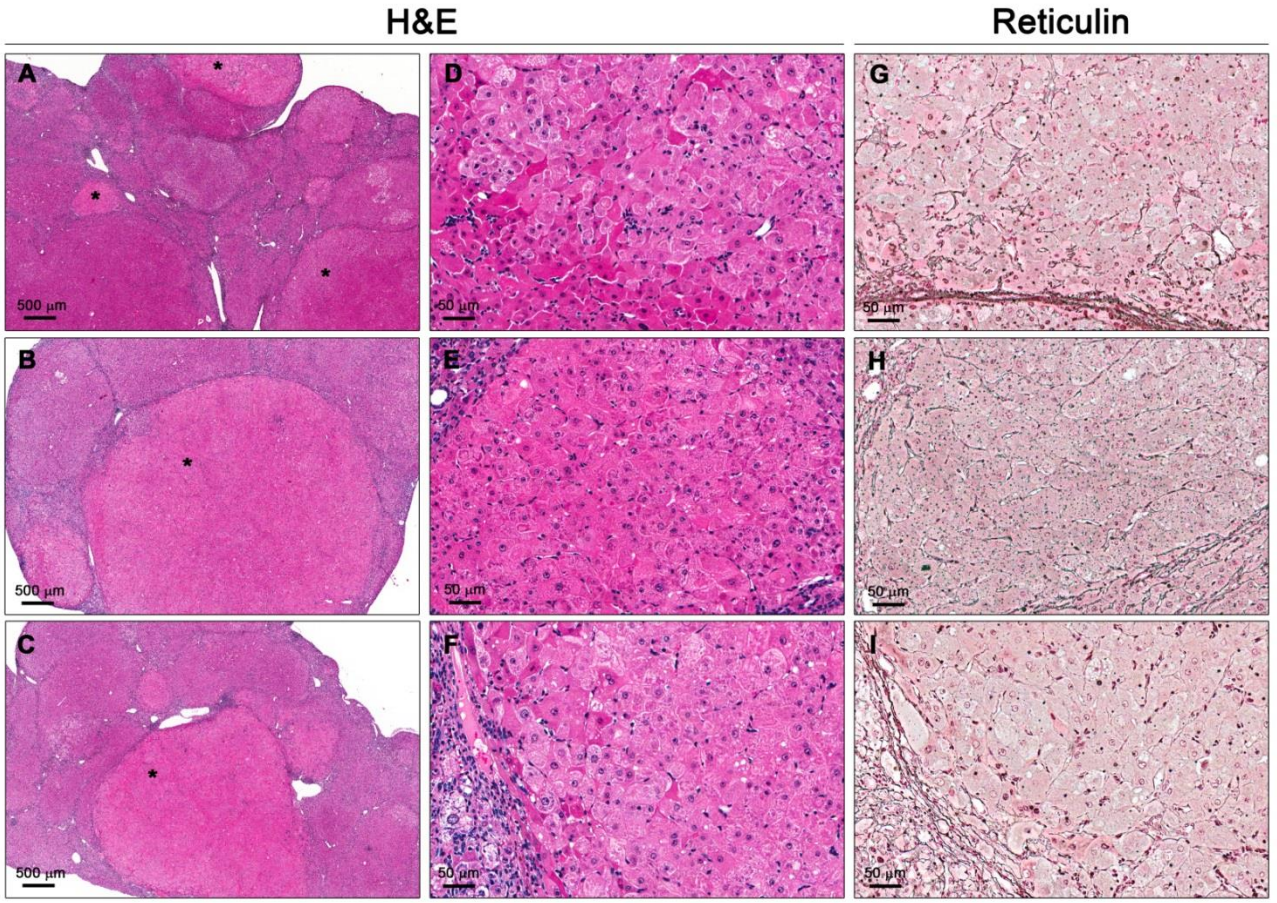

Fig. 5.31: Histology of TAA-induced tumours. Formalin-fixed, paraffin-embedded liver sections of mice treated with TAA for seven months were utilised to analyse the histology of advanced tumours by haematoxylin and eosin, and Reticulin staining. (A-C) show low magnification images of liver sections, and (D-I) illustrate representative images of analysed neoplasms. The scale bar depicts 500 (A-C) and 50 µm (D-I), respectively.

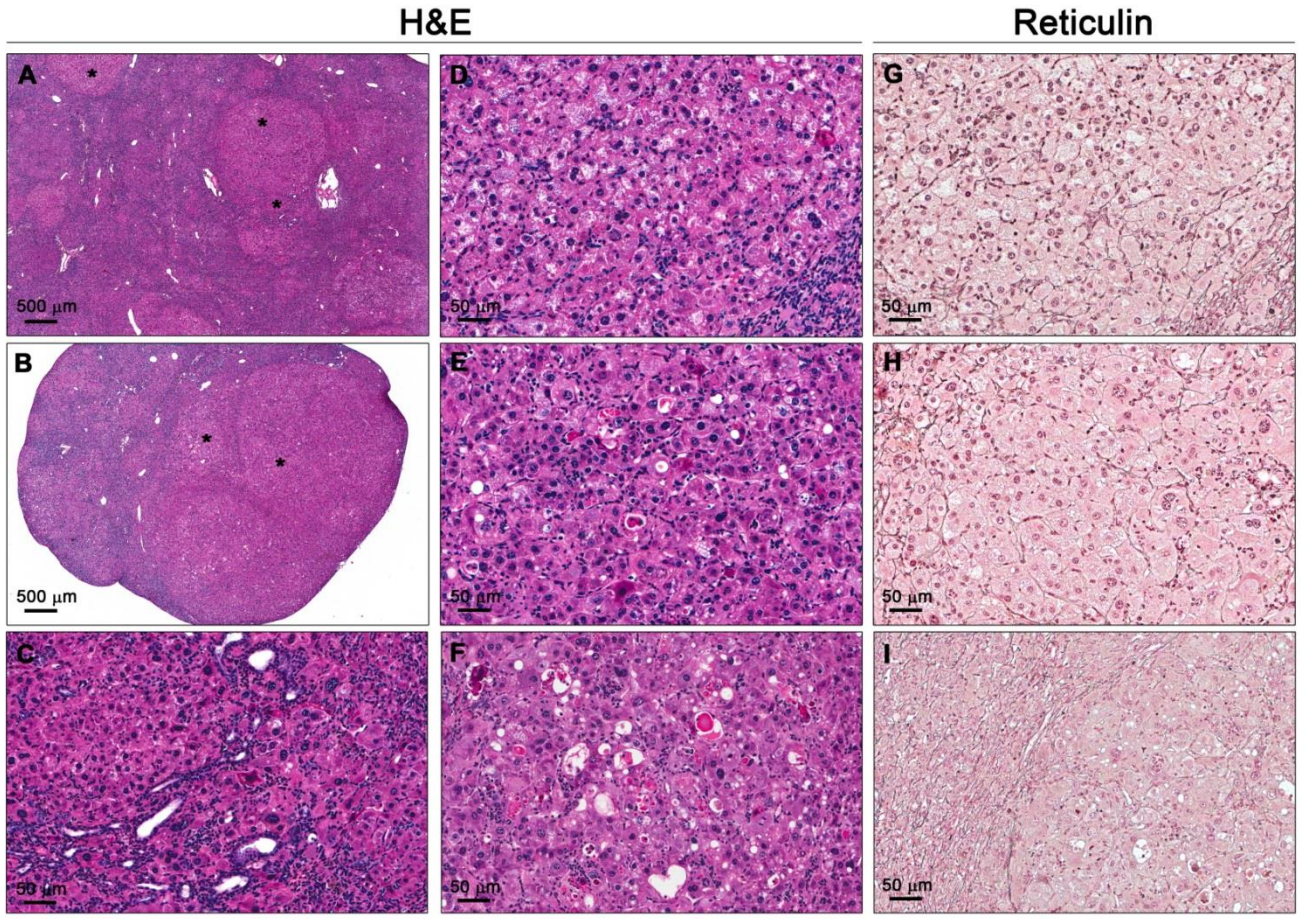

Fig. 5.32: Histology of CDE-induced tumours. The histology of advanced tumours was examined by haematoxylin and eosin, and Reticulin staining using formalin-fixed, paraffin-embedded sections of CDE mice treated for seven months. Low magnification images of liver sections are shown in (A and B), and (C-I) show representative images of analysed neoplasms. The scale bar depicts 500 (A, B), and 50 µm (C-I), respectively.

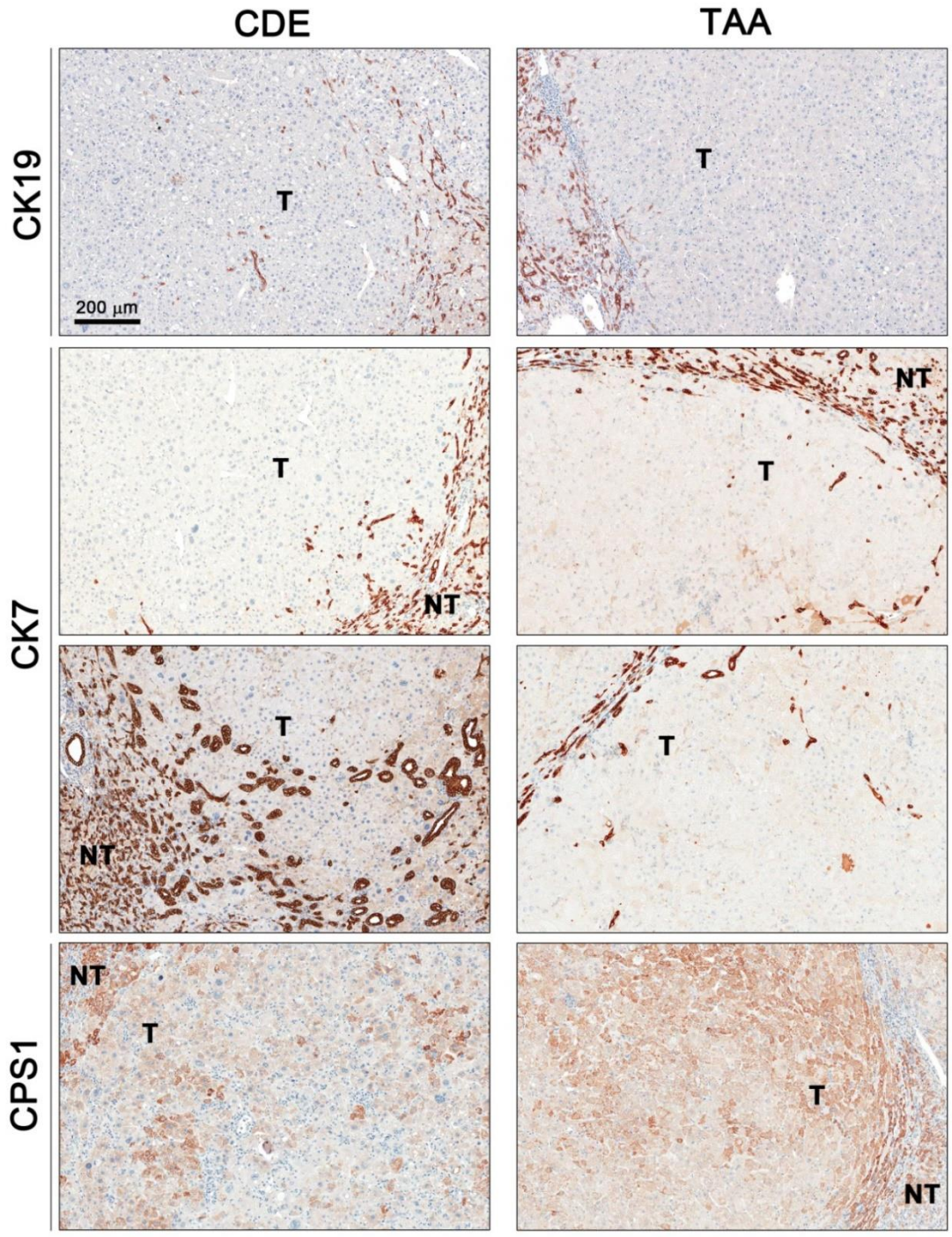

Fig. 5.33: CK7, CK19 and CPS1 expression in CDE- and TAA-induced tumours. Formalin-fixed, paraffin-embedded tissue sections of advanced tumours induced by CDE and TAA treatment for seven months were immunohistochemically labelled for the HCC marker CPS1 and the biliary/LPC and CC markers CK7 and CK19. Representative images are shown and the scale bar represents 200µm. *NT*, non-tumorous tissue; *T*, tumour.

Immunohistochemical evaluation revealed the presence of $CD45^+$ inflammatory cells and $F4/80^+$ KCs in CDE- and TAA-induced HCC, however positively stained cells were more abundant in the CDE model. Moreover, the spatial arrangement and increased magnitude of $F4/80^+$ cells in the tumour mass compared to non-cancerous surrounding tissue was highly distinct in CDE mice, suggesting a massive KC invasion (Fig. 5.34). Furthermore, labelling with the proliferation marker Ki67 demonstrated proliferating hepatocytes and small cell infiltrates in CDE- and TAA-associated HCCs, with a higher proliferative state of CDE tumours (Fig. 5.35). Sirius Red staining identified similar HCC fibrosis patterns in response to both models showing fine and moderate collagen deposition within tumours (Fig. 5.36). Finally, the distribution of LPCs was assessed using immunohistochemistry and the biliary and LPC marker panCK. The data showed that both regimens provoked tumours that hosted $panCK^+$ LPCs and those without panCK expression (Fig. 5.37). Further analysis based on immunofluorescent staining revealed that tumour-embedded LPCs comprised the $EpCAM^+/CD44^+$ subpopulation (Fig. 5.37).

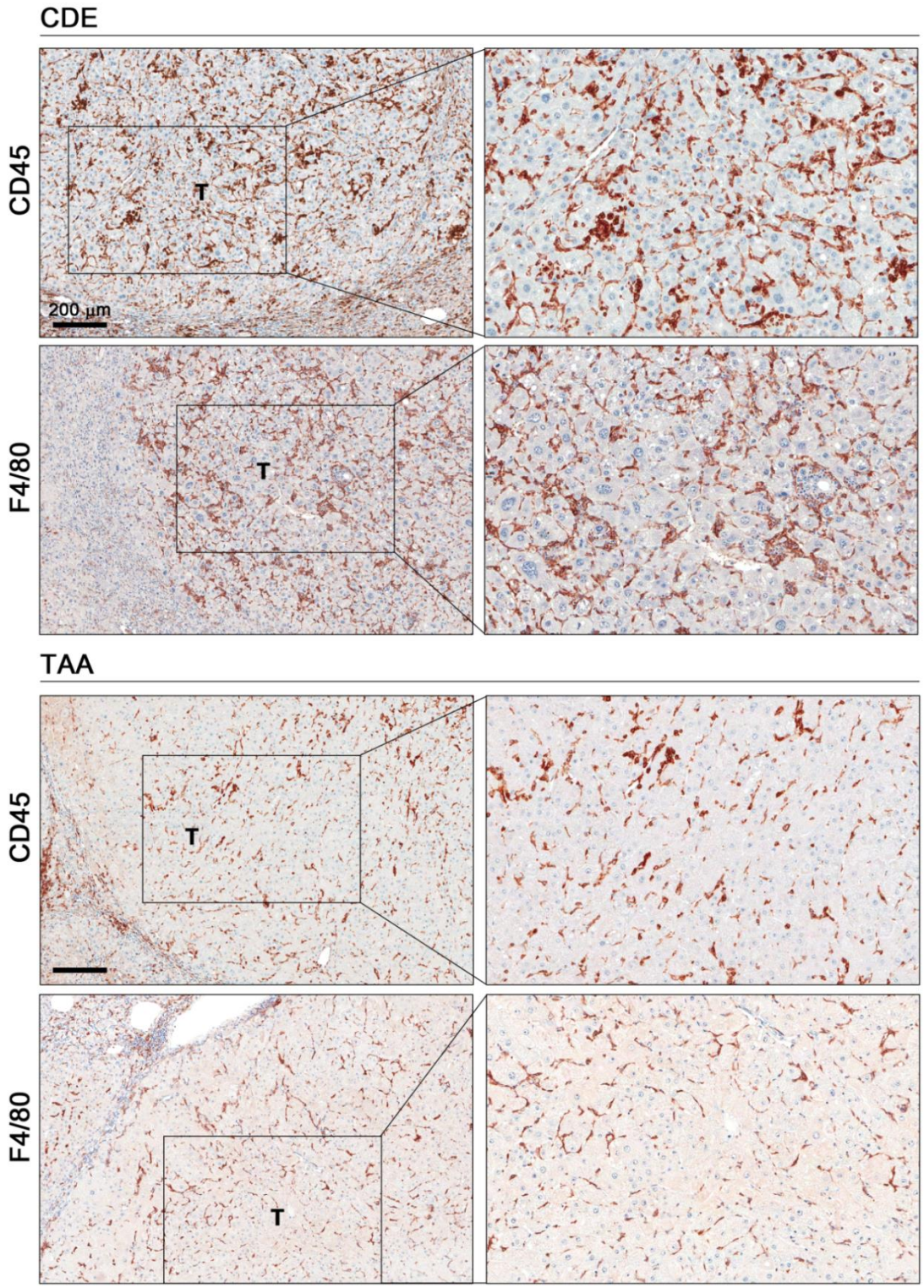

Fig. 5.34: Inflammatory pattern in CDE- and TAA-induced tumours. The inflammatory signature of advanced tumours was evaluated using formalin-fixed, paraffin-embedded tissue sections of mice treated for seven months with CDE or TAA, and immunohistochemical staining for the inflammatory marker CD45 and the KC marker F4/80. Representative images are shown and the scale bar depicts 200 µm. *T*, tumour.

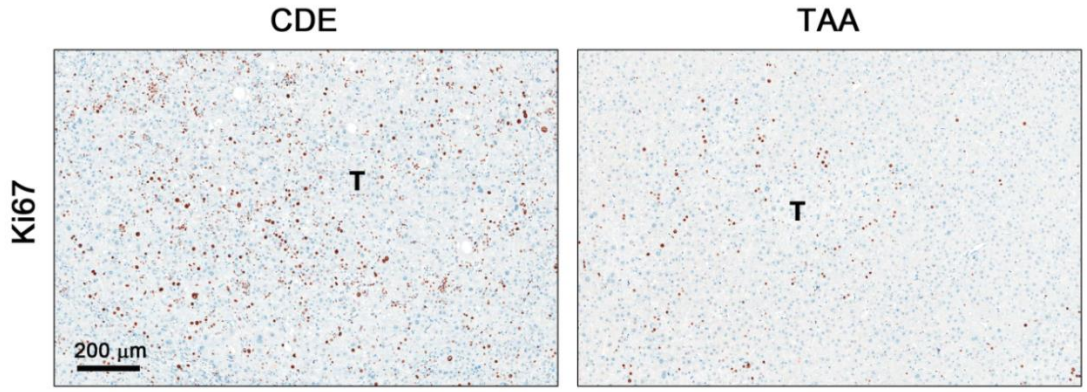

Fig. 5.35: Immunohistochemical assessment of Ki67$^+$ cells in CDE- and TAA-induced tumours. Formalin-fixed, paraffin-embedded liver sections of advanced CDE and TAA tumours were immunohistochemically labelled for the proliferation marker Ki67. Representative images are shown and the scale bar depicts 200 µm. *T*, tumour.

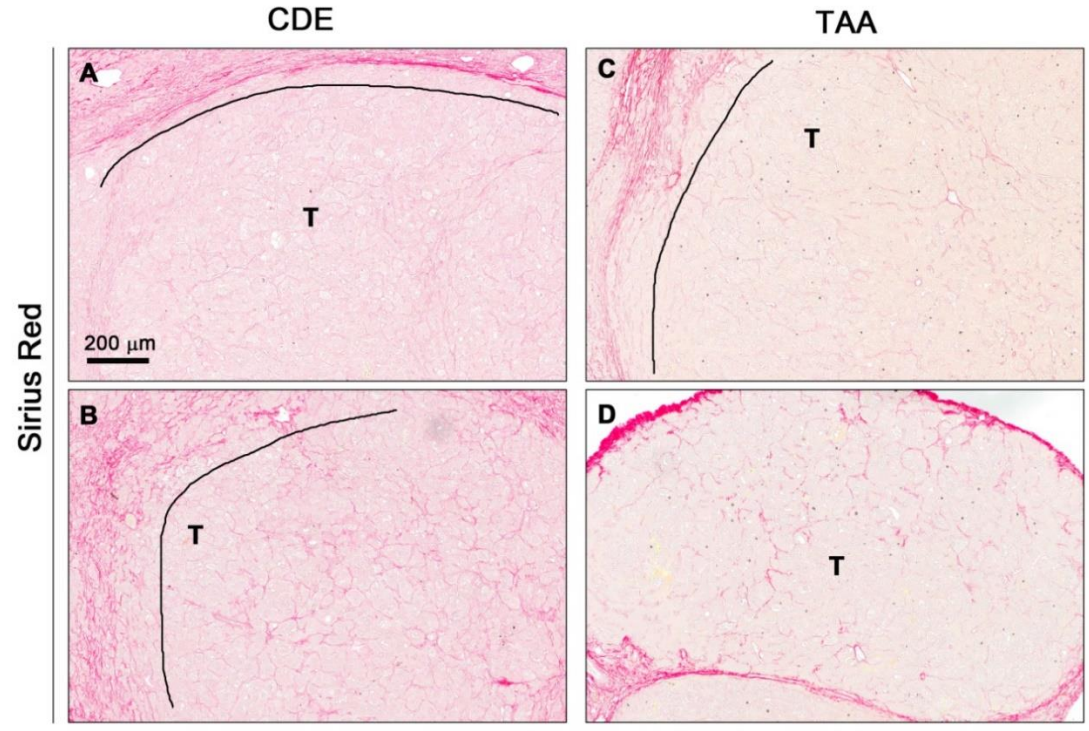

Fig. 5.36: Fibrosis state of CDE- and TAA-induced tumours. Formalin-fixed, paraffin-embedded sections of advanced tumours induced by seven months of CDE (A, low; B, moderate) or TAA (C, low; D; moderate) treatment were assessed for collagen deposition using Sirius Red staining. Representative images are shown and the scale bar depicts 200 µm. *T*, tumour.

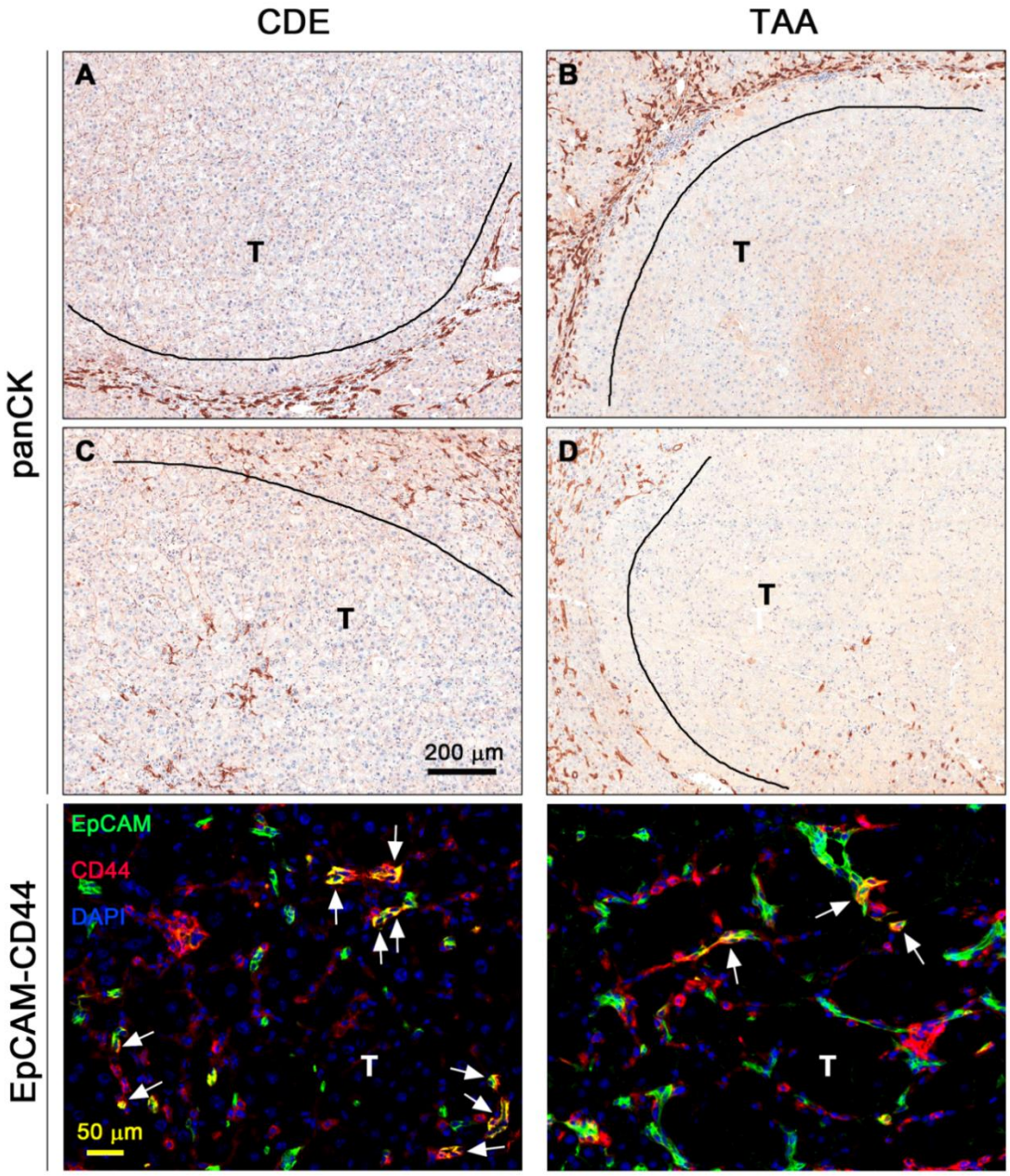

Fig. 5.37: Assessment of LPCs in CDE- and TAA-induced advanced tumours. Formalin-fixed, paraffin-embedded sections of advanced tumours induced by seven months of CDE (A, B) or TAA (C, D) treatment were stained for the cholangiocyte and LPC marker panCK using immunohistochemistry. Corresponding frozen tissue sections were fluorescently labelled with the LPC and CSC marker EpCAM, and CD44. Representative images are shown and the scale bar depicts 200 (immunohistochemical staining) or 50 µm (fluorescent staining), respectively. Arrows highlight examples of $EpCAM^+/CD44^+$ cells. *T*, tumour.

5.5 Discussion

Chapter 3 discussed in detail the dynamics of disease parameters associated with CDE and TAA-induced early stages of injury including the induction, establishment and maintenance phase. As demonstrated in the literature, both treatments represent valuable models for studying hepatocarcinogenesis and are frequently used to investigate HCC, and in the case of TAA also CC (Becker 1983; Knight *et al.* 2008; Darweish *et al.* 2014; Boulter *et al.* 2015). Therefore, the following chapter extends the comprehensive comparison of the two models to a time course of seven months through snapshot analyses after 3, 5 and 7 months, and thus covers stages of injury progression and tumour formation.

The data emphasise that long-term treatment with CDE and TAA generally induces similar kinetics of disease parameters, illustrated by increasing hepatic injury, inflammation, LPC expansion and fibrosis that predispose to cancer development. However, substantial differences were observed in the magnitude and spatial arrangements of investigated parameters at individual time points. Moreover, it is important to mention that TAA treatment caused a much more homogenous tissue response compared to high animal-to-animal variations provoked by the CDE diet. The succession of events for TAA is sustained hepatic injury, progressive inflammation, LPC response and fibrosis and eventually cirrhosis and HCC development - reflecting the pathological dynamics seen in viral hepatitis patients (Ferrell 2000). The CDE model induced excessive hepatic fat loading and progressive hepatic injury, as well as the progressive inflammation, LPC response and fibrosis, and eventually HCC development without cirrhosis. These dynamics resemble the conditions found in NAFLD patients (Ferrell 2000). Investigations of the spatial arrangements of these parameters revealed that the area of tissue damage in the TAA model persisted in centrilobular regions and formed central-to-central bridging septa, illustrated by the panCK$^+$ LPC expansion and the CD45$^+$ inflammatory response. Additionally, Sirius Red-detected collagen deposition produced a consistent fibrogenic pattern directed to the central site of injury. In contrast, evaluation of CDE mice illustrated varying degrees of steatosis predominantly in zone 3, periportal and intralobular inflammation and LPC expansion, and different fibrosis patterns including portal “chicken wire”, zone 3 and lobular perisinusoidal or pericellular fibrosis. Therefore, the CDE regimen may be

considered a model for the more severe form of NAFLD, NASH, which is marked by steatosis, severe lobular inflammation and hepatocyte ballooning (Takahashi and Fukusato 2014).

On the background of progressive CLD, both regimens effectively induced primary liver cancer with advanced tumours emerging after five months of treatment. This demonstrates a rapid tumour development in our cohort of CDE mice compared to other studies, where HCC developed after 12-14 months of CDE treatment (Davies *et al.* 2006; Knight *et al.* 2008). Histological assessment of neoplasms indicated that both models developed HCC, which was confirmed by a $CK7^-/CK19^-/CPS1^+$ phenotype, a profile that is commonly used to distinguish between HCC and CC (Kakar *et al.* 2007). These results differ from studies in the literature that mainly report CC development and only rarely report HCCs in rats in response to TAA treatment (Becker 1983; Al-Bader *et al.* 2000; Guest *et al.* 2014; Sekiya *et al.* 2012). It is worth noting that this study only used male mice for TAA treatment, while TAA-induced CC was mainly observed in female mice (Guest *et al.* 2014). Different genetic backgrounds of mice may also influence study outcomes. Consequently, standardised protocols are needed to induce similar response kinetics to be able to compare results between different laboratories.

Further characterisation of CDE- and TAA-induced HCCs demonstrated the presence of $CD45^+$ inflammatory cells infiltrating the entire tumour mass, a high proliferative state marked by $Ki67^+$ cells and low to moderate fibrosis levels illustrated by Sirius Red-visualised collagen deposition. Interestingly, in contrast to TAA, CDE tumours showed a high abundance of $F4/80^+$ TAMs, which formed a distinct distribution pattern compared to the tissue surrounding area. The immune response in cancer is a general diagnostic tool for poor outcomes, in which TAMs represent the major player in HCC (Capece *et al.* 2013; Zhang *et al.* 2010b). Therefore, the CDE diet represents a valuable model for the study of HCC-related inflammatory modulation. Analogous to the high variation of tissue injury responses, the emerging tumours in the CDE model displayed several different forms of HCC. The morphology of CDE tumours included varying degrees of steatosis and steatohepatitis, as well as $CK7^+$ bile-like structures within the tumour, most likely representing pseudoglandular formations, a typical feature of rapidly proliferating HCCs (Yeh 2010). Several CDE-induced steatotic HCCs resembled the distinctive histological variant that is mainly seen in

patients suffering from NASH and termed steatohepatitic HCC (SH-HCC) (Salomao *et al.* 2010). In future studies, neoplasms will be analysed using immunohistochemical staining for glypican-3, glutamine synthetase and heat shock protein 70. In human diagnostics positive expression of these markers clearly distinguishes HCCs from high grade dysplastic nodules in cirrhotic and hepatocellular adenomas in non-cirrhotic livers (Schlageter *et al.* 2014).

A cohort study in HCV patients demonstrated a positive correlation between the DR, the inflammatory response and the degree of fibrosis (Prakoso *et al.* 2014). Similar results were obtained in CDE- and TAA-induced CLD progression and carcinogenesis. Immunohistochemical staining of panCK$^+$ LPCs strongly suggested a positive correlation between tumour formation and the magnitude of the LPC response in CDE mice. Moreover, the degree of the inflammatory response and tissue fibrosis seemed to be intricately linked to the magnitude of LPC expansion. Due to time constrictions a limited number of animals was analysed and the trend described in this study will be further examined using more mice of this time course. The observed temporal and numerical relationship between investigated disease parameters suggested potential interactions between their cellular components. As described in Chapter 3.4.3, the regeneration niche provoked by CDE and TAA treatment accommodated panCK$^+$ LPC, αSMA$^+$ HSCs and CD45$^+$ inflammatory cells, and most likely orchestrated the tissue response during injury induction (CDE), and the establishment and maintenance phase (TAA). Furthermore, a communication between these cellular players has been proposed in several studies using CDE as initiator of CLD (Van Hul *et al.* 2009; Ruddell *et al.* 2009; Tirnitz-Parker *et al.* 2014; Elsegood *et al.* 2015). Immunofluorescent triple staining of the cellular components of the regeneration niche during carcinogenesis demonstrated a close spatial relationship in tumour-surrounding areas and suggested that the interaction between LPCs, activated HSCs and inflammatory cells may play a role in the modulation of a tumour-favouring microenvironment. Interestingly, immunofluorescent characterisation using different LPC markers illustrated an increasing diversity within the LPC response during both CDE- and TAA-induced progressive CLD and carcinogenesis. Despite a general great overlap, several single positive subpopulations were detected including phenotypes such as panCK$^+$/CK19$^-$, CK19$^+$/EpCAM$^-$, CK19$^-$/EpCAM$^+$ and panCK$^+$/CD133$^-$. They may identify different

stages during lineage commitment and/or define phenotypes that fulfil different roles during liver regeneration and cancer development. A study in chronic viral hepatitis patients suggested $EpCAM^+$ hepatocytes to be a recent progeny of amplifying LPCs (Yoon *et al.* 2011).

LPCs are discussed in the literature as potential precursor cells during hepatocarcinogenesis (see 1.8.4 for review). Data in this chapter support this hypothesis in the CDE and TAA model. Firstly, a correlation between the degree of LPC expansion and tumour development was demonstrated in both regimen, and several HCCs were infiltrated with $panCK^+$ and $CK7^+$ LPCs. Secondly, within the $panCK^+$ LPC population, several CD44-expressing cells were detected. It was previously shown that CD44 identified tumour-initiating cells in the liver when co-expressed with other CSC markers (Yang *et al.* 2008c; Yang *et al.* 2008b; Zhu *et al.* 2010) and thus may represent a valid feature to identify pre-cancerous LPC candidates. The potential pre-cancerous stage of $CD44^+/panCK^+$ LPCs was strengthened by the presence of $CD44^+/EpCAM^+$ cells located in tumours and the surrounding tissue, since EpCAM not only labels LPCs, but also identifies hepatic CSCs (Yamashita *et al.* 2008; Yamashita *et al.* 2009; Kimura *et al.* 2010). In future studies, a potential precursor-product relationship will be further investigated using FACS-isolated $CD44^+$ LPCs and subsequent functional (tumorigenicity assays) and gene expression analysis (HCC- and CSC-associated changes).

CHAPTER 6

Defining the relationship between the DR/LPC response and HCC development in human CLD

6.1 Introduction

A detailed characterisation of the disease parameters associated with CDE- or TAA-induced murine CLD progression and carcinogenesis was provided in the previous chapter. Both regimens provoked tumour development in response to long-term treatment and it was further suggested that there is a positive correlation between LPCs and HCC occurrence in mice. This chapter focuses on human hepatocarcinogenesis and investigates the relationship between the DR, LPC expansion, and HCC development.

The DR and associated LPC activation in human liver disease has been well characterised in chronic cholestatic liver disease, ALD, NAFLD and viral hepatitis (Roskams and Desmet 1998; Lowes *et al.* 1999; Roskams *et al.* 2003a; Clouston *et al.* 2005)). Furthermore, a positive correlation between disease parameters including fibrosis and inflammation, and expanding bile ductules/LPCs was established in HBV- and HCV- infected patients (Libbrecht *et al.* 2000a; Clouston *et al.* 2005; Prakoso *et al.* 2014). Cytokeratins represent the most common markers used to identify the DR and the LPC compartment. In particular, CK7 and CK19 expression were both localised with the DR/LPCs in ALD, obesity, NAFLD, NASH and viral hepatitis (Richardson *et al.* 2007; Jung *et al.* 2008; Meriden *et al.* 2010; Liew *et al.* 2012). A high degree of overlap between the expression profiles of CK7, CK9 and panCK in HCV patients illustrated that these markers identify the same injury response (Prakoso *et al.* 2014). Furthermore, CK7 and EpCAM expression positively correlated with disease severity in alcoholic hepatitis and the authors suggested potential value as mortality predictors in patients (Sancho-Bru *et al.* 2012). Although several immunohistochemical studies demonstrated a positive correlation between the disease severity and the DR/LPC response in CLD patients, the role of expanding LPCs during hepatocarcinogenesis requires further investigation.

6.2 Study Aims

The aim of this chapter was to examine the relationship between the abundance of LPCs, their lobular distribution, and potential tumour occurrence in CLD patients. Therefore, the LPC response has been analysed in two groups of patients (still on-going). The first set of samples was derived from CLD patients with advanced stages of fibrosis and a known history of no HCC development, whereas the second group included patients who later developed HCC.

6.3 Methods

A retrospective study was performed using human biopsy material and de-identified clinical data. Tissue samples of two cohorts were included in the study. These were obtained from the Alfred Hospital in Melbourne (VIC, Australia) and Fremantle Hospital in Fremantle (WA, Australia). The Melbourne cohort comprised 25 liver biopsies obtained from individual CLD patients, who developed HCC one to 12 years after the biopsy (HCC group). The degree of tissue fibrosis and inflammation was evaluated at Royal Alfred Hospital using Scheuer's scoring system (0-4). The Fremantle cohort contained liver biopsies from five patients, who developed HCC six to 12 years after the biopsy (HCC group) and 25 liver biopsies from CLD patients without liver tumours up to the date of commencing this study (followed patient history for 7 to 17 years after biopsy) (non-HCC group). The stage of tissue fibrosis in the second cohort was assessed at Fremantle Hospital using Scheuer's scoring system (0-4). Ductular reactions and LPC responses were evaluated in all patients using paraffin-embedded sections and immunohistochemistry staining for the common biliary cell and LPC marker CK7, EpCAM and Sox9. Histopathological analysis of sections was performed blinded to the clinical data. The appearance of positive CK7 staining was scored according to the magnitude and lobular distribution of the DR and LPCs in whole section scans on a three-point scale, modified after Prakoso *et al.* (Prakoso *et al.* 2014) (Table. 6.1). Due to cohort-specific tissue

fixation methods, the background staining varied greatly between sections, however did not affect the analyses.

Category	**Description**
1 (mild)	DR and/or LPC expansion limited to portal tract
2 (moderate)	DR and/or LPC expansion in zone 1 and up to 50% of zone 2 of the liver lobule
3 (severe)	DR and/or LPC expansion into zones 1, 2 and 3 of the liver lobule

Table. 6.1: Description of the three-point scoring system for the DR/LPC response.

6.4 Results

6.4.1 Patient characteristics of the non-HCC and the HCC group

To evaluate the DR and LPC response in CLD patients and correlate their appearance with tumour formation, two groups of patients have been analysed and compared (Table 6.2). The first group included CLD patients with advanced stages of fibrosis and cirrhosis (F3, 76% and F4, 24% of patients, respectively) but no signs of developing tumours are referred to as non-HCC group. We have previously established that the DR and LPC responses correlate with the severity of the underlying chronic liver disease (Lowes *et al.* 1999; Prakoso *et al.* 2014). As most cases of HCC develop on a background of moderate to severe fibrosis, only F3 and F4 patients were included in the non-HCC group to identify true differences with regards to the appearance and the magnitude of the DR/LPC responses as potential associates of HCC development.

The second set of CLD patients, defined as HCC-group, was derived from patients who later developed HCC and showed various stages of fibrosis and cirrhosis at the time of the biopsy (F0, 3.7%; F1, 7.4%; F2, 22.2%; F3, 11.1%; F4, 37%). Patients with different aetiologies were included in the study; however, CLD was mainly caused by viral hepatitis infections (HBV and HCV). Characteristics of individual patients are shown in Table 6.3 and Table 6.4.

.

	Non-HCC group		*HCC group*	
	n	%	n	%
Total	25	100	27	100
Male	13	52	23	85.2
Age	34-51	-	36-69	-
Mean ± SEM	41.9 ± 1.1	-	50.8 ± 1.9	-
Fibrosis stage				
F0	-	-	1	3.7
F1	-	-	2	7.4
F2	-	-	6	22.2
F3	19	76	3	11.1
F4	6	24	10	37
N/A	-	-	5	18.5

Table 6.2: Patient data of the non-HCC and HCC group. Gender, age and fibrosis stage of patients from the non-tumour and tumour group are listed.

Patient	*Sex*	*Age at biopsy*	*Date of biopsy*	*Fibrosis*	*Inflammation*	*HBV*	*HCV*
N1	M	49	2009	3	N/A		
N2	M	41	2005	3	N/A		
N3	M	39	2005	3	N/A		
N4	M	37	2005	3	N/A		
N5	M	37	2003	3	N/A		yes
N6	M	48	2004	3	N/A		
N7	M	46	2003	3	N/A		yes
N8	M	44	2003	3	N/A		
N9	M	49	2005	3	N/A		
N10	M	40	2001	3	N/A		
N11	M	36	2001	4	N/A		yes
N12	M	41	2002	4	N/A		
N13	M	51	2009	4	N/A		yes
N14	F	40	2009	3	N/A		yes
N15	F	39	2008	3	N/A		
N16	F	38	2003	3	N/A		
N17	F	35	2001	3	N/A		yes
N18	F	34	1999	3	N/A		yes
N19	F	38	2001	3	N/A		yes
N20	F	49	2005	4	N/A		
N21	F	47	2005	4	N/A		
N22	F	47	2004	4	N/A		
N23	F	46	2003	3	N/A		
N24	F	43	2000	3	N/A		yes
N25	F	34	2005	3	N/A		

Table 6.3: Characteristics of individual non-HCC patients. *N/A*, not assessed.

Patient	*Sex*	*Age at biopsy*	*Age at HCC detection*	*Fibrosis*	*Inflammation*	*HBV*	*HCV*
T1	M	44	47	4	2	yes	yes
T2	M	36	47	4	1	no	yes
T3	M	43	44	2	2	no	yes
T4	F	69	79	2	2	no	yes
T5	M	58	63	1	3	yes	no
T6	M	44	56	4	1	yes	yes
T7	M	27	32	2	1	yes	no
T8	M	66	70	1	2	no	yes
T9	M	53	56	2	2	yes	yes
T10	M	56	57	4	3	no	yes
T11	M	55	62	4	2	no	yes
T12	M	45	53	4	2	no	yes
T13	F	56	61	0	1	yes	yes
T14	F	58	64	3	3	yes	yes
T15	M	60	64	3	3	yes	no
T16	M	45	51	3	3	yes	yes
T17	M	57	61	4	3	no	yes
T18	M	45	53	2	1	no	yes
T19	M	45	52	4	3	no	yes
T20	F	57	66	2	2	no	yes
T21	M	47	55	4	N/A	yes	yes
T22	M	48	56	4	2	yes	yes
T23	M	47	57	N/A	N/A		yes
T24	M	47	58	N/A	N/A		yes
T25	M	52	64	N/A	N/A		yes
T26	M	69	75	N/A	N/A		yes
T27	M	42	52	N/A	N/A		yes

Table 6.4: Characteristics of individual HCC patients. *N/A*, not assessed.

6.4.2 Ductular reaction and LPC expansion in the non-HCC vs. HCC group

Immunohistochemical staining of the biliary cell and LPC marker CK7 revealed that the DR mainly appeared in periportal areas identified by increasing numbers of $CK7^+$ biliary structures and irregular strings of bile duct epithelium. Moreover, in the periphery of portal tracts, $CK7^+$ single cells and small groups of cells without a lumen, and therefore defined as LPCs, were detected, which occasionally expanded further into the parenchyma. The magnitude and lobular distribution of the DR and LPCs was evaluated using a three-point scoring system defined as mild (1), moderate (2) and severe responses (3) (Table 6.1 and Fig. 6.1). The non-HCC group mainly showed mild (44%) and moderate responses (48%) with increased ductular structures and limited LPC expansion. On the other hand, in the HCC group all categories were evenly represented (mild, 30%; moderate, 33%; severe, 37%), demonstrating more prominent expansion of LPCs into the parenchyma (Table 6.5 and Fig.6.2). There was a significant positive correlation between the appearance and degree of the DR/LPC response and the risk to develop HCC in CLD patients (Fig. 6.3).

In the HCC group, tissue fibrosis increased significantly with a stronger DR/LPC response, whereas the severity of inflammation did not significantly change between the mild, moderate and severe response group even though a trend of increasing inflammation was observed (Fig. 6.4). However, a significant positive correlation was detected between the severity of the DR/LPC response and the corresponding tissue fibrosis stage (Fig. 6.5A), and tissue inflammation (Fig. 6.5B), respectively. Since the non-HCC group patients were limited to more advanced fibrosis stage (F3 and F4), a correlation was not performed.

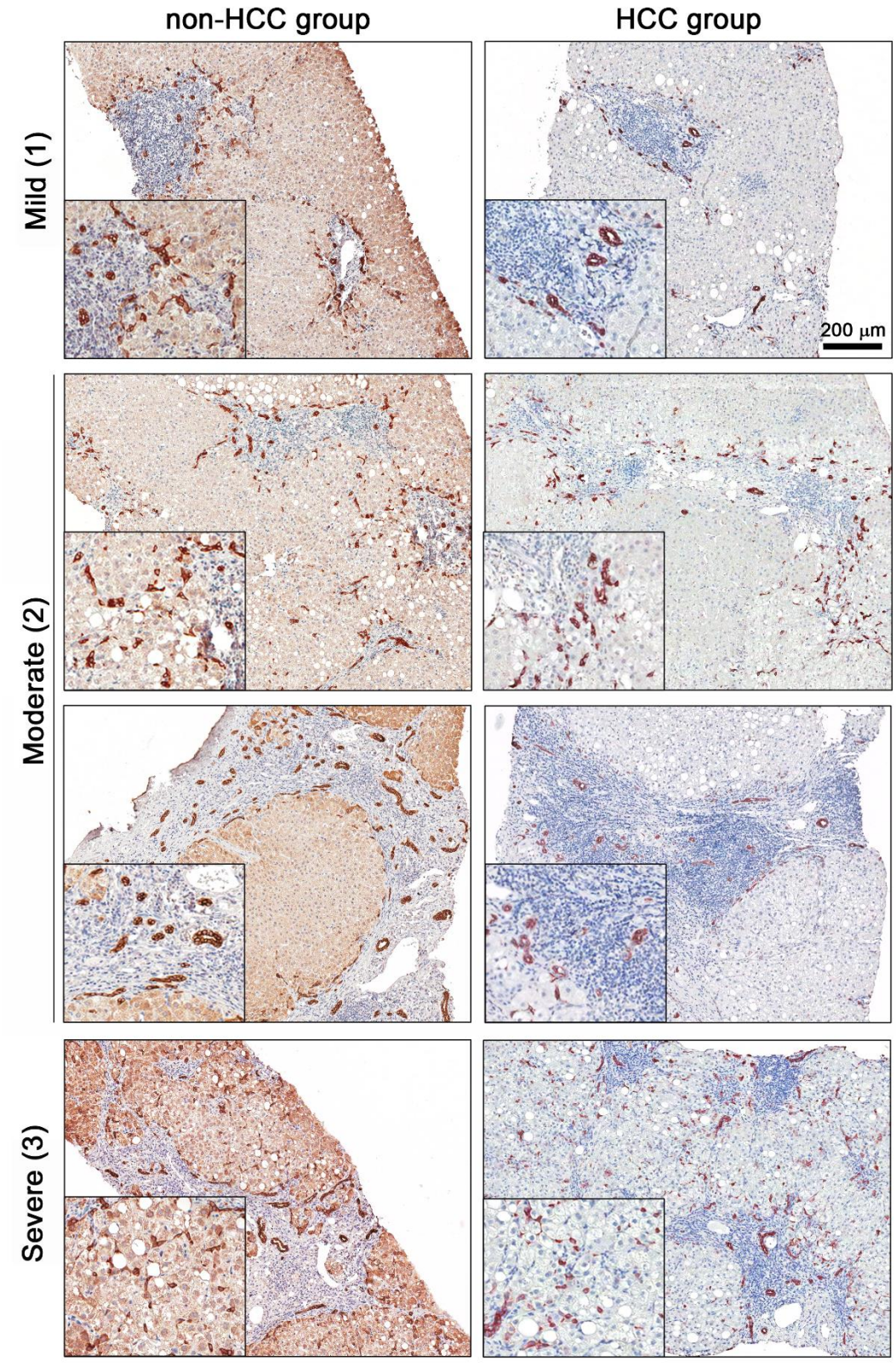

Fig. 6.1: Mild, moderate and severe DR and LPC response. Formalin-fixed, paraffin-embedded sections from patients of the non-HCC and HCC group were immunohistochemically labelled for the biliary cell and LPC marker CK7. Representative images of the mild, moderate and severe DR/ LPC response are shown. The scale depicts 200 µm.

	Non-HCC group		*HCC group*	
	n	%	n	%
Total	25	100	27	100
DR/ LPCs				
1	11	44	8	30
2	12	48	9	33
3	2	8	10	37

Table 6.5: Scoring of the DR and LPC response in the non-HCC and HCC group.

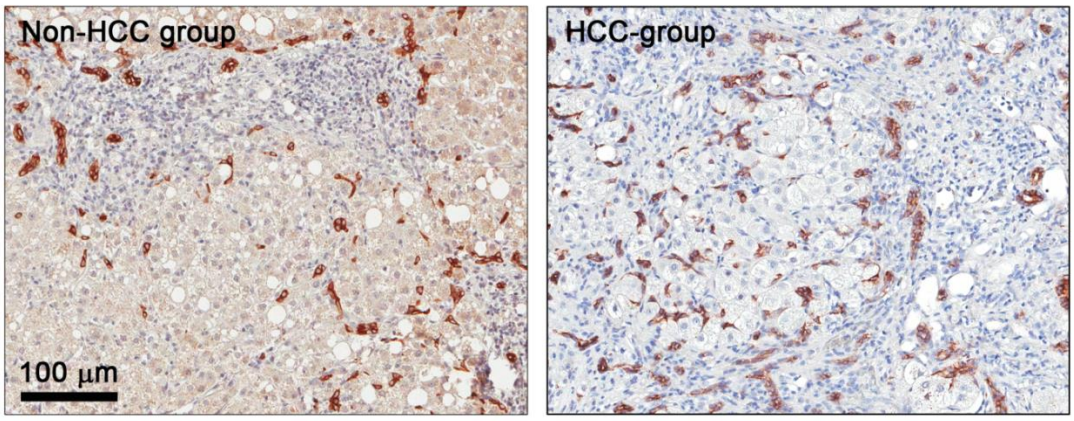

Fig. 6.2: Parenchymal infiltration of CK7$^+$ LPCs in non-HCC and HCC patients. Representative images of parenchymal CK7$^+$ LPC infiltration in livers of non-HCC and HCC patients are shown. The scale depicts 100 µm.

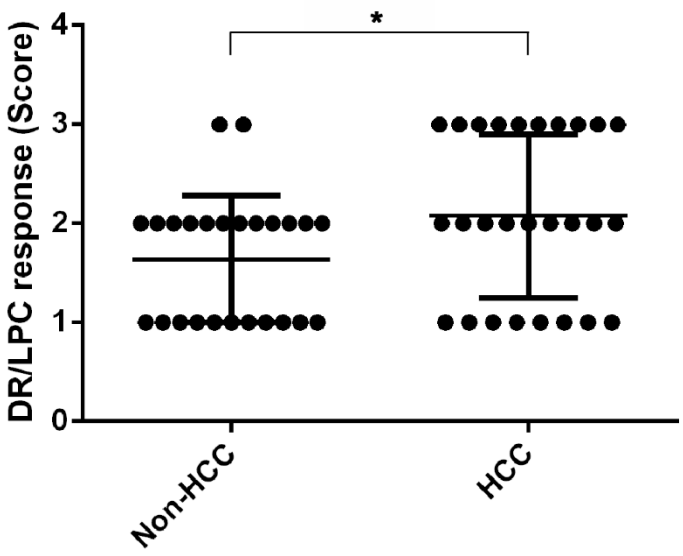

Fig 6.3: DR and LPC response in the non-HCC and HCC group. The graph shows the average score ± SEM for the DR/LPC response in non-HCC and HCC patients. *p > 0.05 (Mann Whitney test)

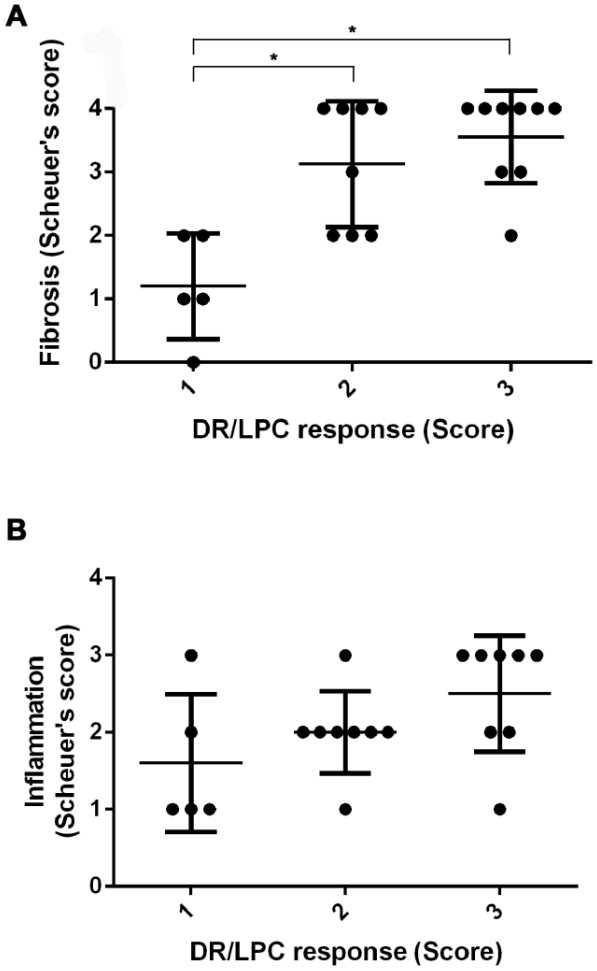

Fig 6.4: The relationship between the DR/LPC response and other CLD disease parameters in the HCC group. This graph shows (A) the fibrosis and (B) inflammation status of HCC patients in the three categories of DR and LPC response. *$p < 0.05$ (Kruskal Wallis test)

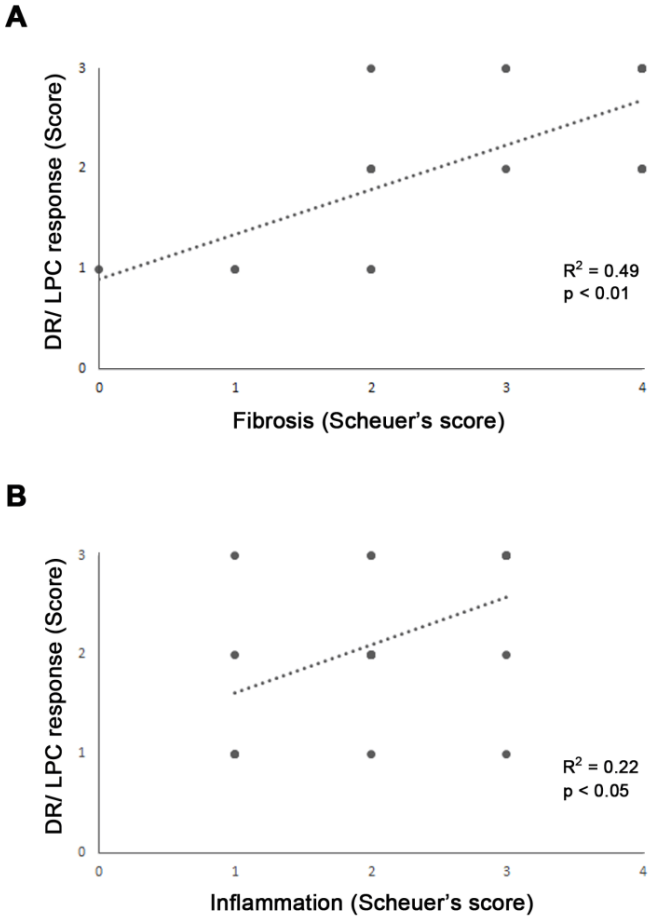

Fig 6.5: The DR/LPC response in correlation to other CLD disease parameters of the HCC group. Stages of the DR/LPC response (1-3) in individual patients of the HCC-group were correlated to (A) the fibrosis score and (B) the inflammation score. Multiple data points may be present overlying an individual point. Shown is the trend line with R^2 and p values state the significance of the correlation.

.

6.5 Discussion

Support for the hypothesis that LPC activation and proliferation might be associated with an increased risk of HCC development in human livers came from several studies that linked LPCs and the DR to progressing injury patterns (Clouston *et al.* 2005; Lowes *et al.* 1999; Prakoso *et al.* 2014; Wood *et al.* 2014). Moreover, pharmacological inhibition of the LPC compartment has been demonstrated to decelerate disease progression and reduce HCC formation (Davies *et al.* 2006; Knight *et al.* 2008; Lee *et al.* 2010a). Additionally, in combined HCC-CC, background activation of LPCs is associated with multifocal occurrence and recurrence (Cai *et al.* 2012).

This chapter investigated the appearance of the DR and LPC response in CLD patients and assessed a potential link to HCC. The samples included in this retrospective study were particularly valuable since the history of patient data as well as their outcome was known. Characterisation of $CK7^+$ DRs/LPC expansions suggested a positive correlation between the magnitude/distribution of the LPC response and HCC development. Furthermore, patients in the HCC group illustrated a more prominent parenchymal infiltration of LPCs, marked by $CK7^+$ single cells and small groups of cells. However, to validate this observation, additional patient cohorts will need to be analysed. In CLD such as ALD, NAFLD and HCV infection, a positive correlation between the degree of fibrosis and LPC expansion has been demonstrated (Roskams *et al.* 2003a; Sancho-Bru *et al.* 2012; Prakoso *et al.* 2014). This study confirmed and extended the previous findings in chronically injured livers of patients, who later developed HCC by showing a positive correlation between LPCs and tissue fibrosis, as well as between LPCs and tissue inflammation, respectively.

Due to the known positive correlation between LPCs and the corresponding tissue fibrosis (Roskams *et al.* 2003a; Clouston *et al.* 2005; Sancho-Bru *et al.* 2012), only F3 and F4 patients were incorporated in the non-HCC group to include samples with increased DRs/LPCs. Due to the shortage of biopsy material from CLD patients with a known long-term course of the disease, all stages of fibrosis were included in the

HCC group. This may cause a potential underestimation of differences in LPC expansion between non-HCC and HCC patients. However, despite this, the study was able to demonstrate a statistically significant association. Therefore, further analyses are planned using a more homogenous set of samples regarding underlying aetiology and fibrosis stage. In addition, a more detailed characterisation of the LPC population using markers associated with human LPCs such as AFP, CD133, CK19 and EpCAM (Spee *et al.* 2010; Porretti *et al.* 2010; Sancho-Bru *et al.* 2012; Villano *et al.* 2014), as well as assessing the proliferation status of LPC subpopulations may reveal a specific phenotype associated with HCC development.

Overall, the results further support the theory that LPCs play a role in human hepatocarcinogensis. Whether there is a direct causation in the form of a precursor-product relationship or a regulatory function of LPCs remains to be determined. However, considering published data and the results of this study, the LPC compartment represents a promising cellular target to therapeutically influence disease outcomes. Furthermore, co-localisation studies may help to identify cell populations with potential tumour-initiating characteristics showing a distinct expression profile in HCC rather than non-HCC patients. The $EpCAM^{+}/CD44^{+}$ and $panCK^{+}/CD44^{+}$ populations found in CDE- and TAA-induced carcinogenesis (see Chapter 5) may be candidate phenotypes that will also be investigated and correlated to disease outcome.

CHAPTER 7

General Discussion

Irrespective of clinical presentations and the underlying cause, most CLDs are accompanied by expanding ductular epithelial cell structures and proliferating LPC arrangements. Together with induced inflammatory, vascular, neural and ECM changes, these cellular components form the injury niche, termed the ductular reaction (Gouw *et al.* 2011; Williams *et al.* 2014). This compartment is activated in response to severe liver injury caused by viral, toxic or carcinogenic stimuli when residual hepatocytes may no longer meet the tissue demand due to cell cycle arrest and senescence. Upon activation LPCs proliferate and repopulate the liver mass by migrating towards the site of injury and differentiating into the major hepatic cell types, hepatocytes and cholangiocytes (Suzuki *et al.* 2008; Sackett *et al.* 2009; Forster *et al.* 2011; Shin *et al.* 2011; Liu *et al.* 2015). These processes are regulated by the local microenvironment, which includes cell-cell and cell-matrix interactions in close association with HSC activation and inflammation (Ruddell *et al.* 2009; Boulter *et al.* 2013; Dwyer *et al.* 2014; Grzelak *et al.* 2014; Tirnitz-Parker *et al.* 2014).

Orthotopic liver transplantation is still the most effective treatment for end-stage CLD and as donors are short in numbers, alternative treatment options are urgently needed. A great potential lies in cell therapy approaches and LPCs have been suggested as promising cellular sources due to their high regenerative potential (Dan and Yeoh 2008; Forster *et al.* 2011). Thus, further studies on LPC-mediated regeneration are required, including the study of appropriate animal models before results can be translated into human injury settings.

The aim of Chapter 3 was to thoroughly characterise and compare two common murine CLD models, based on CDE and TAA treatment, respectively. Evaluation of the injury induction (days 3 and 7), establishment (days 14 and 21) and maintenance phase (day 42) revealed that the injury response dynamics differed significantly between both regimens. In the CDE model, markers of overall liver damage including ALT levels, apoptosis, lipid accumulation and oxidative stress, as well as inflammation and fibrosis peaked during the induction phase before normalising during injury establishment and maintenance. However, in response to increased levels of known regulating factors associated with LPC activation in the induction phase, including TWEAK, TNF, LTβ, IL6, IFNγ and HGF (Matthews *et al.* 2004; Brooling *et al.* 2005; Knight *et al.* 2005c; Ruddell *et al.* 2009; Tirnitz-Parker *et al.*

2010; Ishikawa *et al.* 2012), numbers of LPCs (panCK$^+$ cells) were increasing until they reached a steady-state level in the establishment phase. On the other hand, the TAA model provoked a progressive (chronic) injury response with disease parameters persistently upregulated or gradually increasing throughout the time course of six weeks.

In addition to discrepancies in temporal kinetics, the data illustrated for the first time significant spatial differences between both regimens. The CDE diet induced a mainly periportal injury response, where inflammatory cells, HSCs and LPCs formed the regeneration niche in the induction phase. Since inflammatory cells and myofibroblasts are both known to facilitate LPC activation (Tirnitz-Parker *et al.* 2010; Elsegood *et al.* 2015) portal areas represented the anchoring point for crosstalk-mediated expansion of LPCs and HSCs into the surrounding parenchyma (Ruddell *et al.* 2009). In contrast, TAA-induced centrilobular damage provoked an injury cascade in central areas initiated by injured hepatocytes, inflammatory cells and potentially LSECs, which together may activate HSCs and the formation of the LPC-hosting regeneration niche during later stages of the injury establishment phase. The limited migration of LPCs initiated from portal areas and their accumulation and expansion from central areas may be mediated through relocation of the DR to the damage-burden area. Kaneko and colleagues showed a structural flexibility of the hepatobiliary system in response to tissue injury (Kaneko *et al.* 2015). They demonstrated a unidirectional expansion of biliary branches towards central areas in the TAA model versus CDE-induced branching around portal tracts. Further studies, involving ink injection assays, are planned to investigate this hypothesis. Injection of ink into the common bile duct visualises the potential relocation of functional biliary branches. Consistent with model-specific spatial distribution patterns highlighted in Chapter 3, collagen deposition was induced periportally in the CDE model versus pericentrally in the TAA model. A comparison to human pathologies revealed that the CDE-induced pattern is typically observed in fibrosis resulting from autoimmune or chronic viral hepatitis and chronic biliary diseases or cholestasis (Ferrell 2000), whereas TAA-induced fibrosis resembled the pattern illustrated in ALD or NAFLD (Ferrell 2000).

It is widely accepted that LPCs represent a transit amplifying cell population. To date, there is no LPC specific marker available and they share markers with other cell

types in the liver such as cholangiocytes and hepatocytes, as well as haematopoietic and mesenchymal cells (Petersen *et al.* 1998; Petersen *et al.* 1999; Petersen *et al.* 2003; Yovchev *et al.* 2008; Guest *et al.* 2014). Often a combination of different markers is used to identify distinct LPC populations. The aim of Chapter 4 was to characterise the expression profile of common LPC markers and identify different populations induced by CDE or TAA treatment.

Evaluation of the proliferation status revealed that CDE treatment induced biliary cell and LPC proliferation during the injury induction phase demonstrated by $A6^+/Ki67^+$ cells in portal areas. In contrast, the TAA model provoked increased proliferation of this cell population in central areas consistent with the well-established regeneration niche during the injury maintenance phase. This emphasised diverse LPC response dynamics and as illustrated in Chapter 3 confirmed a CDE-driven periportal induction and further expansion of LPCs into the parenchyma, whereas TAA induced a shift of the LPC compartment from initially portal (during the injury induction phase), to central areas during the maintenance phase.

In addition to differences in timing and location, co-localisation analyses of the common LPC markers A6, CD133, CK19, E-cadherin, EpCAM, MIC1-1C3 and panCK (Suzuki *et al.* 2008; Dorrell *et al.* 2011; Espanol-Suner *et al.* 2012; Schievenbusch *et al.* 2012) revealed distinct expression profiles of cell populations within the pool of LPCs in both regimens. While the CDE model mainly produced homogenous double-positive LPC phenotypes, TAA treatment provoked many single-positive populations such as $panCK^+/A6^-$, $panCK^+/CD133^-$, $panCK^+/MIC1\text{-}1C3^-$, $CK19^+/EpCAM^-$ and $CK19^+/E\text{-}cadherin^-$. Furthermore, CD44 identified a small subpopulation of $panCK^+$ LPCs in the TAA model, whereas CD90 was only demonstrated to be expressed in a limited number of CDE-induced LPCs.

Recently, it has been highly debated whether LPCs truly contribute to tissue repair during CLD. In addition to their hepatocytic differentiation potential *in vitro*, numerous studies have shown that LPCs are capable of replacing damaged hepatocytes in mice *in vivo*. This has been demonstrated following their isolation from CDE- or DDC-injured mouse livers or human livers, and subsequent transplantation into a chronic injury setting (Suzuki *et al.* 2008; Forster *et al.* 2011; Shin *et al.* 2011; Huch *et al.* 2015; Lu *et al.* 2015).

Lineage tracing experiments are valuable strategies to follow distinct LPC phenotypes in their endogenous environment throughout induced liver injury. Using this approach, several studies provided contradictory results regarding the function of LPCs during CLD (Sackett *et al.* 2009; Furuyama *et al.* 2011; Espanol-Suner *et al.* 2012; Tarlow *et al.* 2014a; Lu *et al.* 2015; Shin *et al.* 2015). However, caution has to be taken when interpreting the study outcomes. Chapter 3 illustrated that the temporal and spatial dynamics of disease parameters varied greatly between experimental models. Moreover Chapter 4 highlighted that the induced LPC population included model-specific subpopulations with distinct phenotypes. A study by Lu and colleagues demonstrated that distinct LPC subpopulations showed different characteristics *in vitro*. The assessment of colony formation revealed that the phenotype $EpCAM^{+}/CD24^{+}/CD133^{+}$ developed frequent colonies of packed epithelial cells, whereas the $EpCAM^{+}/CD24^{+}/CD133^{-}$ and $EpCAM^{+}/CD24^{-}/CD133^{-}$ populations generated infrequent small colonies with mesenchymal characteristics (Lu *et al.* 2015). Consequently, the above-mentioned discrepancies between studies focussing on LPC function may reflect the usage of different experimental models and/or markers utilised for labelling potential LPC progenies. Irrespective of the markers used for lineage tracing (Sox9, Foxl1 and OPN), LPCs did not generate new hepatocytes in the DDC model. However, their differentiation into cholangiocytes was reported (Espanol-Suner *et al.* 2012; Tarlow *et al.* 2014a; Shin *et al.* 2015). In contrast, the CDE model generated hepatocytes that originated from OPN^{+} and $Foxl1^{+}$ LPCs (Espanol-Suner *et al.* 2012; Shin *et al.* 2015). It is important to mention that the pathology between both models differs significantly. The DDC model represents a cholestatic liver injury model (Liedtke *et al.* 2013), whereas the CDE model resembles injury dynamics seen in NAFLD, as shown in Chapter 3. Furthermore, studies using CCl_4 induction showed different outcomes, illustrated by (i) Espanol-Suner *et al.*, who generated LPC-derived hepatocytes labelled by OPN, versus (ii) Tarlow *et al.* who excluded the contribution of LPCs in tissue regeneration following Sox9 expression (Espanol-Suner *et al.* 2012; Tarlow *et al.* 2014a).

Further support for marker-specific study outcomes is provided by studies relying on CDE-induced CLD. Tracing of the LPC markers OPN and Foxl1, respectively, revealed that these LPC populations are required for hepatocyte development, whereas Sox9- and CK19-expressing cells were found to only rarely differentiate

into hepatocytic lineage (Espanol-Suner *et al.* 2012; Tarlow *et al.* 2014a; Lu *et al.* 2015; Shin *et al.* 2015). Other factors that may influence these diverse study outcomes include the genetic background and gender of mice, but also variations in the protocol of animal models between different laboratories. The study that claimed a minor contribution of CK19-expressing cells to the replacement of hepatocytes during CDE-induced liver regeneration was performed with female mice (personal communication) (Lu *et al.* 2015), whereas most studies utilise male mice (often not mentioned). It was demonstrated that male and female individuals may produce different consequences in response to liver damage (Durazzo *et al.* 2014). Furthermore, minor tracing of Sox9 into the hepatocytic lineage in response to CDE treatment may be provoked by a lower concentration of ethionine, the carcinogenic compound of the diet (Tarlow *et al.* 2014a). The authors used 0.1% ethionine compared to the traditional 0.15% used in studies that showed hepatocytic LPC differentiation.

Consequently, when using different markers and experimental models, it is not clear whether the same LPC population is targeted/being investigated and importantly, context-specific LPC responses may influence the study outcome. Overall this highlights the importance of a detailed characterisation of the underlying models, and the urgent need for standardised techniques in order to accurately compare results between laboratories using the same experimental models. The results presented in this thesis are an important stepping stone. Further experiments are planned to define CDE- and TAA-induced LPC subpopulations. A multicolour flow cytometry experiment has been designed based on simultaneous labelling of cells with the markers CK19, CD24, CD44, CD133, EpCAM, Fn14, Integrin α5β6, MIC1-1C3 and OPN. With this approach, LPCs will be isolated from CDE and TAA time courses and a "developmental tree" of LPC populations will be generated. Distinct subpopulations will then be isolated for a detailed characterisation and functional analyses.

Despite the availability of HBV vaccination and improved methods to treat HCV infections, the worldwide number of HCC-related deaths is steadily increasing (Altekruse *et al.* 2014; Wang *et al.* 2014). Therefore it is of high interest to study the gradual process of HCC development to be able to therapeutically prevent a transition at the pre-tumorigenic stage.

The CDE and TAA regime represent promising experimental models to study processes related to hepatocarcinogenesis (Becker 1983; Knight *et al.* 2008; Guest *et al.* 2014; Darweish *et al.* 2014; Boulter *et al.* 2015). However, it is fundamental to thoroughly characterise the injury-related parameters and apply the right conditions to specific research questions. Therefore, in addition to the induction, establishment and maintenance phase of the CDE and TAA model analysed in Chapters 3 and 4, the aim of Chapter 5 was to further characterise stages of CLD progression and tumour formation. Investigations on the level of hepatocyte damage, inflammation, LPC expansion and fibrosis revealed that both regimens provoked progressively increasing levels of all investigated disease parameters throughout the time course of seven months. However, substantial differences were observed in the magnitude and spatial arrangements of investigated parameters. In the CDE model, excessive hepatic fat loading and progressive hepatic injury, as well as the progressive inflammation, LPC response and fibrosis, and eventually HCC development without the appearance of cirrhosis resemble the conditions found in NAFLD and NASH patients (Ferrell 2000; Takahashi *et al.* 2014). Inflammation and fibrosis is induced at the site of tissue damage, which is located in periportal and intralobular areas. In contrast, in the TAA model, sustained hepatic injury, progressive inflammation, LPC response, fibrosis and eventually cirrhosis and HCC development reflect the pathological dynamics seen in viral hepatitis patients (Ferrell 2000). Moreover, the localisation of tissue damage and the following injury response remained in pericetral and central-to-central bridging areas. The conditions described in both regimens predisposed the liver to HCC development. Both CDE and TAA treatment induced frequent incidences of primary HCC formation, contradictory to studies in the literature that mainly reported TAA-induced CCs (Becker 1983; Al-Bader *et al.* 2000; Sekiya *et al.* 2012; Guest *et al.* 2014).

Besides their potential beneficial role during tissue regeneration, LPCs have been associated with the formation of liver cancer and have even been proposed to represent one candidate for the cell of origin (Davies *et al.* 2006; Knight *et al.* 2008; Shupe and Petersen 2011; He *et al.* 2013; Guest *et al.* 2014; Lee *et al.* 2010a). Therefore, further studies on their role during hepatocarcinogenesis are needed. Chapter 3 and 4 showed that LPC expansion occurred during phases of injury induction, establishment and maintenance in response to CDE and TAA treatment,

respectively. Moreover, in Chapter 5 it was demonstrated that the number of LPCs further increased during disease progression and carcinogenesis and incorporated several distinct subpopulations including panCK$^+$/CK19$^-$, CK19$^+$/EpCAM$^-$, CK19$^-$/EpCAM$^+$ and panCK$^+$/CD133$^-$ cells. In particular the CDE model suggested a positive correlation between the degree of LPC expansion and HCC development. These data emphasise that LPCs play a role during CDE- and TAA-induced carcinogenesis and will be strengthend through analysis of additional animals from this time course. In addition, several HCCs induced in both regimens included numerous cells with a LPC phenotype within their tumour mass. The identification of potentially pre-cancerous LPC subpopulations that may initiate tumorigenesis supports the hypothesis of a precursor-product relationship. These subpopulations included CD44$^+$/EpCAM$^+$ and CD44$^+$/panCK$^+$ cells with CD44 and EpCAM representing CSC markers (Yamashita *et al.* 2008; Yang *et al.* 2008b; Zhu *et al.* 2010; Yamashita *et al.* 2009; Kimura *et al.* 2010). The characteristics and the tumour-initiating potential of isolated CD44$^+$ LPCs will be further investigated using FACS and subsequent analyses including functional assays (soft agar assay and xenograft transplantation) and the evaluation of an HCC- and CSC-associated gene expression profile.

Previous studies including lineage tracing, immunohistochemistry and gene expression profiling produced contradictory results regarding a potential tumour-initiating potential of LPCs (Sekiya *et al.* 2012; Guest *et al.* 2014; Mu *et al.* 2015; Kowalik *et al.* 2015; Shin *et al.* 2016). A study by Sekiya and colleagues proposed that CC development in TAA-treated mice originates from hepatocytes (Sekiya *et al.* 2012), whereas Guest *et al.*, using the same model, claimed cholangiocytes/LPCs as cellular origin (Guest *et al.* 2014). Recently Mu and colleagues investigated the cell of origin during HCC development using mice with OPN-traced cholangiocytes/LPCs and the injury models DEN, DEN+CCL_4, DEN+CDE, DEN+DDC, and CDE alone. The authors came to the conclusion that HCC originates from hepatocytes and not from the biliary/LPC compartment (Mu *et al.* 2015). However, it should be mentioned that the animals in this study illustrated a weaker LPC response when exposed to the CDE diet than demonstrated in this thesis. Moreover, only 30% of mice developed HCC after one year of treatment or longer, whereas this thesis showed that 45% of mice had developed intermediate and

advanced stages of HCC already after seven months of treatment, possibly reflecting different degrees of induced hepatocyte damage in the two studies. Overall these findings demonstrate that even with the use of the same carcinogenesis-inducing agent (here TAA and CDE), different results can be generated, highlighting once more the importance of standardised protocols between laboratories.

A summary of the injury dynamics observed in the murine CLD models investigated in this thesis, CDE versus TAA, is given in Fig. 7.1. The CDE model provoked a two-phasic injury pattern since the six-week time course induced a rapid increase of disease parameters during the injury induction phase and a normalisation thereafter; whereas, long-term treatment caused a progressive increase. The only outstanding parameter was the LPC compartment, which was activated during the injury induction and co-regulated with the inflammatory and fibrogenic responses. However, in contrast to normalisation of inflammation and fibrosis, LPC numbers further increased in a progressive fashion through to carcinogenesis. On the other hand, the TAA model induced a rather continuously progressive injury response of all investigated parameters throughout the time course.

Since Chapter 5 proposed a correlation between the LPC response and HCC development in mice, the aim of Chapter 6 was to investigate the degree or appearance of the DR and LPC response in CLD patients and to assess a potential link to HCC. Several studies have demonstrated an association between LPC activation and proliferation, and an increased risk of developing HCC (Davies *et al.* 2006; Knight *et al.* 2008; Lee *et al.* 2010a). This hypothesis is supported through data generated by characterising the $CK7^{+}$ DR/LPC response. In particular, a significant positive correlation between the magnitude and distribution of the LPC response and HCC development was demonstrated. Further experiments are planned, which define the characteristics of the illustrated LPC response by analysing expression profiles of markers that have been associated with human LPCs such as AFP, CD133, CK19 and EpCAM (Porretti *et al.* 2010; Spee *et al.* 2010; Sancho-Bru *et al.* 2012; Villano *et al.* 2014). In addition, their proliferation status will be investigated and co-localisation studies with CSC markers might identify potential tumour-initiating phenotypes.

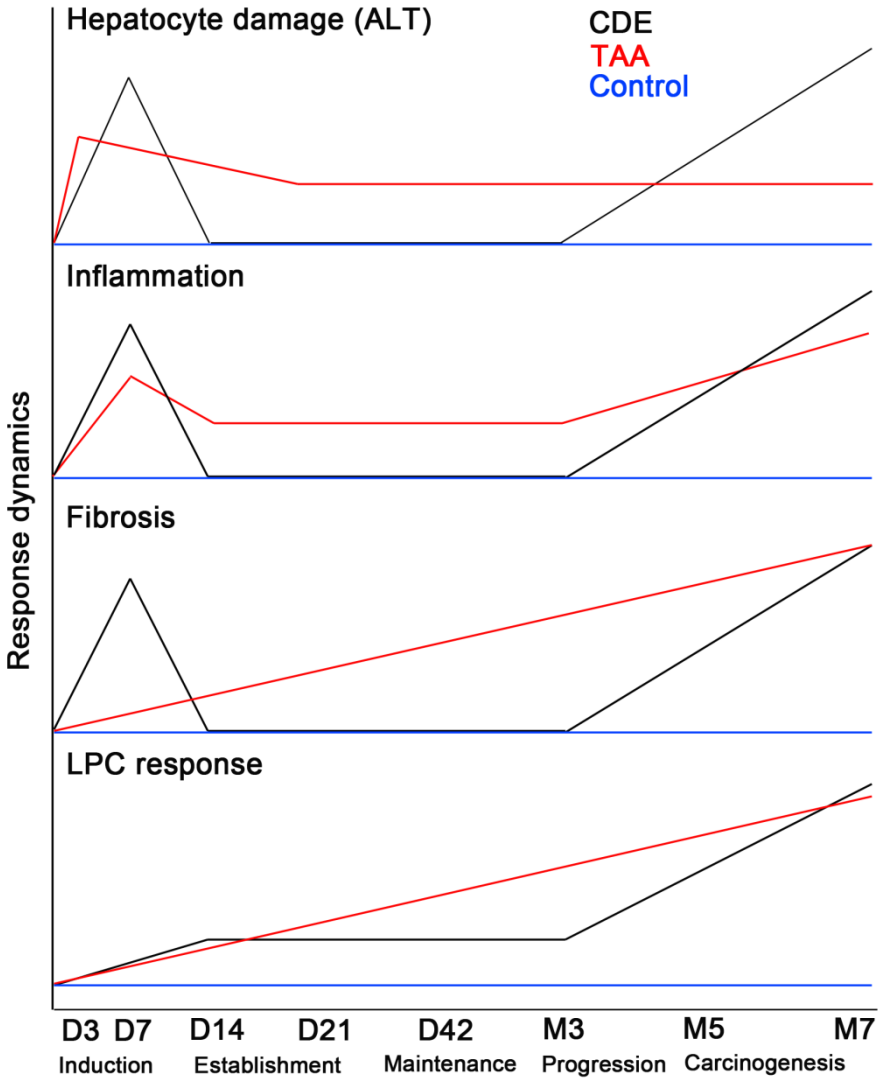

Fig. 7.1: Injury response dynamics in the CDE and TAA model. *D*, day; *M*, month.

In conclusion, this thesis aimed to characterise two common murine CLD models, CDE versus TAA, and to describe the microenvironment and phenotypes of the associated LPC responses during the stages of injury induction, establishment, maintenance, progression and carcinogenesis. Furthermore, the relationship between LPCs and HCC development in humans was investigated. Firstly, it was shown that the dynamics and patterns of disease parameters greatly rely on the stimulus and do not fully represent a particular pathological condition in humans. This thesis highlights the importance of choosing the appropriate experimental conditions including the most suitable model and time point to address specific research questions. Secondly, this thesis introduced the TAA regimen as suitable model for the study of LPC biology during CLD and HCC formation. Thirdly, HCC development in both regimens was associated with the degree of the LPC response, which further suggests their active contribution to the formation of HCC. Whether there is a direct precursor-product relationship or this is mediated through regulation of functions by providing a pro-tumorigenic environment remains to be clarified. Lastly, the magnitude and distribution of the DR/LPC response was positively correlated to HCC formation in CLD patients. This finding may be relevant for clinical applications, since a qualitative assessment of the DR/LPC response will potentially identify patients at greater risk of development of HCC on the background of CLD. Overall this thesis further supports the hypothesis that LPCs represent a promising cellular target to therapeutically influence disease outcomes. Further investigation is required to potentially identify distinct phenotypes that may play different roles in regeneration versus carcinogenesis. With this knowledge therapeutic approaches can be developed that may support LPC-mediated regeneration, while inhibiting cancer development through inactivation of the appropriate phenotypes.

REFERENCES

Aharoni-Simon M., Hann-Obercyger M., Pen S., Madar Z., and Tirosh O. (2011). Fatty Liver Is Associated with Impaired Activity of Ppargamma-Coactivator 1alpha (Pgc1alpha) and Mitochondrial Biogenesis in Mice. *Laboratory Investigation*, **91**: 1018-1028.

Akerman P., Cote P., Yang S.Q., McClain C., Nelson S., Bagby G.J., and Diehl A.M. (1992). Antibodies to Tumor Necrosis Factor-Alpha Inhibit Liver Regeneration after Partial Hepatectomy. *Am J Physiol*, **263**: G579-585.

Akhurst B., Croager E.J., Farley-Roche C.A., Ong J.K., Dumble M.L., Knight B., and Yeoh G.C. (2001). A Modified Choline-Deficient, Ethionine-Supplemented Diet Protocol Effectively Induces Oval Cells in Mouse Liver. *Hepatology*, **34**: 519-522.

Akhurst B., Matthews V., Husk K., Smyth M.J., Abraham L.J., and Yeoh G.C. (2005). Differential Lymphotoxin-Beta and Interferon Gamma Signaling During Mouse Liver Regeneration Induced by Chronic and Acute Injury. *Hepatology*, **41**: 327-335.

Akyol G., Erdem O., and Yilmaz G. (2005). Nonalcoholic Fatty Liver Disease. Correlation with Histology and Viral Hepatitis. *Saudi Med J*, **26**: 1904-1910.

Al-Bader A., Mathew T.C., Abul H., Al-Sayer H., Singal P.K., and Dashti H.M. (2000). Cholangiocarcinoma and Liver Cirrhosis in Relation to Changes Due to Thioacetamide. *Mol Cell Biochem*, **208**: 1-10.

Alexander J., Torbenson M., Wu T.T., and Yeh M.M. (2013). Non-Alcoholic Fatty Liver Disease Contributes to Hepatocarcinogenesis in Non-Cirrhotic Liver: A Clinical and Pathological Study. *J Gastroenterol Hepatol*, **28**: 848-854.

Alison M., Golding M., Lalani E.N., Nagy P., Thorgeirsson S., and Sarraf C. (1997). Wholesale Hepatocytic Differentiation in the Rat from Ductular Oval Cells, the Progeny of Biliary Stem Cells. *J Hepatol*, **26**: 343-352.

Alpini G., Lenzi R., Sarkozi L., and Tavoloni N. (1988). Biliary Physiology in Rats with Bile Ductular Cell Hyperplasia. Evidence for a Secretory Function of Proliferated Bile Ductules. *J Clin Invest*, **81**: 569-578.

Altekruse S.F., Henley S.J., Cucinelli J.E., and McGlynn K.A. (2014). Changing Hepatocellular Carcinoma Incidence and Liver Cancer Mortality Rates in the United States. *Am J Gastroenterol*, **109**: 542-553.

Amarapurkar A.D., Amarapurkar D.N., Vibhav S., and Patel N.D. (2007). Angiogenesis in Chronic Liver Disease. *Ann Hepatol*, **6**: 170-173.

Andrisani O.M., Studach L., and Merle P. (2011). Gene Signatures in Hepatocellular Carcinoma (Hcc). *Semin Cancer Biol*, **21**: 4-9.

Apte U., Thompson M.D., Cui S.S., Liu B., Cieply B., and Monga S.P.S. (2008). Wnt/Beta-Catenin Signaling Mediates Oval Cell Response in Rodents. *Hepatology*, **47**: 288-295.

Arber N., Zajicek G., and Ariel I. (1988). The Streaming Liver. Ii. Hepatocyte Life History. *Liver*, **8**: 80-87.

Aydin A.F., Kusku-Kiraz Z., Dogru-Abbasoglu S., Gulluoglu M., Uysal M., and Kocak-Toker N. (2010). Effect of Carnosine against Thioacetamide-Induced Liver Cirrhosis in Rat. *Peptides*, **31**: 67-71.

Baffy G., Brunt E.M., and Caldwell S.H. (2012). Hepatocellular Carcinoma in Non-Alcoholic Fatty Liver Disease: An Emerging Menace. *J Hepatol*, **56**: 1384-1391.

Bakiri L., and Wagner E.F. (2013). Mouse Models for Liver Cancer. *Mol Oncol*, **7**: 206-223.

Bataller R., and Brenner D.A. (2005). Liver Fibrosis. *J Clin Invest*, **115**: 209-218.

Bateman A.C., and Hubscher S.G. (2010). Cytokeratin Expression as an Aid to Diagnosis in Medical Liver Biopsies. *Histopathology*, **56**: 415-425.

Baum C.M., Weissman I.L., Tsukamoto A.S., Buckle A.M., and Peault B. (1992). Isolation of a Candidate Human Hematopoietic Stem-Cell Population. *Proc Natl Acad Sci U S A*, **89**: 2804-2808.

Baumann U., Crosby H.A., Ramani P., Kelly D.A., and Strain A.J. (1999). Expression of the Stem Cell Factor Receptor C-Kit in Normal and Diseased Pediatric Liver: Identification of a Human Hepatic Progenitor Cell? *Hepatology*, **30**: 112-117.

Becker F.F. (1983). Thioacetamide Hepatocarcinogenesis. *J Natl Cancer Inst*, **71**: 553-558.

Berasain C., Castillo J., Perugorria M.J., Latasa M.U., Prieto J., and Avila M.A. (2009). Inflammation and Liver Cancer: New Molecular Links. *Ann N Y Acad Sci*, **1155**: 206-221.

Bird T.G., Lorenzini S., and Forbes S.J. (2008). Activation of Stem Cells in Hepatic Diseases. *Cell Tissue Res*, **331**: 283-300.

Biswas M., and Chan J.Y. (2010). Role of Nrf1 in Antioxidant Response Element-Mediated Gene Expression and Beyond. *Toxicol Appl Pharmacol*, **244**: 16-20.

Blouin A., Bolender R.P., and Weibel E.R. (1977). Distribution of Organelles and Membranes between Hepatocytes and Nonhepatocytes in the Rat Liver Parenchyma. A Stereological Study. *J Cell Biol*, **72**: 441-455.

Bode H.P., Wang L., Cassio D., Leite M.F., St-Pierre M.V., Hirata K., Okazaki K., Sears M.L., Meda P., Nathanson M.H., and Dufour J.F. (2002). Expression and Regulation of Gap Junctions in Rat Cholangiocytes. *Hepatology*, **36**: 631-640.

Boniver J., and Herfs M.M. (2011). [Cancer Stem Cells]. *Bull Mem Acad R Med Belg*, **166**: 141-145; discussion 146.

Bonnet D., and Dick J.E. (1997). Human Acute Myeloid Leukemia Is Organized as a Hierarchy That Originates from a Primitive Hematopoietic Cell. *Nat Med*, **3**: 730-737.

Boulter L., Guest R.V., Kendall T.J., Wilson D.H., Wojtacha D., Robson A.J., Ridgway R.A., Samuel K., Van Rooijen N., Barry S.T., Wigmore S.J., Sansom O.J., and Forbes S.J. (2015). Wnt Signaling Drives Cholangiocarcinoma Growth and Can Be Pharmacologically Inhibited. *J Clin Invest*, **125**: 1269-1285.

Boulter L., Lu W.Y., and Forbes S.J. (2013). Differentiation of Progenitors in the Liver: A Matter of Local Choice. *J Clin Invest*, **123**: 1867-1873.

Bouwens L., Baekeland M., De Zanger R., and Wisse E. (1986). Quantitation, Tissue Distribution and Proliferation Kinetics of Kupffer Cells in Normal Rat Liver. *Hepatology*, **6**: 718-722.

Bralet M.P., Branchereau S., Brechot C., and Ferry N. (1994). Cell Lineage Study in the Liver Using Retroviral Mediated Gene Transfer. Evidence against the Streaming of Hepatocytes in Normal Liver. *Am J Pathol*, **144**: 896-905.

Bralet M.P., Calise D., Brechot C., and Ferry N. (1996). In Vivo Cell Lineage Analysis During Chemical Hepatocarcinogenesis Using Retroviral-Mediated Gene Transfer. *Lab Invest*, **74**: 871-881.

Brooling J.T., Campbell J.S., Mitchell C., Yeoh G.C., and Fausto N. (2005). Differential Regulation of Rodent Hepatocyte and Oval Cell Proliferation by Interferon Gamma. *Hepatology*, **41**: 906-915.

Brown K.E., Brunt E.M., and Heinecke J.W. (2001). Immunohistochemical Detection of Myeloperoxidase and Its Oxidation Products in Kupffer Cells of Human Liver. *Am J Pathol*, **159**: 2081-2088.

Brunt E.M. (2012). Histopathologic features of hepatocellular carcinoma. *Clinical Liver Disease*, **1**: 194–199.

Budhu A., and Wang X.W. (2006). The Role of Cytokines in Hepatocellular Carcinoma. *J Leukoc Biol*, **80**: 1197-1213.

Butler S.L., Dong H., Cardona D., Jia M., Zheng R., Zhu H., Crawford J.M., and Liu C. (2008). The Antigen for Hep Par 1 Antibody Is the Urea Cycle Enzyme Carbamoyl Phosphate Synthetase 1. *Laboratory Investigation*, **88**: 78-88.

Cai X., Zhai J., Kaplan D.E., Zhang Y., Zhou L., Chen X., Qian G., Zhao Q., Li Y., Gao L., Cong W., Zhu M., Yan Z., Shi L., Wu D., Wei L., Shen F., and Wu M. (2012). Background Progenitor Activation Is Associated with Recurrence after

Hepatectomy of Combined Hepatocellular-Cholangiocarcinoma. *Hepatology*, **56**: 1804-1816.

Campbell J.S., Prichard L., Schaper F., Schmitz J., Stephenson-Famy A., Rosenfeld M.E., Argast G.M., Heinrich P.C., and Fausto N. (2001). Expression of Suppressors of Cytokine Signaling During Liver Regeneration. *J Clin Invest*, **107**: 1285-1292.

Capece D., Fischietti M., Verzella D., Gaggiano A., Cicciarelli G., Tessitore A., Zazzeroni F., and Alesse E. (2013). The Inflammatory Microenvironment in Hepatocellular Carcinoma: A Pivotal Role for Tumor-Associated Macrophages. *Biomed Res Int*, **2013**: 187204.

Carpentier R., Suner R.E., van Hul N., Kopp J.L., Beaudry J.B., Cordi S., Antoniou A., Raynaud P., Lepreux S., Jacquemin P., Leclercq I.A., Sander M., and Lemaigre F.P. (2011). Embryonic Ductal Plate Cells Give Rise to Cholangiocytes, Periportal Hepatocytes, and Adult Liver Progenitor Cells. *Gastroenterology*, **141**: 1432-1438, 1438 e1431-1434.

Chen C.L., Yang H.I., Yang W.S., Liu C.J., Chen P.J., You S.L., Wang L.Y., Sun C.A., Lu S.N., Chen D.S., and Chen C.J. (2008). Metabolic Factors and Risk of Hepatocellular Carcinoma by Chronic Hepatitis B/C Infection: A Follow-up Study in Taiwan. *Gastroenterology*, **135**: 111-121.

Chen J., Li Y., Yu T.S., McKay R.M., Burns D.K., Kernie S.G., and Parada L.F. (2012). A Restricted Cell Population Propagates Glioblastoma Growth after Chemotherapy. *Nature*, **488**: 522-526.

Chiba T., Kamiya A., Yokosuka O., and Iwama A. (2009). Cancer Stem Cells in Hepatocellular Carcinoma: Recent Progress and Perspective. *Cancer Lett*, **286**: 145-153.

Chiba T., Kita K., Zheng Y.W., Yokosuka O., Saisho H., Iwama A., Nakauchi H., and Taniguchi H. (2006). Side Population Purified from Hepatocellular Carcinoma Cells Harbors Cancer Stem Cell-Like Properties. *Hepatology*, **44**: 240-251.

Clouston A.D., Powell E.E., Walsh M.J., Richardson M.M., Demetris A.J., and Jonsson J.R. (2005). Fibrosis Correlates with a Ductular Reaction in Hepatitis C: Roles of Impaired Replication, Progenitor Cells and Steatosis. *Hepatology*, **41**: 809-818.

Coulouarn C., Corlu A., Glaise D., Guenon I., Thorgeirsson S.S., and Clement B. (2012). Hepatocyte-Stellate Cell Cross-Talk in the Liver Engenders a Permissive Inflammatory Microenvironment That Drives Progression in Hepatocellular Carcinoma. *Cancer Res*, **72**: 2533-2542.

Couvelard A., Scoazec J.Y., and Feldmann G. (1993). Expression of Cell-Cell and Cell-Matrix Adhesion Proteins by Sinusoidal Endothelial Cells in the Normal and Cirrhotic Human Liver. *Am J Pathol*, **143**: 738-752.

Cressman D.E., Greenbaum L.E., DeAngelis R.A., Ciliberto G., Furth E.E., Poli V., and Taub R. (1996). Liver Failure and Defective Hepatocyte Regeneration in Interleukin-6-Deficient Mice. *Science*, **274**: 1379-1383.

Dabeva M.D., and Shafritz D.A. (1993). Activation, Proliferation, and Differentiation of Progenitor Cells into Hepatocytes in the D-Galactosamine Model of Liver Regeneration. *Am J Pathol*, **143**: 1606-1620.

Dan Y.Y., and Yeoh G.C. (2008). Liver Stem Cells: A Scientific and Clinical Perspective. *J Gastroenterol Hepatol*, **23**: 687-698.

Darweish M.M., Abbas A., Ebrahim M.A., and Al-Gayyar M.M. (2014). Chemopreventive and Hepatoprotective Effects of Epigallocatechin-Gallate against Hepatocellular Carcinoma: Role of Heparan Sulfate Proteoglycans Pathway. *J Pharm Pharmacol*, **66**: 1032-1045.

Davies R.A., Knight B., Tian Y.W., Yeoh G.C., and Olynyk J.K. (2006). Hepatic Oval Cell Response to the Choline-Deficient, Ethionine Supplemented Model of Murine Liver Injury Is Attenuated by the Administration of a Cyclo-Oxygenase 2 Inhibitor. *Carcinogenesis*, **27**: 1607-1616.

Di Carlo I., Fraggetta F., Lombardo R., Azzarello G., Vasquez E., and Puleo S. (2002). Cd 34 Expression in Chronic and Neoplastic Liver Diseases. *Panminerva Med*, **44**: 365-367.

Ding S.J., Li Y., Tan Y.X., Jiang M.R., Tian B., Liu Y.K., Shao X.X., Ye S.L., Wu J.R., Zeng R., Wang H.Y., Tang Z.Y., and Xia Q.C. (2004). From Proteomic Analysis to Clinical Significance: Overexpression of Cytokeratin 19 Correlates with Hepatocellular Carcinoma Metastasis. *Mol Cell Proteomics*, **3**: 73-81.

Do H., Healey J.F., Waller E.K., and Lollar P. (1999). Expression of Factor Viii by Murine Liver Sinusoidal Endothelial Cells. *Journal of Biological Chemistry*, **274**: 19587-19592.

Dohi T., and Burkly L.C. (2012). The Tweak/Fn14 Pathway as an Aggravating and Perpetuating Factor in Inflammatory Diseases: Focus on Inflammatory Bowel Diseases. *J Leukoc Biol*, **92**: 265-279.

Dooley S., and ten Dijke P. (2012). Tgf-Beta in Progression of Liver Disease. *Cell Tissue Res*, **347**: 245-256.

Dorrell C., Erker L., Lanxon-Cookson K.M., Abraham S.L., Victoroff T., Ro S., Canaday P.S., Streeter P.R., and Grompe M. (2008). Surface Markers for the Murine Oval Cell Response. *Hepatology*, **48**: 1282-1291.

Dorrell C., Erker L., Schug J., Kopp J.L., Canaday P.S., Fox A.J., Smirnova O., Duncan A.W., Finegold M.J., Sander M., Kaestner K.H., and Grompe M. (2011). Prospective Isolation of a Bipotential Clonogenic Liver Progenitor Cell in Adult Mice. *Genes Dev*, **25**: 1193-1203.

Driessens G., Beck B., Caauwe A., Simons B.D., and Blanpain C. (2012). Defining the Mode of Tumour Growth by Clonal Analysis. *Nature*, **488**: 527-530.

Dubois-Pot-Schneider H., Fekir K., Coulouarn C., Glaise D., Aninat C., Jarnouen K., Le Guevel R., Kubo T., Ishida S., Morel F., and Corlu A. (2014). Inflammatory Cytokines Promote the Retrodifferentiation of Tumor-Derived Hepatocyte-Like Cells to Progenitor Cells. *Hepatology*, **60**: 2077-2090.

Dumble M.L., Croager E.J., Yeoh G.C., and Quail E.A. (2002). Generation and Characterization of P53 Null Transformed Hepatic Progenitor Cells: Oval Cells Give Rise to Hepatocellular Carcinoma. *Carcinogenesis*, **23**: 435-445.

Durazzo M., Belci P., Collo A., Prandi V., Pistone E., Martorana M., Gambino R., and Bo S. (2014). Gender Specific Medicine in Liver Diseases: A Point of View. *World J Gastroenterol*, **20**: 2127-2135.

Durnez A., Verslype C., Nevens F., Fevery J., Aerts R., Pirenne J., Lesaffre E., Libbrecht L., Desmet V., and Roskams T. (2006). The Clinicopathological and Prognostic Relevance of Cytokeratin 7 and 19 Expression in Hepatocellular Carcinoma. A Possible Progenitor Cell Origin. *Histopathology*, **49**: 138-151.

Dwyer B.J., Olynyk J.K., Ramm G.A., and Tirnitz-Parker J.E. (2014). Tweak and Ltbeta Signaling During Chronic Liver Disease. *Front Immunol*, **5**: 39.

Elsegood C.L., Chan C.W., Degli-Esposti M.A., Wikstrom M.E., Domenichini A., Lazarus K., van Rooijen N., Ganss R., Olynyk J.K., and Yeoh G.C. (2015). Kupffer Cell-Monocyte Communication Is Essential for Initiating Murine Liver Progenitor Cell-Mediated Liver Regeneration. *Hepatology*, **62**: 1272-1284.

Endo Y., Zhang M., Yamaji S., and Cang Y. (2012). Genetic Abolishment of Hepatocyte Proliferation Activates Hepatic Stem Cells. *PLoS One*, **7**: e31846.

Espanol-Suner R., Carpentier R., Van Hul N., Legry V., Achouri Y., Cordi S., Jacquemin P., Lemaigre F., and Leclercq I.A. (2012). Liver Progenitor Cells Yield Functional Hepatocytes in Response to Chronic Liver Injury in Mice. *Gastroenterology*, **143**: 1564-+.

Evarts R.P., Nagy P., Marsden E., and Thorgeirsson S.S. (1987). In Situ Hybridization Studies on Expression of Albumin and Alpha-Fetoprotein During the Early Stage of Neoplastic Transformation in Rat Liver. *Cancer Res*, **47**: 5469-5475.

Fahimi H.D. (1970). The Fine Structural Localization of Endogenous and Exogenous Peroxidase Activity in Kupffer Cells of Rat Liver. *J Cell Biol*, **47**: 247-262.

Fan B., Malato Y., Calvisi D.F., Naqvi S., Razumilava N., Ribback S., Gores G.J., Dombrowski F., Evert M., Chen X., and Willenbring H. (2012). Cholangiocarcinomas Can Originate from Hepatocytes in Mice. *J Clin Invest*, **122**: 2911-2915.

Farber E. (1956). Similarities in the Sequence of Early Histological Changes Induced in the Liver of the Rat by Ethionine, 2-Acetylamino-Fluorene, and 3'-Methyl-4-Dimethylaminoazobenzene. *Cancer Res*, **16**: 142-148.

Farber J.L., and El-Mofty S.K. (1975). The Biochemical Pathology of Liver Cell Necrosis. *Am J Pathol*, **81**: 237-250.

Fausto N., Campbell J.S., and Riehle K.J. (2006). Liver Regeneration. *Hepatology*, **43**: S45-53.

Ferrell L. (2000). Liver Pathology: Cirrhosis, Hepatitis, and Primary Liver Tumors. Update and Diagnostic Problems. *Mod Pathol*, **13**: 679-704.

Fickert P., Stoger U., Fuchsbichler A., Moustafa T., Marschall H.U., Weiglein A.H., Tsybrovskyy O., Jaeschke H., Zatloukal K., Denk H., and Trauner M. (2007). A New Xenobiotic-Induced Mouse Model of Sclerosing Cholangitis and Biliary Fibrosis. *Am J Pathol*, **171**: 525-536.

Font-Burgada J., Shalapour S., Ramaswamy S., Hsueh B., Rossell D., Umemura A., Taniguchi K., Nakagawa H., Valasek M.A., Ye L., Kopp J.L., Sander M., Carter H., Deisseroth K., Verma I.M., and Karin M. (2015). Hybrid Periportal Hepatocytes Regenerate the Injured Liver without Giving Rise to Cancer. *Cell*, **162**: 766-779.

Forster N., Palmer J.A., Yeoh G., Ong W.C., Mitchell G.M., Slavin J., Tirnitz-Parker J., and Morrison W.A. (2011). Expansion and Hepatocytic Differentiation of Liver Progenitor Cells in Vivo Using a Vascularized Tissue Engineering Chamber in Mice. *Tissue Eng Part C Methods*, **17**: 359-366.

Francavilla A., Ove P., Polimeno L., Sciascia C., Coetzee M.L., and Starzl T.E. (1986). Epidermal Growth Factor and Proliferation in Rat Hepatocytes in Primary Culture Isolated at Different Times after Partial Hepatectomy. *Cancer Res*, **46**: 1318-1323.

Franchitto A., Onori P., Renzi A., Carpino G., Mancinelli R., Alvaro D., and Gaudio E. (2013). Recent Advances on the Mechanisms Regulating Cholangiocyte Proliferation and the Significance of the Neuroendocrine Regulation of Cholangiocyte Pathophysiology. *Ann Transl Med*, **1**: 27.

Friedman S.L. (2008a). Hepatic Stellate Cells: Protean, Multifunctional, and Enigmatic Cells of the Liver. *Physiol Rev*, **88**: 125-172.

Friedman S.L. (2008b). Mechanisms of Hepatic Fibrogenesis. *Gastroenterology*, **134**: 1655-1669.

Fujio K., Evarts R.P., Hu Z., Marsden E.R., and Thorgeirsson S.S. (1994). Expression of Stem Cell Factor and Its Receptor, C-Kit, During Liver Regeneration from Putative Stem Cells in Adult Rat. *Laboratory Investigation*, **70**: 511-516.

Fujio K., Hu Z., Evarts R.P., Marsden E.R., Niu C.H., and Thorgeirsson S.S. (1996). Coexpression of Stem Cell Factor and C-Kit in Embryonic and Adult Liver. *Exp Cell Res*, **224**: 243-250.

Furuyama K., Kawaguchi Y., Akiyama H., Horiguchi M., Kodama S., Kuhara T., Hosokawa S., Elbahrawy A., Soeda T., Koizumi M., Masui T., Kawaguchi M., Takaori K., Doi R., Nishi E., Kakinoki R., Deng J.M., Behringer R.R., Nakamura T., and Uemoto S. (2011). Continuous Cell Supply from a Sox9-Expressing Progenitor Zone in Adult Liver, Exocrine Pancreas and Intestine. *Nat Genet*, **43**: 34-41.

Gandillet A., Alexandre E., Holl V., Royer C., Bischoff P., Cinqualbre J., Wolf P., Jaeck D., and Richert L. (2003). Hepatocyte Ploidy in Normal Young Rat. *Comp Biochem Physiol A Mol Integr Physiol*, **134**: 665-673.

Gao J.H., Wen S.L., Yang W.J., Lu Y.Y., Tong H., Huang Z.Y., Liu Z.X., and Tang C.W. (2013). Celecoxib Ameliorates Portal Hypertension of the Cirrhotic Rats through the Dual Inhibitory Effects on the Intrahepatic Fibrosis and Angiogenesis. *PLoS One*, **8**: e69309.

Gebhardt R. (1988). Different Proliferative Activity in Vitro of Periportal and Perivenous Hepatocytes. *Scand J Gastroenterol Suppl*, **151**: 8-18.

Gebhardt R. (1992). Metabolic Zonation of the Liver: Regulation and Implications for Liver Function. *Pharmacol Ther*, **53**: 275-354.

Golding M., Sarraf C.E., Lalani E.N., Anilkumar T.V., Edwards R.J., Nagy P., Thorgeirsson S.S., and Alison M.R. (1995). Oval Cell Differentiation into Hepatocytes in the Acetylaminofluorene-Treated Regenerating Rat Liver. *Hepatology*, **22**: 1243-1253.

Gomaa A.I., Khan S.A., Toledano M.B., Waked I., and Taylor-Robinson S.D. (2008). Hepatocellular Carcinoma: Epidemiology, Risk Factors and Pathogenesis. *World J Gastroenterol*, **14**: 4300-4308.

Gouw A.S., Clouston A.D., and Theise N.D. (2011). Ductular Reactions in Human Liver: Diversity at the Interface. *Hepatology*, **54**: 1853-1863.

Govaere O., Komuta M., Berkers J., Spee B., Janssen C., de Luca F., Katoonizadeh A., Wouters J., van Kempen L.C., Durnez A., Verslype C., De Kock J., Rogiers V., van Grunsven L.A., Topal B., Pirenne J., Vankelecom H., Nevens F., van den Oord J., Pinzani M., and Roskams T. (2014). Keratin 19: A Key Role Player in the Invasion of Human Hepatocellular Carcinomas. *Gut*, **63**: 674-685.

Greene A.K., and Puder M. (2003). Partial Hepatectomy in the Mouse: Technique and Perioperative Management. *J Invest Surg*, **16**: 99-102.

Grisham J.W., Nopanitaya W., Compagno J., and Nagel A.E. (1975). Scanning Electron Microscopy of Normal Rat Liver: The Surface Structure of Its Cells and Tissue Components. *Am J Anat*, **144**: 295-321.

Grzelak C.A., Martelotto L.G., Sigglekow N.D., Patkunanathan B., Ajami K., Calabro S.R., Dwyer B.J., Tirnitz-Parker J.E., Watkins D.N., Warner F.J., Shackel N.A., and McCaughan G.W. (2014). The Intrahepatic Signalling Niche of Hedgehog Is Defined by Primary Cilia Positive Cells During Chronic Liver Injury. *J Hepatol*, **60**: 143-151.

Guest R.V., Boulter L., Kendall T.J., Minnis-Lyons S.E., Walker R., Wigmore S.J., Sansom O.J., and Forbes S.J. (2014). Cell Lineage Tracing Reveals a Biliary Origin of Intrahepatic Cholangiocarcinoma. *Cancer Res*, **74**: 1005-1010.

Hahn W.C., Counter C.M., Lundberg A.S., Beijersbergen R.L., Brooks M.W., and Weinberg R.A. (1999). Creation of Human Tumour Cells with Defined Genetic Elements. *Nature*, **400**: 464-468.

Hahn W.C., and Weinberg R.A. (2002). Rules for Making Human Tumor Cells. *N Engl J Med*, **347**: 1593-1603.

Hanada S., Strnad P., Brunt E.M., and Omary M.B. (2008). The Genetic Background Modulates Susceptibility to Mouse Liver Mallory-Denk Body Formation and Liver Injury. *Hepatology*, **48**: 943-952.

Haraguchi N., Ishii H., Mimori K., Tanaka F., Ohkuma M., Kim H.M., Akita H., Takiuchi D., Hatano H., Nagano H., Barnard G.F., Doki Y., and Mori M. (2010). Cd13 Is a Therapeutic Target in Human Liver Cancer Stem Cells. *J Clin Invest*, **120**: 3326-3339.

Haraguchi N., Utsunomiya T., Inoue H., Tanaka F., Mimori K., Barnard G.F., and Mori M. (2006). Characterization of a Side Population of Cancer Cells from Human Gastrointestinal System. *Stem Cells*, **24**: 506-513.

Hardwick R.N., Fisher C.D., Canet M.J., Lake A.D., and Cherrington N.J. (2010). Diversity in Antioxidant Response Enzymes in Progressive Stages of Human Nonalcoholic Fatty Liver Disease. *Drug Metab Dispos*, **38**: 2293-2301.

Haybaeck J., Zeller N., Wolf M.J., Weber A., Wagner U., Kurrer M.O., Bremer J., Iezzi G., Graf R., Clavien P.A., Thimme R., Blum H., Nedospasov S.A., Zatloukal K., Ramzan M., Ciesek S., Pietschmann T., Marche P.N., Karin M., Kopf M., Browning J.L., Aguzzi A., and Heikenwalder M. (2009). A Lymphotoxin-Driven Pathway to Hepatocellular Carcinoma. *Cancer Cell*, **16**: 295-308.

He G., Dhar D., Nakagawa H., Font-Burgada J., Ogata H., Jiang Y., Shalapour S., Seki E., Yost S.E., Jepsen K., Frazer K.A., Harismendy O., Hatziapostolou M., Iliopoulos D., Suetsugu A., Hoffman R.M., Tateishi R., Koike K., and Karin M. (2013). Identification of Liver Cancer Progenitors Whose Malignant Progression Depends on Autocrine Il-6 Signaling. *Cell*, **155**: 384-396.

Higgins G.M. and Anderson R.M. (1931). Experimental pathology of the liver. I. Restoration of the liver following partial surgical removal. *Archives of Pathology*, **272**: 186-202.

Hixson D.C., and Allison J.P. (1985). Monoclonal Antibodies Recognizing Oval Cells Induced in the Liver of Rats by N-2-Fluorenylacetamide or Ethionine in a Choline-Deficient Diet. *Cancer Res*, **45**: 3750-3760.

Hixson D.C., Brown J., McBride A.C., and Affigne S. (2000). Differentiation Status of Rat Ductal Cells and Ethionine-Induced Hepatic Carcinomas Defined with Surface-Reactive Monoclonal Antibodies. *Exp Mol Pathol*, **68**: 152-169.

Ho D.W., Yang Z.F., Yi K., Lam C.T., Ng M.N., Yu W.C., Lau J., Wan T., Wang X., Yan Z., Liu H., Zhang Y., and Fan S.T. (2012). Gene Expression Profiling of Liver Cancer Stem Cells by Rna-Sequencing. *PLoS One*, **7**: e37159.

Holic N., Suzuki T., Corlu A., Couchie D., Chobert M.N., Guguen-Guillouzo C., and Laperche Y. (2000). Differential Expression of the Rat Γ-Glutamyl Transpeptidase Gene Promoters Along with Differentiation of Hepatoblasts into Biliary or Hepatocytic Lineage. *Am J Pathol*, **157**: 537-548.

Hoshida Y. (2012). Molecular Epidemiology of Hepatocellular Carcinoma. *Clin Liver Dis (Hoboken)*, **1**: 177-179.

Hu Z., Evarts R.P., Fujio K., Marsden E.R., and Thorgeirsson S.S. (1993). Expression of Hepatocyte Growth Factor and C-Met Genes During Hepatic Differentiation and Liver Development in the Rat. *Am J Pathol*, **142**: 1823-1830.

Huch M., Dorrell C., Boj S.F., van Es J.H., Li V.S., van de Wetering M., Sato T., Hamer K., Sasaki N., Finegold M.J., Haft A., Vries R.G., Grompe M., and Clevers H. (2013). In Vitro Expansion of Single Lgr5+ Liver Stem Cells Induced by Wnt-Driven Regeneration. *Nature*, **494**: 247-250.

Huch M., Gehart H., van Boxtel R., Hamer K., Blokzijl F., Verstegen M.M., Ellis E., van Wenum M., Fuchs S.A., de Ligt J., van de Wetering M., Sasaki N., Boers S.J., Kemperman H., de Jonge J., Ijzermans J.N., Nieuwenhuis E.E., Hoekstra R., Strom S., Vries R.R., van der Laan L.J., Cuppen E., and Clevers H. (2015). Long-Term Culture of Genome-Stable Bipotent Stem Cells from Adult Human Liver. *Cell*, **160**: 299-312.

Hunter A.L., Holscher M.A., and Neal R.A. (1977). Thioacetamide-Induced Hepatic Necrosis. I. Involvement of the Mixed-Function Oxidase Enzyme System. *J Pharmacol Exp Ther*, **200**: 439-448.

Inoue H., Yokoyama F., Kita Y., Yoshiji H., Tsujimoto T., Deguchi A., Nakai S., Morishita A., Uchida N., Masaki T., Watanabe S., and Kuriyama S. (2006). Relationship between the Proliferative Capability of Hepatocytes and the Intrahepatic Expression of Hepatocyte Growth Factor and C-Met in the Course of Cirrhosis Development in Rats. *Int J Mol Med*, **17**: 857-864.

Irving M.G., Roll F.J., Huang S., and Bissell D.M. (1984). Characterization and Culture of Sinusoidal Endothelium from Normal Rat Liver: Lipoprotein Uptake and Collagen Phenotype. *Gastroenterology*, **87**: 1233-1247.

Ishikawa T., Factor V.M., Marquardt J.U., Raggi C., Seo D., Kitade M., Conner E.A., and Thorgeirsson S.S. (2012). Hepatocyte Growth Factor/C-Met Signaling Is Required for Stem-Cell-Mediated Liver Regeneration in Mice. *Hepatology*, **55**: 1215-1226.

Iverson S.V., Comstock K.M., Kundert J.A., and Schmidt E.E. (2011). Contributions of New Hepatocyte Lineages to Liver Growth, Maintenance, and Regeneration in Mice. *Hepatology*, **54**: 655-663.

Iwakiri Y., Shah V., and Rockey D.C. (2014). Vascular Pathobiology in Chronic Liver Disease and Cirrhosis - Current Status and Future Directions. *J Hepatol*, **61**: 912-924.

Jakubowski A., Ambrose C., Parr M., Lincecum J.M., Wang M.Z., Zheng T.S., Browning B., Michaelson J.S., Baetscher M., Wang B., Bissell D.M., and Burkly L.C. (2005). Tweak Induces Liver Progenitor Cell Proliferation. *J Clin Invest*, **115**: 2330-2340.

Jelnes P., Santoni-Rugiu E., Rasmussen M., Friis S.L., Nielsen J.H., Tygstrup N., and Bisgaard H.C. (2007). Remarkable Heterogeneity Displayed by Oval Cells in Rat and Mouse Models of Stem Cell-Mediated Liver Regeneration. *Hepatology*, **45**: 1462-1470.

Jemal A., Bray F., Center M.M., Ferlay J., Ward E., and Forman D. (2011). Global Cancer Statistics. *CA Cancer J Clin*, **61**: 69-90.

Jensen C.H., Jauho E.I., Santoni-Rugiu E., Holmskov U., Teisner B., Tygstrup N., and Bisgaard H.C. (2004). Transit-Amplifying Ductular (Oval) Cells and Their Hepatocytic Progeny Are Characterized by a Novel and Distinctive Expression of Delta-Like Protein/Preadipocyte Factor 1/Fetal Antigen 1. *Am J Pathol*, **164**: 1347-1359.

Jeong D.H., Jang J.J., Lee S.J., Lee J.H., Lim I.K., Lee M.J., and Lee Y.S. (2001). Expression Patterns of Cell Cycle-Related Proteins in a Rat Cirrhotic Model Induced by Ccl4 or Thioacetamide. *J Gastroenterol*, **36**: 24-32.

Jung Y., Brown K.D., Witek R.P., Omenetti A., Yang L., Vandongen M., Milton R.J., Hines I.N., Rippe R.A., Spahr L., Rubbia-Brandt L., and Diehl A.M. (2008). Accumulation of Hedgehog-Responsive Progenitors Parallels Alcoholic Liver Disease Severity in Mice and Humans. *Gastroenterology*, **134**: 1532-1543.

Jungermann K., and Kietzmann T. (1996). Zonation of Parenchymal and Nonparenchymal Metabolism in Liver. *Annu Rev Nutr*, **16**: 179-203.

Kakar S., Gown A.M., Goodman Z.D., and Ferrell L.D. (2007). Best Practices in Diagnostic Immunohistochemistry: Hepatocellular Carcinoma Versus Metastatic Neoplasms. *Arch Pathol Lab Med*, **131**: 1648-1654.

Kamiya A., Kakinuma S., Yamazaki Y., and Nakauchi H. (2009). Enrichment and Clonal Culture of Progenitor Cells During Mouse Postnatal Liver Development in Mice. *Gastroenterology*, **137**: 1114-1126, 1126 e1111-1114.

Kaneda K., Kurioka N., Seki S., Wake K., and Yamamoto S. (1984). Pit Cell-Hepatocyte Contact in Autoimmune Hepatitis. *Hepatology*, **4**: 955-958.

Kaneda K., and Wake K. (1983). Distribution and Morphological Characteristics of the Pit Cells in the Liver of the Rat. *Cell Tissue Res*, **233**: 485-505.

Kaneko K., Kamimoto K., Miyajima A., and Itoh T. (2015). Adaptive Remodeling of the Biliary Architecture Underlies Liver Homeostasis. *Hepatology*, **61**: 2056-2066.

Katoonizadeh A., Nevens F., Verslype C., Pirenne J., and Roskams T. (2006). Liver Regeneration in Acute Severe Liver Impairment: A Clinicopathological Correlation Study. *Liver Int*, **26**: 1225-1233.

Katoonizadeh A., and Poustchi H. (2014). Adult Hepatic Progenitor Cell Niche: How It Affects the Progenitor Cell Fate. *Middle East J Dig Dis*, **6**: 57-64.

Kennedy S., Rettinger S., Flye M.W., and Ponder K.P. (1995). Experiments in Transgenic Mice Show That Hepatocytes Are the Source for Postnatal Liver Growth and Do Not Stream. *Hepatology*, **22**: 160-168.

Kim J.W., Ye Q., Forgues M., Chen Y., Budhu A., Sime J., Hofseth L.J., Kaul R., and Wang X.W. (2004). Cancer-Associated Molecular Signature in the Tissue Samples of Patients with Cirrhosis. *Hepatology*, **39**: 518-527.

Kim T.H., Mars W.M., Stolz D.B., and Michalopoulos G.K. (2000). Expression and Activation of Pro-Mmp-2 and Pro-Mmp-9 During Rat Liver Regeneration. *Hepatology*, **31**: 75-82.

Kim Y.H., Kwak K.A., and Kang J.S. (2014). Expression of Neighbor of Punc E11 in Hepatocarcinogenesis Induced by Diethylnitrosamine. *Oncol Rep*, **32**: 1043-1049.

Kimura O., Takahashi T., Ishii N., Inoue Y., Ueno Y., Kogure T., Fukushima K., Shiina M., Yamagiwa Y., Kondo Y., Inoue J., Kakazu E., Iwasaki T., Kawagishi N., Shimosegawa T., and Sugamura K. (2010). Characterization of the Epithelial Cell Adhesion Molecule (Epcam)+ Cell Population in Hepatocellular Carcinoma Cell Lines. *Cancer Sci*, **101**: 2145-2155.

Kinosita R. (1937). Studies on the Cancerogenic Chemical Substances. *Transactions of the Japanese Society for Pathology*, **27**: 665-727.

Kiernan F. (1833). The Anatomy and Physiology of the Liver. In *Philosophical Transactions of the Royal Society of London*, **123**:711–770.

Kiso S., Kawata S., Tamura S., Inui Y., Yoshida Y., Sawai Y., Umeki S., Ito N., Yamada A., Miyagawa J., Higashiyama S., Iwawaki T., Saito M., Taniguchi N., Matsuzawa Y., and Kohno K. (2003). Liver Regeneration in Heparin-Binding Egf-Like Growth Factor Transgenic Mice after Partial Hepatectomy. *Gastroenterology*, **124**: 701-707.

Knight B., Akhurst B., Matthews V.B., Ruddell R.G., Ramm G.A., Abraham L.J., Olynyk J.K., and Yeoh G.C. (2007a). Attenuated Liver Progenitor (Oval) Cell and Fibrogenic Responses to the Choline Deficient, Ethionine Supplemented Diet in the Balb/C Inbred Strain of Mice. *J Hepatol*, **46**: 134-141.

Knight B., Lim R., Yeoh G.C., and Olynyk J.K. (2007b). Interferon-Gamma Exacerbates Liver Damage, the Hepatic Progenitor Cell Response and Fibrosis in a Mouse Model of Chronic Liver Injury. *J Hepatol*, **47**: 826-833.

Knight B., Matthews V.B., Akhurst B., Croager E.J., Klinken E., Abraham L.J., Olynyk J.K., and Yeoh G. (2005a). Liver Inflammation and Cytokine Production, but Not Acute Phase Protein Synthesis, Accompany the Adult Liver Progenitor (Oval) Cell Response to Chronic Liver Injury. *Immunol Cell Biol*, **83**: 364-374.

Knight B., Matthews V.B., Olynyk J.K., and Yeoh G.C. (2005b). Jekyll and Hyde: Evolving Perspectives on the Function and Potential of the Adult Liver Progenitor (Oval) Cell. *Bioessays*, **27**: 1192-1202.

Knight B., Tirnitz-Parker J.E., and Olynyk J.K. (2008). C-Kit Inhibition by Imatinib Mesylate Attenuates Progenitor Cell Expansion and Inhibits Liver Tumor Formation in Mice. *Gastroenterology*, **135**: 969-979, 979 e961.

Knight B., and Yeoh G.C. (2005c). Tnf/Ltalpha Double Knockout Mice Display Abnormal Inflammatory and Regenerative Responses to Acute and Chronic Liver Injury. *Cell Tissue Res*, **319**: 61-70.

Knight B., Yeoh G.C., Husk K.L., Ly T., Abraham L.J., Yu C., Rhim J.A., and Fausto N. (2000). Impaired Preneoplastic Changes and Liver Tumor Formation in Tumor Necrosis Factor Receptor Type 1 Knockout Mice. *J Exp Med*, **192**: 1809-1818.

Kofman A.V., Morgan G., Kirschenbaum A., Osbeck J., Hussain M., Swenson S., and Theise N.D. (2005). Dose- and Time-Dependent Oval Cell Reaction in Acetaminophen-Induced Murine Liver Injury. *Hepatology*, **41**: 1252-1261.

Kogure K., Ishizaki M., Nemoto M., Kuwano H., and Makuuchi M. (1999). A Comparative Study of the Anatomy of Rat and Human Livers. *J Hepatobiliary Pancreat Surg*, **6**: 171-175.

Kohga K., Tatsumi T., Takehara T., Tsunematsu H., Shimizu S., Yamamoto M., Sasakawa A., Miyagi T., and Hayashi N. (2010). Expression of Cd133 Confers Malignant Potential by Regulating Metalloproteinases in Human Hepatocellular Carcinoma. *J Hepatol*, **52**: 872-879.

Köhn-Gaone J., Dwyer B.J., Grzelak C.A., Miller G., Shackel N.A., Ramm G.A., McCaughan G.W., Elsegood C.L., Olynyk J.K., and Tirnitz-Parker J.E. (2016a). Divergent Inflammatory, Fibrogenic, and Liver Progenitor Cell Dynamics in Two Common Mouse Models of Chronic Liver Injury. *Am J Pathol*, **186**: 1762-1774.

Köhn-Gaone J., Gogoi-Tiwari J., Ramm G.A., Olynyk J.K., and Tirnitz-Parker J.E. (2016b). The Role of Liver Progenitor Cells During Liver Regeneration, Fibrogenesis, and Carcinogenesis. *Am J Physiol Gastrointest Liver Physiol*, **310**: G143-154.

Kollet O., Shivtiel S., Chen Y.Q., Suriawinata J., Thung S.N., Dabeva M.D., Kahn J., Spiegel A., Dar A., Samira S., Goichberg P., Kalinkovich A., Arenzana-Seisdedos F., Nagler A., Hardan I., Revel M., Shafritz D.A., and Lapidot T. (2003). Hgf, Sdf-1, and Mmp-9 Are Involved in Stress-Induced Human Cd34+ Stem Cell Recruitment to the Liver. *J Clin Invest*, **112**: 160-169.

Kon J., Ooe H., Oshima H., Kikkawa Y., and Mitaka T. (2006). Expression of Cd44 in Rat Hepatic Progenitor Cells. *J Hepatol*, **45**: 90-98.

Kordes C., Sawitza I., Gotze S., Herebian D., and Haussinger D. (2014). Hepatic Stellate Cells Contribute to Progenitor Cells and Liver Regeneration. *J Clin Invest*, **124**: 5503-5515.

Kornek M., Raskopf E., Guetgemann I., Ocker M., Gerceker S., Gonzalez-Carmona M.A., Rabe C., Sauerbruch T., and Schmitz V. (2006). Combination of Systemic Thioacetamide (Taa) Injections and Ethanol Feeding Accelerates Hepatic Fibrosis in C3h/He Mice and Is Associated with Intrahepatic up Regulation of Mmp-2, Vegf and Icam-1. *J Hepatol*, **45**: 370-376.

Kowalik M.A., Sulas P., Ledda-Columbano G.M., Giordano S., Columbano A., and Perra A. (2015). Cytokeratin-19 Positivity Is Acquired Along Cancer Progression

and Does Not Predict Cell Origin in Rat Hepatocarcinogenesis. *Oncotarget*, **6**: 38749-38763.

Kuramitsu K., Sverdlov D.Y., Liu S.B., Csizmadia E., Burkly L., Schuppan D., Hanto D.W., Otterbein L.E., and Popov Y. (2013). Failure of Fibrotic Liver Regeneration in Mice Is Linked to a Severe Fibrogenic Response Driven by Hepatic Progenitor Cell Activation. *Am J Pathol*, **183**: 182-194.

Kuwahara R., Kofman A.V., Landis C.S., Swenson E.S., Barendswaard E., and Theise N.D. (2008). The Hepatic Stem Cell Niche: Identification by Label-Retaining Cell Assay. *Hepatology*, **47**: 1994-2002.

Lalor P.F., Lai W.K., Curbishley S.M., Shetty S., and Adams D.H. (2006). Human Hepatic Sinusoidal Endothelial Cells Can Be Distinguished by Expression of Phenotypic Markers Related to Their Specialised Functions in Vivo. *World J Gastroenterol*, **12**: 5429-5439.

Lapidot T., Sirard C., Vormoor J., Murdoch B., Hoang T., Caceres-Cortes J., Minden M., Paterson B., Caligiuri M.A., and Dick J.E. (1994). A Cell Initiating Human Acute Myeloid Leukaemia after Transplantation into Scid Mice. *Nature*, **367**: 645-648.

Lara-Pezzi E., Serrador J.M., Montoya M.C., Zamora D., Yanez-Mo M., Carretero M., Furthmayr H., Sanchez-Madrid F., and Lopez-Cabrera M. (2001). The Hepatitis B Virus X Protein (Hbx) Induces a Migratory Phenotype in a Cd44-Dependent Manner: Possible Role of Hbx in Invasion and Metastasis. *Hepatology*, **33**: 1270-1281.

LaRusso N.F., Ishii M., and Vroman B.T. (1991). The Ins and Outs of Membrane Movement in Biliary Epithelia. *Trans Am Clin Climatol Assoc*, **102**: 245-258; discussion 258-249.

Lee C.M., Knight B., Yeoh G.C., Ramm G.A., and Olynyk J.K. (2005). Lymphotoxin-Beta Production Following Bile Duct Ligation: Possible Role for Kupffer Cells. *J Gastroenterol Hepatol*, **20**: 1762-1768.

Lee J.S., Heo J., Libbrecht L., Chu I.S., Kaposi-Novak P., Calvisi D.F., Mikaelyan A., Roberts L.R., Demetris A.J., Sun Z., Nevens F., Roskams T., and Thorgeirsson S.S. (2006). A Novel Prognostic Subtype of Human Hepatocellular Carcinoma Derived from Hepatic Progenitor Cells. *Nat Med*, **12**: 410-416.

Lee K.P., Lee J.H., Kim T.S., Kim T.H., Park H.D., Byun J.S., Kim M.C., Jeong W.I., Calvisi D.F., Kim J.M., and Lim D.S. (2010a). The Hippo-Salvador Pathway Restrains Hepatic Oval Cell Proliferation, Liver Size, and Liver Tumorigenesis. *Proc Natl Acad Sci U S A*, **107**: 8248-8253.

Lee N.P., Poon R.T., Shek F.H., Ng I.O., and Luk J.M. (2010b). Role of Cadherin-17 in Oncogenesis and Potential Therapeutic Implications in Hepatocellular Carcinoma. *Biochim Biophys Acta*, **1806**: 138-145.

Lee T.K., Castilho A., Cheung V.C., Tang K.H., Ma S., and Ng I.O. (2011). Cd24(+) Liver Tumor-Initiating Cells Drive Self-Renewal and Tumor Initiation through Stat3-Mediated Nanog Regulation. *Cell Stem Cell*, **9**: 50-63.

Lee T.K., Cheung V.C., Lu P., Lau E.Y., Ma S., Tang K.H., Tong M., Lo J., and Ng I.O. (2014a). Blockade of Cd47-Mediated Cathepsin S/Protease-Activated Receptor 2 Signaling Provides a Therapeutic Target for Hepatocellular Carcinoma. *Hepatology*, **60**: 179-191.

Lee T.Y., Chang H.H., Wen C.K., Huang T.H., and Chang Y.S. (2014b). Modulation of Thioacetamide-Induced Hepatic Inflammations, Angiogenesis and Fibrosis by Andrographolide in Mice. *J Ethnopharmacol*, **158 Pt A**: 423-430.

Leite A.R., Correa-Giannella M.L., Dagli M.L., Fortes M.A., Vegas V.M., and Giannella-Neto D. (2007). Fibronectin and Laminin Induce Expression of Islet Cell Markers in Hepatic Oval Cells in Culture. *Cell Tissue Res*, **327**: 529-537.

Lemire J.M., Shiojiri N., and Fausto N. (1991). Oval Cell Proliferation and the Origin of Small Hepatocytes in Liver Injury Induced by D-Galactosamine. *Am J Pathol*, **139**: 535-552.

Lenzi R., Liu M.H., Tarsetti F., Slott P.A., Alpini G., Zhai W.R., Paronetto F., Lenzen R., and Tavoloni N. (1992). Histogenesis of Bile Duct-Like Cells Proliferating During Ethionine Hepatocarcinogenesis - Evidence for a Biliary Epithelial Nature of Oval Cells .3. *Laboratory Investigation*, **66**: 390-402.

Li J., Xin J., Zhang L., Wu J., Jiang L., Zhou Q., Li J., Guo J., Cao H., and Li L. (2014). Human Hepatic Progenitor Cells Express Hematopoietic Cell Markers Cd45 and Cd109. *Int J Med Sci*, **11**: 65-79.

Libbrecht L., Desmet V., and Roskams T. (2005). Preneoplastic Lesions in Human Hepatocarcinogenesis. *Liver Int*, **25**: 16-27.

Libbrecht L., Desmet V., Van Damme B., and Roskams T. (2000a). Deep Intralobular Extension of Human Hepatic 'Progenitor Cells' Correlates with Parenchymal Inflammation in Chronic Viral Hepatitis: Can 'Progenitor Cells' Migrate? *J Pathol*, **192**: 373-378.

Libbrecht L., Desmet V., Van Damme B., and Roskams T. (2000b). The Immunohistochemical Phenotype of Dysplastic Foci in Human Liver: Correlation with Putative Progenitor Cells. *J Hepatol*, **33**: 76-84.

Liedtke C., Luedde T., Sauerbruch T., Scholten D., Streetz K., Tacke F., Tolba R., Trautwein C., Trebicka J., and Weiskirchen R. (2013). Experimental Liver

Fibrosis Research: Update on Animal Models, Legal Issues and Translational Aspects. *Fibrogenesis Tissue Repair*, **6**: 19.

Liew P.L., Wang W., Lee Y.C., Huang M.T., and Lee W.J. (2012). Roles of Hepatic Progenitor Cells Activation, Ductular Reaction Proliferation and Notch Signaling in Morbid Obesity. *Hepatogastroenterology*, **59**: 1921-1927.

Liu H., Zhang W., Jia Y., Yu Q., Grau G.E., Peng L., Ran Y., Yang Z., Deng H., and Lou J. (2013a). Single-Cell Clones of Liver Cancer Stem Cells Have the Potential of Differentiating into Different Types of Tumor Cells. *Cell Death Dis*, **4**: e857.

Liu Y., Cao L., Chen R., Zhou X., Fan X., Liang Y., Jia R., Wang H., Liu G., Guo Y., and Zhao J. (2015). Osteopontin Promotes Hepatic Progenitor Cell Expansion and Tumorigenicity Via Activation of Beta-Catenin in Mice. *Stem Cells*,

Liu Y., Meyer C., Xu C., Weng H., Hellerbrand C., ten Dijke P., and Dooley S. (2013b). Animal Models of Chronic Liver Diseases. *Am J Physiol Gastrointest Liver Physiol*, **304**: G449-468.

Llovet J.M., Ricci S., Mazzaferro V., Hilgard P., Gane E., Blanc J.F., de Oliveira A.C., Santoro A., Raoul J.L., Forner A., Schwartz M., Porta C., Zeuzem S., Bolondi L., Greten T.F., Galle P.R., Seitz J.F., Borbath I., Haussinger D., Giannaris T., Shan M., Moscovici M., Voliotis D., Bruix J., and Group S.I.S. (2008). Sorafenib in Advanced Hepatocellular Carcinoma. *N Engl J Med*, **359**: 378-390.

Llovet J.M., Villanueva A., Lachenmayer A., and Finn R.S. (2015). Advances in Targeted Therapies for Hepatocellular Carcinoma in the Genomic Era. *Nat Rev Clin Oncol*, **12**: 408-424.

Lorenzini S., Bird T.G., Boulter L., Bellamy C., Samuel K., Aucott R., Clayton E., Andreone P., Bernardi M., Golding M., Alison M.R., Iredale J.P., and Forbes S.J. (2010). Characterisation of a Stereotypical Cellular and Extracellular Adult Liver Progenitor Cell Niche in Rodents and Diseased Human Liver. *Gut*, **59**: 645-654.

Low T.Y., Leow C.K., Salto-Tellez M., and Chung M.C. (2004). A Proteomic Analysis of Thioacetamide-Induced Hepatotoxicity and Cirrhosis in Rat Livers. *Proteomics*, **4**: 3960-3974.

Lowes K.N., Brennan B.A., Yeoh G.C., and Olynyk J.K. (1999). Oval Cell Numbers in Human Chronic Liver Diseases Are Directly Related to Disease Severity. *Am J Pathol*, **154**: 537-541.

Lowes K.N., Croager E.J., Abraham L.J., Olynyk J.K., and Yeoh G.C. (2003). Upregulation of Lymphotoxin Beta Expression in Liver Progenitor (Oval) Cells in Chronic Hepatitis C. *Gut*, **52**: 1327-1332.

Lu W.Y., Bird T.G., Boulter L., Tsuchiya A., Cole A.M., Hay T., Guest R.V., Wojtacha D., Man T.Y., Mackinnon A., Ridgway R.A., Kendall T., Williams M.J., Jamieson T., Raven A., Hay D.C., Iredale J.P., Clarke A.R., Sansom O.J., and Forbes S.J. (2015). Hepatic Progenitor Cells of Biliary Origin with Liver Repopulation Capacity. *Nat Cell Biol*, **17**: 971-983.

Lunz J.G., 3rd, Tsuji H., Nozaki I., Murase N., and Demetris A.J. (2005). An Inhibitor of Cyclin-Dependent Kinase, Stress-Induced P21waf-1/Cip-1, Mediates Hepatocyte Mito-Inhibition During the Evolution of Cirrhosis. *Hepatology*, **41**: 1262-1271.

Ma S., Chan K.W., Hu L., Lee T.K., Wo J.Y., Ng I.O., Zheng B.J., and Guan X.Y. (2007). Identification and Characterization of Tumorigenic Liver Cancer Stem/Progenitor Cells. *Gastroenterology*, **132**: 2542-2556.

Ma S., Chan K.W., Lee T.K., Tang K.H., Wo J.Y., Zheng B.J., and Guan X.Y. (2008a). Aldehyde Dehydrogenase Discriminates the Cd133 Liver Cancer Stem Cell Populations. *Mol Cancer Res*, **6**: 1146-1153.

Ma S., Lee T.K., Zheng B.J., Chan K.W., and Guan X.Y. (2008b). Cd133+ Hcc Cancer Stem Cells Confer Chemoresistance by Preferential Expression of the Akt/Pkb Survival Pathway. *Oncogene*, **27**: 1749-1758.

MacPhee P.J., Schmidt E.E., and Groom A.C. (1992). Evidence for Kupffer Cell Migration Along Liver Sinusoids, from High-Resolution in Vivo Microscopy. *Am J Physiol*, **263**: G17-23.

Malarkey D.E., Johnson K., Ryan L., Boorman G., and Maronpot R.R. (2005). New Insights into Functional Aspects of Liver Morphology. *Toxicol Pathol*, **33**: 27-34.

Marquardt J.U., Factor V.M., and Thorgeirsson S.S. (2010). Epigenetic Regulation of Cancer Stem Cells in Liver Cancer: Current Concepts and Clinical Implications. *J Hepatol*, **53**: 568-577.

Matthews V.B., Klinken E., and Yeoh G.C. (2004). Direct Effects of Interleukin-6 on Liver Progenitor Oval Cells in Culture. *Wound Repair Regen*, **12**: 650-656.

McGivern D.R., and Lemon S.M. (2011). Virus-Specific Mechanisms of Carcinogenesis in Hepatitis C Virus Associated Liver Cancer. *Oncogene*, **30**: 1969-1983.

Meriden Z., Forde K.A., Pasha T.L., Hui J.J., Reddy K.R., Furth E.E., and Wells R.G. (2010). Histologic Predictors of Fibrosis Progression in Liver Allografts in Patients with Hepatitis C Virus Infection. *Clin Gastroenterol Hepatol*, **8**: 289-296, 296 e281-288.

Mishra L., Banker T., Murray J., Byers S., Thenappan A., He A.R., Shetty K., Johnson L., and Reddy E.P. (2009). Liver Stem Cells and Hepatocellular Carcinoma. *Hepatology*, **49**: 318-329.

Moustakas A., and Kardassis D. (1998). Regulation of the Human P21/Waf1/Cip1 Promoter in Hepatic Cells by Functional Interactions between Sp1 and Smad Family Members. *Proc Natl Acad Sci U S A*, **95**: 6733-6738.

Mu X., Espanol-Suner R., Mederacke I., Affo S., Manco R., Sempoux C., Lemaigre F.P., Adili A., Yuan D., Weber A., Unger K., Heikenwalder M., Leclercq I.A., and Schwabe R.F. (2015). Hepatocellular Carcinoma Originates from Hepatocytes and Not from the Progenitor/Biliary Compartment. *J Clin Invest*, **125**: 3891-3903.

Nair S., Mason A., Eason J., Loss G., and Perrillo R.P. (2002). Is Obesity an Independent Risk Factor for Hepatocellular Carcinoma in Cirrhosis? *Hepatology*, **36**: 150-155.

Nakagawa H., and Maeda S. (2012). Inflammation- and Stress-Related Signaling Pathways in Hepatocarcinogenesis. *World J Gastroenterol*, **18**: 4071-4081.

Nakatani K., Kaneda K., Seki S., and Nakajima Y. (2004). Pit Cells as Liver-Associated Natural Killer Cells: Morphology and Function. *Med Electron Microsc*, **37**: 29-36.

Natarajan A., Wagner B., and Sibilia M. (2007). The Egf Receptor Is Required for Efficient Liver Regeneration. *Proc Natl Acad Sci U S A*, **104**: 17081-17086.

Newell P., Villanueva A., Friedman S.L., Koike K., and Llovet J.M. (2008). Experimental Models of Hepatocellular Carcinoma. *J Hepatol*, **48**: 858-879.

Nguyen L.N., Furuya M.H., Wolfraim L.A., Nguyen A.P., Holdren M.S., Campbell J.S., Knight B., Yeoh G.C., Fausto N., and Parks W.T. (2007). Transforming Growth Factor-Beta Differentially Regulates Oval Cell and Hepatocyte Proliferation. *Hepatology*, **45**: 31-41.

Nielsen J.S., and McNagny K.M. (2008). Novel Functions of the Cd34 Family. *J Cell Sci*, **121**: 3683-3692.

Nobili V., Carpino G., Alisi A., Franchitto A., Alpini G., De Vito R., Onori P., Alvaro D., and Gaudio E. (2012). Hepatic Progenitor Cells Activation, Fibrosis, and Adipokines Production in Pediatric Nonalcoholic Fatty Liver Disease. *Hepatology*, **56**: 2142-2153.

Novoyatleva T., Schymura Y., Janssen W., Strobl F., Swiercz J.M., Patra C., Posern G., Wietelmann A., Zheng T.S., Schermuly R.T., and Engel F.B. (2013). Deletion of Fn14 Receptor Protects from Right Heart Fibrosis and Dysfunction. *Basic Res Cardiol*, **108**: 325.

Nusse R. (2008). Wnt Signaling and Stem Cell Control. *Cell Res*, **18**: 523-527.

Ochoa B., Syn W.K., Delgado I., Karaca G.F., Jung Y., Wang J., Zubiaga A.M., Fresnedo O., Omenetti A., Zdanowicz M., Choi S.S., and Diehl A.M. (2010). Hedgehog Signaling Is Critical for Normal Liver Regeneration after Partial Hepatectomy in Mice. *Hepatology*, **51**: 1712-1723.

Ohmori S., Shiraki K., Sugimoto K., Sakai T., Fujikawa K., Wagayama H., Takase K., and Nakano T. (2001). High Expression of Cd34-Positive Sinusoidal Endothelial Cells Is a Risk Factor for Hepatocellular Carcinoma in Patients with Hcv-Associated Chronic Liver Diseases. *Hum Pathol*, **32**: 1363-1370.

Okabe M., Tsukahara Y., Tanaka M., Suzuki K., Saito S., Kamiya Y., Tsujimura T., Nakamura K., and Miyajima A. (2009). Potential Hepatic Stem Cells Reside in Epcam+ Cells of Normal and Injured Mouse Liver. *Development*, **136**: 1951-1960.

Okuyama H., Nakamura H., Shimahara Y., Uyama N., Kwon Y.W., Kawada N., Yamaoka Y., and Yodoi J. (2005). Overexpression of Thioredoxin Prevents Thioacetamide-Induced Hepatic Fibrosis in Mice. *J Hepatol*, **42**: 117-123.

Oliva J., French B.A., Qing X., and French S.W. (2010). The Identification of Stem Cells in Human Liver Diseases and Hepatocellular Carcinoma. *Exp Mol Pathol*, **88**: 331-340.

Olle E.W., Ren X., McClintock S.D., Warner R.L., Deogracias M.P., Johnson K.J., and Colletti L.M. (2006). Matrix Metalloproteinase-9 Is an Important Factor in Hepatic Regeneration after Partial Hepatectomy in Mice. *Hepatology*, **44**: 540-549.

Omori N., Omori M., Evarts R.P., Teramoto T., Miller M.J., Hoang T.N., and Thorgeirsson S.S. (1997). Partial Cloning of Rat Cd34 Cdna and Expression During Stem Cell-Dependent Liver Regeneration in the Adult Rat. *Hepatology*, **26**: 720-727.

Paku S., Dezso K., Kopper L., and Nagy P. (2005). Immunohistochemical Analysis of Cytokeratin 7 Expression in Resting and Proliferating Biliary Structures of Rat Liver. *Hepatology*, **42**: 863-870.

Paku S., Nagy P., Kopper L., and Thorgeirsson S.S. (2004). 2-Acetylaminofluorene Dose-Dependent Differentiation of Rat Oval Cells into Hepatocytes: Confocal and Electron Microscopic Studies. *Hepatology*, **39**: 1353-1361.

Paradis V., Zalinski S., Chelbi E., Guedj N., Degos F., Vilgrain V., Bedossa P., and Belghiti J. (2009). Hepatocellular Carcinomas in Patients with Metabolic Syndrome Often Develop without Significant Liver Fibrosis: A Pathological Analysis. *Hepatology*, **49**: 851-859.

Park Y.S., Huh J.W., Lee J.H., and Kim H.R. (2012). Shrna against Cd44 Inhibits Cell Proliferation, Invasion and Migration, and Promotes Apoptosis of Colon Carcinoma Cells. *Oncol Rep*, **27**: 339-346.

Parker G.A., and Picut C.A. (2005). Liver Immunobiology. *Toxicol Pathol*, **33**: 52-62.

Patsenker E., Popov Y., Stickel F., Jonczyk A., Goodman S.L., and Schuppan D. (2008). Inhibition of Integrin Alphavbeta6 on Cholangiocytes Blocks Transforming Growth Factor-Beta Activation and Retards Biliary Fibrosis Progression. *Gastroenterology*, **135**: 660-670.

Patsenker E., Popov Y., Stickel F., Schneider V., Ledermann M., Sagesser H., Niedobitek G., Goodman S.L., and Schuppan D. (2009). Pharmacological Inhibition of Integrin Alphavbeta3 Aggravates Experimental Liver Fibrosis and Suppresses Hepatic Angiogenesis. *Hepatology*, **50**: 1501-1511.

Pekow J.R., Bhan A.K., Zheng H., and Chung R.T. (2007). Hepatic Steatosis Is Associated with Increased Frequency of Hepatocellular Carcinoma in Patients with Hepatitis C-Related Cirrhosis. *Cancer*, **109**: 2490-2496.

Peng Z.W., Ikenaga N., Liu S.B., Sverdlov D.Y., Vaid K.A., Dixit R., Weinreb P.H., Violette S., Sheppard D., Schuppan D., and Popov Y. (2015). Integrin Alphavbeta6 Critically Regulates Hepatic Progenitor Cell Function and Promotes Ductular Reaction, Fibrosis and Tumorigenesis. *Hepatology*,

Petersen B.E., Bowen W.C., Patrene K.D., Mars W.M., Sullivan A.K., Murase N., Boggs S.S., Greenberger J.S., and Goff J.P. (1999). Bone Marrow as a Potential Source of Hepatic Oval Cells. *Science*, **284**: 1168-1170.

Petersen B.E., Goff J.P., Greenberger J.S., and Michalopoulos G.K. (1998). Hepatic Oval Cells Express the Hematopoietic Stem Cell Marker Thy-1 in the Rat. *Hepatology*, **27**: 433-445.

Petersen B.E., Grossbard B., Hatch H., Pi L., Deng J., and Scott E.W. (2003). Mouse A6-Positive Hepatic Oval Cells Also Express Several Hematopoietic Stem Cell Markers. *Hepatology*, **37**: 632-640.

Piao L.S., Hur W., Kim T.K., Hong S.W., Kim S.W., Choi J.E., Sung P.S., Song M.J., Lee B.C., Hwang D., and Yoon S.K. (2012). Cd133+ Liver Cancer Stem Cells Modulate Radioresistance in Human Hepatocellular Carcinoma. *Cancer Lett*, **315**: 129-137.

Pocha C., Kolly P., and Dufour J.F. (2015). Nonalcoholic Fatty Liver Disease-Related Hepatocellular Carcinoma: A Problem of Growing Magnitude. *Semin Liver Dis*, **35**: 304-317.

Polakis P. (2012). Wnt Signaling in Cancer. *Cold Spring Harb Perspect Biol*, **4**:

Porretti L., Cattaneo A., Colombo F., Lopa R., Rossi G., Mazzaferro V., Battiston C., Svegliati-Baroni G., Bertolini F., Rebulla P., and Prati D. (2010). Simultaneous Characterization of Progenitor Cell Compartments in Adult Human Liver. *Cytometry A*, **77**: 31-40.

Potter V.R. (1978). Phenotypic Diversity in Experimental Hepatomas: The Concept of Partially Blocked Ontogeny. The 10th Walter Hubert Lecture. *Br J Cancer*, **38**: 1-23.

Prakoso E., Tirnitz-Parker J.E., Clouston A.D., Kayali Z., Lee A., Gan E.K., Ramm G.A., Kench J.G., Bowen D.G., Olynyk J.K., McCaughan G.W., and Shackel N.A. (2014). Analysis of the Intrahepatic Ductular Reaction and Progenitor Cell

Responses in Hepatitis C Virus Recurrence after Liver Transplantation. *Liver Transpl*, **20**: 1508-1519.

Preisegger K.H., Factor V.M., Fuchsbichler A., Stumptner C., Denk H., and Thorgeirsson S.S. (1999). Atypical Ductular Proliferation and Its Inhibition by Transforming Growth Factor Beta1 in the 3,5-Diethoxycarbonyl-1,4-Dihydrocollidine Mouse Model for Chronic Alcoholic Liver Disease. *Laboratory Investigation*, **79**: 103-109.

Pusztaszeri M.P., Seelentag W., and Bosman F.T. (2006). Immunohistochemical Expression of Endothelial Markers Cd31, Cd34, Von Willebrand Factor, and Fli-1 in Normal Human Tissues. *J Histochem Cytochem*, **54**: 385-395.

Qiu Q., Hernandez J.C., Dean A.M., Rao P.H., and Darlington G.J. (2011). Cd24-Positive Cells from Normal Adult Mouse Liver Are Hepatocyte Progenitor Cells. *Stem Cells Dev*, **20**: 2177-2188.

Rabes H.M. (1976). Kinetics of Hepatocellular Proliferation after Partial Resection of the Liver. *Prog Liver Dis*, **5**: 83-99.

Ramm G.A. (2009). Chemokine (C-C Motif) Receptors in Fibrogenesis and Hepatic Regeneration Following Acute and Chronic Liver Disease. *Hepatology*, **50**: 1664-1668.

Ramm G.A., Shepherd R.W., Hoskins A.C., Greco S.A., Ney A.D., Pereira T.N., Bridle K.R., Doecke J.D., Meikle P.J., Turlin B., and Lewindon P.J. (2009). Fibrogenesis in Pediatric Cholestatic Liver Disease: Role of Taurocholate and Hepatocyte-Derived Monocyte Chemotaxis Protein-1 in Hepatic Stellate Cell Recruitment. *Hepatology*, **49**: 533-544.

Raper S.E., Burwen S.J., Barker M.E., and Jones A.L. (1987). Translocation of Epidermal Growth Factor to the Hepatocyte Nucleus During Rat Liver Regeneration. *Gastroenterology*, **92**: 1243-1250.

Rappaport A.M., Borowy Z.J., Lougheed W.M., and Lotto W.N. (1954). Subdivision of Hexagonal Liver Lobules into a Structural and Functional Unit; Role in Hepatic Physiology and Pathology. *Anat Rec*, **119**: 11-33.

Regev A., Berho M., Jeffers L.J., Milikowski C., Molina E.G., Pyrsopoulos N.T., Feng Z.Z., Reddy K.R., and Schiff E.R. (2002). Sampling Error and Intraobserver Variation in Liver Biopsy in Patients with Chronic Hcv Infection. *Am J Gastroenterol*, **97**: 2614-2618.

Regimbeau J.M., Colombat M., Mognol P., Durand F., Abdalla E., Degott C., Degos F., Farges O., and Belghiti J. (2004). Obesity and Diabetes as a Risk Factor for Hepatocellular Carcinoma. *Liver Transpl*, **10**: S69-73.

Reiberger T., Chen Y., Ramjiawan R.R., Hato T., Fan C., Samuel R., Roberge S., Huang P., Lauwers G.Y., Zhu A.X., Bardeesy N., Jain R.K., and Duda D.G. (2015). An Orthotopic Mouse Model of Hepatocellular Carcinoma with Underlying Liver Cirrhosis. *Nat Protoc*, **10**: 1264-1274.

Reya T., Morrison S.J., Clarke M.F., and Weissman I.L. (2001). Stem Cells, Cancer, and Cancer Stem Cells. *Nature*, **414**: 105-111.

Richardson F.C., Boucheron J.A., Dyroff M.C., Popp J.A., and Swenberg J.A. (1986). Biochemical and Morphologic Studies of Heterogeneous Lobe Responses in Hepatocarcinogenesis. *Carcinogenesis*, **7**: 247-251.

Richardson M.M., Jonsson J.R., Powell E.E., Brunt E.M., Neuschwander-Tetri B.A., Bhathal P.S., Dixon J.B., Weltman M.D., Tilg H., Moschen A.R., Purdie D.M., Demetris A.J., and Clouston A.D. (2007). Progressive Fibrosis in Nonalcoholic Steatohepatitis: Association with Altered Regeneration and a Ductular Reaction. *Gastroenterology*, **133**: 80-90.

Riehle K.J., Dan Y.Y., Campbell J.S., and Fausto N. (2011). New Concepts in Liver Regeneration. *J Gastroenterol Hepatol*, **26 Suppl 1**: 203-212.

Robrechts C., De Vos R., Van den Heuvel M., Van Cutsem E., Van Damme B., Desmet V., and Roskams T. (1998). Primary Liver Tumour of Intermediate (Hepatocyte-Bile Duct Cell) Phenotype: A Progenitor Cell Tumour? *Liver*, **18**: 288-293.

Rodrigo-Torres D., Affo S., Coll M., Morales-Ibanez O., Millan C., Blaya D., Alvarez-Guaita A., Rentero C., Lozano J.J., Maestro M.A., Solar M., Arroyo V., Caballeria J., van Grunsven L.A., Enrich C., Gines P., Bataller R., and Sancho-Bru P. (2014). The Biliary Epithelium Gives Rise to Liver Progenitor Cells. *Hepatology*, **60**: 1367-1377.

Roskams T. (2006). Liver Stem Cells and Their Implication in Hepatocellular and Cholangiocarcinoma. *Oncogene*, **25**: 3818-3822.

Roskams T., and Desmet V. (1998). Ductular Reaction and Its Diagnostic Significance. *Semin Diagn Pathol*, **15**: 259-269.

Roskams T., Yang S.Q., Koteish A., Durnez A., DeVos R., Huang X., Achten R., Verslype C., and Diehl A.M. (2003a). Oxidative Stress and Oval Cell Accumulation in Mice and Humans with Alcoholic and Nonalcoholic Fatty Liver Disease. *Am J Pathol*, **163**: 1301-1311.

Roskams T.A., Libbrecht L., and Desmet V.J. (2003b). Progenitor Cells in Diseased Human Liver. *Semin Liver Dis*, **23**: 385-396.

Rountree C.B., Barsky L., Ge S., Zhu J., Senadheera S., and Crooks G.M. (2007). A Cd133-Expressing Murine Liver Oval Cell Population with Bilineage Potential. *Stem Cells*, **25**: 2419-2429.

Ruddell R.G., Knight B., Tirnitz-Parker J.E., Akhurst B., Summerville L., Subramaniam V.N., Olynyk J.K., and Ramm G.A. (2009). Lymphotoxin-Beta Receptor Signaling Regulates Hepatic Stellate Cell Function and Wound Healing in a Murine Model of Chronic Liver Injury. *Hepatology*, **49**: 227-239.

Saalbach A., Haustein U.F., and Anderegg U. (2000). A Ligand of Human Thy-1 Is Localized on Polymorphonuclear Leukocytes and Monocytes and Mediates the Binding to Activated Thy-1-Positive Microvascular Endothelial Cells and Fibroblasts. *J Invest Dermatol*, **115**: 882-888.

Sackett S.D., Li Z., Hurtt R., Gao Y., Wells R.G., Brondell K., Kaestner K.H., and Greenbaum L.E. (2009). Foxl1 Is a Marker of Bipotential Hepatic Progenitor Cells in Mice. *Hepatology*, **49**: 920-929.

Sakurai T., Kudo M., Umemura A., He G., Elsharkawy A.M., Seki E., and Karin M. (2013). P38alpha Inhibits Liver Fibrogenesis and Consequent Hepatocarcinogenesis by Curtailing Accumulation of Reactive Oxygen Species. *Cancer Res*, **73**: 215-224.

Salomao M., Yu W.M., Brown R.S., Jr., Emond J.C., and Lefkowitch J.H. (2010). Steatohepatitic Hepatocellular Carcinoma (Sh-Hcc): A Distinctive Histological Variant of Hcc in Hepatitis C Virus-Related Cirrhosis with Associated Nafld/Nash. *Am J Surg Pathol*, **34**: 1630-1636.

Sancho-Bru P., Altamirano J., Rodrigo-Torres D., Coll M., Millan C., Jose Lozano J., Miquel R., Arroyo V., Caballeria J., Gines P., and Bataller R. (2012). Liver Progenitor Cell Markers Correlate with Liver Damage and Predict Short-Term Mortality in Patients with Alcoholic Hepatitis. *Hepatology*, **55**: 1931-1941.

Sarraf C., Lalani E.N., Golding M., Anilkumar T.V., Poulsom R., and Alison M. (1994). Cell Behavior in the Acetylaminofluorene-Treated Regenerating Rat Liver. Light and Electron Microscopic Observations. *Am J Pathol*, **145**: 1114-1126.

Sasaki K., Kon J., Mizuguchi T., Chen Q., Ooe H., Oshima H., Hirata K., and Mitaka T. (2008). Proliferation of Hepatocyte Progenitor Cells Isolated from Adult Human Livers in Serum-Free Medium. *Cell Transplant*, **17**: 1221-1230.

Schepers A.G., Snippert H.J., Stange D.E., van den Born M., van Es J.H., van de Wetering M., and Clevers H. (2012). Lineage Tracing Reveals Lgr5+ Stem Cell Activity in Mouse Intestinal Adenomas. *Science*, **337**: 730-735.

Schievenbusch S., Sauer E., Curth H.M., Schulte S., Demir M., Toex U., Goeser T., and Nierhoff D. (2012). Neighbor of Punc E 11: Expression Pattern of the New Hepatic Stem/Progenitor Cell Marker During Murine Liver Development. *Stem Cells Dev*, **21**: 2656-2666.

Schlageter M., Terracciano L.M., D'Angelo S., and Sorrentino P. (2014). Histopathology of Hepatocellular Carcinoma. *World J Gastroenterol*, **20**: 15955-15964.

Schmitt-Graff A., Kruger S., Bochard F., Gabbiani G., and Denk H. (1991). Modulation of Alpha Smooth Muscle Actin and Desmin Expression in Perisinusoidal Cells of Normal and Diseased Human Livers. *Am J Pathol*, **138**: 1233-1242.

Schuppan D., Schmid M., Somasundaram R., Ackermann R., Ruehl M., Nakamura T., and Riecken E.O. (1998). Collagens in the Liver Extracellular Matrix Bind Hepatocyte Growth Factor. *Gastroenterology*, **114**: 139-152.

Scoazec J.Y., and Feldmann G. (1991). In Situ Immunophenotyping Study of Endothelial Cells of the Human Hepatic Sinusoid: Results and Functional Implications. *Hepatology*, **14**: 789-797.

Sekiya S., and Suzuki A. (2012). Intrahepatic Cholangiocarcinoma Can Arise from Notch-Mediated Conversion of Hepatocytes. *J Clin Invest*, **122**: 3914-3918.

Sell S. (1978). Distribution of Alpha-Fetoprotein- and Albumin-Containing Cells in the Livers of Fischer Rats Fed Four Cycles of N-2-Fluorenylacetamide. *Cancer Res*, **38**: 3107-3113.

Sell S. (1990). Is There a Liver Stem Cell? *Cancer Res*, **50**: 3811-3815.

Shaib Y., and El-Serag H.B. (2004). The Epidemiology of Cholangiocarcinoma. *Semin Liver Dis*, **24**: 115-125.

Shapiro L., and Weis W.I. (2009). Structure and Biochemistry of Cadherins and Catenins. *Cold Spring Harb Perspect Biol*, **1**: a003053.

Shi G.M., Xu Y., Fan J., Zhou J., Yang X.R., Qiu S.J., Liao Y., Wu W.Z., Ji Y., Ke A.W., Ding Z.B., He Y.Z., Wu B., Yang G.H., Qin W.Z., Zhang W., Zhu J., Min Z.H., and Wu Z.Q. (2008). Identification of Side Population Cells in Human Hepatocellular Carcinoma Cell Lines with Stepwise Metastatic Potentials. *J Cancer Res Clin Oncol*, **134**: 1155-1163.

Shi X., Leng L., Wang T., Wang W., Du X., Li J., McDonald C., Chen Z., Murphy J.W., Lolis E., Noble P., Knudson W., and Bucala R. (2006). Cd44 Is the Signaling Component of the Macrophage Migration Inhibitory Factor-Cd74 Receptor Complex. *Immunity*, **25**: 595-606.

Shin S., Upadhyay N., Greenbaum L.E., and Kaestner K.H. (2015). Ablation of Foxl1-Cre-Labeled Hepatic Progenitor Cells and Their Descendants Impairs Recovery of Mice from Liver Injury. *Gastroenterology*, **148**: 192-202 e193.

Shin S., Walton G., Aoki R., Brondell K., Schug J., Fox A., Smirnova O., Dorrell C., Erker L., Chu A.S., Wells R.G., Grompe M., Greenbaum L.E., and Kaestner K.H. (2011). Foxl1-Cre-Marked Adult Hepatic Progenitors Have Clonogenic and Bilineage Differentiation Potential. *Genes Dev*, **25**: 1185-1192.

Shin S., Wangensteen K.J., Teta-Bissett M., Wang Y.J., Mosleh-Shirazi E., Buza E.L., Greenbaum L.E., and Kaestner K.H. (2016). Genetic Lineage Tracing Analysis of

the Cell of Origin of Hepatotoxin-Induced Liver Tumors in Mice. *Hepatology*, **64**: 1163-1177.

Shinozuka H., Lombardi B., Sell S., and Iammarino R.M. (1978). Early Histological and Functional Alterations of Ethionine Liver Carcinogenesis in Rats Fed a Choline-Deficient Diet. *Cancer Res*, **38**: 1092-1098.

Shupe T., and Petersen B.E. (2011). Potential Applications for Cell Regulatory Factors in Liver Progenitor Cell Therapy. *Int J Biochem Cell Biol*, **43**: 214-221.

Sidney L.E., Branch M.J., Dunphy S.E., Dua H.S., and Hopkinson A. (2014). Concise Review: Evidence for Cd34 as a Common Marker for Diverse Progenitors. *Stem Cells*, **32**: 1380-1389.

Sleyster E.C., and Knook D.L. (1982). Relation between Localization and Function of Rat Liver Kupffer Cells. *Laboratory Investigation*, **47**: 484-490.

Smedsrod B., De Bleser P.J., Braet F., Lovisetti P., Vanderkerken K., Wisse E., and Geerts A. (1994). Cell Biology of Liver Endothelial and Kupffer Cells. *Gut*, **35**: 1509-1516.

Smith L.M., Nesterova A., Ryan M.C., Duniho S., Jonas M., Anderson M., Zabinski R.F., Sutherland M.K., Gerber H.P., Van Orden K.L., Moore P.A., Ruben S.M., and Carter P.J. (2008). Cd133/Prominin-1 Is a Potential Therapeutic Target for Antibody-Drug Conjugates in Hepatocellular and Gastric Cancers. *Br J Cancer*, **99**: 100-109.

Smith P.G., Tee L.B., and Yeoh G.C. (1996). Appearance of Oval Cells in the Liver of Rats after Long-Term Exposure to Ethanol. *Hepatology*, **23**: 145-154.

Solt D., and Farber E. (1976). New Principle for the Analysis of Chemical Carcinogenesis. *Nature*, **263**: 701-703.

Solt D.B., Hay J.B., and Farber E. (1977). Comparison of the Blood Supply to Diethylnitrosamine-Induced Hyperplastic Nodules and Hepatomas and to the Surrounding Liver. *Cancer Res*, **37**: 1686-1691.

Spangrude G.J., Heimfeld S., and Weissman I.L. (1988). Purification and Characterization of Mouse Hematopoietic Stem Cells. *Science*, **241**: 58-62.

Spee B., Carpino G., Schotanus B.A., Katoonizadeh A., Vander Borght S., Gaudio E., and Roskams T. (2010). Characterisation of the Liver Progenitor Cell Niche in Liver Diseases: Potential Involvement of Wnt and Notch Signalling. *Gut*, **59**: 247-257.

Strain A.J., Ismail T., Tsubouchi H., Arakaki N., Hishida T., Kitamura N., Daikuhara Y., and McMaster P. (1991). Native and Recombinant Human Hepatocyte Growth Factors Are Highly Potent Promoters of DNA Synthesis in Both Human and Rat Hepatocytes. *J Clin Invest*, **87**: 1853-1857.

Suarez-Causado A., Caballero-Diaz D., Bertran E., Roncero C., Addante A., Garcia-Alvaro M., Fernandez M., Herrera B., Porras A., Fabregat I., and Sanchez A. (2015). Hgf/C-Met Signaling Promotes Liver Progenitor Cell Migration and Invasion by an Epithelial-Mesenchymal Transition-Independent, Phosphatidyl Inositol-3 Kinase-Dependent Pathway in an in Vitro Model. *Biochim Biophys Acta*, **1853**: 2453-2463.

Suetsugu A., Nagaki M., Aoki H., Motohashi T., Kunisada T., and Moriwaki H. (2006). Characterization of Cd133+ Hepatocellular Carcinoma Cells as Cancer Stem/Progenitor Cells. *Biochem Biophys Res Commun*, **351**: 820-824.

Sun B., and Karin M. (2012). Obesity, Inflammation, and Liver Cancer. *J Hepatol*, **56**: 704-713.

Suzuki A., Sekiya S., Onishi M., Oshima N., Kiyonari H., Nakauchi H., and Taniguchi H. (2008). Flow Cytometric Isolation and Clonal Identification of Self-Renewing Bipotent Hepatic Progenitor Cells in Adult Mouse Liver. *Hepatology*, **48**: 1964-1978.

Svistounov D., Warren A., McNerney G.P., Owen D.M., Zencak D., Zykova S.N., Crane H., Huser T., Quinn R.J., Smedsrod B., Le Couteur D.G., and Cogger V.C. (2012). The Relationship between Fenestrations, Sieve Plates and Rafts in Liver Sinusoidal Endothelial Cells. *PLoS One*, **7**: e46134.

Tabibian J.H., Masyuk A.I., Masyuk T.V., O'Hara S.P., and LaRusso N.F. (2013). Physiology of Cholangiocytes. *Compr Physiol*, **3**: 541-565.

Takahashi Y., and Fukusato T. (2014). Histopathology of Nonalcoholic Fatty Liver Disease/Nonalcoholic Steatohepatitis. *World J Gastroenterol*, **20**: 15539-15548.

Takase H.M., Itoh T., Ino S., Wang T., Koji T., Akira S., Takikawa Y., and Miyajima A. (2013). Fgf7 Is a Functional Niche Signal Required for Stimulation of Adult Liver Progenitor Cells That Support Liver Regeneration. *Genes Dev*, **27**: 169-181.

Takase S., Leo M.A., Nouchi T., and Lieber C.S. (1988). Desmin Distinguishes Cultured Fat-Storing Cells from Myofibroblasts, Smooth Muscle Cells and Fibroblasts in the Rat. *J Hepatol*, **6**: 267-276.

Tarlow B.D., Finegold M.J., and Grompe M. (2014a). Clonal Tracing of Sox9+ Liver Progenitors in Mouse Oval Cell Injury. *Hepatology*, **60**: 278-289.

Tarlow B.D., Pelz C., Naugler W.E., Wakefield L., Wilson E.M., Finegold M.J., and Grompe M. (2014b). Bipotential Adult Liver Progenitors Are Derived from Chronically Injured Mature Hepatocytes. *Cell Stem Cell*, **15**: 605-618.

Tatematsu M., Kaku T., Medline A., and Farber E. (1985). Intestinal Metaplasia as a Common Option of Oval Cells in Relation to Cholangiofibrosis in Liver of Rats Exposed to 2-Acetylaminofluorene. *Laboratory Investigation*, **52**: 354-362.

Tee L.B., Kirilak Y., Huang W.H., Morgan R.H., and Yeoh G.C. (1994). Differentiation of Oval Cells into Duct-Like Cells in Preneoplastic Liver of Rats Placed on a Choline-Deficient Diet Supplemented with Ethionine. *Carcinogenesis*, **15**: 2747-2756.

Theise N.D., Saxena R., Portmann B.C., Thung S.N., Yee H., Chiriboga L., Kumar A., and Crawford J.M. (1999). The Canals of Hering and Hepatic Stem Cells in Humans. *Hepatology*, **30**: 1425-1433.

Theise N.D., Yao J.L., Harada K., Hytiroglou P., Portmann B., Thung S.N., Tsui W., Ohta H., and Nakanuma Y. (2003). Hepatic 'Stem Cell' Malignancies in Adults: Four Cases. *Histopathology*, **43**: 263-271.

Thenappan A., Li Y., Kitisin K., Rashid A., Shetty K., Johnson L., and Mishra L. (2010). Role of Transforming Growth Factor Beta Signaling and Expansion of Progenitor Cells in Regenerating Liver. *Hepatology*, **51**: 1373-1382.

Thorgeirsson S.S. (1996). Hepatic Stem Cells in Liver Regeneration. *FASEB J*, **10**: 1249-1256.

Thurman R.G., and Kauffman F.C. (1985). Sublobular Compartmentation of Pharmacologic Events (Scope): Metabolic Fluxes in Periportal and Pericentral Regions of the Liver Lobule. *Hepatology*, **5**: 144-151.

Tian Y.W., Smith P.G.J., and Yeoh G.C.T. (1997). The Oval-Shaped Cell as a Candidate for a Liver Stem Cell in Embryonic, Neonatal and Precancerous Liver: Identification Based on Morphology and Immunohistochemical Staining for Albumin and Pyruvate Kinase Isoenzyme Expression. *Histochemistry and Cell Biology*, **107**: 243-250.

Tirnitz-Parker J.E., Glanfield A., Olynyk J.K., and Ramm G.A. (2013). Iron and Hepatic Carcinogenesis. *Crit Rev Oncog*, **18**: 391-407.

Tirnitz-Parker J.E., Olynyk J.K., and Ramm G.A. (2014). Role of Tweak in Coregulating Liver Progenitor Cell and Fibrogenic Responses. *Hepatology*, **59**: 1198-1201.

Tirnitz-Parker J.E., Tonkin J.N., Knight B., Olynyk J.K., and Yeoh G.C. (2007). Isolation, Culture and Immortalisation of Hepatic Oval Cells from Adult Mice Fed a Choline-Deficient, Ethionine-Supplemented Diet. *Int J Biochem Cell Biol*, **39**: 2226-2239.

Tirnitz-Parker J.E., Viebahn C.S., Jakubowski A., Klopcic B.R., Olynyk J.K., Yeoh G.C., and Knight B. (2010). Tumor Necrosis Factor-Like Weak Inducer of Apoptosis Is a Mitogen for Liver Progenitor Cells. *Hepatology*, **52**: 291-302.

Tirnitz-Parker J.E.E., Yeoh G.C.T., and Olynyk J.K. (2012). "Liver Progenitor Cells, Cancer Stem Cells and Hepatocellular Carcinoma." In *Liver Regeneration*, ed. Baptista P.M.: Intech.

Tonkin J.N., Knight B., Curtis D., Abraham L.J., and Yeoh G.C. (2008). Bone Marrow Cells Play Only a Very Minor Role in Chronic Liver Regeneration Induced by a Choline-Deficient, Ethionine-Supplemented Diet. *Stem Cell Res*, **1**: 195-204.

Toshikuni N., Arisawa T., and Tsutsumi M. (2014). Hepatitis C-Related Liver Cirrhosis - Strategies for the Prevention of Hepatic Decompensation, Hepatocarcinogenesis, and Mortality. *World J Gastroenterol*, **20**: 2876-2887.

Treyer A., and Musch A. (2013). Hepatocyte Polarity. *Compr Physiol*, **3**: 243-287.

Tyson G.L., and El-Serag H.B. (2011). Risk Factors for Cholangiocarcinoma. *Hepatology*, **54**: 173-184.

Ueberham E., Aigner T., Ueberham U., and Gebhardt R. (2007). E-Cadherin as a Reliable Cell Surface Marker for the Identification of Liver Specific Stem Cells. *J Mol Histol*, **38**: 359-368.

Uenishi T., Kubo S., Yamamoto T., Shuto T., Ogawa M., Tanaka H., Tanaka S., Kaneda K., and Hirohashi K. (2003). Cytokeratin 19 Expression in Hepatocellular Carcinoma Predicts Early Postoperative Recurrence. *Cancer Sci*, **94**: 851-857.

Van Eyken P., Sciot R., and Desmet V.J. (1988). A Cytokeratin Immunohistochemical Study of Alcoholic Liver Disease: Evidence That Hepatocytes Can Express 'Bile Duct-Type' Cytokeratins. *Histopathology*, **13**: 605-617.

Van Hul N.K., Abarca-Quinones J., Sempoux C., Horsmans Y., and Leclercq I.A. (2009). Relation between Liver Progenitor Cell Expansion and Extracellular Matrix Deposition in a Cde-Induced Murine Model of Chronic Liver Injury. *Hepatology*, **49**: 1625-1635.

Vestentoft P.S., Jelnes P., Hopkinson B.M., Vainer B., Mollgard K., Quistorff B., and Bisgaard H.C. (2011). Three-Dimensional Reconstructions of Intrahepatic Bile Duct Tubulogenesis in Human Liver. *BMC Dev Biol*, **11**: 56.

Villano G., Turato C., Quarta S., Ruvoletto M., Ciscato F., Terrin L., Semeraro R., Paternostro C., Parola M., Alvaro D., Bernardi P., Gatta A., and Pontisso P. (2014). Hepatic Progenitor Cells Express Serpinb3. *BMC Cell Biol*, **15**: 5.

Villanueva A., Alsinet C., Yanger K., Hoshida Y., Zong Y., Toffanin S., Rodriguez-Carunchio L., Sole M., Thung S., Stanger B.Z., and Llovet J.M. (2012). Notch Signaling Is Activated in Human Hepatocellular Carcinoma and Induces Tumor Formation in Mice. *Gastroenterology*, **143**: 1660-1669 e1667.

Visvader J.E., and Lindeman G.J. (2008). Cancer Stem Cells in Solid Tumours: Accumulating Evidence and Unresolved Questions. *Nat Rev Cancer*, **8**: 755-768.

Wake K. (1971). "Sternzellen" in the Liver: Perisinusoidal Cells with Special Reference to Storage of Vitamin A. *Am J Anat*, **132**: 429-462.

Wallace M.C., Hamesch K., Lunova M., Kim Y., Weiskirchen R., Strnad P., and Friedman S.L. (2015). Standard Operating Procedures in Experimental Liver Research: Thioacetamide Model in Mice and Rats. *Lab Anim*, **49**: 21-29.

Wang B., Zhao L., Fish M., Logan C.Y., and Nusse R. (2015). Self-Renewing Diploid Axin2(+) Cells Fuel Homeostatic Renewal of the Liver. *Nature*, **524**: 180-185.

Wang F.S., Fan J.G., Zhang Z., Gao B., and Wang H.Y. (2014). The Global Burden of Liver Disease: The Major Impact of China. *Hepatology*, **60**: 2099-2108.

Wang X., Willenbring H., Akkari Y., Torimaru Y., Foster M., Al-Dhalimy M., Lagasse E., Finegold M., Olson S., and Grompe M. (2003). Cell Fusion Is the Principal Source of Bone-Marrow-Derived Hepatocytes. *Nature*, **422**: 897-901.

Webber E.M., Bruix J., Pierce R.H., and Fausto N. (1998). Tumor Necrosis Factor Primes Hepatocytes for DNA Replication in the Rat. *Hepatology*, **28**: 1226-1234.

Webber E.M., FitzGerald M.J., Brown P.I., Bartlett M.H., and Fausto N. (1993). Transforming Growth Factor-Alpha Expression During Liver Regeneration after Partial Hepatectomy and Toxic Injury, and Potential Interactions between Transforming Growth Factor-Alpha and Hepatocyte Growth Factor. *Hepatology*, **18**: 1422-1431.

Webber E.M., Godowski P.J., and Fausto N. (1994). In Vivo Response of Hepatocytes to Growth Factors Requires an Initial Priming Stimulus. *Hepatology*, **19**: 489-497.

Widmann J.J., Cotran R.S., and Fahimi H.D. (1972). Mononuclear Phagocytes (Kupffer Cells) and Endothelial Cells. Identification of Two Functional Cell Types in Rat Liver Sinusoids by Endogenous Peroxidase Activity. *J Cell Biol*, **52**: 159-170.

Williams M.J., Clouston A.D., and Forbes S.J. (2014). Links between Hepatic Fibrosis, Ductular Reaction, and Progenitor Cell Expansion. *Gastroenterology*, **146**: 349-356.

Wisse E. (1972). An Ultrastructural Characterization of the Endothelial Cell in the Rat Liver Sinusoid under Normal and Various Experimental Conditions, as a Contribution to the Distinction between Endothelial and Kupffer Cells. *J Ultrastruct Res*, **38**: 528-562.

Wisse E., De Zanger R.B., Jacobs R., and McCuskey R.S. (1983). Scanning Electron Microscope Observations on the Structure of Portal Veins, Sinusoids and Central Veins in Rat Liver. *Scan Electron Microsc*, 1441-1452.

Wisse E., van't Noordende J.M., van der Meulen J., and Daems W.T. (1976). The Pit Cell: Description of a New Type of Cell Occurring in Rat Liver Sinusoids and Peripheral Blood. *Cell Tissue Res*, **173**: 423-435.

Wood M.J., Gadd V.L., Powell L.W., Ramm G.A., and Clouston A.D. (2014). Ductular Reaction in Hereditary Hemochromatosis: The Link between Hepatocyte Senescence and Fibrosis Progression. *Hepatology*, **59**: 848-857.

Wu K., Ding J., Chen C., Sun W., Ning B.F., Wen W., Huang L., Han T., Yang W., Wang C., Li Z., Wu M.C., Feng G.S., Xie W.F., and Wang H.Y. (2012a). Hepatic Transforming Growth Factor Beta Gives Rise to Tumor-Initiating Cells and Promotes Liver Cancer Development. *Hepatology*, **56**: 2255-2267.

Wu S.D., Ma Y.S., Fang Y., Liu L.L., Fu D., and Shen X.Z. (2012b). Role of the Microenvironment in Hepatocellular Carcinoma Development and Progression. *Cancer Treat Rev*, **38**: 218-225.

Xie Z., Choong P.F., Poon L.F., Zhou J., Khng J., Jasinghe V.J., Palaniyandi S., and Chen C.S. (2008). Inhibition of Cd44 Expression in Hepatocellular Carcinoma Cells Enhances Apoptosis, Chemosensitivity, and Reduces Tumorigenesis and Invasion. *Cancer Chemother Pharmacol*, **62**: 949-957.

Yabushita K., Yamamoto K., Ibuki N., Okano N., Matsumura S., Okamoto R., Shimada N., and Tsuji T. (2001). Aberrant Expression of Cytokeratin 7 as a Histological Marker of Progression in Primary Biliary Cirrhosis. *Liver*, **21**: 50-55.

Yamada Y., Kirillova I., Peschon J.J., and Fausto N. (1997). Initiation of Liver Growth by Tumor Necrosis Factor: Deficient Liver Regeneration in Mice Lacking Type I Tumor Necrosis Factor Receptor. *Proc Natl Acad Sci U S A*, **94**: 1441-1446.

Yamashita T., Budhu A., Forgues M., and Wang X.W. (2007). Activation of Hepatic Stem Cell Marker Epcam by Wnt-Beta-Catenin Signaling in Hepatocellular Carcinoma. *Cancer Res*, **67**: 10831-10839.

Yamashita T., Forgues M., Wang W., Kim J.W., Ye Q., Jia H., Budhu A., Zanetti K.A., Chen Y., Qin L.X., Tang Z.Y., and Wang X.W. (2008). Epcam and Alpha-Fetoprotein Expression Defines Novel Prognostic Subtypes of Hepatocellular Carcinoma. *Cancer Res*, **68**: 1451-1461.

Yamashita T., Honda M., Nakamoto Y., Baba M., Nio K., Hara Y., Zeng S.S., Hayashi T., Kondo M., Takatori H., Yamashita T., Mizukoshi E., Ikeda H., Zen Y., Takamura H., Wang X.W., and Kaneko S. (2013). Discrete Nature of Epcam+ and Cd90+ Cancer Stem Cells in Human Hepatocellular Carcinoma. *Hepatology*, **57**: 1484-1497.

Yamashita T., Ji J., Budhu A., Forgues M., Yang W., Wang H.Y., Jia H., Ye Q., Qin L.X., Wauthier E., Reid L.M., Minato H., Honda M., Kaneko S., Tang Z.Y., and Wang X.W. (2009). Epcam-Positive Hepatocellular Carcinoma Cells Are Tumor-Initiating Cells with Stem/Progenitor Cell Features. *Gastroenterology*, **136**: 1012-1024.

Yang J.D., Nakamura I., and Roberts L.R. (2011). The Tumor Microenvironment in Hepatocellular Carcinoma: Current Status and Therapeutic Targets. *Semin Cancer Biol*, **21**: 35-43.

Yang L., Faris R.A., and Hixson D.C. (1993). Characterization of a Mature Bile Duct Antigen Expressed on a Subpopulation of Biliary Ductular Cells but Absent from Oval Cells. *Hepatology*, **18**: 357-366.

Yang L., Li S., Hatch H., Ahrens K., Cornelius J.G., Petersen B.E., and Peck A.B. (2002). In Vitro Trans-Differentiation of Adult Hepatic Stem Cells into Pancreatic Endocrine Hormone-Producing Cells. *Proc Natl Acad Sci U S A*, **99**: 8078-8083.

Yang W., Yan H.X., Chen L., Liu Q., He Y.Q., Yu L.X., Zhang S.H., Huang D.D., Tang L., Kong X.N., Chen C., Liu S.Q., Wu M.C., and Wang H.Y. (2008a). Wnt/Beta-Catenin Signaling Contributes to Activation of Normal and Tumorigenic Liver Progenitor Cells. *Cancer Res*, **68**: 4287-4295.

Yang Z.F., Ho D.W., Ng M.N., Lau C.K., Yu W.C., Ngai P., Chu P.W., Lam C.T., Poon R.T., and Fan S.T. (2008b). Significance of Cd90+ Cancer Stem Cells in Human Liver Cancer. *Cancer Cell*, **13**: 153-166.

Yang Z.F., Ngai P., Ho D.W., Yu W.C., Ng M.N., Lau C.K., Li M.L., Tam K.H., Lam C.T., Poon R.T., and Fan S.T. (2008c). Identification of Local and Circulating Cancer Stem Cells in Human Liver Cancer. *Hepatology*, **47**: 919-928.

Yao Z.M., and Vance D.E. (1988). The Active Synthesis of Phosphatidylcholine Is Required for Very Low Density Lipoprotein Secretion from Rat Hepatocytes. *J Biol Chem*, **263**: 2998-3004.

Yaswen P., Hayner N.T., and Fausto N. (1984). Isolation of Oval Cells by Centrifugal Elutriation and Comparison with Other Cell Types Purified from Normal and Preneoplastic Livers. *Cancer Res*, **44**: 324-331.

Yeh M.M. (2010). Pathology of Combined Hepatocellular-Cholangiocarcinoma. *J Gastroenterol Hepatol*, **25**: 1485-1492.

Yeh M.M., and Brunt E.M. (2014). Pathological Features of Fatty Liver Disease. *Gastroenterology*, **147**: 754-764.

Yin S., Li J., Hu C., Chen X., Yao M., Yan M., Jiang G., Ge C., Xie H., Wan D., Yang S., Zheng S., and Gu J. (2007). Cd133 Positive Hepatocellular Carcinoma Cells Possess High Capacity for Tumorigenicity. *Int J Cancer*, **120**: 1444-1450.

Yokoi Y., Namihisa T., Kuroda H., Komatsu I., Miyazaki A., Watanabe S., and Usui K. (1984). Immunocytochemical Detection of Desmin in Fat-Storing Cells (Ito Cells). *Hepatology*, **4**: 709-714.

Yoon S.M., Gerasimidou D., Kuwahara R., Hytiroglou P., Yoo J.E., Park Y.N., and Theise N.D. (2011). Epithelial Cell Adhesion Molecule (Epcam) Marks Hepatocytes Newly Derived from Stem/Progenitor Cells in Humans. *Hepatology*, **53**: 964-973.

Yovchev M.I., Grozdanov P.N., Joseph B., Gupta S., and Dabeva M.D. (2007). Novel Hepatic Progenitor Cell Surface Markers in the Adult Rat Liver. *Hepatology*, **45**: 139-149.

Yovchev M.I., Grozdanov P.N., Zhou H., Racherla H., Guha C., and Dabeva M.D. (2008). Identification of Adult Hepatic Progenitor Cells Capable of Repopulating Injured Rat Liver. *Hepatology*, **47**: 636-647.

Zajicek G., Oren R., and Weinreb M., Jr. (1985). The Streaming Liver. *Liver*, **5**: 293-300.

Zatloukal K., French S.W., Stumptner C., Strnad P., Harada M., Toivola D.M., Cadrin M., and Omary M.B. (2007). From Mallory to Mallory-Denk Bodies: What, How and Why? *Exp Cell Res*, **313**: 2033-2049.

Zhang A., London R., Schulz F.M., Giguere-Simmonds P.W., Delriviere L., Chandraratana H., Hardy K., Zheng S., Olynyk J.K., and Yeoh G. (2010a). Human Liver Progenitor Cell Lines Are Readily Established from Non-Tumorous Tissue Adjacent to Hepatocellular Carcinoma. *Stem Cells Dev*, **19**: 1277-1284.

Zhang D.Y., and Friedman S.L. (2012). Fibrosis-Dependent Mechanisms of Hepatocarcinogenesis. *Hepatology*, **56**: 769-775.

Zhang M., and Thorgeirsson S.S. (1994). Modulation of Connexins During Differentiation of Oval Cells into Hepatocytes. *Exp Cell Res*, **213**: 37-42.

Zhang W., Zhu X.D., Sun H.C., Xiong Y.Q., Zhuang P.Y., Xu H.X., Kong L.Q., Wang L., Wu W.Z., and Tang Z.Y. (2010b). Depletion of Tumor-Associated Macrophages Enhances the Effect of Sorafenib in Metastatic Liver Cancer Models by Antimetastatic and Antiangiogenic Effects. *Clin Cancer Res*, **16**: 3420-3430.

Zhu Z., Hao X., Yan M., Yao M., Ge C., Gu J., and Li J. (2010). Cancer Stem/Progenitor Cells Are Highly Enriched in Cd133+Cd44+ Population in Hepatocellular Carcinoma. *Int J Cancer*, **126**: 2067-2078.

APPENDIX

The full text of the publications listed on page vi of this thesis are unable to be reproduced here due to copyright restrictions.

They can instead be accessed via the following locations:

American Journal of Physiology Gastrointestinal and Liver Physiology: http://dx.doi.org/10.1152/ajpgi.00215.2015

American Journal of Pathology: http://dx.doi.org/10.1016/j.ajpath.2016.03.005

Oncotarget: http://dx.doi.org/10.18632/oncotarget.7836